

Poly(Alkyl Methacrylate-co-Acrylic Acid) Copolymers of Varying Architecture for Improved Adhesion



The
University
Of
Sheffield.

Sarah Louise Canning

A Thesis submitted for the Degree of Doctor of Philosophy

Department of Chemistry, University of Sheffield

March 2015

Acknowledgements

I would firstly like to thank my supervisory team, Prof. Steve Rimmer and Prof. Mark Geoghegan at the University of Sheffield and Dr Trevor Wear, Dr Stuart Reynolds and Dr Jon Morgan at Domino UK Ltd for all their help, support and guidance throughout this project. Thanks also go to the rest of the R&D team at Domino for being so welcoming to me.

Domino UK Ltd and the EPSRC are gratefully acknowledged for providing financial support for the project.

To everyone in the Chemistry Department at the University of Sheffield, I'm grateful for their assistance and for making the department such a friendly place to work. I particularly want to thank Melanie Hannah for her technical assistance and support. I am grateful to Richard Bottomley for allowing me to borrow equipment from the teaching labs, to Rob Hanson for his help with chromatography, to Sue Bradshaw for her assistance with NMR, and to Jenny Louth for elemental analysis. Thank you also to Pete Farran and Nick Smith for their storekeeping and footballing excellence, and to Pauline Bould for being a cheerful face every morning.

I am very grateful to Dr Svet Tsokov in the EM Department for training me to use the TEM and for his continued advice, and to Chris Hill who assisted with the SEM imaging.

I must thank Dr Ann Terry and Dr Steve King, instrument scientists at the ISIS facility, for their assistance with the SANS experiments. I am also extremely grateful to Prof. Patrick Fairclough for his help with fitting the SANS data.

I'm thankful to all the members of the Geoghegan group past and present, especially Jason Zhang who trained me on the AFM with utmost patience.

I must also thank the past and present members of F floor and the Rimmer group for their advice, support and friendship over the past three and a half years, particularly Laura Platt, Laura Shallcross, Simon Finnegan and Pavintorn (Mew) Teratanatorn.

I also want to thank the undergraduate students who have worked with me on summer placements, Sammi Hassan, Joe Ferner and Natalie Paul; I appreciate their hard work and enthusiasm.

Thanks to Lizzy Jones and Vicki Cunningham for being excellent friends and housemates, I'm glad we've experienced this journey together.

Thank you to Nathan Rutland for his support, patience and understanding (not to mention top banter!) You made the writing process much less painful than I expected. I hope I can return the favour when your turn comes.

Finally I want to thank my family for their continuous support and encouragement throughout my studies and my entire life. I want to dedicate this thesis to my grandmother Pam Penhale, who will always be an inspiration to me.

Abstract

Amphiphilic copolymers composed of hydrophilic polyacrylic acid segments and hydrophobic poly(alkyl methacrylate) segments were targeted as adhesion-promoting additives for use in printing inks. Methyl, butyl and lauryl methacrylates were chosen to vary hydrophobicity. Initially, a phase transfer-catalysed backbone functionalisation and a reversible addition-fragmentation chain transfer (RAFT)-controlled grafting step were employed to form graft copolymers, although polyacrylic acid homopolymer was also produced. The lauryl methacrylate synthesis proved more difficult due to the steric effect of the long alkyl chain. Branched and linear poly(alkyl methacrylate-acrylic acid) copolymers were then synthesised using RAFT, in either a one-pot polymerisation, producing random copolymers, or a two-step procedure forming block copolymers. Molecular weights of close to 20 000 g mol⁻¹ were achieved, with methacrylate:acrylic acid ratios close to 1:1, as targeted. Branching was confirmed through calculation of Mark-Houwink parameters using GPC with viscometric detection, and a ¹³C NMR method was developed to identify block or random monomer sequence distribution. Due to their amphiphilic nature, the copolymers were found to self-assemble in water to form macromolecular structures. These varied according to architecture, monomer distribution, and hydrophobicity of the methacrylate segment. Small angle neutron scattering was used to study the copolymers in a range of solvent systems. Whilst Gaussian coils were formed in d-THF and self-assembled spheres or multi-lamellar micelles were formed in D₂O, the copolymers were found to aggregate into fractal structures in intermediate solvency conditions. The behaviour of the copolymers when coated on polyolefin substrates was studied by contact angle measurements, and the random materials created more polar surfaces compared to the segmented analogues. A force spectroscopy technique showed potential for accurate comparison of copolymer adhesion. Ink formulations containing the butyl methacrylate copolymers jetted well on both thermal inkjet and drop on demand printers. Adhesion was assessed using industry standard tests, and better overall performance was observed for the branched copolymers.

List of Abbreviations

α	Mark-Houwink parameter
γ_L	surface energy of liquid
γ_{LS}	surface energy of liquid-solid interface
γ_S	surface energy of solid
AA	acrylic acid
AFM	atomic force microscope
AIBN	azobisisobutyronitrile
ACVA	4,4'-azobis (4-cyanovaleric acid)
ANOVA	analysis of variance
ATRP	atom transfer radical polymerisation
BMA	butyl methacrylate
BN	α -bromonaphthalene
CDCl ₃	deuterated chloroform
CIJ	continuous inkjet
CRP	controlled radical polymerisation
CTA	chain transfer agent
\bar{D}	dispersity
DB	degree of branching
d-DMSO	deuterated dimethyl sulfoxide
d-EtOH	deuterated ethanol
D _f	fractal dimension

D ₂ O	deuterium oxide
DOD	drop on demand
D _p	degree of polymerisation
d-THF	deuterated THF
EG	ethylene glycol
<i>g</i> '	contraction factor
GPC	gel permeation chromatography
HB	highly branched
HD	1,2-hexanediol
HDPE	high density polyethylene
I(Q)	scattering intensity
IV, [η]	intrinsic viscosity
K	Mark-Houwink parameter
LDPE	low density polyethylene
LMA	lauryl methacrylate
MMA	methyl methacrylate
M _n	number-average molecular weight
M _w	weight-average molecular weight
nMA	alkyl methacrylate monomer
NIP	non-impact printing
NMP	nitroxide mediated polymerisation
NMR	nuclear magnetic resonance
Q	scattering vector

PAA	polyacrylic acid
PALS	phase analysis light scattering
PE	polyethylene
PnMA	poly(alkyl methacrylate) (n = M methyl, B butyl or L lauryl)
PNIPAM	poly(<i>N</i> -isopropyl acrylamide)
PP	polypropylene
P(Q)	form factor
PTC	phase transfer catalysis
RAFT	reversible addition-fragmentation chain transfer polymerisation
RB	repeat units per branch
R_g	radius of gyration
RI	refractive index
SANS	small angle neutron scattering
SCVP	self condensing vinyl polymerisation
SEM	scanning electron microscopy
SLD	scattering length density
S(Q)	structure factor
tBA	t-butyl acrylate
TBAB	tetrabutyl ammonium bromide
TEM	transmission electron microscopy
TIJ	thermal inkjet
VBC	4-vinylbenzyl chloride

Chapter 3. Synthesis of Poly(Alkyl Methacrylate-<i>g</i>-Acrylic Acid) Graft Copolymers	39
3.1 Introduction	39
3.2 Synthesis of P(nMA- <i>co</i> -VBC) Backbones	42
3.3 Functionalisation of P(nMA- <i>co</i> -VBC) Backbones using Phase Transfer Catalysis	45
3.4 Grafting Polyacrylic Acid Side Chains from Functionalised Backbones	51
3.5 Investigation into the Effect of Alkyl Methacrylate Monomer on Grafting of Polyacrylic Acid Side Chains from Functionalised Backbones	56
3.6 Conclusions	62
Chapter 4. Synthesis of Poly(Alkyl Methacrylate-<i>co</i>-Acrylic Acid) Block and Random Copolymers with Highly Branched and Linear Architectures	63
4.1. Introduction	63
4.2. Highly Branched Block P(nMA- <i>b</i> -AA) Copolymers	66
4.3. Highly Branched Block P(AA- <i>b</i> -nMA) Copolymers	70
4.4. Highly Branched Random P(nMA- <i>co</i> -AA) Copolymers	72
4.5. Linear Block P(nMA- <i>b</i> -AA) Copolymers	74
4.6. Linear Random P(nMA- <i>co</i> -AA) Copolymers	77
4.7. ¹³ C NMR to Study Monomer Sequence Distribution	78
4.8. GPC-Viscometry	82
4.9. Conclusions	87
Chapter 5. Solution Behaviour of Poly(Alkyl Methacrylate-<i>co</i>-Acrylic Acid) Copolymers	89
5.1. Introduction	89
5.2. Poly(Alkyl Methacrylate- <i>co</i> -Acrylic Acid) Copolymers in Water	90
5.3. Small Angle Neutron Scattering	107
5.4. Conclusions	128
Chapter 6. Formation of Onion Micelles from the Self-Assembly of HB P(BMA-<i>b</i>-AA) in Water	131
6.1. Introduction	131
6.2. Self-Assembly of HB P(nMA- <i>b</i> -AA) Copolymers in Water	132
6.3. Discussion of Formation of Onion Micelles	155
6.4. Release Studies from HB P(nMA- <i>b</i> -AA) Micelles	156
6.5. Conclusions	162
Chapter 7. Surface Properties and Adhesion Behaviour	165
7.1. Introduction	165
7.2. Surface Analysis by Contact Angle Measurements	168
7.3. AFM Force Spectroscopy	183

7.4. Method for Removal of RAFT End Groups	188
7.5. Conclusions	189
Chapter 8. Materials Testing for Printing Applications	191
8.1. Introduction	191
8.2. Synthesis of Copolymers for Printing	191
8.3. Copolymers in Ink Formulations	193
8.3.1. Viscometry of Copolymer Inks	194
8.4. Thermal Inkjet Printing with Domino G Series	200
8.4.1. Decap Time	201
8.4.2. Adhesion Testing	204
8.4.3. Jet Xpert	209
8.5. Drop on Demand Printing with Fujifilm Dimatix	214
8.5.1. Print Setting Optimisation	215
8.5.2. Printing onto Substrates	218
8.5.3. Printing Polymer Solutions	219
8.5.3.1. Viscometry	220
8.5.3.2. Printing Tests	222
8.6. Summary	224
8.7. Conclusions	225
Chapter 9. Conclusions and Future Work	227
9.1. Conclusions	227
9.2. Future Work	231
Chapter 10. Experimental	235
10.1. Materials	235
10.2. Synthesis of Pyrrole-1-carbodithioic Acid	235
10.3. Free Radical Copolymerisation of Alkyl Methacrylate and 4-Vinylbenzyl Chloride to form P(nMA-co-VBC) Backbone	236
10.4. Functionalisation of P(LMA-co-VBC) Linear Copolymers with Pyrrole-1-carbodithioic Acid	237
10.5. Functionalisation of P(nMA-co-VBC) Linear Copolymers with Pyrrole-1-carbodithioic Acid using Phase Transfer Catalysis	238
10.6. Grafting of Acrylic Acid onto P(nMA-co-VBC) Backbones via RAFT Polymerisation to form P(nMA-co-VBC-g-AA) Graft Copolymers	239
10.7. Grafting of t-Butyl Acrylate onto P(LMA-co-VBC) Backbones via RAFT Polymerisation to form P(LMA-co-VBC-g-tBA) Graft Copolymers	241
10.8. Hydrolysis of P(LMA-co-VBC-g-tBA) to P(LMA-co-VBC-g-AA)	242

10.9.	Synthesis of Benzyl-1-pyrrole Carbodithioate	242
10.10.	RAFT Polymerisation of Alkyl Methacrylates using Benzyl-1-pyrrole Carbodithioate to form Linear P(nMA) Chain Transfer Agent	243
10.11.	Synthesis of Linear P(nMA- <i>b</i> -AA) Block Copolymers via RAFT Polymerisation of P(nMA) Macro-Chain Transfer Agent and Acrylic Acid	244
10.12.	RAFT Polymerisation of Alkyl Methacrylates and Acrylic Acid using Benzyl-1-pyrrole Carbodithioate to form Linear Random P(nMA- <i>co</i> -AA) Copolymers	245
10.13.	Synthesis of 4-Vinylbenzyl-1-pyrrole Carbodithioate	247
10.14.	RAFT Polymerisation of Alkyl Methacrylates using 4-Vinylbenzyl-1-pyrrole Carbodithioate to form Highly Branched P(nMA) Macro-Chain Transfer Agent	248
10.15.	Synthesis of HB P(nMA- <i>b</i> -AA) Block Copolymers via RAFT Polymerisation of HB P(nMA) Macro-Chain Transfer Agent and Acrylic Acid	249
10.16.	RAFT Polymerisation of Acrylic Acid using 4-Vinylbenzyl-1-pyrrole Carbodithioate to form HB PAA Macro-Chain Transfer Agent	250
10.17.	Synthesis of HB P(AA- <i>b</i> -nMA) Block Copolymers via RAFT Polymerisation of HB PAA Macro-Chain Transfer Agent and Alkyl Methacrylates	251
10.18.	RAFT Polymerisation of Alkyl Methacrylates and Acrylic Acid using 4-Vinylbenzyl-1-pyrrole Carbodithioate to form HB Random P(nMA- <i>co</i> -AA) Copolymers	252
10.19.	Removal of RAFT End Groups using Polymer-Supported Borohydride Reducing Agent	253
10.20.	Preparation of Copolymer Dispersions	254
10.20.1.	Preparation of Copolymer Dispersions at a Range of pH	254
10.21.	Annealing of Copolymer Dispersions	254
10.22.	Encapsulation and Release of Rhodamine B	254
10.23.	Equipment and Instrumentation	255
10.23.1.	Freeze-Pump-Thaw Polymerisation	255
10.23.2.	¹ H and ¹³ C NMR	255
10.23.3.	Elemental Analysis	255
10.23.4.	Mass Spectrometry	255
10.23.5.	Gel Permeation Chromatography	255
10.23.6.	Particle Sizing Analysis	256
10.23.7.	Zeta Potential Measurements	256
10.23.8.	Transmission Electron Microscopy	256
10.23.9.	Scanning Electron Microscopy	257

10.23.10.	Small Angle Neutron Scattering	257
10.23.11.	UV-Vis Spectrometry	257
10.23.12.	Atomic Force Microscopy	257
10.23.13.	Contact Angle Measurements	258
10.23.14.	ATR-FTIR	258
10.23.15.	Density Measurements	258
10.23.16.	Viscometry	258
10.23.17.	Printing Studies	258
References		261
Appendix 1: Analysis of Variance (ANOVA)		271
Appendix 2: Parameters Obtained from Model Fitting to SANS Data		275
Appendix 3: Model Fitting to SANS Data		283

1. Introduction

1.1 Introduction to Polymer Architecture and Synthesis

1.1.1 Polymer Architectures

The simplest polymers are linear chains formed from a great number of monomer units, which can be either homopolymers, meaning that only one type of monomer is used, or copolymers consisting of two different monomers. Copolymers can be categorised as statistical, alternating, block or graft depending on the distribution of the monomers within the polymer chain, as shown in **Figure 1.1**.

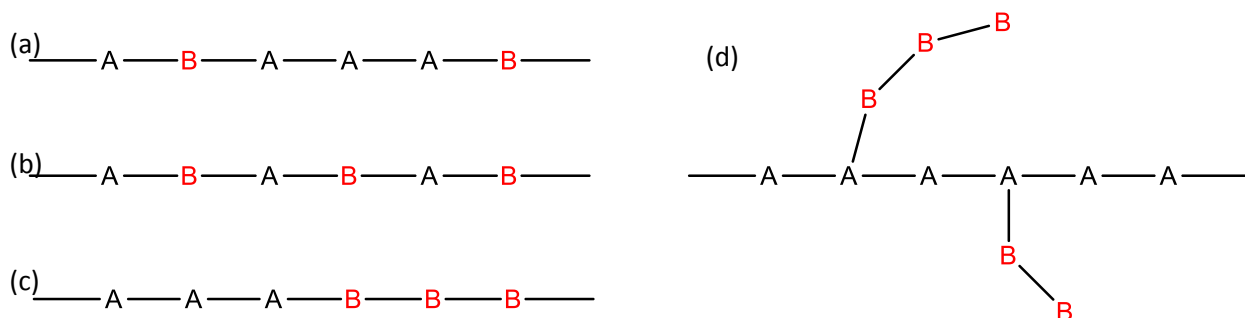


Figure 1.1 Possible copolymer architectures: (a) statistical (b) alternating (c) block (d) graft

More complex polymer structures can be produced with branched or crosslinked chains, enabling the formation of more elaborate polymer architectures such as stars¹, dendrimers², combs³ and pom-poms.⁴

1.1.2 Branched Polymers

Branched polymers have become a focus of research in the field of polymer science, due to their interesting and versatile properties. This is not unexpected, considering that many natural macromolecular systems incorporate branched structures; such as amylopectin, which is one of the primary components of starch; and glycogen,

which is a multibranched polysaccharide that stores glucose in the human body. The structure of these biopolymers is shown in **Figure 1.2**. A wide variety of branched polymeric architectures are possible, some of which are shown in **Figure 1.3**. Each structure possesses different physical and biological properties and therefore they lend themselves to a diverse range of possible applications.

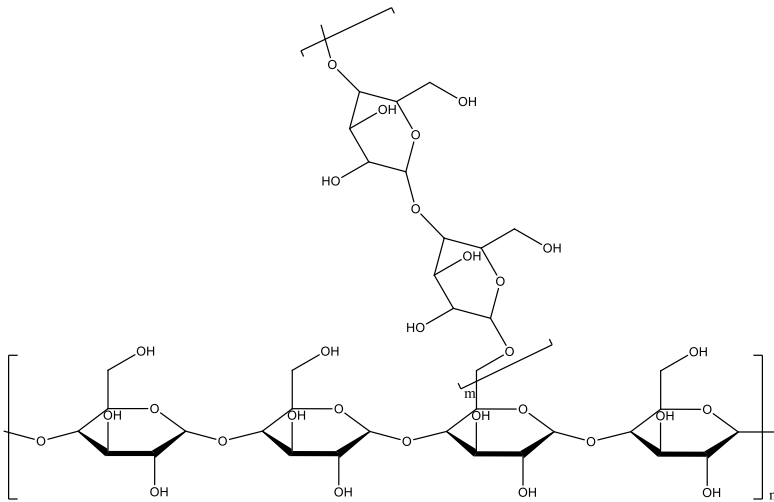


Figure 1.2 Representative chemical structure of biopolymers amylopectin and glycogen. Both polysaccharides are composed of the same glucose repeat units but glycogen contains more frequent branching.

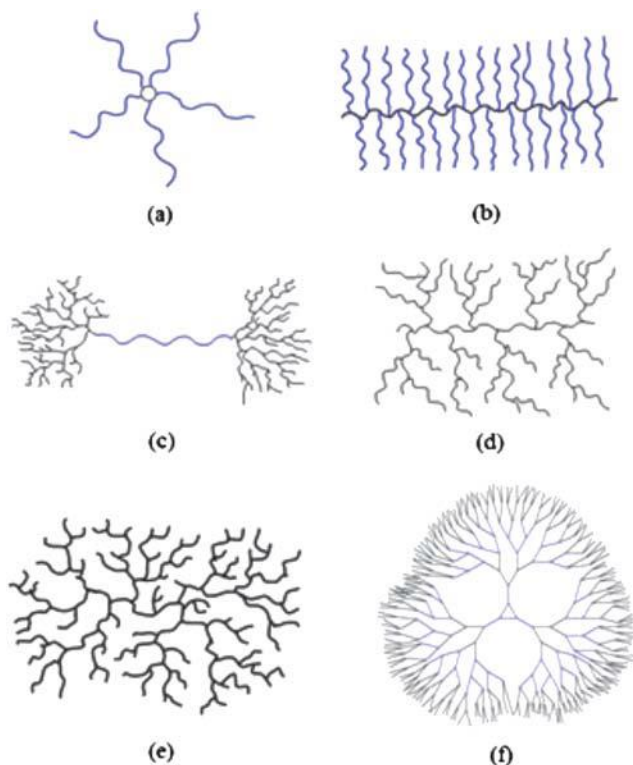


Figure 1.3 Examples of branched polymer architectures (a) star (b) brush (c) pom-pom (d) dendrigraft (e) highly/hyper-branched (f) dendrimer. Reprinted with permission from England et al.⁵

Dendrimers are considered to be the perfect branched architecture, due to their advantageous properties. They exist as single molecular species with a high degree of branching, conferring high degrees of symmetry to the molecule in addition to a large number of functional groups on the surface. They also have excellent solubility and very low solution viscosity. These factors make dendrimers ideal candidates for applications ranging from drug carriers⁶ to catalyst supports⁷. However dendrimers have one major drawback in that they are difficult to produce, requiring complex syntheses that involve many purification steps. These are costly and time-intensive processes which are hard to scale up. As a consequence, dendrimers are not suited to industrial use.

Highly branched (HB) polymers are therefore a more attractive alternative since they are far easier to synthesise and possess many of the properties which make dendrimers so desirable, as well as additional useful properties. In comparison to linear analogues, HB polymers have improved solubilities as well as tunable solution

behaviour and low solution and melt viscosities. They possess large numbers of functional end groups, which can potentially be further modified to suit specific applications. For example HB-poly(*N*-isopropyl acrylamide) (PNIPAM) with glycine-arginine-glycine-aspartic acid-serine (GRGDS) peptide end groups has been used to develop a useful process in cell biology for lifting and releasing cells from their culture substrate, making use of the property that GRGDS groups bind to cell surfaces⁸. There are drawbacks to HB materials, however, including irregular branching and uneven statistical functional group distribution throughout the macromolecule⁹. HB polymers also tend to have broad molecular weight distributions. Disperse branched polymers can be difficult to analyse, sometimes requiring time-consuming fractionation steps in order to obtain full characterisation. Despite these issues, HB macromolecules are still an area of much current research.

1.1.3 Graft Polymers

According to the IUPAC definition¹⁰, graft polymers consist of macromolecules in which one of several blocks (grafts) are attached to the main polymer chain (backbone) as side chains. In the case of graft copolymers, the backbone and grafts are formed from different monomers. These graft polymers possess interesting properties compared to their linear counterparts of similar molecular weight¹¹, which can be used to tune the polymers for specific applications. These properties include wormlike morphologies, compact molecular dimensions and notable chain end effects as a result of their confined and compact structures.¹²⁻¹⁵

One feature of wormlike graft copolymers is that when they are spread on particular surfaces, the repulsion of the adsorbed side chains not only extends the backbone of the polymer, but in addition can induce spontaneous scission of backbones of graft copolymers.¹⁶ This possibility must be considered when designing surface-targeted macromolecules. However, it can also be exploited to target specific weaker bonds in the copolymer structure, for example, by including disulfides which could be selectively broken while other bonds remain intact.^{16, 17}

In addition to one-dimensional graft copolymers which are formed by tethering two different polymer chains together via a stable linkage, grafting to the surface of a planar, spherical or cylindrical solid is possible, forming two-dimensional or three-

dimensional graft copolymers, respectively. The study of the properties and preparation of these surface-grafted polymers is a particular focus for current research.¹⁸

Another important area of research is the design and preparation of graft copolymers possessing desired functional groups, lengths of backbone and side chains, grafting densities and chemical compositions. This is due to the need for special molecular structures to suit specific applications in wide-ranging fields, from biomedical applications to nanoscience.^{19, 20} Recent advances in controlled radical polymerisation (CRP) have enabled the synthesis of well-defined polymers and copolymers in a variety of branched and graft architectures. These will be discussed in the following section.

1.1.4 Methods of Polymer Synthesis

There are many different methods of polymerisation which can be used to create specific polymer architectures. These methods can be divided into two groups, step-growth polymerisation or chain polymerisation, depending on the mechanism of polymerisation. In step-growth polymerisation, polymers are formed from monomers containing functional groups such $-\text{OH}$, $-\text{COOH}$ and $-\text{COCl}$.²¹ This generally involves a series of condensation reactions, sometimes resulting in the elimination of small molecules such as H_2O or HCl .

Chain polymerisation, also known as addition polymerisation, is used to polymerise monomers containing vinyl groups. This occurs via the activation of a double bond by either an ionic or free-radical initiator to produce a kinetic chain, which grows through repeated monomer addition to the growing chain until it undergoes a termination reaction. The examples of this polymerisation mechanism are ionic polymerisation, including both cationic and anionic, and free radical polymerisation.

Ionic polymerisation encompasses both cationic and anionic techniques, where polymerisation proceeds via a kinetic chain mechanism.²² In this method the formation and stabilisation of a carbonium ion or carbanion, for cationic and anionic polymerisations respectively, depend on the nature of the group R in the vinyl monomer $\text{CH}_2=\text{CHR}$.²⁴ For this reason, only a limited range of monomers can be polymerised by ionic techniques due to electronic requirements: for successful cationic polymerisation,

electron-donating groups are necessary to stabilise the delocalisation of positive charge in the π -orbitals of the double bond, whereas anionic polymerisation requires electron-withdrawing substituents. Other drawbacks are the requirement for stringent reaction conditions often requiring high catalyst concentrations, rigorously dry solvents and low temperatures,²⁵ in addition to rapid reaction rates and a tendency to attain poor reproducibility. Consequently, ionic polymerisation is unsuited to use in industry where stringent reaction conditions are inconvenient for large-scale use.

The most common method of polymerisation is free radical, which can be performed under milder reaction conditions than ionic polymerisation using a much wider range of monomers, including those with functionality.²³ Radical polymerisation has been described as ‘the most versatile and scalable chain growth polymerisation available for the synthesis of functional polymers’.²⁴ The main disadvantage of this technique is that it provides poor control over polymer properties such as molecular weight and dispersity. In recent years, living radical polymerisation techniques, also known as controlled radical polymerisation, have been developed. These methods offer much greater control over the properties of the polymer produced.

1.1.4.1 Controlled Radical Polymerisation

Living polymerisation was initially limited to anionic polymerisation and was so-called because the living anionic systems experience no termination reactions except those caused by impurities in the system.²⁴ In living radical polymerisation or controlled radical polymerisation (CRP) as it will be henceforth referred to, the reaction systems still undergo bimolecular termination reactions but the rate of termination is suppressed relative to the rate of propagation of radical chains. This causes the formation of a rapid dynamic equilibrium between radical growing chains and dormant species where the radical has been capped. This reduces the overall concentration of the propagating radical chain ends and therefore minimises termination reactions such as combination and disproportionation. Consequently chain growth occurs in a living-like fashion and a high degree of control is possible, yielding well-defined polymers.²⁶

There are three principal mechanisms of CRP, which are nitroxide-mediated polymerisation (NMP), atom transfer radical polymerisation (ATRP) and reversible addition-fragmentation chain transfer polymerisation (RAFT).

1.1.4.1.1 Nitroxide-Mediated Polymerisation

The first of the CRP techniques to be developed was NMP, which was first described by Rizzardo et al.²⁷ The mechanism of NMP proceeds with reversible termination by coupling. The polymer radical is capped with a nitroxide, such as 2,2,6,6-tetramethylpiperidiny-1-oxy (TEMPO), which combines with carbon-centred radicals to form stable alkoxyamines.

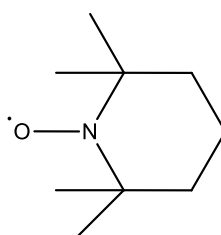


Figure 1.4 - 2,2,6,6-tetramethylpiperidiny-1-oxy (TEMPO)

NMP has been successfully used to polymerise a range of monomers including acrylates²⁸, methacrylates²⁹, styrenes³⁰ and vinyl acetate.³¹ Other alkoxyamine structures have been developed, such as phosphonate³² and arene³³ nitroxides, which are more versatile than TEMPO and can be used in the polymerisation of acrylates, acrylamides and acrylonitrile monomers. These give much improved control and at low molecular weights can give dispersities as low as 1.05.³⁴ However, there are also disadvantages to NMP. Relatively few of the nitroxide or alkoxyamine initiators are commercially available and the reactions require high temperatures compared to other CRP techniques. Rates of reaction are generally very slow and therefore long reaction times are necessary to reach high conversions, often accompanied by a loss of control over the polymerisation.

1.1.4.1.2 Atom Transfer Radical Polymerisation

ATRP was developed in 1995 by Sawamoto and co-workers³⁵, and also separately by Wang and Matyjaszewski.³⁶ It involves an alkyl halide initiator and a transition metal catalyst. Chain growth is controlled by the transfer of terminal halogen atoms from the chain ends of the polymer to the metal complex. This rapid reversible capping leads to suppression of the instantaneous concentration of propagating polymer radicals, thereby minimising termination and providing good control over the molecular weight distribution of the polymer.³⁷ Typically copper (I) halide is used, together with a nitrogen-based complexing ligand such as 4,4' di-tert butyl bipy.³⁸ ATRP is a versatile technique which can be carried out in bulk or in various solvents. ATRP is very tolerant of protic solvents, and polymerisations have been successfully conducted in alcohols and even water.³⁹ It has a high tolerance for functional groups on both monomer and initiator, such as allyl, amino, epoxy, hydroxy and vinyl groups.²⁴ An example of the successful use of ATRP is the synthesis of low dispersity linear poly(2-hydroxypropyl methacrylate), which can be obtained in very high yield with a short reaction time.⁴⁰ The primary disadvantage of ATRP is that a relatively large amount of metal from the catalyst (0.1-1% of the reaction mixture) needs to be removed from the final polymer product.⁴¹

1.1.4.1.3 Reversible Addition-Fragmentation Chain Transfer Polymerisation

The RAFT process was developed by Rizzardo and co-workers in 1998.⁴² RAFT polymerisation differs from the other variations of CRP in that the chain growth is controlled by reversible chain transfer rather than chain capping. This is made possible due to the use of a chain transfer agent (CTA), which is typically a dithioester-based compound with the general structure as shown in **Figure 1.5**.

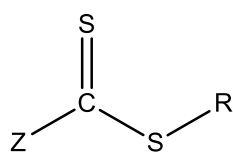
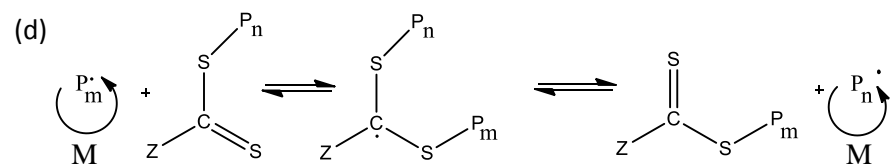
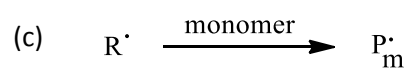
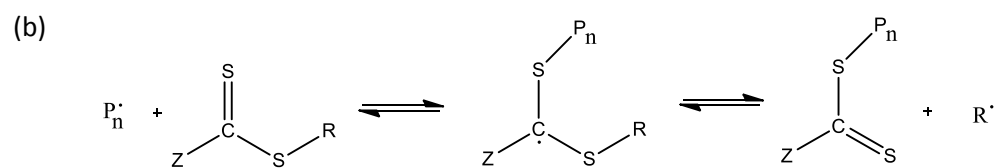
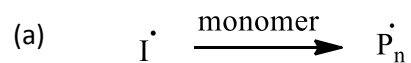


Figure 1.5 – General structure of a dithioester chain transfer agent

The mechanism for RAFT polymerisation is shown in **Scheme 1.1** below. The polymerisation is initiated using a conventional free radical initiator, generally a peroxide such as benzyl peroxide (BPO) or an azo compound like azobisisobutyronitrile (AIBN). This initiator decomposes, as in conventional free radical polymerisation, to give two radical species I^\bullet which then go on to react with monomer, forming polymer radicals, P_n^\bullet . These propagating radicals react with the CTA to form a radical adduct which then fragments to produce a dormant chain capped by the dithioester group and another species, R^\bullet . This radical species is capable of initiating further polymerisation, which occurs in the reinitiation step producing another propagating radical polymer chain, P_m^\bullet . This results in the formation of the chain-end transfer equilibrium, which is an equilibrium between the dormant polymer chains and propagating radicals. It is this equilibrium which confers the pseudo-living character of the polymerisation since there is only a small concentration of propagating species present at any time so the possibility of bimolecular termination reactions occurring is reduced. This is illustrated in a schematic diagram in **Figure 1.6**. The equilibrium also controls the chain length of the polymer produced. On average each chain grows simultaneously as the equilibrium between dormant and propagating chains is so rapid compared to the rate of propagation.⁴³ This results in the formation of polymer chains with equal lengths, hence near-monodisperse polymer can be prepared.



Scheme 1.1. The mechanism of RAFT polymerisation: (a) initiation (b) addition-fragmentation (c) reinitiation (d) chain-end transfer equilibrium

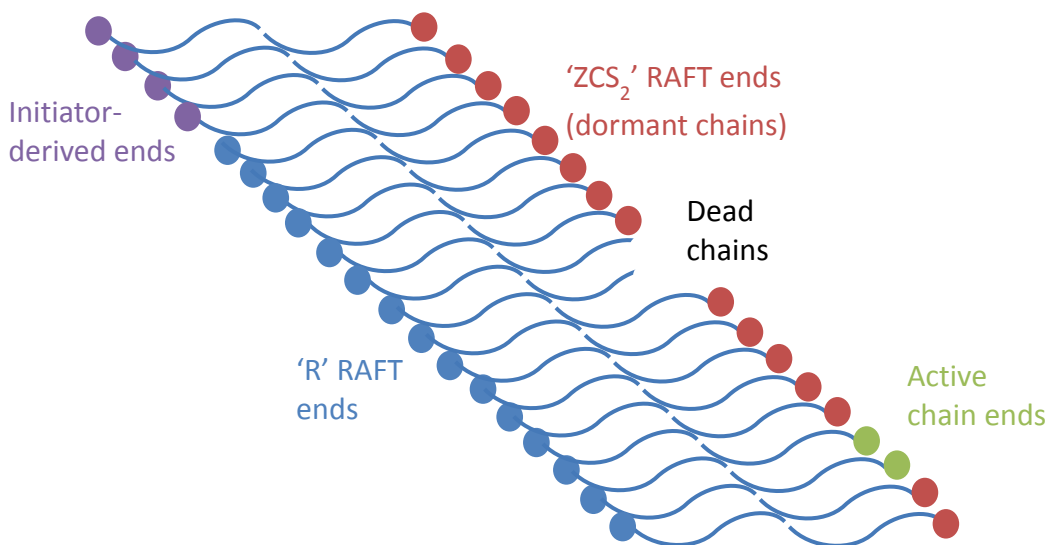


Figure 1.6. Schematic diagram of RAFT polymerisation showing the fraction of polymer chains having each different end group derived from either initiator or CTA. Redrawn from Thang et al.⁴³

The fraction of polymer molecules with dithioester end groups is increased in comparison to the fraction of chains terminated by normal bimolecular termination by maximising the amount of chain transfer. This requires the use of CTAs with high chain transfer constants, and using these in high concentrations relative to the amount of initiator present. Under these conditions, RAFT polymerisation proceeds with narrow molecular weight distributions, usually with a dispersity (\mathcal{D}) of less than 1.2 and sometimes below 1.1. Kinetic modelling experiments have shown that the effective transfer constant must be greater than 100 in order to achieve a dispersity of 1.1 at low conversion.⁴⁴ Higher molecular weight polymers or block copolymers can be produced by further monomer addition.

The choice of groups Z and R in the CTA is important to the success of the RAFT process. To ensure the CTA has a high transfer constant, Z needs to be a substituent which activates the C=S bond towards radical addition. It also needs to stabilise the intermediate radical adduct formed by addition of the propagating radical. Common Z substituents are alkyl or aryl groups. R needs to be a good homolytic leaving group compared to the polymer chain P_n^\bullet ,⁴⁵ which will form a stable radical R^\bullet

capable of reinitiating polymerisation. The optimum choice of CTA depends on the class of monomer which is being polymerised. For example, benzyl dithiobenzoate is useful for the polymerisation of acrylates⁴⁶ whereas tertiary cyanoalkyl trithiocarbonates are suited to methacrylate and styrenic monomers.⁴³ Additionally the CTA can be designed to contain a specific chemical functionality, which will be located on the terminal chain ends of the polymer following polymerisation, enabling the simple introduction of functionality into a polymer.

Another family of CTAs is the xanthates, which have the general structure as shown in **Figure 1.7**. The process which employs these reagents is known as macromolecular design via the interchange of xanthates⁴⁷, or MADIX. Xanthates have much lower chain transfer constants than the dithioester-based reagents, 0.6-3.5 compared to values as high as 6000, and tend to produce polymers with broader molecular weight distributions. However, there are advantages to their use in that xanthates are easier to produce and can be used for the polymerisation of monomers such as vinyl acetate which are inhibited by dithiobenzoate CTAs.^{48, 49}

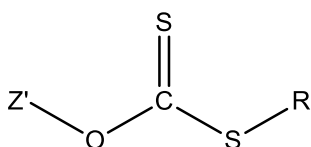


Figure 1.7 – General structure of a xanthate

RAFT is an extremely versatile technique and can be performed in a wide variety of reaction conditions, including bulk,⁵⁰ both organic and aqueous solutions,⁵¹ and suspension.⁵² It is compatible with an extensive range of monomers including those with functionality, and is also tolerant of functionality in the CTA and the initiator. This allows the synthesis of polymers with pendant chain or end group functionality without any need for deprotection. The main disadvantage of RAFT polymerisation is that few RAFT agents are commercially available, so it is necessary to synthesise them. This can sometimes require complicated synthetic and purification procedures.

1.1.4.2 Branched Copolymer Synthesis

In 1952 Flory reported the synthesis of hyperbranched polymers from the condensation of monomers with the structures AB_2 or AB_n , where A and B are different functional groups and condensation is restricted to only reactions between these two groups.⁵³ This led to the creation of unique branched structures which avoid gelation. Until this point, hyperbranched polymers were only formed as part of crosslinked networks, and the formation of intermolecular branching during polymerisations was considered an unwanted side-reaction. However the first synthesis of a hyperbranched structure was not published until the work of Kim and Webster in 1988.⁵⁴ This covered the synthesis of hyperbranched polyphenylenes from polycondensation of AB_2 monomers, and initiated the recognition of the useful properties of branched polymers.

Most examples of hyperbranched polymers are synthesised by step-growth polymerisation through the polycondensation of AB_n -type monomers. For example an AB_2 monomer produces branching units every time both B groups on one monomer react with A groups on other monomers. Other monomers have been used with B functionalities up to AB_8 .⁵⁵ It was found that the degree of branching (DB) increased with increasing functionality, from 32% for AB_2 to 84% for AB_8 monomers. However examples of hyperbranched polymers with a DB of 100% are limited and involve complicated reaction conditions and expensive catalysts in the production of polymers which have high dispersities, low molecular weights and are often symmetrically imperfect.^{56, 57} The synthesis of branched polymers by step-growth polymerisation is subject to a lack of control over the polymer size and structure, leading to particularly broad molecular weight distributions.

Self condensing vinyl polymerisation (SCVP) is a method of producing branched polymers that yields better control over both branching and molecular weight distribution. SCVP was first reported by Fréchet et al. in 1995.⁵⁸ It employs a monomer with the general structure $A=B-C^*$, where C^* is a group capable of initiating the polymerisation of the vinyl group $A=B$. The activated group C^* could be a radical, anion, cation or carbanion. The process is initiated by the addition of a C^* group to the vinyl group of another monomer, creating a dimer having one $A=B$ vinyl group and two active sites, B^* and C^* .⁵⁹ Subsequently both B^* and C^* can react with the vinyl groups of other monomers in the same manner to create a branched structure. The method has

been applied in conjunction with radical polymerisation, in particular CRP methods to allow control over molecular weight and minimisation of gelation.

SCVP has been applied successfully to branched polymer synthesis using both NMP⁶⁰ and ATRP,⁶¹ but here the focus will be on the use of SCVP in RAFT polymerisations. The first work on RAFT SCVP covered the synthesis of branched polymers via the incorporation of a polymerisable dithioester CTA into the polymerisation of styrene.⁶² However, this led to the creation of a weak link in the polymer as the reactive dithioester group was incorporated into the main chain. The method was later adapted using different branching CTAs which placed the dithioester groups at the chain ends instead, where the chain strength is not affected.⁶³ This approach was used to synthesise one of the first examples of a HB block copolymer, HB poly(*N*-isopropyl acrylamide-*block*-glycerol monomethacrylate).⁶⁴

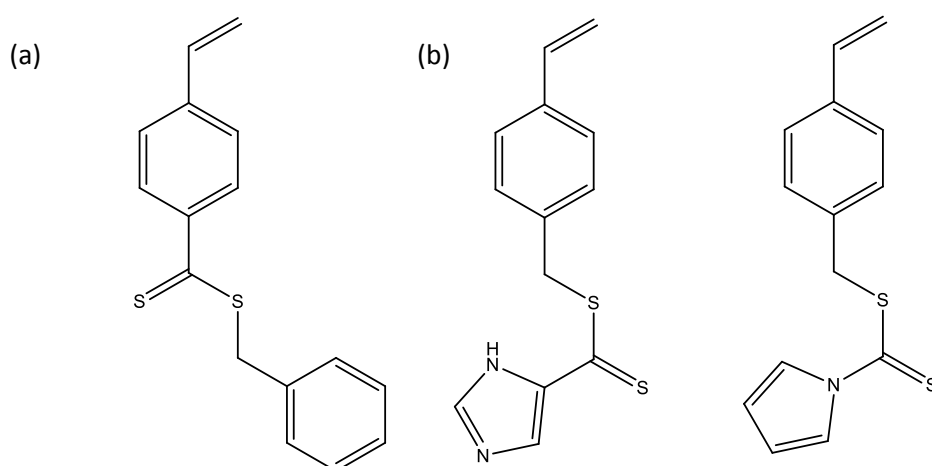


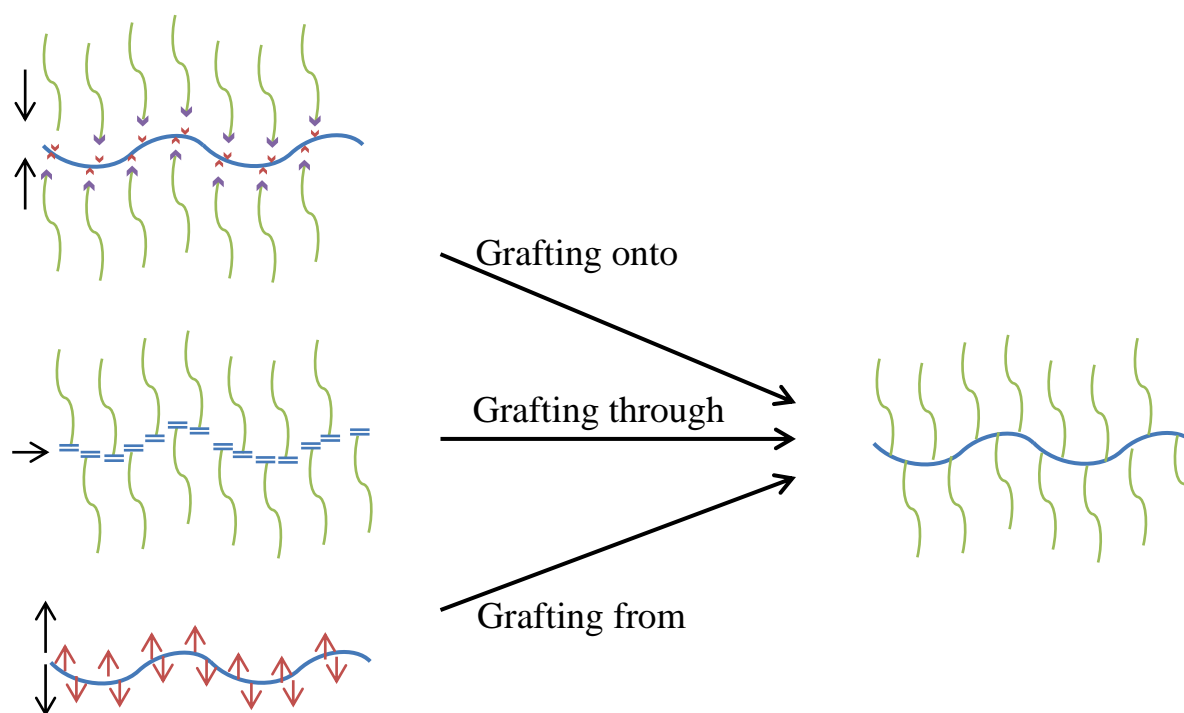
Figure 1.8 (a) The RAFT branching monomer designed by Yang et al.⁴⁰ and (b) those developed by Carter et al.⁴¹ which place the dithioester group at the chain ends

An important feature of RAFT polymerisation, as mentioned previously, is that the dithioester groups originating from the CTA are retained in the polymer structure, enabling the synthesis of block copolymers and more complex architectures. This is

clearly even more significant for a HB polymer as they contain many more end groups within the molecule. This can be exploited to great advantage as an opportunity to add useful functionality to a polymer. This can be achieved by either using a CTA containing the desired functional groups, which will become end groups in the polymer structure, or by post-polymerisation modification of the dithioester chain ends to achieve the target functionality.⁶⁵ The first approach has been used to synthesise HB polymers with imidazole groups at the chain ends, which have been applied in protein purification⁶⁶ and have potential application in drug delivery.⁶⁷ The post-modification approach has been used to convert the dithioester end groups of a HB PNIPAM polymer to carboxylic acid ends through reaction with an excess of 4,4'-azobis (4-cyanovaleric acid) (ACVA) initiator, allowing the subsequent attachment of a charged peptide sequence, RGD (arginine-glycine-aspartic acid).⁸ This enabled the formation of stable sub-micron stimuli-responsive particles above the lower critical solution temperature due to the additional stability afforded by the polar chain ends.

1.1.4.3 Graft Copolymer Synthesis

There are three different strategies which can be employed to synthesise graft copolymers, defined as grafting-from, grafting-onto and grafting-through. **Scheme 1.2** gives a pictorial representation of these approaches.



Scheme 1.2. The three strategies for the synthesis of graft copolymers, redrawn from Huang et al.¹¹

1.1.4.3.1 Grafting-Onto

The grafting-onto approach involves attaching certain side chains onto a linear backbone via a coupling reaction. The backbone and side chains are prepared independently so they can be synthesised by whichever method of polymerisation is most appropriate for each one, and the chain lengths can be easily modified. However, the method of coupling does need to be very efficient and any unreacted side chains need to be removed in order to achieve high grafting densities and narrow molecular weight distributions. A successful example of this technique is the Cu(I)-catalysed 1,3-dipolar cycloaddition reaction of an azide with an alkyne, known as a ‘click reaction’, which proceeds with high reaction efficiency, mild reaction conditions, good functional group tolerance and few byproducts.⁶⁸ Matyjaszewski et al reported the synthesis of PHEMA-g-PEO molecular brushes using a combination of ATRP and click reactions, where the azide-terminated PEO side chains were coupled to the PHEMA-alkyne backbone by the click reaction.⁶⁹

1.1.4.3.2 Grafting-Through

Another way to synthesise graft copolymers is to polymerise macromonomers which have a polymerisable end group. This approach allows control of the grafting density and the length of side chains by adjusting the degree of polymerisation of the side chains and the backbone. Many graft copolymers have been prepared by this method using a combination of polymerisation techniques such as ring opening polymerisation (ROP)⁷⁰, ring opening metathesis polymerisation (ROMP)⁷¹, CRP⁷² and living anionic polymerisation.⁷³

Theoretically, graft copolymers with 100% grafting density could be prepared using the grafting-through strategy, meaning that every repeating unit contained one side chain. However, in controlled radical polymerisations it is difficult to completely eliminate side reactions, particularly at high conversions. Moreover, the complete conversion of macromonomers is difficult, due to issues with low reactivity in addition to steric hindrance between the functionalised chain end of the macromonomer and the reactive site of the propagating graft copolymer.¹¹ The separation of unreacted macromonomers is also not simple.

1.1.4.3.3 Grafting-From

This strategy involves the formation of side chains from a macromonomer containing an initiation group, also called a macroinitiator, which can be obtained either directly from the initiation group-containing monomer or through the introduction of initiating functional groups to a precursor. This is a particularly attractive strategy for the synthesis of well-defined graft copolymers when using CRP, since the low concentration of instantaneous propagating species limits the coupling and termination reactions and the gradual growth of the side chains means that the steric effect is reduced.¹¹ For the grafting-onto and grafting-through strategies this is inevitable. Additionally the grafting-from approach avoids the need to remove unreacted macroinitiator, which complicates the other techniques. Graft copolymers have been formed using this strategy employing ATRP⁷⁴, NMP-ATRP⁷⁵ and RAFT-ATRP⁷⁶, among other techniques.

1.2 Introduction to Inkjet Printing

1.2.1 Types of Printing

Printing is defined as ‘the process of transferring ink onto a substrate via a printing plate’.⁷⁷ Many different printing technologies have been developed over the years. The so-called ‘conventional printing’ technologies can be divided into four main categories depending on the type of image carrier used: letterpress, gravure, lithography and screen printing. **Figure 1.9** shows a schematic diagram of the image carrier in each of these cases.

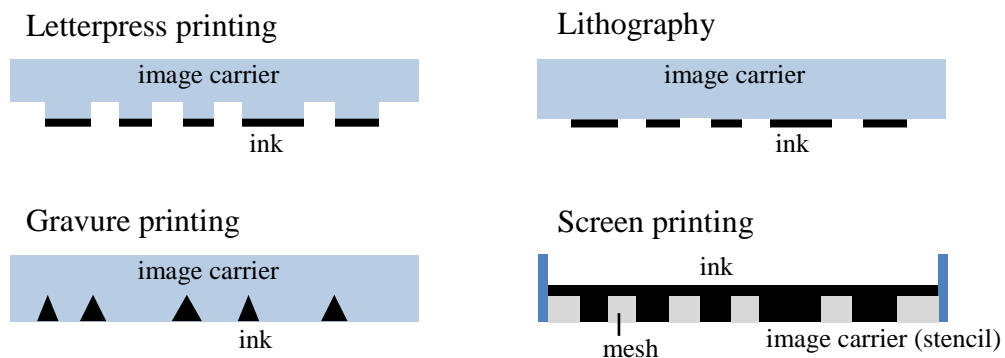


Figure 1.9. The principles of the main ‘conventional printing’ technologies. Redrawn from Kipphan.⁷⁷

In letterpress printing, also known as relief printing, the printing elements such as lines, dots and letters are raised on the printing plate. This means that ink adheres to the printing elements when the printing plate is inked and is then transferred to the substrate under pressure. The main examples of this technology are letterpress, which was the primary printing technology until a few decades ago, and flexography, which is widely used in the printing of packaging. Traditional letterpress printing uses a hard printing plate, usually made of lead, whereas in flexography a soft, flexible rubber or plastic plate is used.

In lithography, however, the printing and non-printing elements are planographic, i.e. at the same level, but are composed of different materials with correspondingly different chemical and physical surface properties. Wetting is firstly

carried out to render the non-printing elements ink-repellent, so that when the plate is inked the ink is only taken up by the printing areas. Offset printing is the primary example of lithography, and is an indirect printing technology where the ink is transferred first to an intermediate carrier and consequently from there to the substrate.

Gravure printing involves the use of recessed printing elements on the printing plate. The surface of the gravure cylinder is 'flooded' with low viscosity ink and subsequently passed under a doctor blade which removes the excess ink and leaves only ink remaining in the recesses. The printing substrate is then pressed against the gravure cylinder and takes up the ink from the recesses. The main examples of this technology are rotogravure printing, as well as copperplate stamping and die-stamping.

Finally in the fourth technology, screen printing, the printing plate is composed of a fine mesh. The non-printing elements of the mesh are blocked by a coating known as the 'stencil'. Similarly to gravure printing, the screen plate is covered with ink over which a blade is passed over. The pressure of the blade causes the ink to be pushed through the screen onto the substrate below.

The conventional printing technologies all possess a common feature which is that the image carriers have a physically stable structure. This means that they are not variable but rather are used to reproduce the same image many times. An alternative type of printing technology is known as 'non-impact printing technology' or NIP technology where either a new printing plate is imaged for each print, as in electrophotography, or the ink is directly transferred onto the substrate without the need for a carrier, as in inkjet printing. This allows the printing of subsequent pages with different content.

1.2.2 Inkjet Printing

Inkjet printing encompasses a range of technologies which all involve the jetting of ink droplets from a small aperture on a printhead to a specific position on the substrate to create an image. The basis of modern inkjet printing, discovered by Felix Savart in 1833, is that a laminar flow jet can be broken up into a train of droplets by acoustic energy.⁷⁸ The break-up of a liquid jet stream occurs because the surface energy of a liquid sphere is smaller than that of a cylinder but has the same volume.⁷⁹

Inkjet printing enables the delivery and precise positioning of small volumes of liquid at high rates of repetition under digital control.⁸⁰ There are two key advantages to inkjet printing technologies, which are the noncontact method of deposition and the precise control over both the amount and position of the deposited material. Of the range of inkjet technologies there are two primary groups: drop on demand (DOD) and continuous inkjet (CIJ).^{81, 82} These inkjet printers produce ink droplets with sizes in the range 10-150 μm and picolitre drop volumes. **Figure 1.10** shows the division of inkjet printing technologies into these two groups followed by further classification into sub-groups.

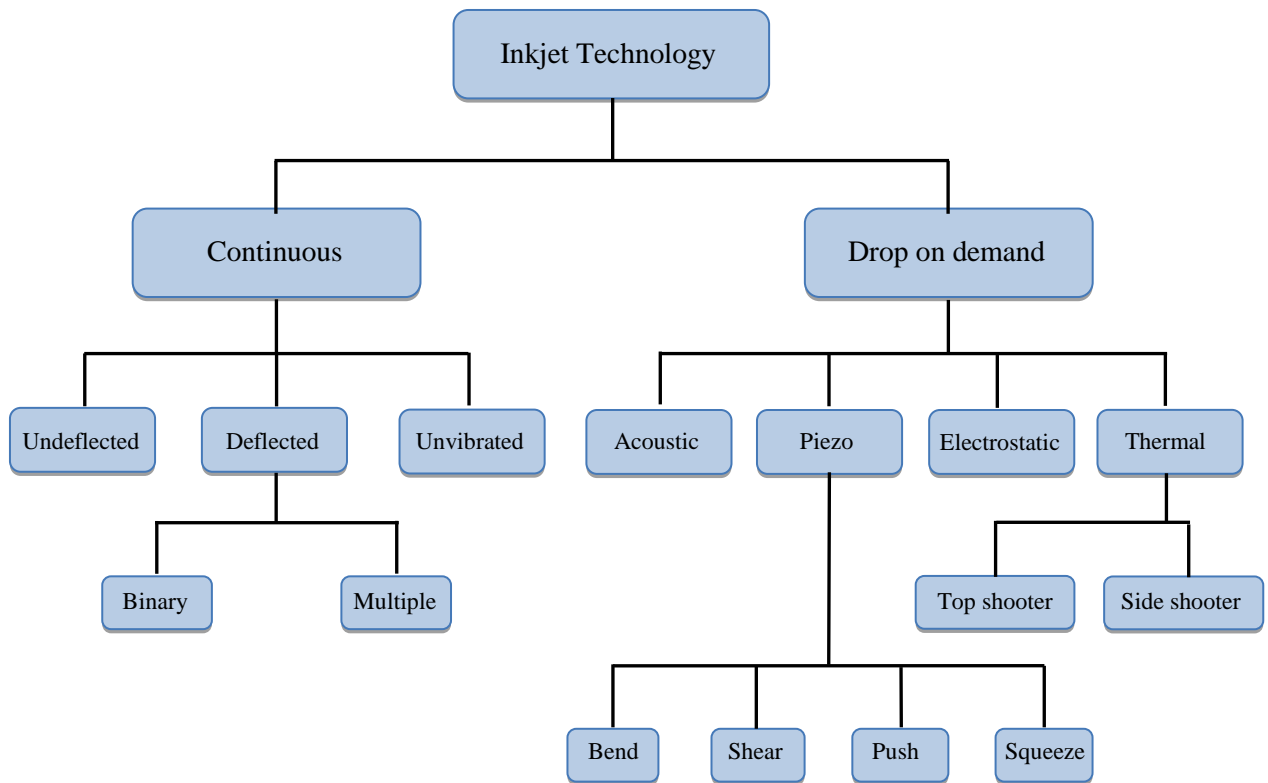


Figure 1.10. Classification of inkjet printing technologies, adapted from Goedde and Yuen.⁷⁹

1.2.2.1 Continuous Inkjet

Continuous inkjet printing produces droplets through the use of an electric charge which is applied selectively to the drops of ink, whose size and spacing is controlled through the application of a pressure wave pattern to the aperture.⁸³ The

charged drops are deflected into a gutter and then recirculated back into the ink reservoir, whilst the uncharged drops travel onto the media to create the image.⁸¹ This process is illustrated in **Figure 1.11** below. The droplet separation is determined by both the frequency of modulation and the speed of the jet. CIJ generally produces droplets of 80-100 μm diameter with speeds of 20 ms^{-1} and printing frequencies of over 250 kHz. CIJ is mostly used in coding and marking applications. The major issue with this type of printing is that it can be unreliable due to concerns such as nozzle clogging and issues with the ink recirculation system.

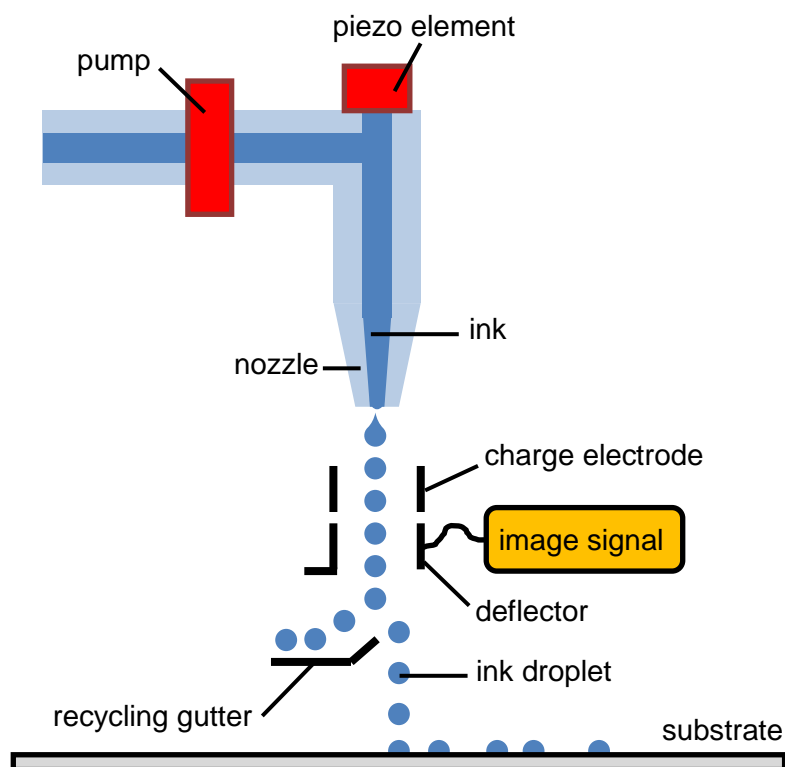


Figure 1.11. Schematic diagram of CIJ printing system, redrawn from DP3 Project website.⁸⁴

1.2.2.2 Drop on Demand

In drop on demand printing, ink droplets are produced in response to a digital waveform. The ejection of ink droplets occurs only when they are required to create the image on the media. When a voltage pulse is applied, mechanical motion of the piezoelectric ceramic creates a pressure wave which ejects ink droplets. A schematic diagram of DOD printing is shown in **Figure 1.12**. There are four different modes for

the generation of droplets using a piezoelectric device, as seen in **Figure 1.10**. These are the squeeze method, which uses a hollow tube of piezoelectric material to squeeze the ink chamber when a voltage is applied; the bend mode, which ejects droplets through the bending of a wall of the ink chamber; the push mode, in which a piezoelectric element is used to push against an ink chamber wall and eject drops; and also the shear mode, where the electric field is perpendicular to the piezo-ceramic polarisation.⁸⁵

A development of DOD printing is the bubble jet or thermal inkjet (TIJ) printer. In this system ink droplets are ejected from the nozzle by the growth and subsequent collapse of a water vapour bubble, which is located above a thermal transducer near the nozzle.⁸⁶ This heats the ink above its boiling point causing a local expansion of the ink and therefore the formation of a droplet.

In DOD printing the printhead is integral with the cartridge and therefore is replaced every time the cartridge is empty. This solves certain reliability issues as the printhead does not have to sustain long term use. Typically, droplets of 15-55 μm diameter are produced with drop speeds of 3-15 ms^{-1} and printing frequencies of up to 100 kHz. DOD is mostly applied in graphics and text printing.

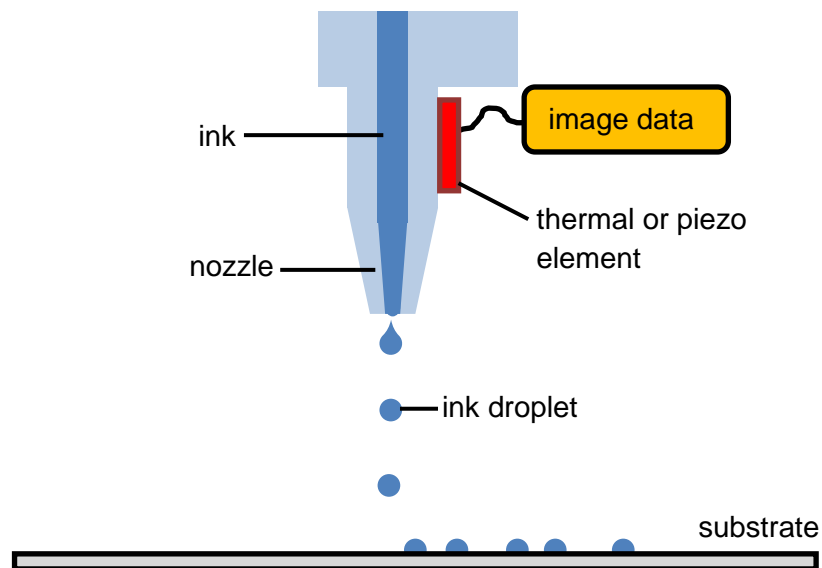


Figure 1.12. Schematic diagram of DOD printing system, redrawn from DP3 Project website.⁸⁴

1.2.3 Ink Formulations and the Use of Polymers in Inkjet Printing

Inkjet inks tend to have complex formulations. In order to appeal to customers, inks need to possess a combination of consistency and reliability, desired colour properties and good print image quality. In addition to conventional design requirements such as long shelf life and safety considerations, there are required physicochemical properties for each intended printing application. Inks need to have viscosities within the right range to provide appropriate flow properties; if the viscosity is too low the ink will leak through the print head, whereas if the viscosity is too high the ink may not flow from the print head. The maximum viscosity of an ink which can be used in inkjet printing restricts the achievable amount of solids possible in the formulation. Industrial print heads typically require ink viscosities of below 25 cP, depending on the inkjet technology used. The ideal viscosity range for piezoelectric actuation is between 8 and 15 cP whilst thermal print heads require inks with much lower viscosity, often below 3 cP. In order to meet these conditions, the achievable amount of solids in the ink is often below 10 percent.⁸⁷

Surface tension is another important parameter which governs the spread and penetration of ink drops on the substrate. Excessively high surface tension results in drops which are too small meaning they are unable to spread properly. Consequently, white gaps may be seen within the printed image. Conversely, if the surface tension is too low then drops may spread too far causing bleeding and over-banding. Additionally drops may become too large, adversely affecting print resolution, as a combination of viscosity and surface tension determines the ink drop size. Conductivity is also an important consideration for ink formulations, in addition to particle size, component solubility and colour intensity.

Inkjet ink is composed of a functional material and a liquid vehicle which is a carrier for this functional material.⁸⁸ This vehicle is composed of solvent; additives; and usually a binder which acts to bind the functional materials to the substrate after printing. Additives impart a specific function, for example surfactants, preservatives or photoinitiators. The selection of the various components of the vehicle depends on both the printing technology being used and the ultimate function of the printed pattern. The functional materials are generally either dyes, which are dissolved in the ink vehicle, or pigments, which are dispersed in the form of micro- or nanoparticles. The function of

both is to impart colour to the ink. In the case of pigment-based inks, a stabilising agent or dispersant is also required to improve colloidal stability and prevent aggregation of the pigment particles. To minimise the likelihood of nozzle blocking, the particle size needs to be significantly smaller than the diameter of the nozzle.⁸⁹

Polymers are a component of many printing ink formulations. Their use tends to be more common in inks developed for application in CIJ printers as these are predominantly formulated in organic solvents, whereas DOD printers generally use water-based inks. Polymers can be used in various ways within the field of printing. Polymers are commonly incorporated into ink formulations both to stabilise dispersions of particles and to control the behaviour of the ink drops once they reach the substrate.⁸⁰ Other examples of the use of polymers in printing are to act as dyes to impart colour to the ink or to enable UV curing of the ink.⁸¹ Additionally in some cases the polymers themselves compose the functional part of the fluid, for example in additive manufacturing where printing involves direct deposition of the final material. This project, however, will focus on the use of polymers as additives to improve the adhesion of ink onto the printing substrate.

It has long been known that the addition of long chain macromolecules can seriously affect the break-up of liquid jets which are generated by flow through a nozzle, even when present at low concentrations.⁹⁰⁻⁹² High extensional strains are experienced in these flows, which means that the presence of polymers can significantly delay the break-up of jets, particularly linear polymers which unfold in extensional flow. This can be a problem even when the polymers are present at concentrations below c^* , the critical overlap concentration.⁹³ Below this concentration, individual polymer coils rarely overlap, whilst above it the coils penetrate deeply into each other and the chains become entangled. At low concentrations, high molecular weight polymers are useful in preventing the formation of satellite drops, although this reduces jet speeds. However at higher concentrations the main ink drops fail to detach and can even be drawn back up towards the nozzle, meaning that there is a critical polymer concentration at which jetting completely fails for each drive stimulus.⁹⁴ There is therefore a need to understand the behaviour of polymers in inkjet printing.

1.2.4 Future Applications for Inkjet Printing

Inkjet printing was originally developed for use in graphical printing. However there are significant features of the technology which lend it to application in other areas. Inkjet printing has the potential to provide the foundations of a manufacturing process in which a functional fluid can be delivered in very precise quantities at a specific location within a defined working volume.⁸⁰ In graphics printing the functional fluid is an ink which delivers defined amounts of colour to certain locations on a two-dimensional substrate. It has now been demonstrated that inkjet printing technology can also be used to produce three-dimensional objects in an additive manufacturing process, with accurate control over printed features in three orthogonal directions.^{95, 96}

Additive manufacturing is attractive due to the lack of limits to the complexity and repeats of the pattern, the ability to rapidly change the inks, the fact that no mould is required and that only small capital investment is required. Also, significantly, since the process is additive rather than subtractive and also because materials are selectively deposited, less material is wasted, leading to greater sustainability and reduced costs. This technology has already been applied as a fabrication tool in various areas of technology, for example: displays,^{97, 98} plastic electronics,⁹⁹ microelectronics,¹⁰⁰ microelectromechanical systems (MEMS),¹⁰¹ microfluidics,¹⁰² and sensors.¹⁰³ It has been used in manufacturing applications such as rapid prototyping,¹⁰⁴ and the manufacture of ceramic components.¹⁰⁵ Inkjet printing also offers great potential in the life sciences fields including medicine,¹⁰⁶ regenerative medicine and tissue engineering,¹⁰⁷⁻¹⁰⁹ biology,¹¹⁰ and enzyme-based sensors.¹¹¹

1.2.5 Limitations and Challenges of Inkjet Printing

Inkjet printing faces competition from other technologies even in the more traditional field of graphic printing. Consequently the capabilities of inkjet printing need to be extended to meet the requirements already fulfilled by competing technologies. Some of the limiting factors affecting inkjet printing technology are ink performance, printing speed, reliability and problems with substrates.

In terms of ink performance, the main obstruction to the implementation of inkjet printing is the requirement for odour-free inks which are safe if ingested,

experience low migration of monomers and other components, and are able to withstand the processing, packaging and distribution process while still providing the necessary print quality. Many years were needed to develop such inks for conventional printing technologies, and the achievement of these conditions is harder within the constraints of inkjet ink formulations. For example the substrate speed is restricted for inkjet printing, in part due to the greater volume of ink required to reach the necessary colour density compared to traditional printing methods. Also, inkjet inks can lack some of the opacity and brilliance displayed by other technologies due to the limits on viscosity for inkjet printing inks, which in turn limit the solid content. The final functionality is governed by the pigment. Inkjet inks typically contain less than 10 per cent pigment compared to greater than 25 per cent pigment content for offset lithography inks. Inkjet inks need to achieve high solid loadings in order to improve coverage and therefore increase throughput. Overall the development of appropriate inks is the biggest challenge facing inkjet printing⁸⁰. An understanding of ink rheology and its effect on the formation of droplets has only recently developed far enough to allow accurate predictions about ink performance.⁸²

Despite several advantages that inkjet printing holds over conventional printing processes, namely its versatility and level of digital control leading to quicker turnaround times and ability to print long pattern repeats, the actual rate of ink delivery is in general slower than in conventional printing processes. For example the typical linear throughput of inkjet printing is 1 ms^{-1} compared with 5 ms^{-1} for offset lithography and 10 ms^{-1} for flexography. Inkjet printing is able to achieve excellent print quality but at the expense of print speed. To address this issue, inkjet printing needs to produce smaller drop sizes while managing to maintain the volume flow rate.

The major factor affecting the reliability of inkjet printing systems is the formation of small drops in addition to the main printing drops, known as satellite drops.¹¹² The ejected drop of ink emerges as a jet which is followed by a ligament or 'tail' which is still connected to the ink inside the nozzle. The ligament then parts, with some of the ink returning to the nozzle. The rest of the ligament either joins the drop or breaks up into smaller satellite drops, as shown in **Figure 1.13**.¹¹³

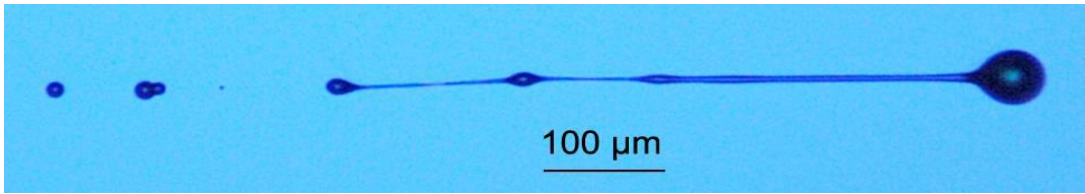


Figure 1.13. High-speed photograph of a jet in-flight after it has detached from the nozzle, showing the break-up of the ligament to form satellites. Reprinted with permission from Hutchings et al.¹¹³

Although all inkjet technologies are susceptible to satellite formation, DOD systems tend to form them more readily meaning that satellite avoidance is more problematic for these systems than for CIJ printers. In DOD printing the satellites tend to be small and lacking in momentum, meaning that they do not reach the substrate but instead are attracted to the nearest surface such as that of the nozzles. Nozzle contamination can affect the formation of the main drops leading to printing failures. Satellite avoidance can be achieved by the use of non-Newtonian inks and optimised drive waveforms.¹¹⁴ Satellite drops formed in CIJ printing possess a higher charge-to-mass ratio than the main drops as a result of the charging geometry; this can result in the satellites being attracted to the charging plates within the printheads causing contamination and ultimately printhead failure when the buildup prevents ink delivery to the substrate. Satellites can be avoided by attaining the right combination of frequency, viscosity, jet velocity and drive amplitude.¹¹⁵

Another factor which can adversely affect the implementation of inkjet printing is its suitability for certain substrates. The ‘printability’ of a substrate is governed by both the nature of the substrate and its surface condition. The nature of a substrate is characterised by its porosity, which determines the permeability and therefore printability of a substrate, and governs the capacity of a substrate to absorb inks. Uncoated papers are macro-porous whereas coated papers and cardboards are micro-porous and synthetic and non-absorbent substrates are either slightly micro-porous or completely non-porous.¹¹⁶ The surface condition of a substrate is defined by parameters including smoothness or roughness, cleanliness or the presence of impurities, and surface energy.¹¹⁷ Smoothness tends to be the dominating factor in the case of printing on paper and cardboard, while for synthetic substrates the surface energy dominates.

The transfer and spreading of an ink is dependent on the surface energy of the material delivering the ink, the surface tension of the ink itself and the surface energy of the substrate. In order to facilitate good printability, the substrate must have a higher surface energy than the ink, with attractive forces strong enough to promote good transfer and spreading, which itself enables good adhesion.¹¹⁸ Other factors affecting adhesion include the substrate composition and the structure of the substrate layer surface. Adhesion will be discussed in the next section.

As a consequence of this requirement, the adhesion of inks to low surface energy substrates such as polyolefins presents a problem for the printing industry, and creates an obstacle to the adoption of inkjet printing technology for applications such as packaging where polyolefinic substrates are commonplace. Possible solutions to this problem will be explored in the rest of this thesis.

1.2.6 Mechanisms of Adhesion

Adhesion results from the interatomic and intermolecular interaction at the interface of two surfaces.¹¹⁹ It is a topic which encompasses many scientific disciplines including surface chemistry, polymer chemistry, physics and rheology. In recent years the need for a better understanding of adhesion has increased as a result of the demands of industry. According to current literature, there are three main mechanisms of adhesion: mechanical coupling, molecular bonding and thermodynamic adhesion.¹²⁰ The mechanism of mechanical coupling is based on the adhesive 'keying' into the substrate surface¹²¹, so the adhesive and substrate are interlocked. There is some debate, however; on one side of the argument it is believed that greater adhesion is provided by mechanical interlocking whilst other researchers believe that surface roughening simply increases the surface area for more molecular bonding interactions.¹²²

Molecular bonding is the most widely accepted adhesion mechanism. It involves intermolecular forces between the substrate and the adhesive, comprising van der Waals forces, dipole-dipole interactions and chemical interactions, which include ionic, covalent and metallic bonding. This mechanism describes the strength of the adhesive interface by both interfacial forces and the presence of polar groups.¹²⁰ The major requirement for molecular bonding mechanisms is that there is intimate contact between

the two substrates; however this contact alone can be insufficient for good adhesion due to the presence of cracks, defects and air bubbles at the interface.¹²¹

The third proposed mechanism of adhesion between the liquid and surface is thermodynamic adsorption. Polymer surfaces, particularly those involving polar constituents, have a tendency to respond to the orientational forces of the medium to which the polymer is exposed. In this manner, in neutral environments such as air, the thermodynamics of the system attempt to minimise the surface free energy by orienting the non-polar substituents of the polymer into the surface region. However when in contact with polar substances such as water or polar organic solvents, thermodynamics requires that the interfacial tension between medium and polymer is minimised in order to obtain good adhesion.¹²³ The advantage of this mechanism over the others is that it does not require a molecular interaction to obtain good adhesion, but an equilibrium process at the interface.¹²⁰

1.2.7 Polymers for the Promotion of Adhesion

There are a variety of methods which have been developed to promote polymer adhesion, involving either modification of the surface itself (frequently polypropylene (PP) or polyethylene (PE)) or the use of an additive to promote the adhesion process.

1.2.7.1 Surface Modification

One frequently used technique is the chemical treatment of the surfaces which are undergoing adhesion, resulting in the creation of new functional groups at the interface of the two materials. Reagents such as oxidisers and acids have been used to treat polymer surfaces and have been shown to increase the polarity of the surfaces. This causes an increase in molecular forces between the materials and therefore increases the strength of adhesion. An example of this was reported by Van Calster et al. who introduced amine groups to the surface of dielectric epoxy resin surfaces in a two-step wet chemical process, leading to improved adhesion with electrochemically deposited metals, for application in electrical circuit fabrication.¹²⁴ Solvents can also be used to chemically treat the surfaces, as they can cause molecular changes at an interface which strengthen adhesion. For example, Chen et al. have used X-ray

photoelectron spectroscopy (XPS) and wetting angle measurements to show that rearrangements occur at the surface of polyurethane when the environment at the surface is changed from air to water.¹²⁵ If the polyurethane is immersed in a suitable organic solvent for a short amount of time first, the rearrangement in water can be stimulated since the motility of the molecular chains near the surface is increased, and consequently polar group formation on the surface of the polyurethane is augmented. Renewable materials have recently become a focus in polymer science. A composite of PP reinforced with natural flax fibres was treated with a zein coupling agent, which is a protein consisting of a mixture of amino acids and glutamic acid. Zein treatment was found to confer improved mechanical properties as a result of better interfacial adhesion between the PP and flax layers. This occurred due to the amphiphilic nature of the zein meaning it can interact strongly with both the polar flax fibres and the non-polar PP matrix.¹²⁶

Another technique which improves adhesion through the alteration of the surface is plasma treatment. This often induces the formation of oxygen-containing functional groups which cause increased wetting of the surface and therefore better adhesion. It has been reported that C=O groups in particular, but also C-O, O-C=O, -OH and -OOH, aid adhesion at the surface of polymers such as PP.¹²⁷ Adjusting the parameters of the plasma treatment including the power, pressure, gas flow and the length of the treatment allows for changes to be made to the surface without altering the bulk properties of the material.¹²⁸ Boschmans et al. studied the surface composition of PP films as a function of plasma treatment time using Time-of-Flight (TOF) static secondary ion mass spectrometry (S-SIMS).¹²⁹ They found that even short atmospheric plasma treatments of less than 6 seconds were enough to significantly change the surface via the formation of oxygen functionalities. The type of plasma used in the surface modification significantly affects both the wettability and the overall adhesion properties of the polymer. Dilsiz et al. demonstrated that both allylcyanoide and a mixture of xylene, air and oxygen plasmas can be used to improve the degree of adhesion between polymeric carbon fibres and their matrix.¹³⁰ Conversely, a comparison of PP modification by a pure argon plasma and a mixed argon/oxygen plasma found that while both treatments increased the surface free energy of the sample, use of only the argon gas introduced slightly more oxygen-containing functional groups onto the surface, in addition to producing a smoother, more wettable surface as

determined by AFM. Boronat et al. optimised the sample distance and treatment rates of the plasma treatment of LDPE in a simulation of industrial conditions. Plasma exposure was found to increase the polar component of the surface energy and therefore improve the surface properties of the material; however this improvement deteriorated over an ageing period of 21 days.¹³¹

Better adhesion can also be obtained by the use of chlorinated polymers. These can be formed either via the polymerisation of chlorinated monomers or by the post-polymerisation chemical modification of polymers with chlorinated reagents. Chlorinated polyethylene (CPE) resins and chlorinated paraffins have been used as adhesive layers between polyolefins and coatings or synthetic resins. For example, Steenbakkers-Menting et al. successfully used powder chlorinated PE to improve the adhesion between ultrahigh molecular weight PE (UHMW-PE) and nitrile rubber (NBR).¹³² Abdullin et al. also found that the chlorination of polymers improved their adhesive properties; in this case by the addition of chlorine atoms to the unsaturated bonds of low molecular weight 1,2-polybutadiene, which was shown to improve adhesion to substrates such as steel.¹³³ An alternative approach is to modify the surface of the substrate itself. This was done by Aronson et al. in a two-step process involving the immersion of HDPE in an aqueous solution containing sodium hypochlorite and acetic anhydride.¹³⁴ They showed that the surface chlorine concentration at the molecular level is proportional to some extent to the strength of adhesion at the macroscopic mechanical level, and additionally the adhesion strength can be increased through optimisation of the reaction conditions and reactants used for surface treatment. Fluorination has also been shown to improve the adhesion and printability of polymer substrates. Kharitonova et al. studied the effects of direct fluorination and found that it can be effectively used to enhance the commercial properties of a range of polymers in several ways, including better adhesion performance.¹³⁵

1.2.7.2 Copolymer Adhesives

Rather than modifying the substrates themselves, copolymer additives can be added to the interface to improve adhesion. The influence of copolymer architecture on adhesion has been investigated. Tirrell et al. concluded that there exists a chain architecture-adhesion relationship which accounts for the influence of surface

architecture on block copolymer adhesion.¹³⁶ A Monte Carlo simulation was performed to investigate the effect of random, alternating or blocky structure within an AB copolymer chain where A denotes a monomer that was adhesive to the surface and B denotes a monomer that was not. It was found that the structure of the adsorbed copolymer film was influenced not only by the fraction of adhesive monomers A within the chain but also their arrangement. With fixed composition, genuine differences were seen between the random, alternating and blocky structures, with the best adhesion observed for diblock and triblock copolymer arrangements.¹³⁷ In another study of the effects of copolymer structure on adhesion, in this case focusing on multiblock polyurethane graft copolymers, it was found that the adhesion depended on the hard segment content within the polymer, with the association of crystallised domains improving both the adhesiveness and cohesiveness of the materials.¹³⁸ Block and graft copolymers have been used to improve adhesion through their addition to the interface between two surfaces, where they act as a molecular bridge between the two polymers.¹³⁹

One instance of the use of block copolymer additives to improve adhesion behaviour makes use of a maleic anhydride copolymer as a coupling agent.¹⁴⁰ The adhesion between PP and amorphous polyamide (aPA) was hugely improved by the addition of maleic anhydride grafted PP (PP-g-MA), which underwent a coupling reaction with the primary amine groups on aPA. Similarly, Boyer et al. improved the adhesion of PP onto poly(vinylidene fluoride) (PVDF) by using PP-g-PMMA graft copolymers.¹⁴¹ Peel tests were carried out to quantify adhesion and it was found that the peel forces increased by a factor of 15 with the use of the adhesion promoter compared to adhesion without promoters.

According to Cho et al.¹⁴² the mechanical strength of the interface between immiscible polymers is very weak since there is little chain entanglement between the polymers as a result of the large enthalpic repulsion between the components.¹⁴² Copolymer additives can be used as reactive interfacial agents to compatibilise immiscible and incompatible polymers through improvement of the interfacial properties. The reactive interfacial agent possesses specific functional groups and can engender the formation of block or graft copolymers at the interface. For example, the interfacial adhesion strength between PS and a styrene maleic anhydride (SMA) random copolymer was improved by the addition of an amine-terminated polystyrene (ω -amino

PS) as a reactive compatibiliser. In another instance of reactive compatibilisation, a styrene maleic anhydride random copolymer (P(SMA-8 wt% MA)) and poly[methylene(phenylene isocyanate)] (PMPI) were demonstrated to bridge the interface of PET and PS, as PSMA is completely miscible with PS, and PMPI can react with PET and PSMA simultaneously to form PET-*co*-PMPI-*co*-PSMA copolymers at the interface with PS. This was found to improve the mechanical properties of the material.¹⁴³ Reactive compatibilisation has become a widely-used method to reduce the interfacial tension between two immiscible materials through the in-situ formation of copolymers.¹⁴⁴

As an alternative method to the use of discrete block or graft copolymers as additives, polymer grafts can be formed in situ at the interface. This can be achieved using plasma graft polymerisation, where plasma treatment is used to activate the surface so that the desired monomer can be polymerised onto or from it to form grafts. Gupta et al. used this technique to graft acrylic acid onto PET films.¹⁴⁵ Characterisation by atomic force microscopy (AFM), XPS and contact angle measurements confirmed that surface roughness was increased and contact angles decreased after grafting. This allowed the immobilisation of collagen onto the films to provide a substrate for the growth of human muscle cells. Plasma graft polymerisation has also been used to graft the hydrophilic monomers acrylamide (AAM), glycidyl methacrylate (GMA) and 2-hydroxyethyl methacrylate (HEMA) onto expanded poly(tetrafluoroethylene) (ePTFE) film. A significant increase in peel strength was reported.¹⁴⁶ Another example of in situ graft polymerisation without the use of plasma was the creation of reactive polymer blends of polystyrene modified with carboxylic acid (PS-*m*COOH) and random copolymers of poly(methyl methacrylate-*co*-glycidyl methacrylate) (PMMA-GMA).¹⁴⁷ A reaction occurred between the carboxylic acid in PS-*m*COOH and PMMA in PMMA-GMA to form the copolymer PMMA-*g*-PS, which was found to stabilise the interfacial morphology and therefore improve the adhesion between the two polymers.

1.2.7.2.1 Use of Amphiphilic Graft Copolymers as Adhesion Promoters

There are several recent examples in the literature concerning the synthesis of amphiphilic graft copolymers and their use in the promotion of adhesion. Fu et al. synthesised a range of amphiphilic poly(higher α -olefin-*co*-para-methylstyrene)-*g*-poly(ethylene glycol) and poly(higher α -olefin-*co*-acrylic acid)-*g*-poly(ethylene glycol) graft copolymers using Ziegler-Natta catalytic polymerisation.¹⁴⁸ It was found that these

could be used to modify the surface of linear low density polyethylene (LLDPE) film by spin coating, which was shown to improve the wettability of the surface. The higher the PEG content of the copolymer, the lower the water contact angle was. Initially the adhesion between the amphiphilic graft copolymer and the LLDPE film was poor so annealing was carried out to induce crystallisation. This led to enrichment of the PEG segments at the interface and therefore fixing of the copolymer at the interface with LLDPE, which further increases surface wettability.

Another example made use of the grafting-through approach to prepare amphiphilic poly(cyclooctene-*g*-PEG), with polycyclooctene as the hydrophobic backbone and PEG as the hydrophilic side chains.¹⁴⁹ The first stage of the synthesis was to prepare the macromonomer cyclooctene-PEG, which was then copolymerised with cyclooctene by ring opening metathesis polymerisation (ROMP). Again it was found that the higher the PEG content, the lower the water contact angle meaning that the surface has been rendered more hydrophilic.

Yilmaz et al. also synthesised amphiphilic graft copolymers, in this case consisting of a hydrophobic polysulfane (PSU) backbone and hydrophilic PAA side chains.¹⁵⁰ These were made by the synthesis of P^tBA via ATRP which was subsequently grafted onto azide-functionalised PSU by click chemistry. Finally the PSU-*g*-P^tBA polymers were hydrolysed using trifluoroacetic acid to give PSU-*g*-PAA. The hydrophilicity of the copolymers was shown to increase on grafting, which reduced the protein fouling and cell adhesion properties of the materials compared to the unmodified PSU precursor. This shows that amphiphilic graft copolymers can also be used to prevent adhesion, depending on their structure and characteristics.

This thesis aims to investigate the effect of amphiphilic copolymer additives of varying architecture on the adhesion of printed ink to low energy polyolefinic substrates. The aims and objectives of the work will be introduced in the next chapter.

2. Aims and Project Outline

2.1 Aims

The overall aim of this work is the design of polymeric additives which will improve the adhesion of ink to ‘difficult’ polyolefin substrates, for example polyethylene and polypropylene, which pose problems due to their low surface energy and hydrophobic nature. This adhesion will occur via migration of the additive to the interface between the dye and the substrate following deposition from a carrier fluid during the inkjet printing process.

These additives will consist of amphiphilic copolymers, with hydrophobic backbones and charged pendant chains. The aim is to design such materials so that they can form interfacial layers with the hydrophobic backbone adsorbed to the polyolefin substrate and the charged groups adsorbed to the dye or pigment particles. In this way they can be used to form an adhesive bridge between the dye and the substrate.

These copolymer additives will be prepared with equivalent monomer composition but with a range of different architectures and monomer distributions, in order to compare their behaviour and allow investigation of the effect of copolymer structure on material properties, both in solution and in the solid state, in addition to comparison of their printing performance.

Initially, graft copolymers will be synthesised, employing an adaptation of the method used by Carter et al.¹⁵¹ These materials will consist of a linear alkyl methacrylate and vinylbenzyl chloride copolymer backbone with poly(acrylic acid) side chains, synthesised via a grafting-from approach using the RAFT polymerisation technique. Different analogues will be prepared using methyl, butyl and lauryl methacrylate monomers to allow study of the effect of varying the hydrophobicity of the methacrylate block.

Copolymers will also be prepared in branched architectures, again following and modifying the previous work of Carter et al,^{63, 64} in addition to linear analogues of the materials. Random and block versions of these copolymer materials will be synthesised in a simple modification of the polymerisation procedure where a ‘one pot’ reaction dictates random copolymer formation whilst sequential monomer addition allows the

synthesis of block copolymers due to the pseudo-living character of RAFT polymerisation.

This set of ‘model’ amphiphilic copolymers will be characterised using techniques including NMR spectroscopy, GPC and GPC-viscometry. They will be dispersed into aqueous solution and their behaviour studied using: Phase Analysis Light Scattering (PALS) to measure particle size and zeta potential; TEM to measure morphology and an alternative measure of particle size; and SANS to allow further study of solution conformation and size. The surface behaviour of the copolymers will be characterised by contact angle measurements. Finally the suitability of the materials for the intended application in inkjet printing will be assessed by a range of printing techniques.

2.2 Project Outline

1. Optimise a method of RAFT grafting-from polymerisation.
2. Synthesise amphiphilic poly(alkyl methacrylate-*g*-acrylic acid) graft copolymers using methacrylate monomers with varying alkyl chain length.
3. Synthesise analogous copolymers with linear and highly branched structures using RAFT polymerisation, in both block and random monomer distributions.
4. Explore the solution properties of these materials.
5. Investigate the adhesion behaviour of these materials at surfaces using contact angle measurements.
6. Test materials in printing studies.

3. Synthesis of Poly(Alkyl Methacrylate-*g*-Acrylic Acid) Graft Copolymers

In this chapter, methyl, butyl and lauryl methacrylate versions of poly(alkyl methacrylate-*g*-acrylic acid) graft copolymers are synthesised. The application of phase transfer catalysis to the functionalisation of poly(alkyl methacrylate-*co*-vinylbenzyl chloride) backbones with a dithioic acid is found to improve the efficiency of this step. Poorer grafting is observed for the lauryl methacrylate analogue and is found to be due to the steric effect of the long chain.

3.1 Introduction

As previously described, a major advantage of the RAFT polymerisation technique is that it can be used to produce complex macromolecular architectures, including both block copolymers¹⁵² and star polymers.^{153, 154} Branched polymer architectures have also been produced using RAFT, initially by Yang et al.,⁶² using a RAFT agent containing a dithioester group and an additional polymerisable double bond. The branching mechanism followed the self-condensing vinyl polymerisation principle introduced by Fréchet.⁵⁸ A similar route was used to prepare HB poly(*N*-isopropyl acrylamide)s with a range of applications.^{63, 64, 155} Separating the copolymerisation and branching reactions in a similar manner to the iterative graft-on-graft polymerisations employed by Fréchet et al.,⁷⁵ Deffieux et al.¹⁵⁶ and Hirao et al.^{157, 158} can be achieved by functionalising a linear polymer chain with dithioate ester groups. This method can be used to produce graft polymers.

4-Vinylbenzyl chloride (VBC), also known as 4-chloromethyl styrene, is an important dual functional monomer containing a benzyl chloride group that can undergo functionalisation reactions before or after polymerisation.¹⁵⁹ VBC polymers react with various nucleophilic reagents at fairly high yields, depending on the steric hindrance. Quinn et al. made use of this property in their work involving the synthesis of comb, star and graft polymers using RAFT.¹⁶⁰ This built on earlier work where the thiocarbonylthio group was incorporated pendant to an existing polymer chain to provide sites from which more sophisticated polymeric architectures could be assembled.^{152, 161} Quinn et al., however, used VBC as a comonomer along with styrene to form a linear backbone, which was converted into a polyfunctional RAFT agent by nucleophilic substitution of the benzyl chloride of VBC with dithiobenzoate. Styrene

branches were then grown from these in-situ RAFT agent moieties to form polymers of various architectures.¹⁶⁰ Vosloo et al. used a similar approach to synthesise comblike PBMA, but using *N*-acryloxysuccinimide (NAS), an activated ester, as a comonomer instead of VBC with BMA in the backbone.¹⁶² This backbone was then functionalised with the RAFT agent benzyl 2-(2-hydroxyethylamino)-1-methyl-2-oxoethyl trithiocarbonate, allowing the subsequent controlled growth of BMA branches via RAFT polymerisation. Carter et al. went on to adapt this technique for the synthesis of functional graft PNIPAM, using P(NIPAM-*co*-VBC) copolymers to form the backbone which was then functionalised with 4(5)-imidazole dithioic acid or *N*-pyrrole dithioic acid to give linear dithioate functional polymers.¹⁵¹ These were then used as macromolecular transfer agents to grow PNIPAM grafts via controlled RAFT polymerisation.

Acrylic acid is a weak polyelectrolyte which has frequently been used as a hydrophilic component of block and graft copolymers, as demonstrated in the examples previously mentioned in Chapter 1. Unlike the other CRP techniques, the RAFT method allows the polymerisation of acidic monomers such as AA without the need for protecting group chemistry.¹⁶³ The methacrylate class of monomers are also suitable for use in RAFT polymerisation.¹⁶⁴ These were chosen to form the hydrophobic portion of the amphiphilic copolymers. The hydrophobicity can be varied depending on the choice of methacrylate monomer. Lauryl methacrylate (LMA) was chosen as the initial hydrophobic monomer since it is the last, and therefore most hydrophobic, of the amorphous alkyl methacrylates. Polymers formed from the polymerisation of higher methacrylate monomers with alkyl chains longer than 12 carbon atoms can crystallise and are therefore more difficult to process. LMA has also been used previously as a non-polar component of amphiphilic block copolymers.^{165, 166}

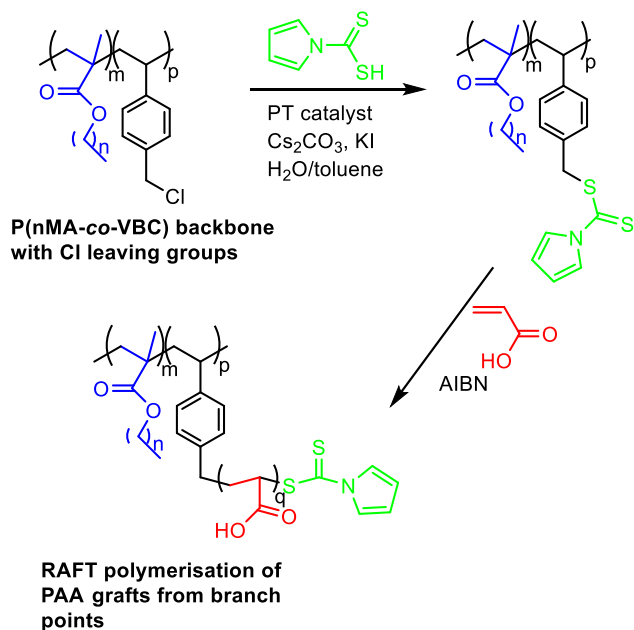
Reactions between substances located partly in an organic phase and partly in an aqueous phase are often slow and inefficient. Phase Transfer Catalysis (PTC) was developed as a method to solve this problem using quaternary ammonium and phosphonium salts to catalyse two-phase organic reactions.¹⁶⁷ The catalyst facilitates the migration of anions across the interface between the two phases. PTC can be applied to reactions including nucleophilic substitution, carbene reactions, alkylation of ketones and nitriles, Wittig reactions, and the formation of ethers and esters. There are many advantages of the technique, such as mild experimental conditions, simple experimental

procedures, inexpensive and environmentally benign reagents and solvents and also the potential for large-scale reactions.¹⁶⁸ It is one of the most important synthetic methods used in various fields of organic chemistry, and widespread industrial applications have also been established.¹⁶⁹

Although initially developed as a technique for organic synthesis, PTC has also been applied to polymer chemistry, both in polymer synthesis and the chemical modification of polymers. Rasmussen and Smith reported the first phase transfer catalysed free radical polymerisation which was carried out on butyl acrylate using various crown ethers as PT catalysts.¹⁷⁰ The use of PTC to aid polymerisation has subsequently become more widespread since it provides high reaction rates at low temperatures. The use of PTC has been mostly restricted to free radical polymerisations with vinyl monomers using water-soluble initiators.¹⁷¹

It was reported in some of the early work combining PTC with polymer modification that PTC can be successfully employed for the reaction of amines and alcohols with chloromethylated polymers and copolymers.¹⁷² In some cases this led to 100% conversion of chloromethyl groups. A wide variety of functionalities were introduced into chloromethylated PS resins using PTC techniques.¹⁷³ Adogen 464 and tetra-n-butylammonium chloride and hydroxide were employed as catalysts, and excellent yields of functionalised polymer were reported. Similar modification of chloromethyl-containing polymers using PTC will be attempted in this work.

The procedure for graft copolymer synthesis developed by Carter et al. was used as the basis for this work. The methodology involves the functionalisation of poly(methacrylate-*co*-VBC) (P(nMA-*co*-VBC)) backbones using a dithioic acid, creating an in-situ CTA. This is followed by the growth of poly(acrylic acid) grafts from the styryl branch points in a RAFT-mediated polymerisation, as outlined in **Scheme 3.1**. Phase Transfer Catalysis was investigated as a way to improve the post-polymerisation modification of the P(nMA-*co*-VBC) backbone, as the success of this step dictates the extent of grafting that can be achieved to form the final copolymer.



Scheme 3.1. Procedure for the synthesis of graft copolymers from a copolymer backbone containing functionalisable groups

3.2 Synthesis of P(nMA-co-VBC) Backbones

Linear backbones were synthesised using non-controlled conventional free radical polymerisation of alkyl methacrylates and VBC. Three different alkyl methacrylate monomers with varying lengths of alkyl chain; methyl, butyl, and lauryl, were used to investigate the effect this had on both the synthesis of the graft copolymers and the properties of the polymer materials. **Table 3.1** shows the molecular weight data obtained for these copolymer backbones. The presence of the comonomer was confirmed via ¹H NMR spectroscopy and chlorine content, which was obtained from elemental analysis.

Table 3.1. Results of Free Radical Polymerisation of Alkyl Methacrylates with Vinyl Benzyl Chloride to Form P(nMA-*co*-VBC) Backbones

polymer	feed ratio nMA:VBC	polymer ratio nMA:VBC ^a	M _n ^b /g mol ⁻¹	M _w ^b /g mol ⁻¹	Đ ^b	Cl content ^c /%	conversion ^a /%
P(MMA- <i>co</i> - VBC)	15:1	16.5:1	10700	29700	2.78	1.93	96.1
P(BMA- <i>co</i> - VBC)	15:1	15.4:1	9700	21700	2.22	1.49	98.3
P(LMA- <i>co</i> - VBC)	15:1	16.9:1	23100	59200	2.56	1.03	99.8

^a determined by ¹H NMR ^b determined by GPC (THF, PMMA standards) ^c determined by elemental analysis

A molar mass of approximately 20000 g mol⁻¹ was targeted, since the polymers currently used in printing inks tend to be of low molecular weight in order to minimise viscosity, as detailed in Section 1.3. The relationship between initiator concentration and molecular weight for polymers synthesised by non-controlled conventional free radical polymerisation follows the relation:

$$x_n \propto [I]^{-\frac{1}{2}} \quad \text{Equation 3.1}$$

where x_n is the kinetic chain length, related to molecular weight, and $[I]$ is the initiator concentration. Therefore a greater amount of initiator is required to make shorter polymer chains. An initiator concentration of 4 wt% was used for these polymerisations following initial studies which showed that when higher concentrations of initiator were used, although lower molecular weight polymers were produced, product yields fell making the process impractical.

Integration of the ^1H NMR spectra was used to calculate the actual ratios of comonomers that were incorporated into the copolymer, as demonstrated by **Figure 3.1**. The copolymers were found to contain slightly more methacrylate than expected but the final product ratios are very similar to the monomer feeds. Changing the ratio of methacrylate to VBC allows control over the grafting density of the graft copolymers, as the VBC units provide the grafting points. A ratio of 15:1 nMA:VBC was used for all further polymerisations to maintain consistency.

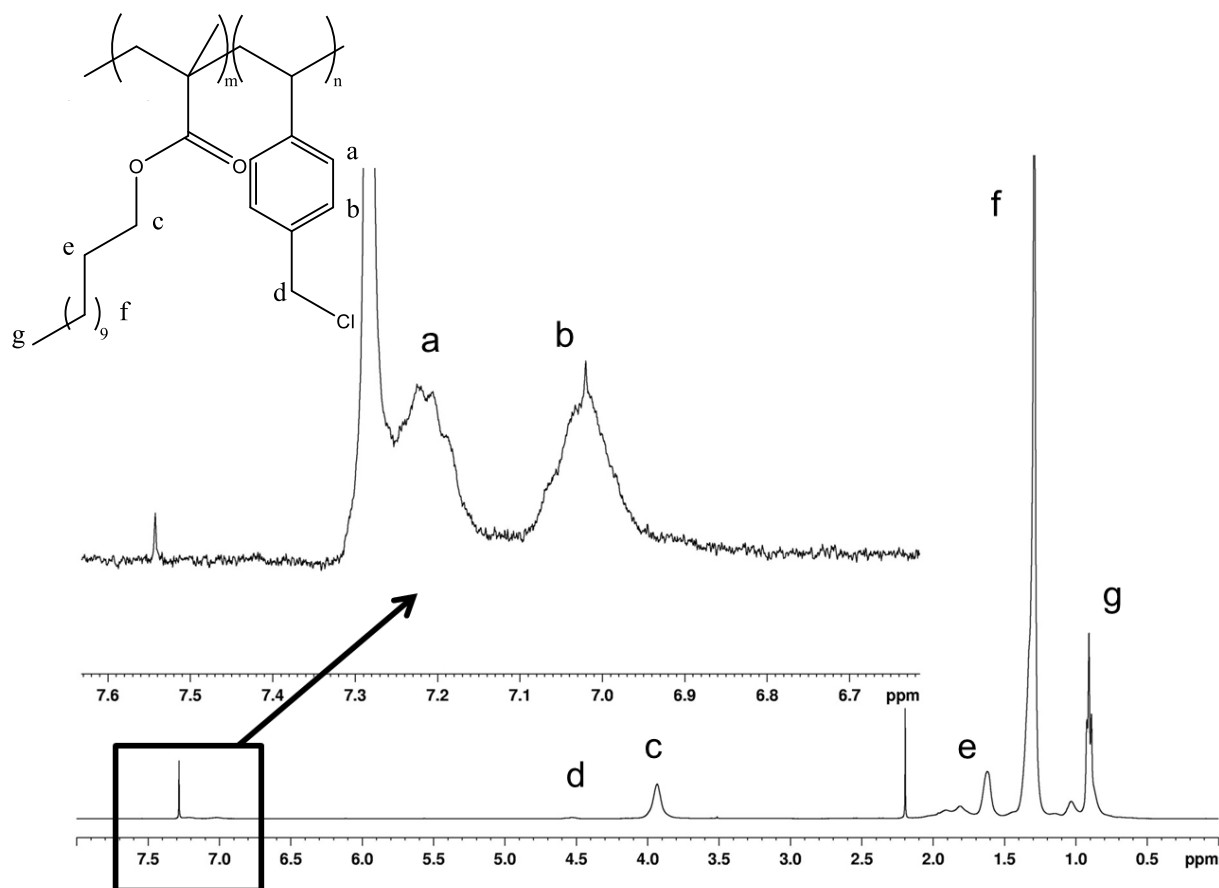


Figure 3.1. ^1H NMR spectrum of P(LMA-*co*-VBC). The actual ratio of comonomers in the backbone is calculated by comparing the integrals of the LMA methylene peak c against the benzyl peak b of VBC.

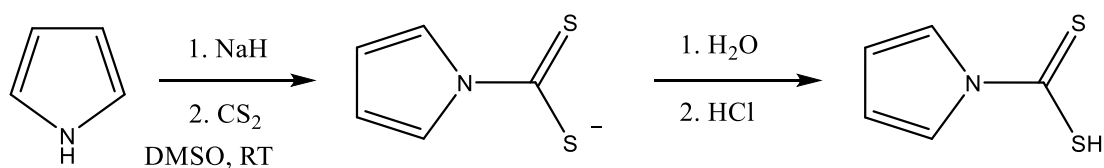
The distribution of the grafts along the copolymer backbone depends on the distribution of the VBC and nMA monomer units within the chain, which in turn depends on the reactivities of the two monomers. The grafts should be randomly distributed along the backbone if the reactivity ratios of the two monomers are similar and are both close to one, whereas an alternating copolymer is more likely if the

reactivity ratios are similar and close to zero. Luo et al. carried out a study on the copolymerisation of methyl methacrylate and VBC and found the reactivity ratios to be 0.3 for MMA and 0.7 for VBC.¹⁷⁴ It was concluded that the system tended towards random copolymer formation, with VBC more likely to be polymerised in the initial stages and MMA later on in the polymerisation as the reactivity ratio for VBC, r_{VBC} , is more than twice r_{MMA} , the reactivity ratio of MMA. This suggests that the copolymer composition will be similar for the P(nMA-*co*-VBC) backbone copolymers. A method of confirming copolymer composition will be explored in Section 4.7.

3.3 Functionalisation of P(nMA-*co*-VBC) Backbones using Phase Transfer Catalysis

Pyrrole-1-carbodithioic acid was used to modify the VBC group in the backbone via nucleophilic substitution to create an in-situ RAFT agent, providing an active site for the growth of poly(acrylic acid) (PAA) grafts. The synthesis of pyrrole-1-carbodithioate involved first using sodium hydride to promote the formation of N-pyrrole anions, which then reacted with carbon disulphide to form dithioate anions. The reaction underwent an acid work up to give the desired product, as shown in **Scheme 3.2**. Both ¹H NMR and elemental analysis were used to confirm product purity.

Scheme 3.2. Synthesis of Pyrrole-1-carbodithioic Acid



The next step was to functionalise the backbone polymers by the nucleophilic substitution of the N-pyrrole dithioester groups of pyrrole-1-carbodithioic acid at the methylene chloride position of the VBC moieties. Initial studies were carried out using the P(LMA-*co*-VBC) backbone in a variety of solvent systems to investigate the optimal conditions for this reaction. Previous work by Carter et al. was carried out on PNIPAM.¹⁵¹ Dioxane was used as the reaction solvent, with potassium iodide and caesium carbonate as additive and base respectively. Toluene was found to be the most suitable solvent for the new system since dioxane, although yielding the highest degrees

of functionalisation due to its non-polar nature and ability to complex ions via the oxygen atom, led to crosslinking of the material rendering it unprocessable for further reactions. Temperature studies showed that increasing the reaction temperature had little positive effect on the degree of functionalisation, and in some cases actually led to a reduction in functional group conversion, indicating that the reaction should be carried out at room temperature. Despite these optimisation steps, initial conversions of methylene chloride groups to dithioester groups were low, as seen in **Table 3.2**.

Table 3.2. Summary of Results From Reaction Time Study of the Functionalisation of P(LMA-*co*-VBC) Backbones with Pyrrole-1-carbodithioic Acid in Toluene at Room Temperature

reaction time /hours	degree of functionalisation ^a /%	S content ^b /%
8	6	0.87
24	9	0.11
72	25	0.93
120	8	0.88

^acalculated from ¹H NMR, ^bfrom elemental analysis

It was proposed that these low conversions occurred due to the heterogeneous nature of the reaction, since the base was insoluble in the reaction solvent. Therefore the reaction was repeated using phase transfer catalysis (PTC), which involves a heterogeneous reaction system. In this particular reaction system the organic phase was toluene and contained the P(nMA-*co*-VBC) backbone with the pyrrole-1-carbodithioic acid. The aqueous phase contained the base, caesium carbonate, in addition to potassium iodide which was added to promote the reaction. The phase transfer catalyst, when used, was also added to the aqueous phase.

A study was carried out to test the hypothesis that the use of a two-phase reaction system, specifically the use of a phase transfer catalyst, would increase the degree of functionalisation of the polymer. The results are summarised in **Table 3.3**.

Table 3.3. Summary of Results for the Functionalisation of P(LMA-*co*-VBC) Copolymer Backbones With and Without the Use of a Phase Transfer Catalyst

reagents	yield /%	degree of functionalisation ^a /%
Cs ₂ CO ₃	94	37
Cs ₂ CO ₃ /KI	71	49
Cs ₂ CO ₃ /KI/HTAB	98	60

^a from ¹H NMR

All three reaction mixtures contained both toluene and aqueous phases, with caesium carbonate base dissolved in the water. Additionally the second reaction contained potassium iodide and the third both potassium iodide and a phase transfer catalyst, hexadecyl trimethyl ammonium bromide (HTAB). For all compositions the two-phase processes proved to be a clean way to carry out the functionalisation as the layers could be easily separated at the end of the reaction and high mass yields of the polymer could be recovered. The results showed that the addition of KI produced a clear increase in the degree of functionalisation, and that the use of a phase transfer catalyst caused a significant further increase.

Following these preliminary experiments, more work was undertaken to compare the suitability of different types of phase transfer catalysts for this reaction system. Phase transfer catalysts can be classified into two groups: accessible and anion activating. The same reaction was carried out using two accessible catalysts, hexadecyl trimethyl ammonium chloride (HTAC) and hexadecyl trimethyl ammonium bromide (HTAB), and two anion activating catalysts, tetrabutyl ammonium chloride (TBAC) and tetrabutyl ammonium bromide (TBAB). **Figure 3.2** shows the structure of these

catalysts. For nucleophilic substitution, or displacement, reactions, anion activating catalysts are usually found to be most effective.¹⁶⁸

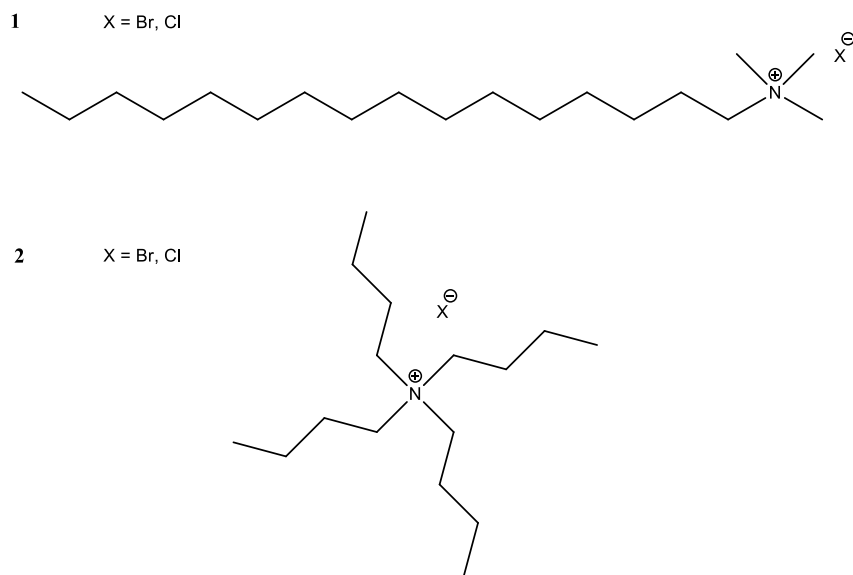


Figure 3.2. Structures of phase transfer catalysts that were used to aid the functionalisation of P(LMA-*co*-VBC) backbones **1**. HTAB/HTAC and **2**. TBAB/TBAC

Table 3.4. Summary of Results for the Functionalisation of P(LMA-*co*-VBC) Copolymer Backbones Using a Range of Phase Transfer Catalysts

catalyst	class	degree of functionalisation ^a	yield
		/%	/%
HTAC	accessible	57.6	88
HTAB	accessible	46.4	95
TBAC	anion activating	63.9	97
TBAB	anion activating	65.6	100

^a from ¹H NMR

The results in **Table 3.4** show that the anion activating catalysts were indeed the most suitable for this system. TBAB provided both the highest conversion and the highest product yield of the four reactions, making it the clear choice for further use.

The presence of the *N*-pyrrole dithioester groups was confirmed by the pyrrole CH resonances at $\delta 6.46$ and $\delta 7.72$ in the ^1H NMR spectra, as shown in **Figure 3.3**. The pyrrole signals occur far enough upfield and downfield from the broad aromatic region arising from the benzyl protons to allow accurate calculation of conversion by comparative integration of these pyrrole protons compared to the -S-CH₂- methylene protons at $\delta 4.55$, with an estimated uncertainty of $\pm 5\%$. Elemental analysis was also used to assess functionalisation since the materials should contain sulfur in place of chlorine. In addition, Gel Permeation Chromatography (GPC) shows changes to the materials on functionalisation, as there is an apparent increase in the size of the polymer backbone as a result of its altered conformation in solution due to the introduction of the more hydrophobic dithioester groups into the structure. Another indicator of functionalisation is the dramatic change in the colour of the materials, from clear P(nMA-*co*-VBC) backbones to dark brown functionalised materials.

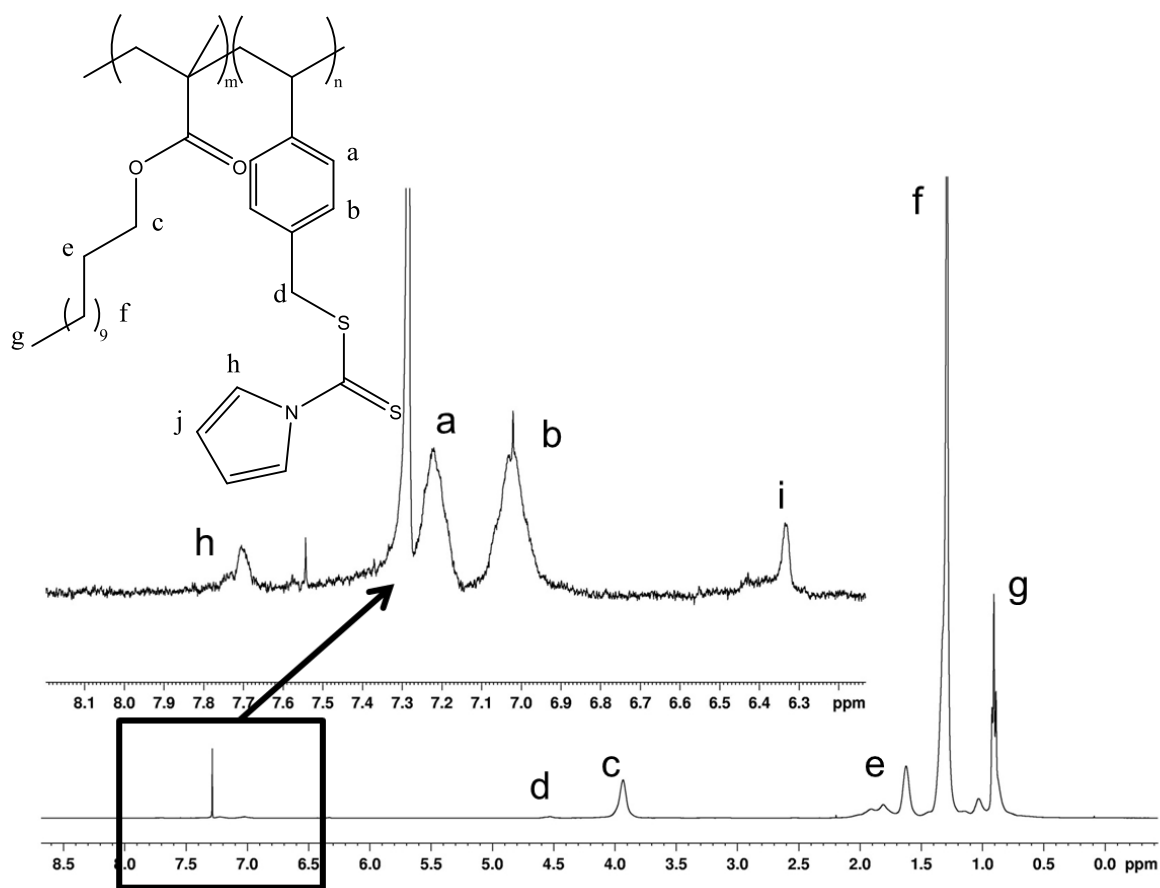


Figure 3.3. ^1H NMR spectrum of functionalised P(LMA-*co*-VBC). The degree of functionalisation of the vinylbenzyl chloride units in the backbone is calculated by comparing the integrals of the pyrrole resonance i against the -S-CH₂- methylene resonance d of VBC

Following these optimisations, the reaction was carried out on a set of methyl, butyl and lauryl P(nMA-*co*-VBC) backbones to yield functionalised materials. The results are summarised in **Table 3.5**. Under the same conditions the highest degree of functionalisation was achieved for P(BMA-*co*-VBC). P(LMA-*co*-VBC) gave a substantially lower degree of functionalisation.

Table 3.5. Results of Functionalisation of P(nMA-co-VBC) Backbones Using TBAB as the Phase Transfer Catalyst

polymer	M_n^b /g mol ⁻¹	M_w^b /g mol ⁻¹	\bar{D}^b	degree of functionalisation ^a /%
P(MMA-co-VBC)	13400	25900	1.93	64.0
P(BMA-co-VBC)	26300	34800	2.32	73.7
P(LMA-co-VBC)	20700	44800	2.17	45.3

^a determined by ¹H NMR, ^b determined by GPC (THF, PMMA standards)

3.4 Grafting Polyacrylic Acid Side Chains from Functionalised Backbones

Following modification of the polymer backbones with pyrrole dithioester groups, grafts of poly(acrylic acid) (PAA) were added by RAFT-controlled polymerisation from the backbones to create ‘comb-like’ materials. **Table 3.6** summarises the results of the backbone modification and grafting step.

Table 3.6. Results of Synthesis of Graft P(nMA-*co*-VBC-*g*-AA) Copolymers from Functionalised Backbones

polymer	M_n^b /g mol ⁻¹	M_w^b /g mol ⁻¹	\bar{D}^b	degree of functionalisation ^a /%	ratio nMA:AA ^a
P(MMA- <i>co</i> - VBC)	13400	25900	1.93	64.0	-
P(MMA- <i>co</i> - VBC- <i>g</i> -AA)	10500	46700	4.45	-	0.77:1
P(BMA- <i>co</i> - VBC)	26300	34800	2.32	73.7	-
P(BMA- <i>co</i> - VBC- <i>g</i> -AA)	5200	57300	10.98	-	1.11:1
P(LMA- <i>co</i> - VBC)	20700	44800	2.17	45.3	-
P(LMA- <i>co</i> - VBC- <i>g</i> -AA)	18800	54400	2.90	-	-

^a determined by ¹H NMR, ^b determined by GPC (THF, PMMA standards)

Analysis of the MMA and BMA graft copolymers showed peaks due to PAA in the ¹H NMR spectra, which were not observed in the P(LMA-*co*-VBC-*g*-AA) spectra. In order to analyse the carboxylic acid-containing materials using a GPC system with THF eluent, the acid groups were methylated with trimethylsilyldiazomethane¹⁷⁵ to prevent the acid groups interacting with the column, which would distort the results. **Figure 3.4** shows a comparison of the GPC chromatograms for the functionalised backbones and the resulting graft copolymers.

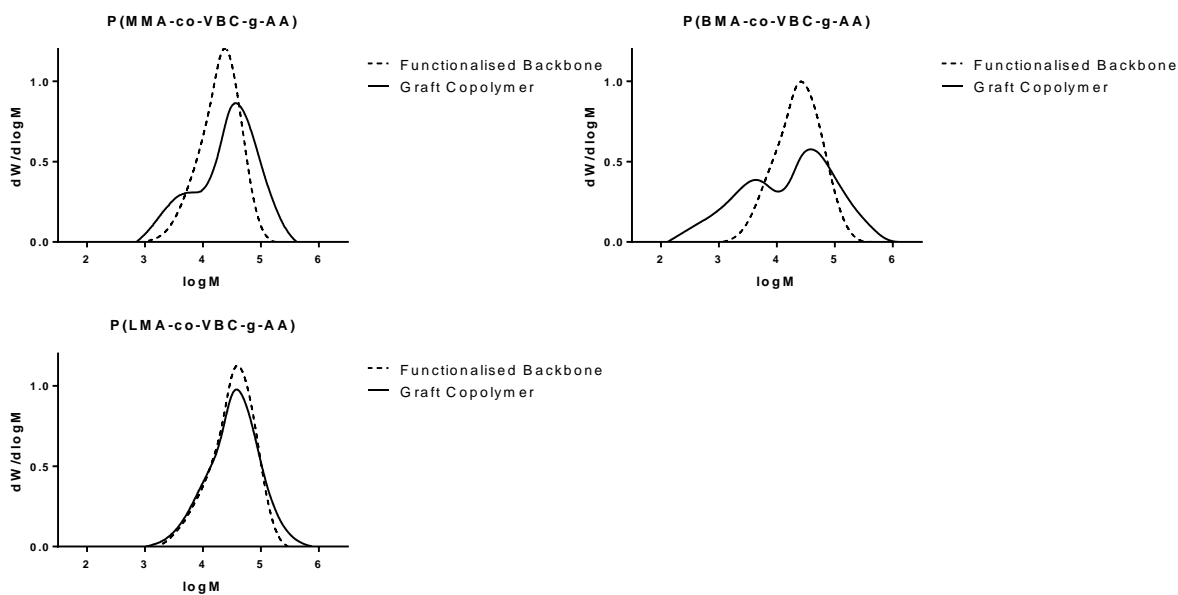
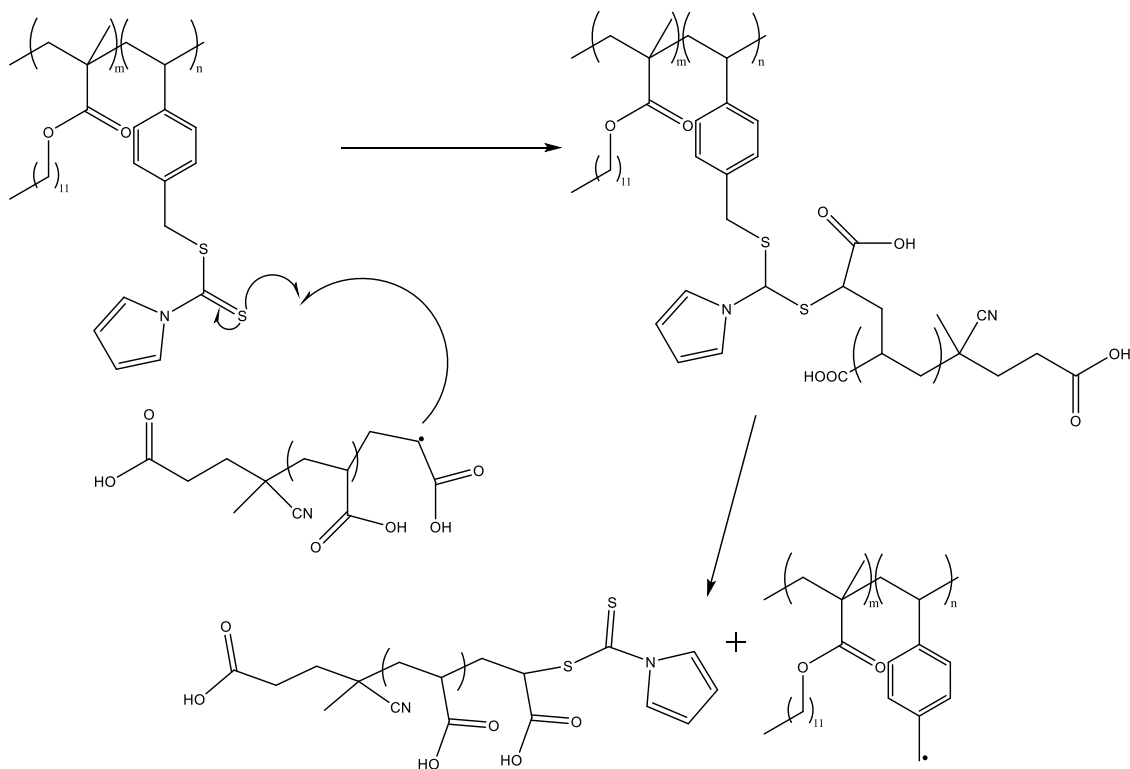


Figure 3.4. Molecular weight distributions determined by GPC (THF, PMMA standards) for: **A)** P(MMA-*co*-VBC-*g*-AA) graft polymer (solid line) and the functionalised P(MMA-*co*-VBC) backbone from which it is derived (dashed line) **B)** P(BMA-*co*-VBC-*g*-AA) graft polymer (solid line) and the functionalised P(BMA-*co*-VBC) backbone from which it is derived (dashed line) **C)** P(LMA-*co*-VBC-*g*-AA) graft polymer (solid line) and the functionalised P(LMA-*co*-VBC) backbone from which it is derived (dashed line)

The graft copolymers had broad molar mass distributions and hence large dispersities due to the branched nature of the graft copolymers. The graft materials show an increase in molecular weight from the functionalised backbones, indicating the growth of PAA chains from the functionalised sites. From the bimodal distribution of the chromatograms it can be seen that the graft copolymer products contained two different species, neither of which appear to correspond to the dithioate-functional backbone materials. This is particularly evident for the P(MMA-*co*-VBC-*g*-AA) and P(BMA-*co*-VBC-*g*-AA) polymers, whilst the P(LMA-*co*-VBC-*g*-AA) polymer shows only a slight shoulder at the low molecular weight side of the peak. The observed lower molecular weight peak is due to the presence of linear PAA homopolymers which are produced as a byproduct of the RAFT reaction. Propagating linear PAA chains attack

the dithioester groups on the polymer backbone, and this controls the molecular weight, yielding low molecular weight PAA. The mechanism is illustrated in **Scheme 3.3**.



Scheme 3.3. Formation of linear PAA during grafting from a dithioester-functionalised backbone

The molar mass distributions were deconvoluted to allow calculation of the molecular weight averages for the two species. This involved assuming that the peaks were the sum of two Gaussian distributions, and performing an initial Gaussian fit to the full distribution followed by deconvolution into the two peaks. Good fits to the raw data were achieved. The results of this deconvolution are shown in **Figure 3.5**. Meanwhile **Table 3.7** shows the calculated results for the molar masses of the graft copolymers and the PAA homopolymer for each material. A measure of grafting was also reported by calculating the mass fraction of graft copolymer in each product mixture.

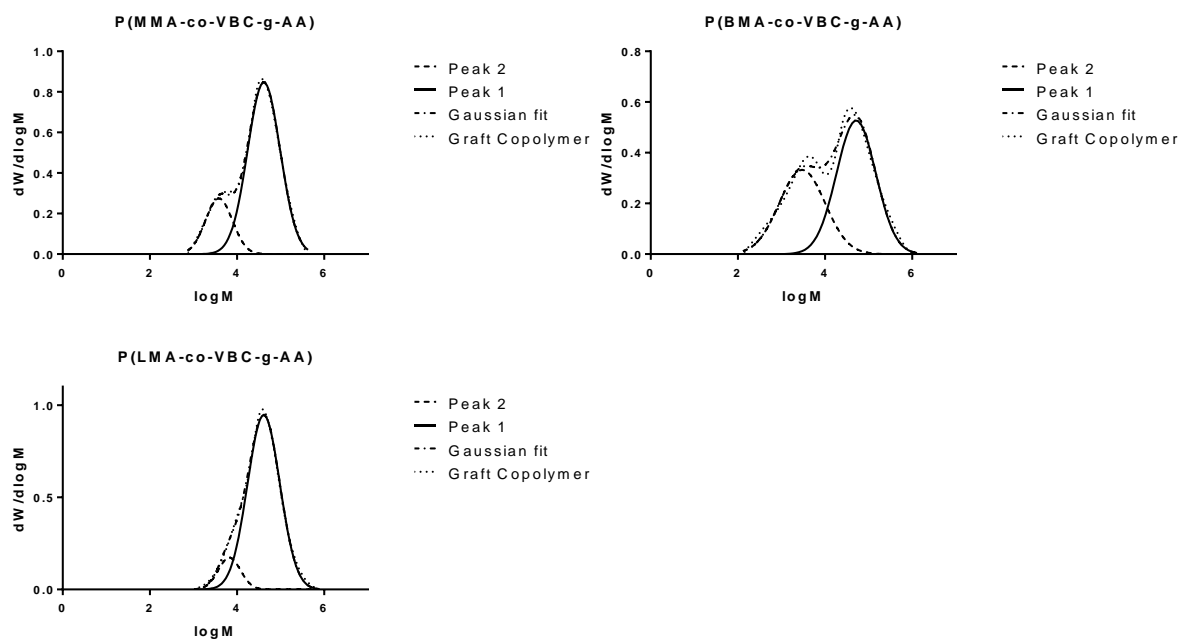


Figure 3.5. Results of deconvolution of molar mass distributions of the P(nMA-co-VBC-g-AA) graft copolymers shown in Figure 3.4: raw data for graft copolymer (dotted line), Gaussian fit to graft copolymer (alternating dotted-dashed line), peak 1 corresponding to graft copolymer (solid line), peak 2 corresponding to PAA homopolymer (dotted line).

Table 3.7. Results of Deconvolution of Molecular Weight Distributions of Graft P(nMA-*co*-VBC-*g*-AA) Copolymers

Polymer	component	M_n/g mol^{-1}	M_w/g mol^{-1}	\bar{D}	% Graft /wt%
P(MMA- <i>co</i> -VBC- <i>g</i> -AA)	graft copolymer	30500	61700	2.02	79
	homopolymer	3200	5300	1.66	
P(BMA- <i>co</i> -VBC- <i>g</i> -AA)	graft copolymer	33700	95200	2.82	58
	homopolymer	23000	34800	1.51	
P(LMA- <i>co</i> -VBC- <i>g</i> -AA)	graft copolymer	30400	62600	2.06	89
	homopolymer	5800	8200	1.41	

Deconvolution showed that each graft copolymer product also contained a proportion of PAA homopolymer, with the BMA material containing both the largest amount of PAA and the highest molar mass PAA. However the graft copolymer was the major fraction in each case. The molar mass averages obtained from the deconvoluted peaks show a much clearer increase in molecular weight from the initial functionalised backbones following grafting. Attempts to remove this remaining homopolymer through various techniques including: repeated reprecipitation; dialysis against water, which is a good solvent for PAA but not for the graft copolymer; and preparative HPLC all proved unsuccessful. Therefore the presence of this extra homopolymer will be noted in the testing of the graft copolymer materials in the following chapters.

3.5 Investigation into the Effect of Alkyl Methacrylate Monomer on Grafting of Polyacrylic Acid Side Chains from Functionalised Backbones

Although the presence of graft copolymer was confirmed for all three materials, MMA, BMA and LMA, the amount of grafting was lower for P(LMA-*co*-VBC-*g*-AA) as evidenced by the smaller increase in molecular weight from backbone to graft

copolymer compared to the other materials. This suggested that the long alkyl chains of LMA were likely to be affecting the growth of grafts by preventing the acrylic acid units from diffusing to the growing chain ends, so little growth of grafts occurred. We proposed this effect to be due to either sterics or an inherent incompatibility of the extremely hydrophobic nature of the lauryl chain with the hydrophilic acrylic acid monomer.

In order to test this theory, we attempted to synthesise P(LMA-*co*-VBC-*g*-AA) via an alternative route involving grafting of t-butyl acrylate (^tBA) to the P(LMA-*co*-VBC) backbone, as tBA and P(LMA-*co*-VBC) are both hydrophobic and therefore any inherent incompatibility would be avoided. This would be followed by hydrolysis of the P^tBA side chains to PAA. The results of these reactions are summarised in **Table 3.8**, with the molecular weight distributions of each polymer overlaid in **Figure 3.6**. The ¹H NMR spectra showed no evidence of PtBA and additionally no PAA resonances following hydrolysis, despite the apparent increase in molecular weight following the grafting step. The molecular weight distributions were deconvoluted in the same manner as carried out on the P(nMA-*co*-VBC-*g*-AA) copolymers in the previous section. The results can be seen in **Table 3.9** and **Figure 3.7**. The presence of homopolymer was detected for these polymers too. The graft copolymer was the major component in both cases, with 86% by mass graft copolymer present in the P(LMA-*co*-VBC-*g*-tBA) material, increasing to 97% following hydrolysis to P(LMA-*co*-VBC-*g*-AA). The results of this alternative synthetic route to P(LMA-*co*-VBC-*g*-AA) yielded very similar results to the initial synthetic method. This suggests that if grafting is prevented for this polymer, it is the steric effect of the lauryl chain which prevents grafting rather than a polymer-polymer incompatibility effect. However, as the GPC data appears to suggest that grafting has occurred, and that homopolymer has also been formed, it is possible that the lack of evidence of PAA in the ¹H NMR is an artefact and does not mean that there is no PAA in the copolymer.

Table 3.8. Results of Synthesis of Graft P(LMA-*co*-VBC-*g*-AA) Copolymers from Functionalised Backbones

Polymer	M_n^b /g mol ⁻¹	M_w^b /g mol ⁻¹	\bar{D}^b	degree of functionalisation ^a /%	ratio nMA:AA ^a
P(LMA- <i>co</i> -VBC)	23100	59200	2.56	-	-
functionalised P(LMA- <i>co</i> -VBC)	20700	44800	2.17	45.3	-
P(LMA- <i>co</i> -VBC- <i>g</i> -tBA)	36500	81400	2.23	-	NA
P(LMA- <i>co</i> -VBC- <i>g</i> -AA)	33600	99800	2.97	-	NA

^a determined by ¹H NMR, ^b determined by GPC (THF, PMMA standards)

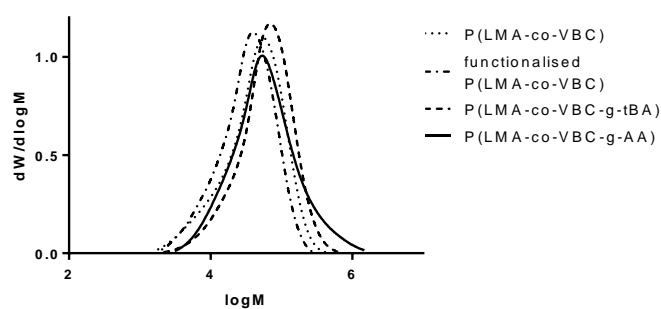


Figure 3.6. Molecular weight distributions determined by GPC (THF, PMMA standards) for: P(LMA-*co*-VBC-*g*-tBA) graft polymer (dashed line), P(LMA-*co*-VBC-*g*-AA) graft polymer (solid line), the functionalised P(LMA-*co*-VBC) backbone from which it is derived (alternating dotted and dashed line) and the starting P(LMA-*co*-VBC) polymer (dotted line)

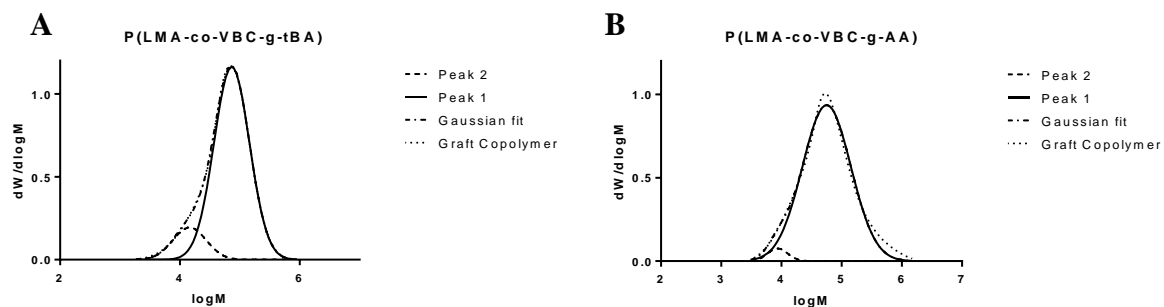


Figure 3.7. Results of deconvolution of molar mass distributions of the A) P(LMA-*co*-VBC-*g*-AA) and B) P(LMA-*co*-VBC-*g*-AA) graft copolymers shown in Figure 3.6: raw data for graft copolymer (dotted line), Gaussian fit to graft copolymer (alternating dotted-dashed line), peak 1 corresponding to graft copolymer (solid line), peak 2 corresponding to PAA homopolymer (dotted line).

Table 3.9. Results of Deconvolution of Molecular Weight Distributions of Graft P(LMA-*co*-VBC-*g*-tBA) and P(LMA-*co*-VBC-*g*-AA) Copolymers

Polymer	component	M_n/g mol^{-1}	M_w/g mol^{-1}	\bar{D}	% Graft /wt%
P(LMA- <i>co</i> -VBC- <i>g</i> -tBA)	graft copolymer	60700	96100	1.58	86
	homopolymer	12400	18600	1.50	
P(LMA- <i>co</i> -VBC- <i>g</i> -AA)	graft copolymer	40200	93100	2.31	97
	homopolymer	8200	9500	1.15	

Additionally, P(HMA-*co*-VBC-*g*-AA) was synthesised to investigate whether an increase in alkyl chain length from BMA, with 4 carbon atoms, to HMA, with 6 carbon atoms, would have any effect on the amount of PAA in the material.

Table 3.10. Results of Synthesis of Graft P(HMA-*co*-VBC-*g*-AA) Copolymers from Functionalised Backbones

Polymer	M_n^b /g mol ⁻¹	M_w^b /g mol ⁻¹	\bar{D}^b	degree of functionalisation ^a /%	ratio nMA:AA ^a
P(HMA- <i>co</i> -VBC)	17200	37200	2.16	-	-
functionalised P(HMA- <i>co</i> -VBC)	31100	70200	2.26	53.1	-
P(HMA- <i>co</i> -VBC- <i>g</i> -AA)	27100	60600	2.23	-	5.90:1

^a determined by ¹H NMR, ^b determined by GPC (THF, PMMA standards)

The results are summarised in **Table 3.10**, with **Figure 3.8** showing a comparison of the molecular weight distributions for the three copolymers. It was found that grafting was successful for the HMA polymer but the ratio of methacrylate to acrylic acid in the material increased from 1.1:1.0 for P(BMA-*co*-VBC-*g*-AA) to 5.9:1.0 for P(HMA-*co*-VBC-*g*-AA), indicating that the amount of acrylic acid grafted on to the HMA backbone was less than 20% of the amount achieved for BMA. This suggests that the steric effect of the alkyl chain length begins to have significance for alkyl methacrylate monomers with chains longer than BMA.

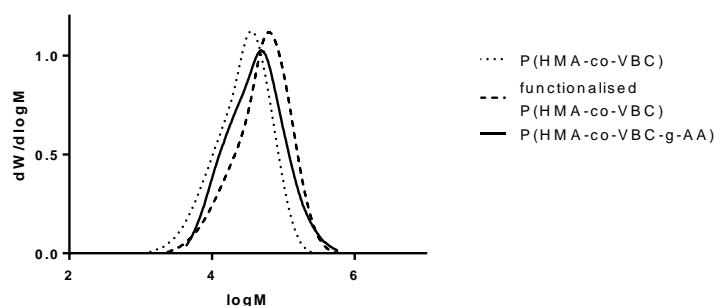


Figure 3.8. Molecular weight distributions determined by GPC (THF, PMMA standards) for: P(HMA-*co*-VBC-*g*-AA) graft polymer (solid line), the functionalised P(HMA-*co*-VBC) backbone from which it is derived (dashed line) and the starting P(HMA-*co*-VBC) polymer (dotted line)

The data was deconvoluted to investigate the presence of homopolymer. **Figure 3.9** demonstrates that a small amount of homopolymer was present but as a minor component, with the graft copolymer comprising 88% of the polymer by mass.

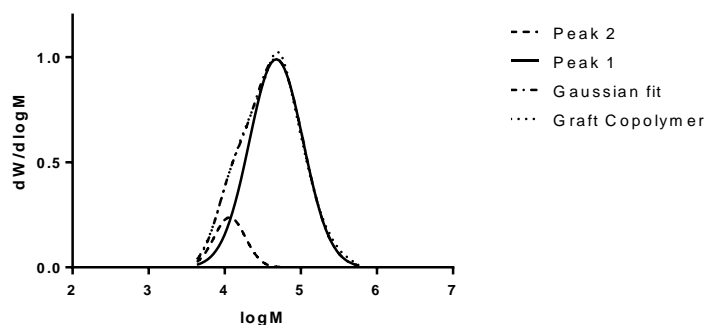


Figure 3.9. Results of deconvolution of molar mass distributions of the P(HMA-*co*-VBC-*g*-AA) graft copolymers shown in Figure 3.8: raw data for graft copolymer (dotted line), Gaussian fit to graft copolymer (alternating dotted-dashed line), peak 1 corresponding to graft copolymer (solid line), peak 2 corresponding to PAA homopolymer (dotted line).

Table 3.11. Results of Deconvolution of Molecular Weight Distributions of Graft P(HMA-*co*-VBC-*g*-AA) Copolymers

Polymer	component	M_n/g mol^{-1}	M_w/g mol^{-1}	\bar{D}	% Graft /wt%
P(HMA- <i>co</i> -VBC- <i>g</i> -AA)	graft copolymer	36800	69700	1.89	88
	homopolymer	11000	13400	1.23	

3.6 Conclusions

Graft poly(alkyl methacrylate-*co*-acrylic acid) copolymers were synthesised in a three-step procedure whereby firstly alkyl methacrylate was copolymerised with VBC to form the backbone. This was then functionalised with pyrrole-1-carbodithioic acid to create in-situ RAFT functional groups pendant to the main chain. It was found that the degree of functionalisation could be much improved by using a heterogeneous reaction system combined with the use of a phase transfer catalyst. The third step involved the growth of PAA grafts from the pendant RAFT groups. Methyl, butyl and lauryl methacrylate analogues of P(nMA-*co*-VBC-*g*-AA) were produced.

The presence of PAA following the grafting reaction was confirmed for P(MMA-*co*-VBC-*g*-AA) and P(BMA-*co*-VBC-*g*-AA) by ¹H NMR and by the appearance of higher molecular weight material in the molecular weight distributions obtained from GPC. Lower molecular weight PAA homopolymer was also observed, however deconvolution of the GPC chromatograms confirmed that the graft copolymer was the main component in all cases.

However, little evidence was found to confirm the successful synthesis of P(LMA-*co*-VBC-*g*-AA). An alternative synthetic route to the target was attempted via grafting of tBA and subsequent hydrolysis to PAA, to investigate whether there was an inherent incompatibility between AA and the hydrophobic backbone. Again, the success of this reaction could not be confirmed and it was postulated that there is a steric effect arising from the long alkyl chain of LMA which is inhibiting grafting. The synthesis of P(HMA-*co*-VBC-*g*-AA) was attempted and found to be successful, although significantly less PAA was grafted than for the MMA and BMA analogues. This suggested that the alkyl chain length could be beginning to have an effect.

4. Synthesis of Poly(Alkyl Methacrylate-*co*-Acrylic Acid) Block and Random Copolymers with Highly Branched and Linear Architectures

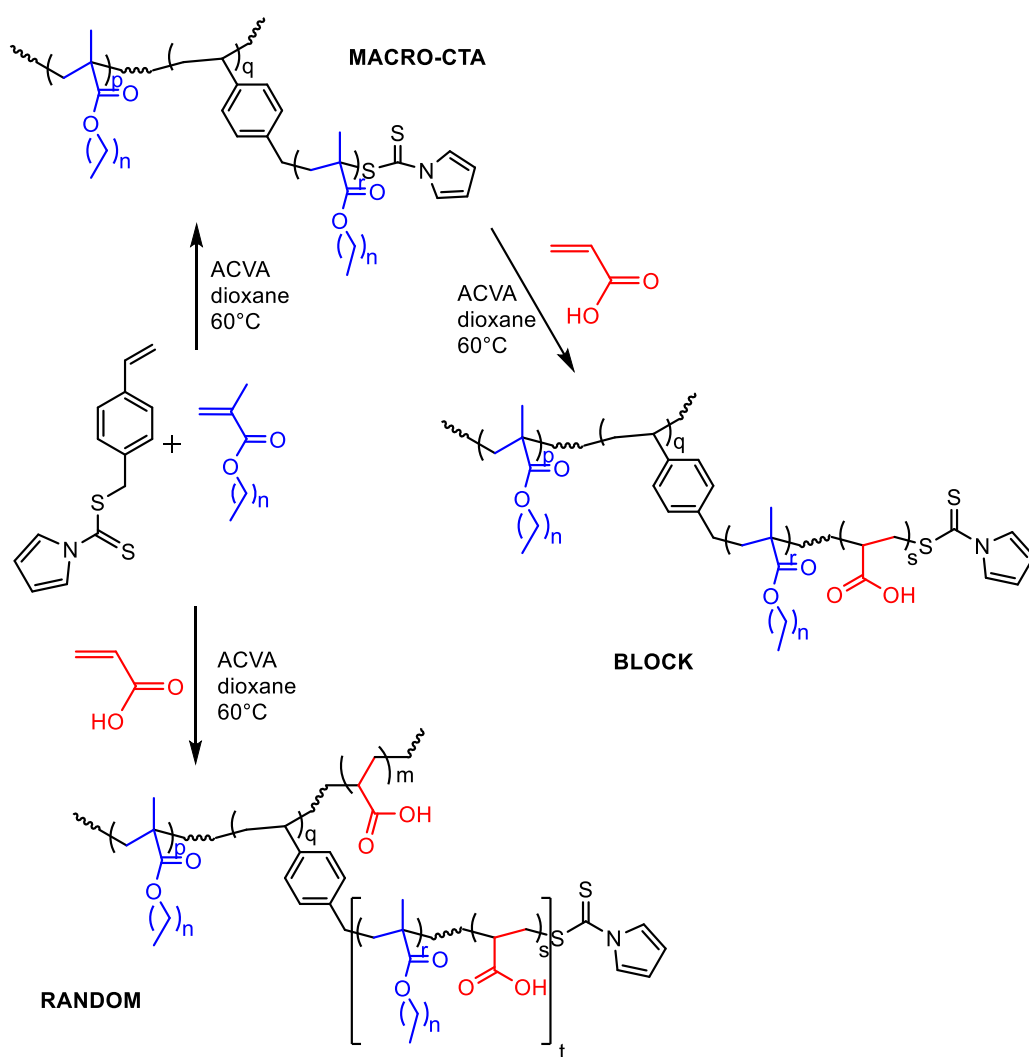
Poly(alkyl methacrylate-acrylic acid) copolymers are synthesised in a range of architectures and monomer sequence distributions: linear and branched copolymers are produced using variations on the same synthesis with a mono- or di-functional RAFT agent, whilst random copolymers are produced in a one-pot synthesis and block copolymers are made by sequential block-addition. ^{13}C NMR is used to confirm block or random monomer sequence distribution, and GPC with viscometric detection is used to verify linear, branched or graft topology.

4.1 Introduction

As previously mentioned, branched polymers, encompassing dendritic, multibranched and highly branched (HB) architectures, exhibit unique properties in terms of solution behaviour and rheology due to the large number of chain ends per molecule that they possess in comparison to linear analogues.^{176, 177} In addition to the utility of these material properties, the chain ends offer the possibility of adding further chemical functionality to the polymer.¹⁷⁸ These branched materials can be produced by chain growth polymerisation via the use of a branching monomer which acts as either monomer and transfer agent¹⁷⁹ or monomer and initiator.⁵⁸ These two functions can be combined in approaches using the addition-fragmentation mechanism to form branched polymers.¹⁸⁰ RAFT polymerisation uses this approach with the additional advantage of being able to modify the end groups of the branched polymer.

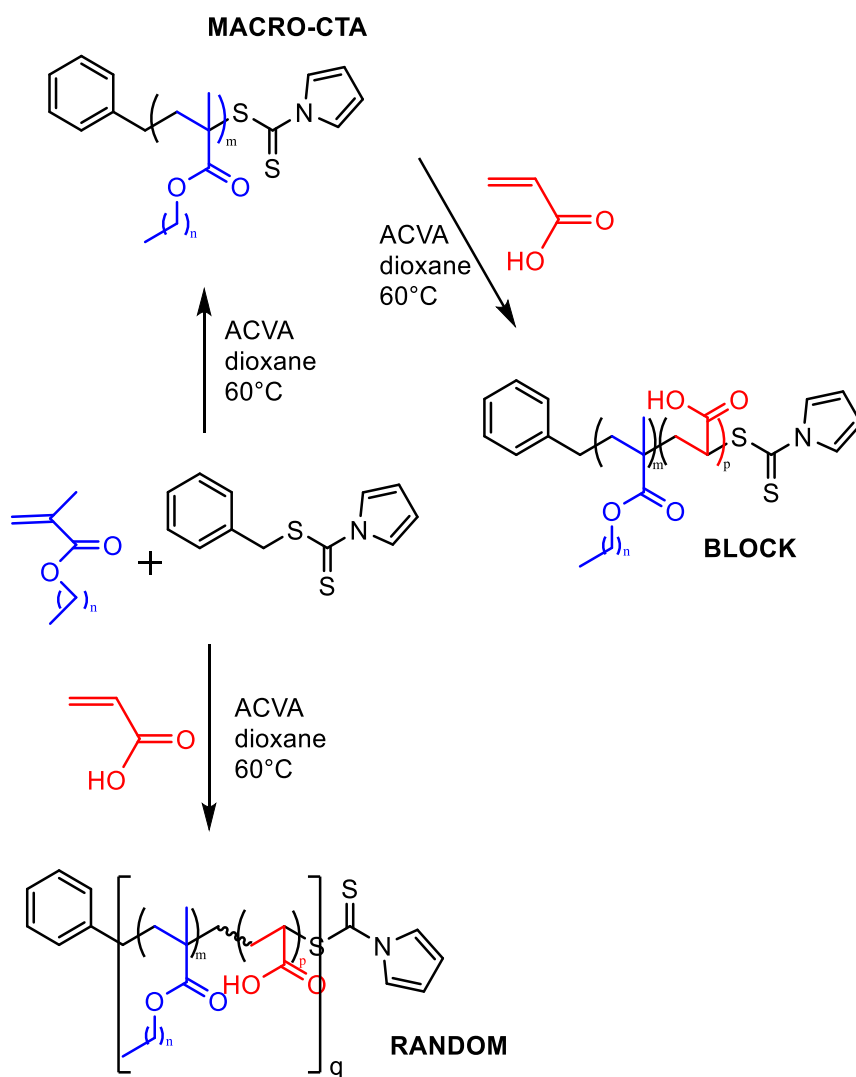
Carter et al. used RAFT to synthesise HB copolymers of NIPAM and 1,2-propandiol-3-methacrylate (P(NIPAM-*co*-GMA)) (GMA = glycerol monomethacrylate) in block and statistical distributions, and proceeded to demonstrate the dependence of the thermal response of these materials on copolymer composition, copolymer sequence distribution and degree of branching.⁶⁴ This was one of the first examples of the synthesis of HB block copolymers using RAFT. More examples have been reported since, such as the work of Peleshanko et al. who synthesised amphiphilic HB polyethylene oxide-*b*-polystyrene (PEO-*b*-PS) copolymers by both RAFT and NMP and found RAFT to give more control over dispersity.¹⁸¹

Scheme 4.1 shows how it is possible to prepare HB block and random copolymers with pyrrole dithioester groups at the chain ends. Combination of both monomers, alkyl methacrylate and acrylic acid, with the RAFT chain transfer agent (CTA) at the start of polymerisation leads to random copolymerisation with monomer sequence dictated by reactivity, as discussed in Chapter 3. Sequential monomer addition, however, initially produces the HB homopolymer, called the macro-CTA, which is then further chain extended by a second monomer to yield HB block copolymer architecture.



Scheme 4.1. Synthesis of HB P(nMA-*b*-AA) block and HB P(nMA-*co*-AA) random copolymers with pyrrole chain ends prepared by RAFT polymerisation

The same synthetic procedure can be used to prepare analogues of these copolymers with linear architectures using a different RAFT agent, benzyl-1-pyrrolicarbodithioate. This has the same structure as the branching RAFT agent used to prepare the HB polymers, 4-vinylbenzyl-1-pyrrolicarbodithioate, but without the vinyl group meaning that it possesses only one polymerisation site and therefore linear polymers are formed. **Scheme 4.2** demonstrates the methodology.



Scheme 4.2. Synthesis of linear P(nMA-*b*-AA) block and linear P(nMA-*co*-AA) random copolymers with pyrrole chain ends prepared by RAFT polymerisation

4.2 Highly Branched Block P(nMA-*b*-AA) Copolymers

The formation of the HB PnMA polymers was enabled by the use of the RAFT CTA 4-vinylbenzyl-1-pyrrole carbodithioate, a dithioate ester that also possesses alkene functionality. This was synthesised via base mediated nucleophilic addition of pyrrole to carbon disulfide, followed by nucleophilic addition with vinylbenzyl chloride. Copolymerisation of each alkyl methacrylate (methyl, butyl and lauryl) with the RAFT CTA produced HB polymers due to the dual action of the CTA: copolymerisation of the styryl double bond and reversible addition-fragmentation chain transfer with the dithioate group.

The structures in **Scheme 4.1** demonstrate that the pyrrole groups are situated at the chain ends of the polymer whereas the styryl groups create a branching point within the polymer structure. Analysis of these polymers by ^1H NMR showed the presence of the pyrrole groups at the ends of the polymer branches at $\delta = 6.34$ and 7.72 ppm. Broad peaks due to the styryl units were also observed between 7.30 and 7.45 ppm. These can be seen in the expanded region of **Figure 4.1**. Average values of degrees of branching (DB) were calculated by first comparing the methacrylate protons at around 0.90 ppm to the aromatic protons from the styryl and pyrrole groups in the region $6.34 - 7.72$ ppm to give the average number of repeat units per branch (RB). DB is then calculated as the reciprocal of the RB value. The associated error in the measurement of the integration of NMR signals was estimated to be $\pm 5\%$.⁶³

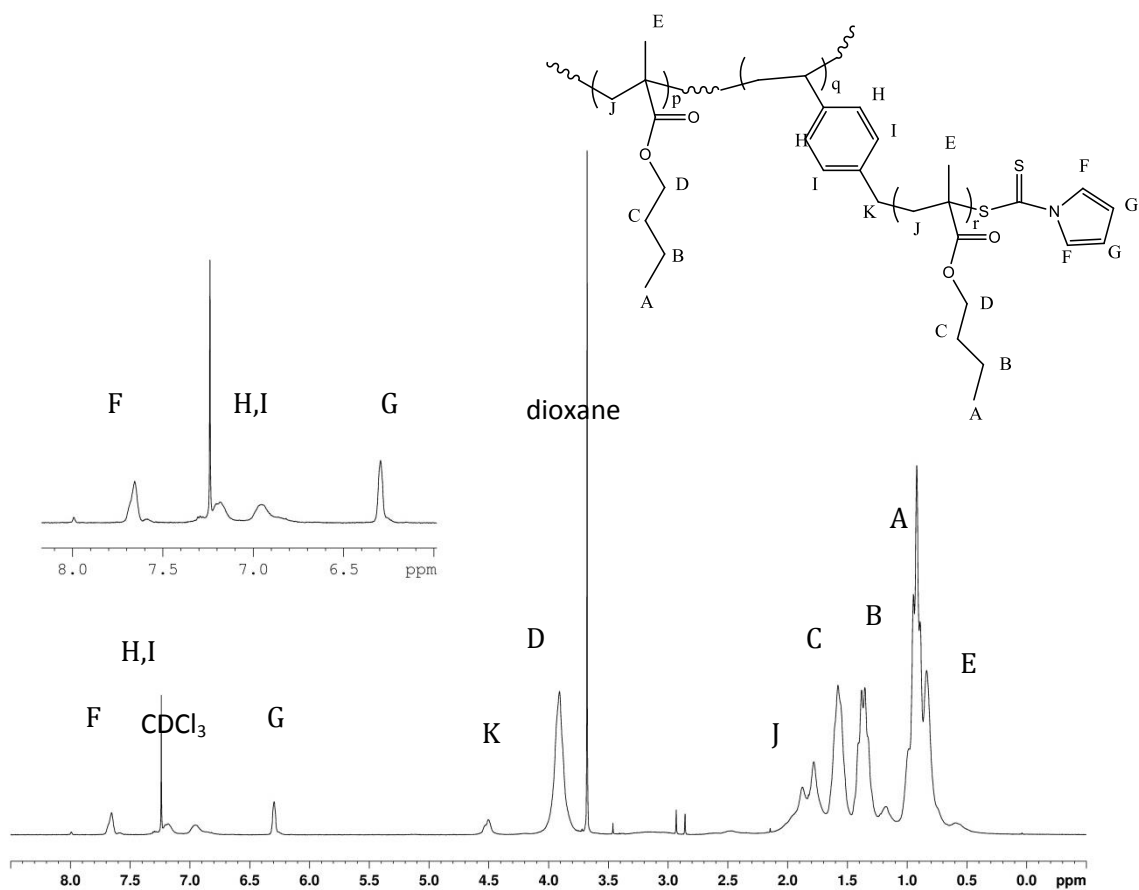


Figure 4.1. ^1H NMR spectrum of HB PBMA, with the expanded region showing the peaks due to the pyrrole groups (F and G) and the peaks due to the styryl group (H and I)

Table 4.1. Results of RAFT Polymerisation of Alkyl Methacrylates to Form HB PnMA Macro-CTAs and HB P(nMA-*b*-AA) Block Copolymers

polymer	conversion ^a /%	molar feed ratio nMA:AA	molar ratio nMA:AA	DB ^a	M _n ^b / g mol ⁻¹	M _w ^b / g mol ⁻¹	Đ ^b
PMMA	55	-	-	0.25	13500	27300	2.02
PBMA	88	-	-	0.36	18000	35800	1.99
PLMA	77	-	-	0.25	30800	64700	2.10
HB P(MMA- <i>b</i> - AA)	93	0.7:1.0	1.1:1.0	0.24	29500	118300	4.00
HB P(BMA- <i>b</i> - AA)	97	0.5:1.0	1.4:1.0	0.12	40000	139900	3.50
HB P(LMA- <i>b</i> -AA)	99	0.3:1.0	0.7:1.0	N/A	34800	328000	9.44

^a determined by ¹H NMR ^b determined by GPC (THF, PMMA standards)

Table 4.1 displays the results of the syntheses of both the homopolymer macro-CTAs, and also the copolymers. ¹H NMR analysis showed the appearance of peaks in the ¹H NMR spectra of the copolymers at $\delta = 1.63$ and 2.22 ppm due to PAA. The ratio of methacrylate to acrylic acid within the copolymers could also be calculated from the ¹H NMR spectra. The amount of PAA in all three copolymers was less than the feed ratio, although the HB P(MMA-*b*-AA) had the closest results to the feed ratio with a factor of 1.6 times as much PMMA in the copolymer than was intended. However, less PAA was observed for the HB P(BMA-*b*-AA) and HB P(LMA-*b*-AA) materials, with 2.8 times as much PBMA in the HB P(BMA-*b*-AA) copolymer and 2.3 times as much PLMA in the HB P(LMA-*b*-AA). This could be due to the steric influence of the increasing alkyl chain length affecting the ability of the AA monomer to approach the

active sites. However, this does not explain why more PAA was observed in the HB P(LMA-*b*-AA) material than the HB P(BMA-*b*-AA), despite the longer alkyl chain of LMA. DB was calculated for all of the macro-CTAs and the block copolymers, except for HB P(LMA-*b*-AA) where the pyrrole and styryl groups could not be clearly seen in the ^1H NMR spectrum meaning that the calculation could not be performed. HB PBMA was the most branched of the macro-CTAs but the corresponding block copolymer was much less branched, whereas the DB was fairly constant for HB PMMA and the corresponding copolymer. A decrease in DB would be expected, as linear PAA chains are being added to a branched PnMA unit, leading to a greater number of repeat units per branch.

The copolymers were methylated with trimethylsilyldiazomethane, as described previously in Chapter 3, to allow analysis by GPC using THF as the eluent without column interactions becoming a problem. An increase in molar mass was observed following addition of the second block to the copolymers. Much larger dispersities were also seen for the copolymers compared to the macro-CTAs. These are presented in **Figure 4.2**, where the traces with the dashed line show the macro-CTA data and the solid lines show the copolymer data. The HB P(LMA-*b*-AA) copolymer in particular exhibits a very broad and multimodal molecular weight distribution. This can be indicative of a highly branched polymer, but also suggests the possible presence of other species, for example the low molecular weight peak could be PAA homopolymer and the high molecular weight peak could be explained by the formation of copolymer di- or trimers.

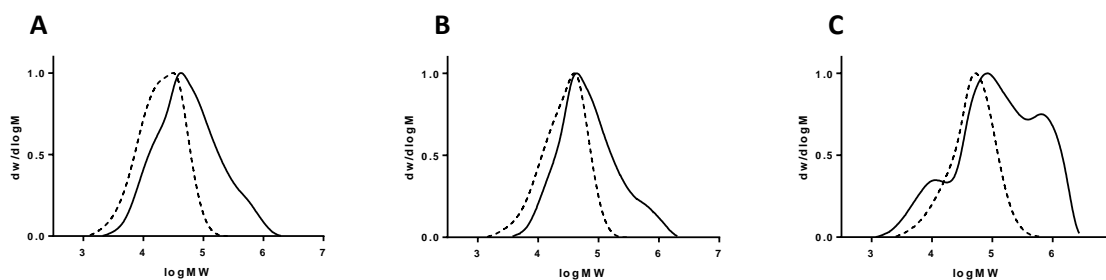


Figure 4.2. A comparison of molecular weight distributions obtained from GPC: A) HB PMMA (dashed line) and HB P(MMA-*b*-AA) (solid line), B) HB PBMA (dashed line) and HB P(BMA-*b*-AA) (solid line) and C) HB PLMA (dashed line) and HB P(LMA-*b*-AA) (solid line)

4.3 Highly Branched Block P(AA-*b*-nMA) Copolymers

The previous synthesis was adapted to form a block copolymer with the hydrophobic and hydrophilic segments reversed. Firstly a HB PAA macro-CTA was synthesised to form the core, followed by the addition of PnMA chains to form the second blocks of the HB copolymers. The results of the syntheses are summarised in **Table 4.2**. Calculation of integrals from the ^1H NMR spectra showed that a greater degree of branching was seen than for the PnMA macro-CTAs, possible due to the smaller size of the AA monomer. Again the ^1H NMR analysis showed RAFT groups remaining in the polymer, enabling the addition of the second block.

Table 4.2. Results of RAFT Polymerisation of Acrylic Acid to Form HB PAA Macro-CTA and HB P(AA-*b*-nMA) Block Copolymer

polymer	conversion ^a /%	molar feed ratio nMA:AA	molar ratio nMA:AA ^a	DB ^a	M _n ^b / g mol ⁻¹	M _w ^b / g mol ⁻¹	Đ ^b
HB PAA	88	-	-	0.33	13600	84200	6.10
HB P(AA- <i>b</i> -MMA)	78	0.7:1.0	1.1:1.0	0.13	12600	119200	9.43
HB P(AA- <i>b</i> -BMA)	93	0.5:1.0	1.7:1.0	0.09	13000	146000	11.20
HB P(AA- <i>b</i> -LMA)	81	0.3:1.0	0.4:1.0	0.26	23000	75200	3.26

^a determined by ^1H NMR ^b determined by GPC (THF, PMMA standards)

The dispersity of the PAA macro-CTA is much larger than those of the alkyl methacrylate macro-CTAs shown in Table 4.1. The PAA macro-CTA had to be methylated before GPC analysis was carried out. As the PAA macro-CTA contains a much greater number of acid groups than materials with PAA grafted on or added as a second block, it is possible that they were not fully methylated and some acid

functionality remained, leading to column interaction and an inaccurate GPC result. Alternatively this RAFT CTA may be less well suited to acrylic acid than to the methacrylate monomers leading to a loss of control over the polymerisation and consequently a large dispersity; the choice of RAFT CTA needs to be optimized for the desired system.¹⁸² Clearly this is not trivial for the synthesis of copolymers comprised of monomers such as acrylic acid and alkyl methacrylates with vastly different properties. As a result, some compromises in reactivity are required to allow the desired materials to be synthesised.

Table 4.2 also summarises the results of the copolymer syntheses. In the case of these copolymers it was the HB P(AA-*b*-LMA) analogue which had a molar ratio closest to the feed ratio, as determined by measuring the integrals in the ¹H NMR spectra. HB P(AA-*b*-MMA) and HB P(AA-*b*-BMA) showed a greater amount of methacrylate in the polymers than the proportion in the feed. All three copolymers have a lower DB than the macro-CTA, which is as expected since more linear units have been added onto the branched core so the number of repeat units per branch should have increased therefore incurring a decrease in DB. The HB P(AA-*b*-LMA) copolymer had the lowest decrease in DB from that of the macro-CTA, since this copolymer had the least amount of methacrylate added.

Comparison of the molecular weight distributions obtained from GPC analysis of the macro-CTA and block copolymers are shown in **Figure 4.3**. It can be clearly seen that the PAA macro-CTA, represented on the distributions as the dashed trace, has a very broad bimodal distribution. The lower molecular weight peak is not seen on the chromatograms of the block copolymers. A larger higher molecular weight shoulder is seen for the HB P(AA-*b*-MMA) and HB P(AA-*b*-BMA) copolymers. This is not observed for the HB P(AA-*b*-LMA) copolymer, and consequently no real increase is observed in M_n and M_w values for this material.

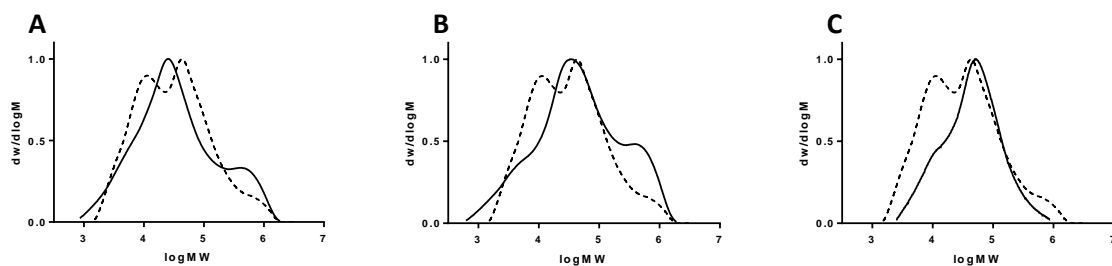


Figure 4.3. A comparison of molecular weight distributions obtained from GPC: A) HB PAA (dashed line) and HB P(AA-*b*-MMA) (solid line), B) HB PAA (dashed line) and HB P(AA-*b*-BMA) (solid line) and C) HB PAA (dashed line) and HB P(AA-*b*-LMA) (solid line)

4.4 Highly Branched Random P(*n*MA-*co*-AA) Copolymers

The same synthetic route was used to successfully synthesise HB P(*n*MA-*co*-AA) random copolymers by adding both monomers into a one-pot synthesis, as shown in **Scheme 4.1**. **Table 4.3** summarises the results. It can be seen that the longer the alkyl chain of the methacrylate monomer, the more PAA was incorporated into the copolymer. This is likely to be because MMA reacts much faster than AA whereas LMA is much slower to react than MMA and is therefore more comparable with the rate of AA polymerisation. This is also why the DB is higher for the P(LMA-*co*-AA) copolymer. DB is the reciprocal of RB, and P(LMA-*co*-AA) will have shorter branches as the rate of polymerisation is slower.

Table 4.3. Results of Syntheses of HB Random P(nMA-*co*-AA) Copolymers

polymer	conversion ^a /%	molar feed ratio nMA:AA	molar ratio nMA:AA ^a	DB ^a	M _n ^b / g mol ⁻¹	M _w ^b / g mol ⁻¹	Đ ^b
HB P(MMA- <i>co</i> -AA)	55	0.7:1.0	6.1:1.0	0.14	7400	31300	4.23
HB P(BMA- <i>co</i> -AA)	52	0.5:1.0	5.1:1.0	0.14	6500	20000	3.07
HB P(LMA- <i>co</i> -AA)	55	0.3:1.0	0.8:1.0	0.28	4100	13200	3.22

^a determined by ¹H NMR ^b determined by GPC (THF, PMMA standards)

The molecular weight distributions of the three random copolymers are shown in **Figure 4.4**. These were obtained following methylation of the copolymers. The HB P(LMA-*co*-AA) copolymer had the lowest molecular weight of the three materials. Again this is possibly due to the slower reaction rate of the LMA monomer. The HB P(MMA-*co*-AA) and HB P(BMA-*co*-AA) copolymers had much more similar distributions, and all three copolymers had significantly lower molecular weights than the HB block materials. This suggests that the one-pot reaction allows a greater degree of control over the polymerisations compared to the stepwise block copolymer syntheses.

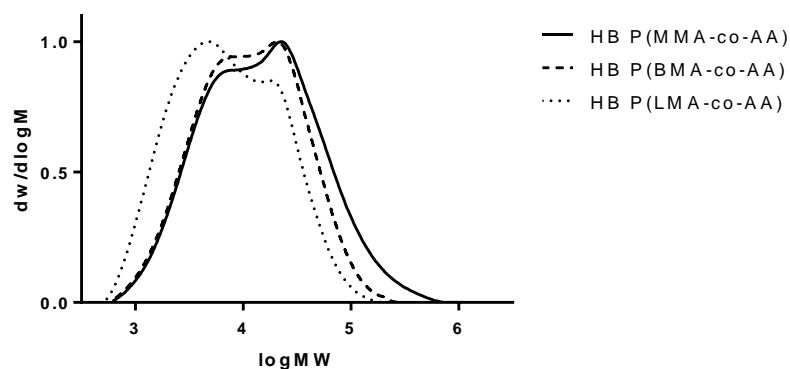


Figure 4.4. A comparison of molecular weight distributions obtained from GPC: A) HB P(MMA-*co*-AA) (solid line), B) P(BMA-*co*-AA) (dashed line) and C) HB P(LMA-*co*-AA) (dotted line)

4.5 Linear Block P(*n*MA-*b*-AA) Copolymers

An analogous synthetic procedure was carried out to synthesise linear versions of the block copolymers. A different RAFT agent was used, benzyl-1-pyrrolicarbodithioate, which has the same structure as that used for the HB polymers, 4-vinylbenzyl-1-pyrrolicarbodithioate, but without the vinyl group which allows polymerisation from a second site. **Figure 4.5** shows a comparison of the two structures.

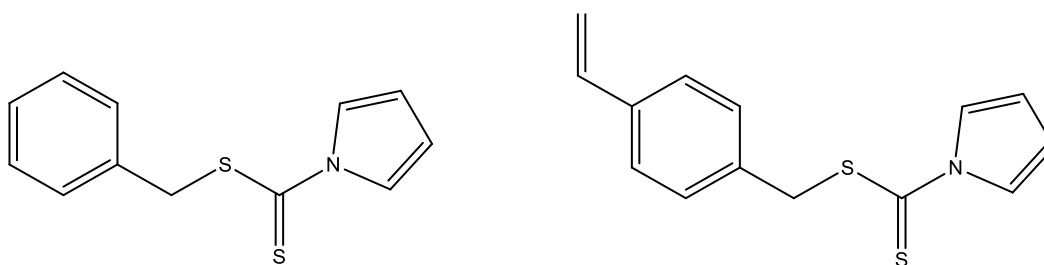


Figure 4.5. A comparison of the structures of the branching RAFT agent, 4-vinylbenzyl-1-pyrrolicarbodithioate, and the linear RAFT agent benzyl-1-pyrrolicarbodithioate

Table 4.4 summarises the results of the macro-CTA and block copolymer syntheses. All three polymerisations of the macro-CTAs went to fairly high conversion. The molecular weights of the PMMA and PBMA materials are consistent, although much higher values were obtained for the PLMA polymer. All polymers exhibit a dispersity of between 2 and 3, which is fairly high for linear chains.

^1H NMR showed that the actual molar ratios of PnMA and PAA in the copolymers were similar to the molar feed ratios, although less PAA was present in the P(LMA-*b*-AA) polymer. The polymerisations of P(MMA-*b*-AA) and P(BMA-*b*-AA) went to very high conversion, whilst the P(LMA-*b*-AA) reaction only reached a conversion of 40%. This is likely to be due to the slower reactivity of LMA. Increases in molecular weight were observed for P(MMA-*b*-AA) and P(BMA-*b*-AA), accompanied by larger dispersities. An increase in lower molecular weight species was also observed for the P(MMA-*b*-AA) and P(BMA-*b*-AA) polymers, which is possibly due to the presence of PAA homopolymer. This was not the case for the P(LMA-*b*-AA) polymer, however, which actually decreased in molecular weight. This could be due to the very high hydrophobicity of the long alkyl unit of LMA affecting the solution conformation of the polymer. This would have an effect on the hydrodynamic volume, which is what is measured by GPC rather than the actual molecular weight of the polymer. **Figure 4.5** presents a comparison of the molecular weight distributions of the macro-CTAs and block copolymers.

Table 4.4. Results of RAFT Polymerisation of Methacrylate Monomer to Form Linear PnMA Macro-CTAs and Block Copolymers

polymer	conversion ^a /%	molar feed ratio nMA:AA	molar ratio nMA:AA ^a	M_n^b / g mol ⁻¹	M_w^b / g mol ⁻¹	\mathcal{D}^b
PMMA	82	-	-	20700	40400	1.95
PBMA	88	-	-	21200	43900	2.07
PLMA	92	-	-	59700	137500	2.30
P(MMA- <i>b</i> -AA)	99	0.7:1.0	0.8:1.0	10600	43100	4.06
P(BMA- <i>b</i> -AA)	99	0.5:1.0	0.4:1.0	9200	50300	5.47
P(LMA- <i>b</i> -AA)	40	0.3:1.0	1.1:1.0	46000	104200	2.27

^a determined by ¹H NMR ^b determined by GPC (THF, PMMA standards)

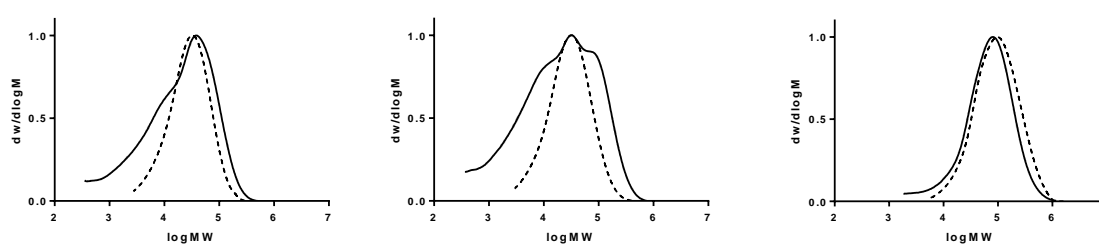


Figure 4.6. A comparison of molecular weight distributions obtained from GPC: A) PMMA (dashed line) and P(MMA-*b*-AA) (solid line), B) PBMA (dashed line) and P(BMA-*b*-AA) (solid line) and C) PLMA (dashed line) and P(LMA-*b*-AA) (solid line)

4.6 Linear Random P(nMA-co-AA) Copolymers

Linear random copolymers were synthesised using the linear RAFT agent in one-pot syntheses, the results of which are displayed in **Table 4.5**. In contrast to the linear block materials, less PAA was present in the copolymer for the P(MMA-co-AA) and P(BMA-co-AA) and more PAA in the P(LMA-co-AA) polymer. The molecular weight data, shown in Figure 4.7, indicates that these reactions were well-controlled as the M_n and M_w values for the three polymers were similar and the dispersity values were much lower than those of the linear block copolymers.

Table 4.5. Results of Syntheses of Linear Random P(nMA-co-AA) Copolymer

polymer	conversion ^a /%	molar feed ratio nMA:AA	actual ratio nMA:AA ^a	M_n^b / g mol ⁻¹	M_w^b / g mol ⁻¹	\bar{D}^b
P(MMA-co-AA)	65	0.7:1.0	1.7:1.0	12000	23400	1.95
P(BMA-co-AA)	87	0.5:1.0	2.2:1.0	10000	19800	1.96
P(LMA-co-AA)	71	0.3:1.0	0.5:1.0	8600	16100	1.86

^a determined by ¹H NMR ^b determined by GPC (THF, PMMA standards)

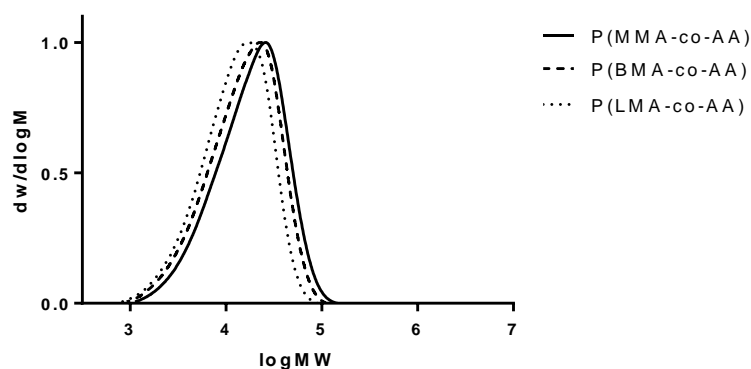


Figure 4.7. A comparison of molecular weight distributions obtained from GPC: A) P(MMA-co-AA) (solid line), B) P(BMA-co-AA) (dashed line) and C) P(LMA-co-AA) (dotted line)

4.7 ¹³C NMR to Study Monomer Sequence Distribution

The statistical analysis of polymers was developed by Bovey¹⁸³ and Price,¹⁸⁴ who showed that copolymer statistics could be used to analyse the abundance of monomer sequences within polymer chains using NMR spectroscopy. ¹³C NMR has been shown to be an effective technique for measuring or estimating the triad composition of a copolymer.^{185, 186} The differential nuclear Overhauser effect (NOE) enhancement is approximately equal for similar carbons within different chemical sequences.¹⁸⁷ Additionally, it is generally accepted that for non-protonated carbons with restricted mobility, such as those within polymers, the residual spin-lattice relaxation times (T_1) are of similar order.¹⁸⁷ These assumptions form the basis of the study of copolymer structure using ¹³C NMR spectroscopy.

Triads are a sequence of three monomer units within a polymer chain. In a copolymer composed of two different monomer units, there are six different triad possibilities. If the monomers are represented by A and B, the possible triads are:

AAA, BBB, ABA, BAB, AAB, BAA, ABB, BBA

These eight triads can be reduced to six as AAB and BAA are equivalent and undistinguishable by spectroscopy since the sequences differ only by directionality. The same is true for ABB and BBA. Therefore the six triads are:

AAA, BBB, ABA, BAB, AAB, ABB

The copolymers we are considering in this case contain the monomers acrylic acid and butyl methacrylate. Therefore both monomers contain a carboxyl functional group. This group is sensitive to the effects of the chain microstructure, enabling the identification of triads.¹⁸⁸ If a copolymer contained all of these sequences of monomer units, we would expect to see a distribution of six peaks. This would be more likely in a random copolymer where the two monomers would be randomly distributed throughout the sequence. In a block copolymer, on the other hand, we would expect there to be long sequences of AAA and BBB triads with only a very small region where the two sequences meet; hence we would expect to see few peaks due to the presence of few of the possible triads.

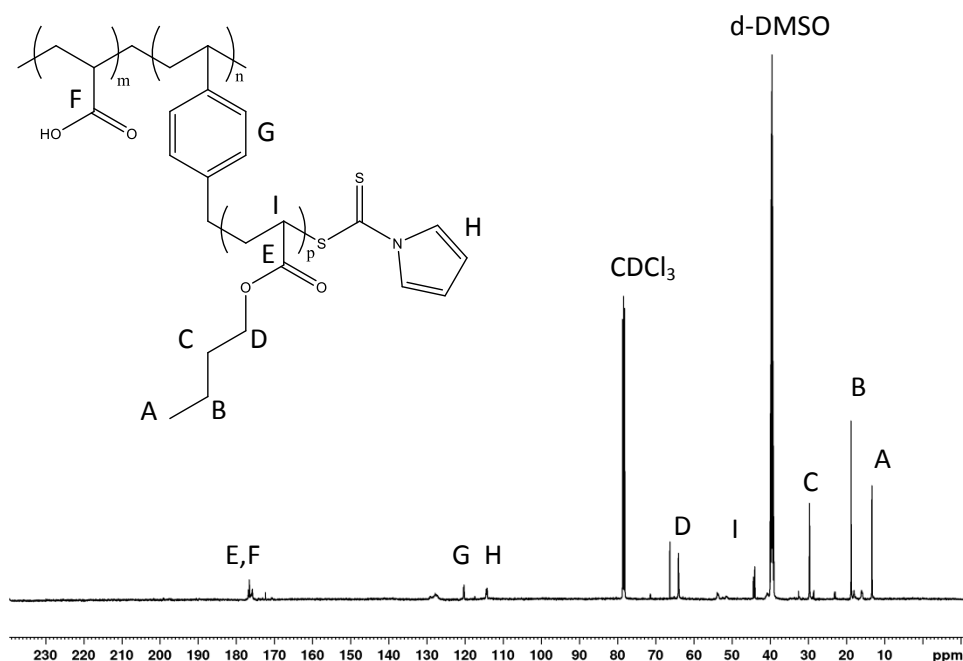


Figure 4.8. An example of a ^{13}C NMR spectrum of a P(BMA-*b*-AA) copolymer: in this case HB P(AA-*b*-BMA)

^{13}C NMR studies were carried out on the set of P(BMA-*co*-AA) copolymers which were synthesised for use in printing studies. The synthesis and characterisation of these materials is reported in Section 8.2 of Chapter 8. **Figure 4.8** shows an example of the ^{13}C NMR spectra obtained from the copolymers. The same peaks are seen for all materials as they are all composed from the same monomers. The region of interest is the carbonyl region, which occurs between 174 and 178 ppm. **Figure 4.9** below shows an expansion of this region for each copolymer, demonstrating the distribution of peaks observed.

Fine structure was observed in the carboxyl peaks of the ^{13}C NMR spectra of the PBMA and PAA homopolymers. This arises due to the effects of polymer tacticity.¹⁸⁹ Unfortunately as a result, the fine structure in the copolymer carbonyl peaks cannot be attributed solely to the copolymeric effect of the triads. However, the results can nevertheless serve as an empirical guide to the monomer sequence distribution within the copolymers. When the spectra of the branched and linear random copolymers are

compared with those of the block and graft materials, it is seen the random copolymers have much broader distributions of peaks with a lot more noise in the signal. However, in the block and graft copolymers where the BMA and AA monomers are present as long separate sequences of each monomer, discrete distributions of sharp peaks are seen. This enables a facile method of identification between block and random copolymers.

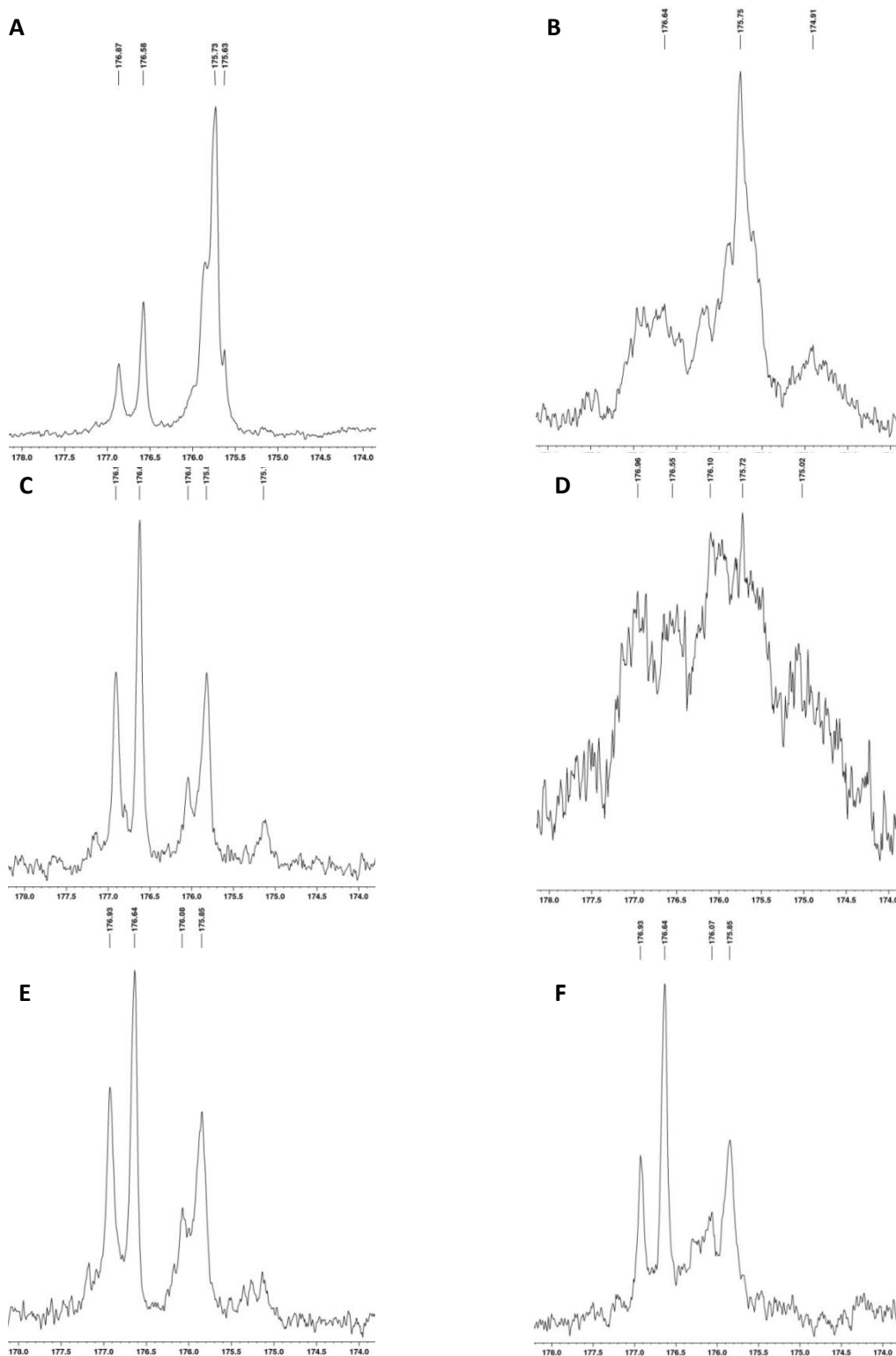


Figure 4.9. Carbonyl region of ^{13}C NMR spectra of P(BMA-*b*-AA) copolymers showing the distribution of triad peaks: A) linear P(BMA-*b*-AA) B) linear P(BMA-*co*-AA) C) graft P(BMA-*co*-VBC-*g*-AA) D) HB random P(BMA-*co*-AA) E) HB block P(BMA-*b*-AA) F) HB block P(AA-*b*-BMA). The scale represents chemical shift in ppm.

4.8 GPC-Viscometry

Conventional Gel Permeation Chromatography (GPC) typically employs a Refractive Index (RI) detector to obtain a measure of polymer size in terms of the hydrodynamic radius. The RI detector provides a signal which is proportional to the concentration of the sample as it elutes from the column. Thus a weight distribution is obtained as the signal voltage varies with elution time in response to the variation in sample concentration. However, RI detection alone does not provide information on the shape of the polymer molecules, as it only separates components by size.

Full characterisation of polymer systems can be obtained by using a triple detection system, which combines RI detection with viscometric and light scattering detectors. This allows determination of the distributions of molecular weight, intrinsic viscosity and size over the full molecular weight range.¹⁹⁰ However this equipment was not available within the department, so a dual detection system coupling RI and viscometry was employed.

The principle of universal calibration is based on the direct proportionality of the product of intrinsic viscosity ($[\eta]$ or IV), and molecular weight to the hydrodynamic volume. This allows the creation of a calibration curve giving the size of polymer molecules over the retention volume, which is independent of the chemical structure and composition of the polymer standards used.¹⁹¹ This solves one main issue with conventional calibration which is the difficulty of finding appropriate standards with similar chemical structure to the sample being studied. This is particularly difficult for the study of copolymers.

Analysis of the copolymer samples with the dual detection GPC system provided distributions of intrinsic viscosity and absolute molecular weight for each copolymer. Copolymers were methylated before analysis to prevent interaction between the column and the carboxylic groups on the PAA segments, using the same method outlined in Chapter 3.

Further information can be obtained from these data. **Equation 4.1** gives the Mark-Houwink relation, where $[\eta]$ is the intrinsic viscosity, M is the molar mass, and K and α are the Mark-Houwink parameters.

$$[\eta] = KM^\alpha \qquad \text{Equation 4.1}$$

The value of the α parameter provides empirical information on the conformation of the polymer, and hence the level of branching. For an ideal polymer coil in solution the α value is typically between 0.6 and 0.8. More compact structures such as branched polymers have lower values of α ; below 0.5 can be expected. Construction of a Mark-Houwink plot of $\log IV$ against $\log MW$ allows determination of α from calculation of the gradient.

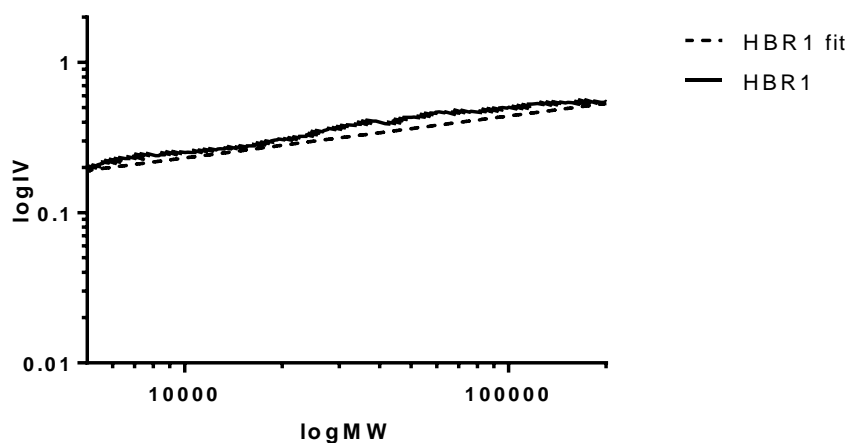


Figure 4.10. Mark-Houwink plot of \log intrinsic viscosity (IV) against \log molecular weight (MW) showing comparison of raw data (solid line) and fitted data (dashed line)

Figure 4.10 shows the Mark-Houwink plot for one of the copolymers, HBR1 (HB P(MMA-*co*-AA)). The raw data obtained from the viscometer is shown as the solid line and a fit to the data is shown as the dashed line. The fitted data are used in the following graphs to enable clearer representation of the results.

Figure 4.11 is a combined Mark-Houwink plot of the full set of copolymers. The key is explained in the figure caption. The three groups of materials, linear, branched and graft, are plotted in different colours for clarity. It can be observed that the linear copolymers, shown in purple, have steeper gradients than those of the branched copolymers, shown in blue. The graft copolymers, shown in green, have gradients between those of the linear and branched materials. This is reasonable as at a basic level a graft copolymer is a series of linear chains, with periodic branching; hence somewhere between a linear and a branched polymer.

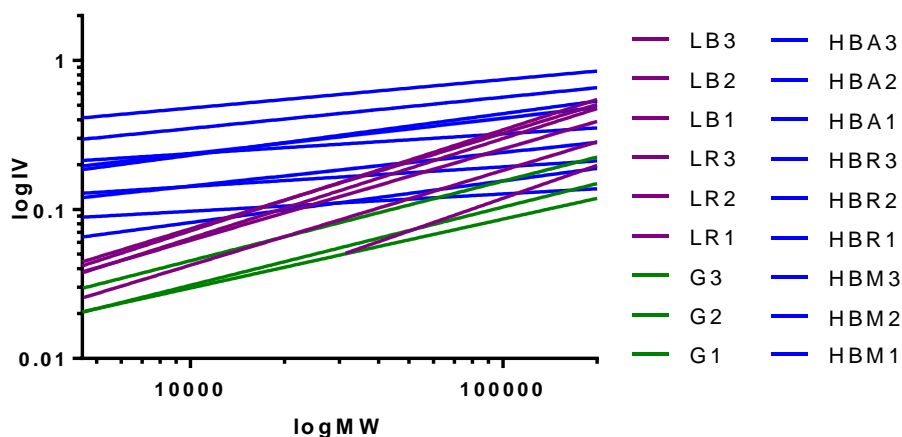


Figure 4.11. Mark-Houwink plot of log intrinsic viscosity (IV) against log molecular weight (MW) showing comparison of linear copolymers (purple), graft copolymers (green) and branched copolymers (blue) (key: letters refer to architecture and distribution HBR = highly branched random, HBM = highly branched methacrylate core, HBA = highly branched acrylic acid core, G = graft, LB = linear block and LR = linear random, numbers refer to methacrylate monomer 1 = MMA, 2 = BMA and 3 = LMA)

Calculated values of α for each copolymer are plotted in **Figure 4.12**. The three sets of branched copolymers, HBM (HB block with methacrylate core), HBR (HB random), and HBA (HB block with acrylic acid core), were all found to have α below 0.4. This is consistent with a compact, branched structure. The graft copolymers, G, had values of α between 0.4 and 0.6 meaning that they fall within the border region. The structures are more compact than an ideal linear chain but do not possess a high degree of branching. However, the linear copolymers, LB (linear block) and LR (linear random), were found to have α between 0.6 and 0.8, as expected for linear chains.

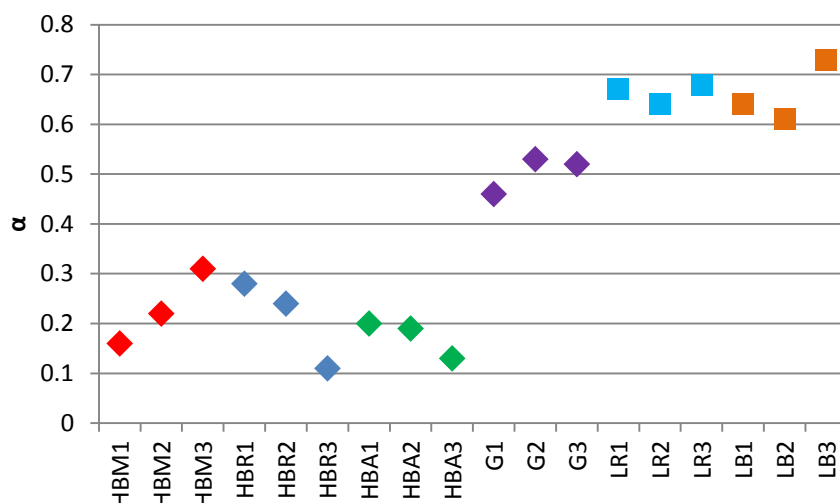


Figure 4.12. A graph showing the values of the Mark-Houwink parameter α obtained as the gradient of the Mark-Houwink plot of $\log IV$ against $\log MW$ for each copolymer (key: letters refer to architecture and distribution HBM = highly branched methacrylate core (red), HBR = highly branched random (dark blue), HBA = highly branched acrylic acid core (green), G = graft (purple), LB = linear block (light blue) and LR = linear random (orange), numbers refer to methacrylate monomer 1 = MMA, 2 = BMA and 3 = LMA)

Another quantitative measure of branching is provided by the contraction factor, g' . This is given by a ratio of the intrinsic viscosity of a branched polymer to the intrinsic viscosity of a linear polymer of equivalent chemical structure and molecular weight, as shown in **Equation 4.2**.

$$g' = \frac{[\eta]_{branched}}{[\eta]_{linear}} \quad \text{Equation 4.2}$$

Values of g' were calculated for each of the branched and graft copolymers. The equivalent linear block copolymer was used as the linear analogue for the HB block and graft copolymers (P(MMA-*b*-AA) for HB P(MMA-*b*-AA) and P(BMA-*b*-AA) for HB P(BMA-*b*-AA) etc.). The equivalent linear random copolymer was used for the HB random copolymers.

Figure 4.13 demonstrates the relationship between contraction factor g' and log molecular weight. The data would be expected to scale according to degree of branching, with the polymers having the most extensive branching at the bottom of the graph and the least branched polymers at the top. Values of g' for all polymers are expected to converge to $g' = 1$ at the low molecular weight limit. However the data from this set of copolymers show significant deviations from the expected behaviour. An almost linear relationship is seen for the set of graft copolymers, with g' values converging to $g' = 1$ at low molecular weight as expected. Conversely, g' is seen to decrease with increasing molecular weight for the three sets of branched copolymers. The data sets are not ordered according to the degree of branching as assessed by the α values, as would have been expected, but rather appear to be grouped according to composition. This appears to show that there are differences in intrinsic viscosity between the different compositional groups of copolymers, as the three branched groups, HBM, HBA and HBR are clearly separated. This suggests that the intrinsic viscosity is influenced by copolymer composition.

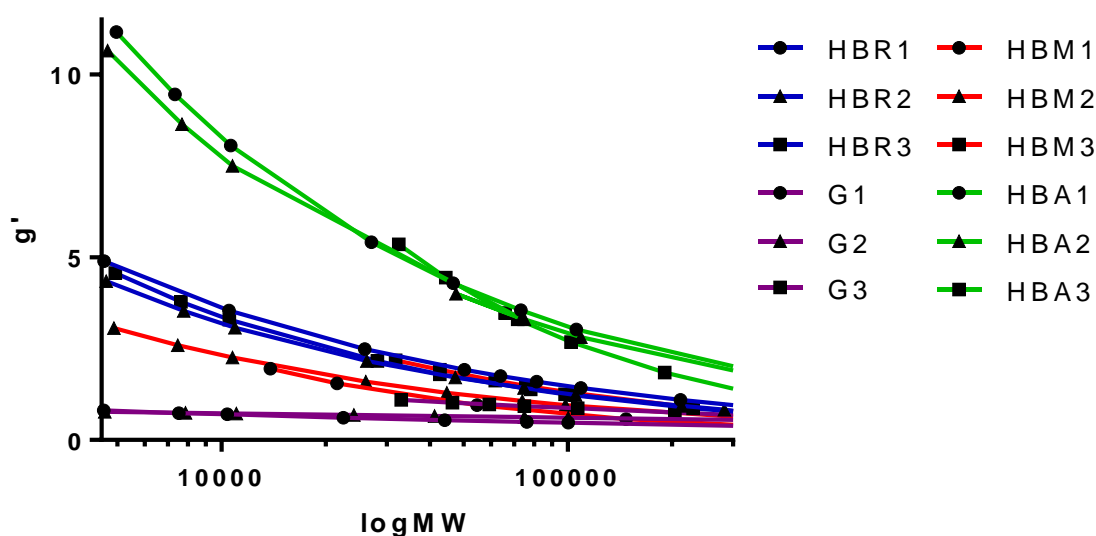


Figure 4.13. A graph showing the contraction factor g' against log molecular weight for each copolymer (key: letters refer to architecture and distribution HBR = highly branched random (blue), HBM = highly branched methacrylate core (red), HBA = highly branched acrylic acid core (green), G = graft (purple), numbers refer to methacrylate monomer 1 = MMA, 2 = BMA and 3 = LMA)

4.9 Conclusions

Poly(alkyl methacrylate-*co*-acrylic acid) copolymers have been successfully synthesised in a range of architectures. Branched copolymers were produced via a combination of RAFT and SCVP employing a CTA with both dithioester and vinyl functional groups. The same synthetic route was used to synthesise linear copolymers using a version of the same CTA having only the dithioester group. A two-step polymerisation procedure enabled the production of block copolymers by first creating a macro-CTA by polymerising the first monomer followed by chain extension with the second monomer to form a diblock. Two versions of the branched block copolymer were synthesised, one with the hydrophobic block forming the core and hydrophilic side chains, and the other with the opposite structure. Random copolymer analogues were also produced through a one-pot reaction. Methyl, butyl and lauryl methacrylate version of each copolymer were made, resulting in a set of 15 different copolymers.

An M_n of 20000 g mol^{-1} was targeted because this is low enough for printing applications. Variation in M_w and M_n values was observed, although the majority of the copolymers fell within the desired range. Broad molecular weight distributions were observed for the branched copolymers. The linear block copolymers also displayed much larger dispersity values than expected for linear copolymers. Coupled with the particularly broad distribution of the HB PAA macro-CTA, this suggests that this particular RAFT CTA does not provide good control over the polymerisation of PAA. Given the very different characteristics of acrylic acid and the alkyl methacrylate monomers, however, it would be difficult to optimise a reaction system to suit both.

^{13}C NMR provides an empirical method of confirming a block or random monomer sequence distribution within a copolymer chain through studying the distribution of peaks in the carbonyl region. However, the effects of tacticity mean that statistical models need to be used to allow deconvolution of this region and the extraction of further information. GPC with a dual detection system of RI and viscometry was used to analyse the copolymers following methylation. Values of the Mark-Houwink parameter α were calculated and found to be above 0.5 for the linear copolymers and less than 0.5 for the branched copolymers, as expected. The graft copolymers had intermediate α values as would be expected for a structure which is a combination of linear and branched structure in terms of the backbone and side chains. The relationship between contraction factor, g' , and copolymer molecular weight was investigated. The graft copolymers behaved as expected, with g' converging to 1 at low molecular weight. Significant deviations were observed for the branched copolymers, however, with g' increasing as molecular weight decreased. The contraction factors did not scale according to degree of branching, as would be expected, but were found to group according to composition. This suggested that IV is influenced by copolymer composition.

5. Solution Behaviour of Poly(Alkyl Methacrylate-co-Acrylic Acid) Copolymers

In this chapter, the poly(alkyl methacrylate-acrylic acid) copolymers are dispersed into water using the solvent switch method. Their solution behaviour is studied using Transmission Electron Microscopy and Phase Analysis Light Scattering to allow comparison of particle size, morphology and zeta potential. Additionally, SANS is used to study the copolymers in a range of different solvent systems.

5.1 Introduction

Amphiphilic copolymers are known to self-assemble into macromolecular structures in a solvent which is selective for one block of the copolymer.¹⁹² This occurs due to association of the insoluble blocks to form cores, with the soluble blocks forming outer corona. The structures formed are most commonly spherical micelles,¹⁹³ wormlike micelles¹⁹⁴ or vesicles,¹⁹⁵ depending on the composition of the block copolymers, the solvent polarity, and the relative solubilities of the blocks in the solvent.¹⁹⁶ This work has largely been carried out with linear di- and tri-block copolymers. It has been proposed that in these cases the morphology of the self-assembled structures is determined by the ratio of the volumes of the core-forming block and the outer block, therefore packing of the hydrophobes influences the observed morphology.¹⁹⁷

Relatively much less research into the self-assembly behaviour of copolymers with more complex architectures has appeared in the literature, although this area has seen progress in recent years. The self-assembly behaviour of complex structures including graft,¹⁹⁸ hyperbranched¹⁹⁹ and star²⁰⁰ polymers has been studied. These polymer architectures have shown unusual properties in comparison to linear block copolymers, including varieties of morphology, material properties, mechanisms of self-assembly, and smart response among others.²⁰¹ These provide unique advantages in supramolecular self-assembly. As a result, HB polymers in particular have found applications in biomedicine, ranging from drug delivery, purification, detection and delivery of proteins to antifouling materials.²⁰²

5.2 Poly(Alkyl Methacrylate-*co*-Acrylic Acid) Copolymers in Water

It was found that these copolymer materials could be dispersed into water using the solvent switch method. This involved the dropwise addition of water at a controlled rate using a syringe pump into a stirring solution of the amphiphilic copolymer in THF, followed by evaporation of the THF to form an aqueous dispersion of copolymer. This procedure is represented in the schematic diagram in **Figure 5.1**. A combination of transmission electron microscopy (TEM), particle sizing and zeta potential measurements, and small angle neutron scattering (SANS) was used to characterise the dispersions of each different copolymer. Since water is a good solvent for polyacrylic acid and a poor solvent for the hydrophobic polymethacrylates, it was hypothesised that the materials would display some kind of self-assembly behaviour.

The structures formed by block copolymers during self-assembly depend on the balance between thermodynamic and kinetic control. Thermodynamic control results in the formation of stable equilibrium structures whereas kinetic trapping can result in ‘freezing’ of intermediate structures. This balance is governed by several factors including solution pH, ionic strength and concentration. These studies were carried out at the pH of the deionised water without any addition of acid, base or salts to buffer pH (except where stated in the pH study) to simplify the system, and all dispersions were prepared at the same concentration (0.5 w/w%).

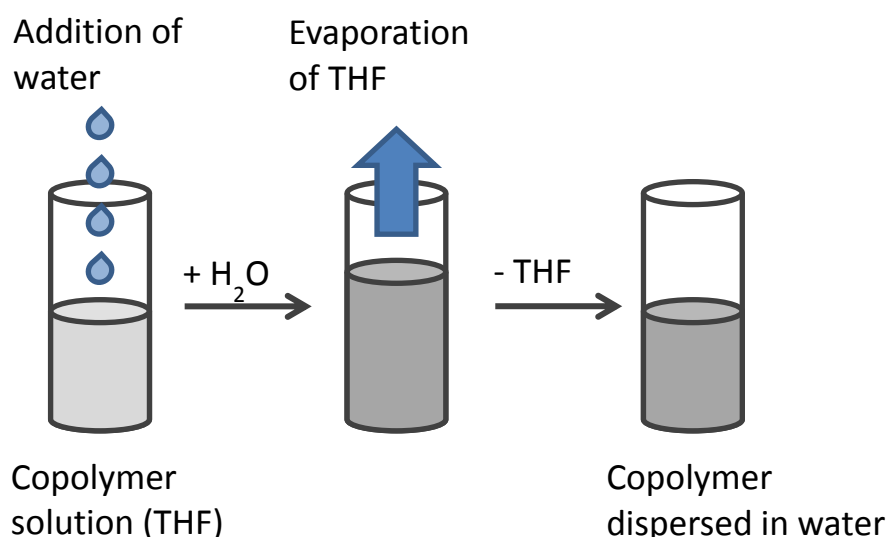


Figure 5.1. Schematic illustration of method for the preparation of copolymer dispersions involving a solvent switch from THF to water

TEM was carried out on carbon-coated copper grids which were plasma-treated to allow the dispersions to be adsorbed onto the surface. Any remaining water from the dispersions was removed by vacuum drying, meaning that TEM permits visualisation of the dried dispersions. This means that it cannot be assumed that the images are accurately depicting the solution structure of the copolymers. Mean particle sizes were obtained by using ImageJ image analysis software to enable the measurement of enough particles to represent a statistically significant sample; where possible this was at least 100 particles.

Particle sizes and zeta potentials were measured on a ZetaPALS instrument, which uses Phase Analysis Light Scattering (PALS) to measure the electrophoretic mobility and therefore surface charge of samples through analysing their phase shift, avoiding the application of large electric fields. A mean particle size is measured together with the associated standard error. The dispersity index (DI) is also obtained through producing a fit to the correlation data using cumulants analysis. A dimensionless number is obtained which indicates the dispersity of the sample: values below 0.05 are only seen for very highly uniform standards whilst values greater than 0.70 indicate a very broad size distribution. When used to measure zeta potentials, both a mean value and associated standard error are obtained.

A fourth method for the analysis of solution behaviour is SANS. Fitting of appropriate models to the neutron scattering profiles of the different copolymers leads to the calculation of particle sizes. SANS gives average diameters as the scattering is recorded from the whole sample. The SANS experiments are further discussed in Section 5.3.

Table 5.1 and **Figure 5.2** show the results for the graft copolymer dispersions. The MMA and BMA materials appear to be forming spherical micelles in solution. Similar particle sizes are observed from SANS and PALS whereas the sizes measured from the TEM images are much smaller. This can be explained by the difference in the techniques, as the two scattering techniques measure the hydrated particle size whilst TEM measures the dried particle size. The BMA spheres are more disperse, as reflected in the particle sizing results. The TEM images show that both dispersions appear to be aggregating, which is often observed for PAA. The measured zeta potential values for both materials are below -30 mV which is generally considered to be the threshold

below which dispersions can be considered to be stable. However, the LMA graft copolymer does not display the same behaviour. The measured zeta potentials and results of the SANS and the particle sizing indicate a stable dispersion of particles slightly larger than those of the MMA and BMA materials. Conversely the TEM images show much larger oily-looking structures, with sizes of some particles approaching the micron range. These could be formed by the coalescence of smaller particles. It is also possible that these are artefacts caused by the drying process.

The P(LMA-*co*-VBC-*g*-AA) copolymer displayed different behaviour to the other graft materials previously, with difficulties experienced in determining whether PAA grafts were present in the material, as outlined in Chapter 3. The dispersion preparation procedure was attempted using the functionalised P(LMA-*co*-VBC) backbone but was unsuccessful as the polymer precipitated out of solution. This suggests that there must be some PAA present in the ‘graft’ polymer to enable an aqueous dispersion to be formed.

Table 5.1. Summary of Results for the Characterisation of Dispersions of Graft P(nMA-*co*-VBC-*g*-AA) Copolymers in Water Using Particle Sizing and Zeta Potential Measurements, TEM and SANS

sample	mean diameter (TEM) /nm	mean diameter (PALS) /nm	DI	mean zeta potential /mV	mean diameter (SANS) /nm
P(MMA- <i>co</i> -VBC- <i>g</i> -AA)	27.7 ± 0.4	106.5 ± 1.7	0.187 ± 0.025	-38 ± 2	114.5 ± 0.2
P(BMA- <i>co</i> -VBC- <i>g</i> -AA)	32.4 ± 0.4	112.9 ± 1.1	0.236 ± 0.006	-31 ± 1	109.3 ± 0.2
P(LMA- <i>co</i> -VBC- <i>g</i> -AA)	471.4 ± 23.2	159.9 ± 0.5	0.140 ± 0.007	-45 ± 4	116.4 ± 0.5

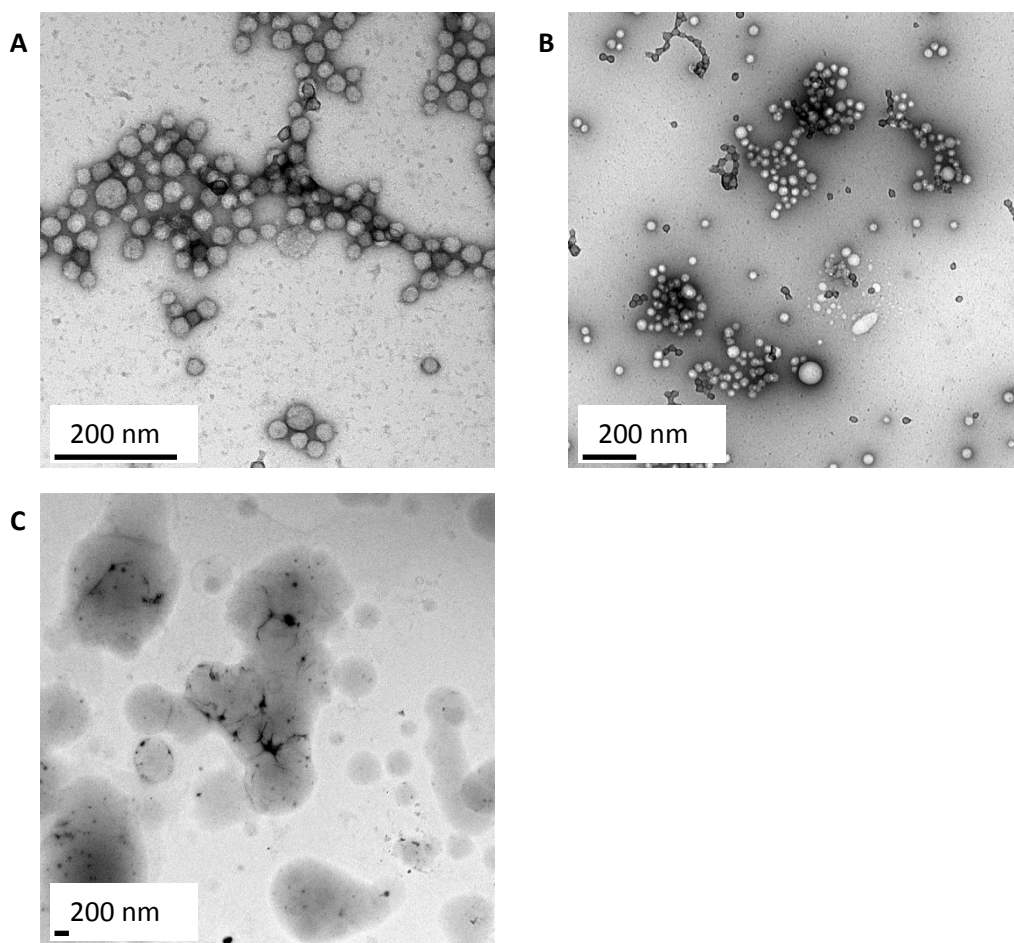


Figure 5.2. TEM micrographs of dispersions of graft P(nMA-co-VBC-g-AA) copolymers in water, stained with uranyl formate: **A** P(MMA-co-VBC-g-AA), **B** P(BMA-co-VBC-g-AA) and **C** P(LMA-co-VBC-g-AA).

The HB random copolymer dispersions were studied by the same techniques. The results are found in **Table 5.2** and **Figure 5.3**. For the MMA and BMA materials, larger diameters were observed by all three techniques compared to those of the graft copolymers. The TEM images show large spheres which appear to have smooth surfaces. The average zeta potentials indicate very stable dispersions. Conversely, very different results are seen for HB P(LMA-co-AA). The TEM image shows large collapsed structures instead of assembled micellar structures. Large mean diameters were obtained from all techniques and a high dispersity was observed, coupled with an average zeta potential which is much smaller and with a much higher standard error,

indicating the absence of a stable colloidal dispersion. This is likely to be due to the comparatively much larger hydrophobic component of the LMA copolymer due to the long alkyl chain. This means that the hydrophobic segment dominates and is unable to be sufficiently stabilised by the hydrophilic PAA segments.

Table 5.2. Summary of Results for the Characterisation of Dispersions of HB random P(nMA-*co*-AA) Copolymers in Water Using Particle Sizing and Zeta Potential Measurements, TEM and SANS

sample	mean diameter (TEM) /nm	mean diameter (PALS) /nm	DI	mean zeta potential /mV	mean diameter (SANS) /nm
HB P(MMA- <i>co</i> -AA)	181.8 ± 12.4	205.8 ± 0.8	0.091 ± 0.011	-50 ± 1	276.6 ± 4.9
HB P(BMA- <i>co</i> -AA)	263.9 ± 6.9	271.1 ± 0.8	0.122 ± 0.010	-53 ± 1	277.4 ± 4.5
HB P(LMA- <i>co</i> -AA)	302.1 ± 23.4	404.2 ± 12.1	0.381 ± 0.013	-13 ± 7	355.2 ± 5.6

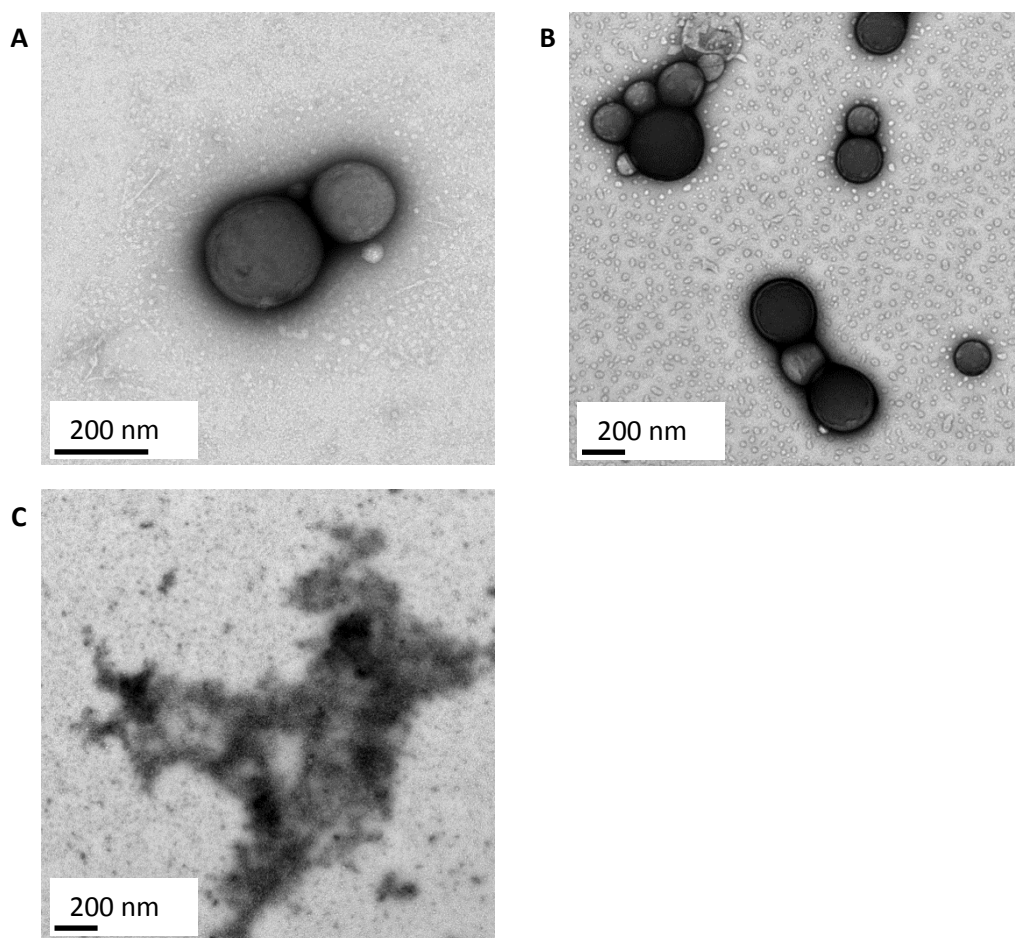


Figure 5.3. TEM micrographs of dispersions of HB random P(nMA-*co*-AA) copolymers in water, stained with uranyl formate: **A** HB P(MMA-*co*-AA), **B** HB P(BMA-*co*-AA) and **C** HB P(LMA-*co*-AA).

Stable dispersions were observed for all three HB block copolymers with PAA cores, with measured zeta potentials close to -30 mV. A range of particle sizes were seen between the samples, shown in **Table 5.3**, with the same trends observed in mean diameters measured by both TEM and PALS. Again the TEM results were substantially smaller due to the drying of the particles onto the grids. SANS data were not obtained for these samples. The HB P(AA-*b*-BMA) copolymer formed particles smaller than those of the MMA analogue. HB P(AA-*b*-LMA) however formed much larger particles with a higher standard error and larger dispersity. Well defined spheres with some

dispersity can be seen in the images in **Figure 5.4** for all three copolymers, which form small aggregates.

Table 5.3. Summary of Results for the Characterisation of Dispersions of HB Block P(AA-*b*-nMA) Copolymers in Water Using Particle Sizing and Zeta Potential Measurements and TEM

sample	mean diameter (TEM) /nm	mean diameter (PALS) /nm	DI	mean zeta potential /mV
HB P(AA- <i>b</i> -MMA)	33.1 ± 0.9	124.8 ± 0.9	0.156 ± 0.008	-33 ± 1
HB P(AA- <i>b</i> -BMA)	29.6 ± 0.6	77.0 ± 0.5	0.188 ± 0.007	-31 ± 1
HB P(AA- <i>b</i> -LMA)	49.8 ± 1.1	279.5 ± 16.1	0.224 ± 0.010	-30 ± 1

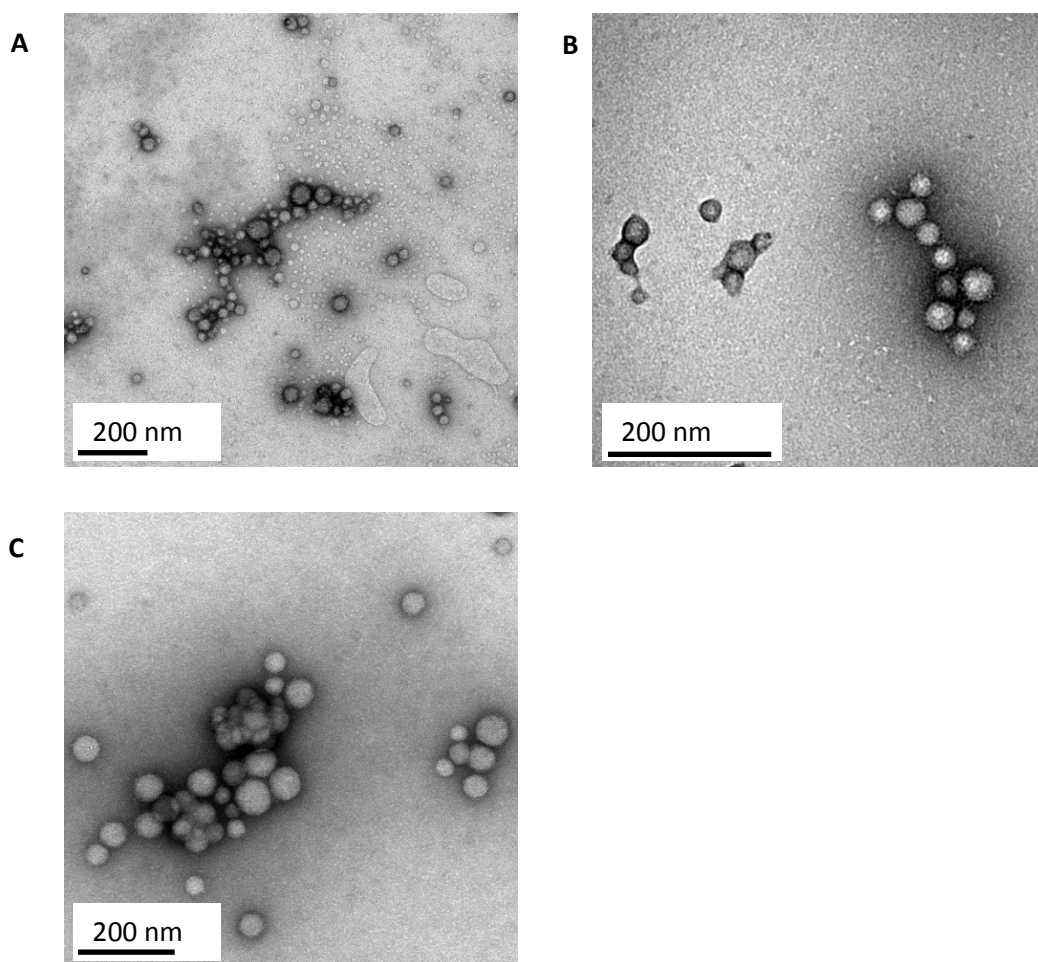


Figure 5.4. TEM micrographs of dispersions of HB block P(AA-*b*-nMA) copolymers in water, stained with uranyl formate: **A** HB P(AA-*b*-MMA), **B** HB P(AA-*b*-BMA) and **C** HB P(LMA-*b*-AA).

The linear block dispersions of all three copolymers showed very similar results in terms of particle sizing, with measured diameters between 245 and 280 nm by PALS and 100 and 140 nm by TEM. SANS data were not obtained for these samples. All three dispersions displayed very narrow dispersity values. The measured zeta potentials indicated high stability as all were below -40 mV. However, the TEM images indicated the presence of mixed phases of both large networks and collapsed large spheres or vesicles. Mean diameters were calculated from the TEM images by measuring both the collapsed structures and the segments of the networks. These mixed phases were seen

for both P(MMA-*b*-AA) and P(BMA-*b*-AA), whilst P(LMA-*b*-AA) appeared to form isolated collapsed structures. These results do not agree with the very low dispersities seen from the PALS results, unless the structures seen in the TEM images are artefacts of the drying process.

Table 5.4. Summary of Results for the Characterisation of Dispersions of Linear Block P(nMA-*b*-AA) Copolymers in Water Using Particle Sizing and Zeta Potential Measurements and TEM

sample	mean diameter (TEM) /nm	mean diameter (PALS) /nm	DI	mean zeta potential /mV
P(MMA- <i>b</i> -AA)	140.6 ± 6.8	261.4 ± 1.3	0.068 ± 0.014	-47 ± 1
P(BMA- <i>b</i> -AA)	108.9 ± 4.1	278.8 ± 1.5	0.068 ± 0.016	-42 ± 1
P(LMA- <i>b</i> -AA)	133.1 ± 13.3	244.9 ± 1.6	0.069 ± 0.015	-73 ± 2

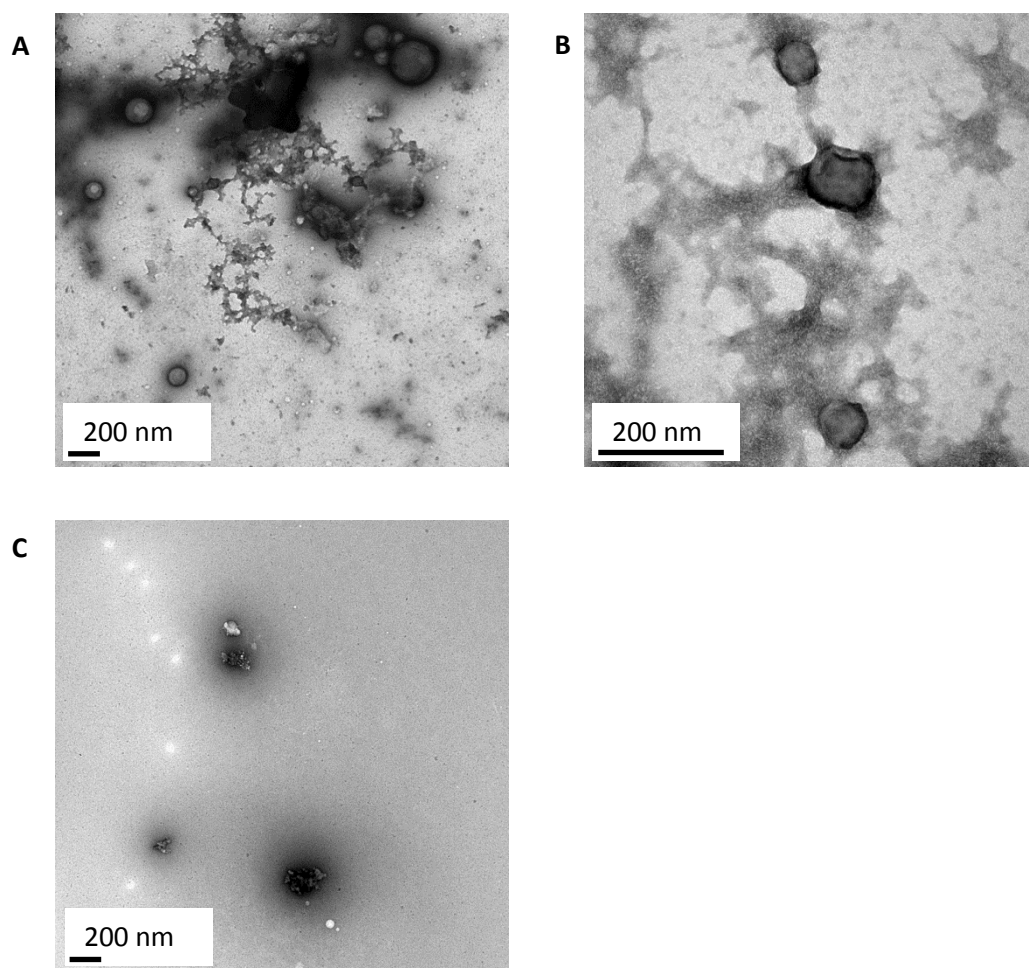


Figure 5.5. TEM micrographs of dispersions of linear block P(nMA-*b*-AA) copolymers in water, stained with uranyl formate: **A** P(MMA-*b*-AA), **B** P(BMA-*b*-AA) and **C** P(LMA-*b*-AA).

The solution characterisation of the dispersions of linear random copolymers shows that they are most similar to the HB random dispersions. The results of the different methods of measuring particle size show that these copolymers form the largest self-assembled structures, with the P(MMA-*co*-AA) forming the smallest of the set and P(LMA-*co*-AA) the largest. The zeta potentials for the MMA and BMA analogues show very stable colloids, whereas the zeta potential of the LMA material is much smaller and has a larger standard error, indicating instability in the surface charge. This same trend is seen in the HB random copolymer dispersions. The dispersity is also

much greater for P(LMA-*co*-AA) which confirms more variation in the self-assembled structures formed from this material.

Table 5.5. Summary of Results for the Characterisation of Dispersions of Linear Random P(nMA-*co*-AA) Copolymers in Water Using Particle Sizing and Zeta Potential Measurements, TEM and SANS

sample	mean diameter (TEM) /nm	mean diameter (PALS) /nm	DI	mean zeta potential /mV	mean diameter (SANS) /nm
P(MMA- <i>co</i> -AA)	360.6 ± 12.3	215.4 ± 0.9	0.099 ± 0.013	-47 ± 2	286.5 ± 1.2
P(BMA- <i>co</i> -AA)	354.1 ± 18.6	238.1 ± 0.7	0.088 ± 0.011	-49 ± 2	251.0 ± 4.7
P(LMA- <i>co</i> -AA)	245.7 ± 15.1	140.8 ± 19.6	0.361 ± 0.014	-11 ± 4	181.4 ± 1.3

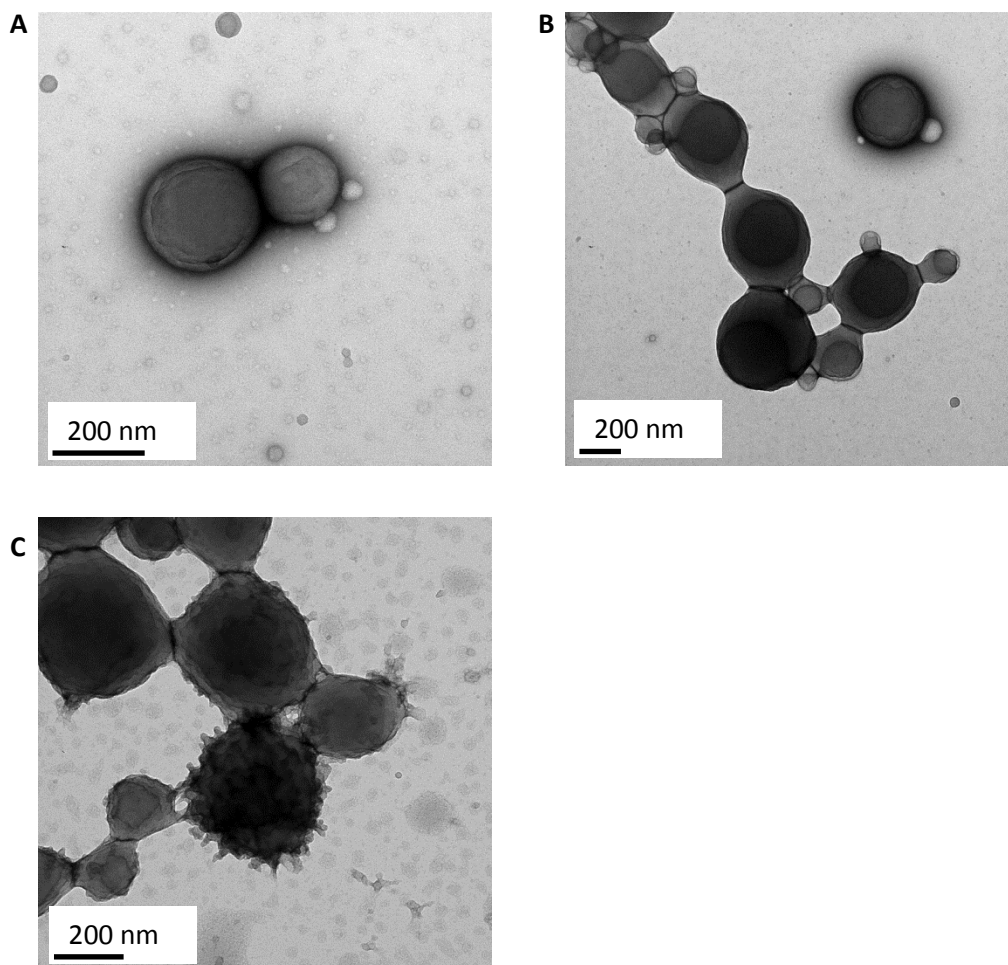


Figure 5.6 TEM micrographs of dispersions of linear random P(nMA-*co*-AA) copolymers in water, stained with uranyl formate: **A** P(MMA-*co*-AA), **B** P(BMA-*co*-AA) and **C** P(LMA-*co*-AA).

Dispersions of the HB block copolymers with PnMA forming the cores were also studied by TEM, PALS and SANS. The results are summarised in **Table 5.6**. This set of copolymers is a particularly notable example of the effect of changing the hydrophobicity of the hydrophobic block through varying the alkyl methacrylate monomer used. The TEM images in **Figure 5.7** show that vastly different structures were formed from each copolymer. The HB P(MMA-*b*-AA) formed spherical micelles with an apparent rough surface, whereas the HB P(LMA-*b*-AA) formed the smaller structures of the three, elliptical micelles with a central dimple. The most interesting structures, however, were the lamellar ‘onion’ micelles formed by the HB P(BMA-*b*-

AA) copolymers. All three dispersions were shown to be stable by the zeta potential results. In this case, the mean diameters measured from the TEM images are not all considerably smaller than those measured from the scattering techniques. The average PALS result for HB P(BMA-*b*-AA) is smaller due to the presence of two species within the sample resulting in a bimodal distribution; hence the resulting overall mean is between the diameters of the larger and smaller particles. The behaviour of the dispersions of this set of HB P(nMA-*b*-AA) copolymers will be studied in more detail in Chapter 6.

Table 5.6. Summary of Results for the Characterisation of Dispersions of HB block P(nMA-*b*-AA) Copolymers in Water Using Particle Sizing and Zeta Potential Measurements, TEM and SANS

sample	mean diameter (TEM) /nm	mean diameter (PALS) /nm	DI	mean zeta potential /mV	mean diameter (SANS) /nm
HB P(MMA- <i>b</i> -AA)	168.9 ± 5.3	159.4 ± 0.9	0.129 ± 0.011	-55 ± 1	136.8 ± 4.9
HB P(BMA- <i>b</i> -AA)	164.1 ± 5.5	82.5 ± 0.7	0.100 ± 0.015	-50 ± 1	162.7 ± 5.4
HB P(LMA- <i>b</i> -AA)	43.8 ± 0.6	59.5 ± 0.8	0.019 ± 0.016	-41 ± 10	70.7 ± 0.2

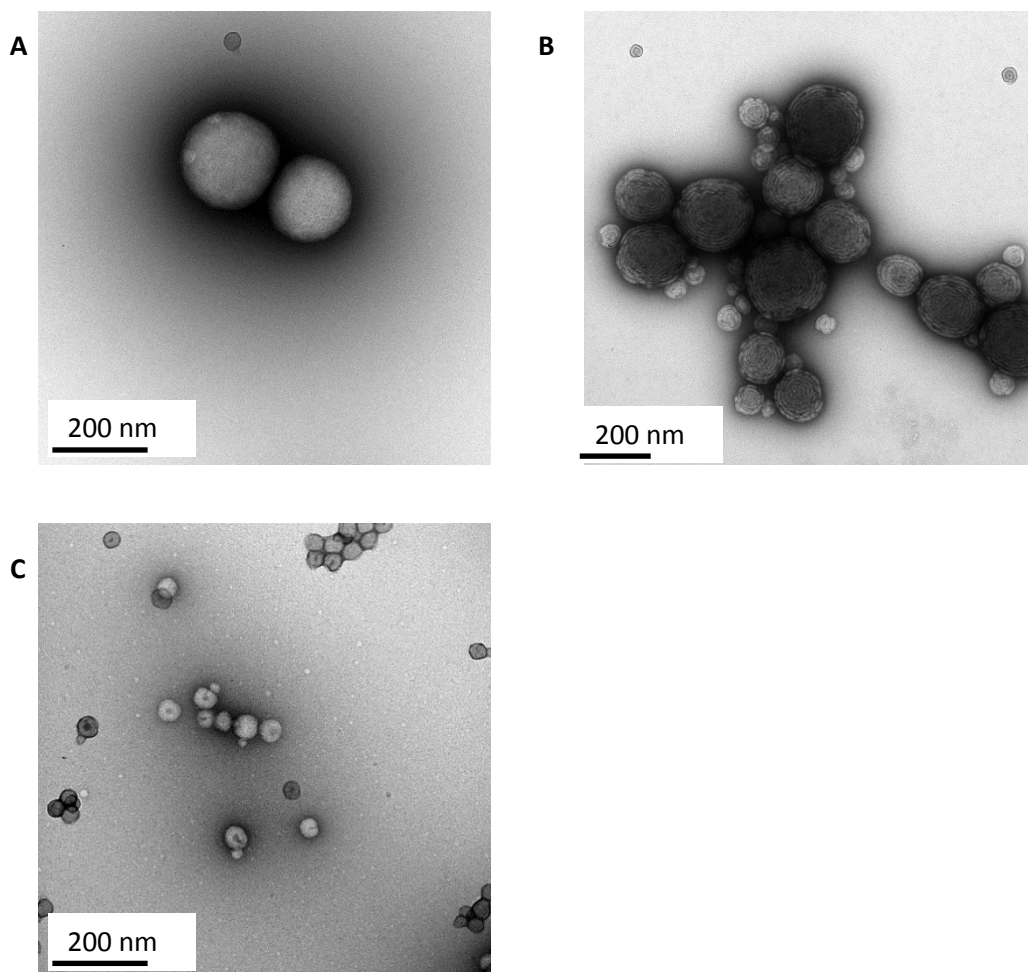


Figure 5.7. TEM micrographs of dispersions of HB block P(nMA-*b*-AA) copolymers in water, stained with uranyl formate: **A** HB P(MMA-*b*-AA), **B** HB P(BMA-*b*-AA) and **C** HB P(LMA-*b*-AA).

It can be seen that the architecture, the monomer distribution and the choice of alkyl methacrylate controlling the hydrophobicity of the hydrophobic block all have an effect on the self-assembled structures formed by the copolymers when dispersed in water. These observed differences between copolymers encompass particle structure, size and surface roughness. **Figure 5.8** shows a comparison of the spherical particles formed by HB P(AA-*b*-BMA) and HB P(BMA-*co*-AA). Both copolymers are composed of the same monomers in the same architecture but one has a random distribution whereas the other is a block copolymer. This difference appears to result in small rough-surfaced spheres for the block copolymer whereas the random analogue forms larger

smooth spheres. It should be noted that it is not necessary to have a segmented structure to form spheres: an aspect that is often not alluded to in the block copolymer literature.

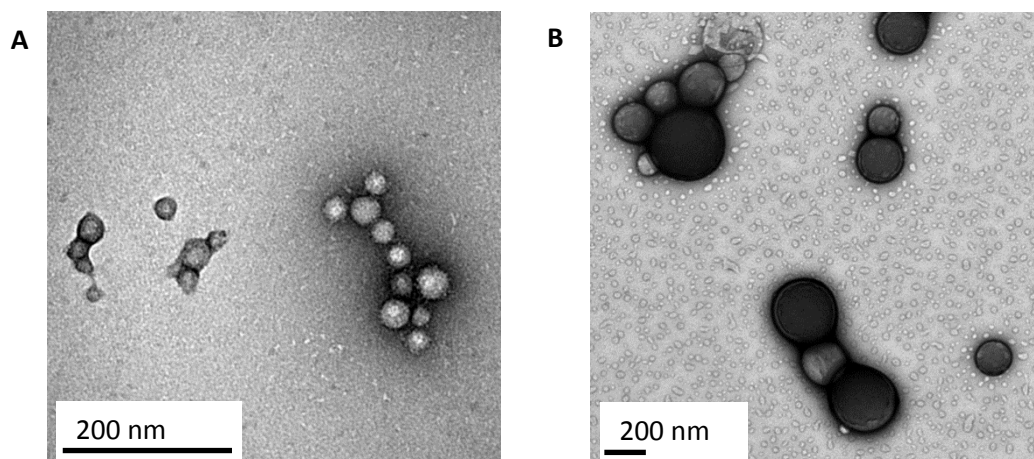


Figure 5.8. TEM micrographs of dispersions of P(nMA-AA) copolymers in water, stained with uranyl formate, showing the difference in surface roughness between the block and random HB structures: **A** HB P(AA-*b*-BMA) and **B** HB P(BMA-*co*-AA).

Zeta potential measurements were carried out on dispersions of all eighteen of the poly(methacrylate-acrylic acid) copolymers in water. The results of these were seen in Tables 5.1-5.6. Each value was obtained from 5 measurement cycles, which were repeated in triplicate, and both mean values and standard errors calculated. Statistical analysis on these data was then carried out using the analysis of variance test (ANOVA). The procedure for the ANOVA test is explained in **Appendix 1**.

Table 5.7. Statistical Analysis of Zeta Potential Measurements for the Characterisation of Dispersions of P(nMA-co-AA) Copolymers in Water using ANOVA

Source of Variation	F	F _{crit}	P	P < 0.05?
Interaction	23.71	2.16	<0.0001	Y
Hydrophobicity	10.52	3.32	P = 0.0003	Y
Architecture	25.52	2.53	<0.0001	Y

Table 5.8. Schematic to illustrate how column factor and row factor are represented in two-way ANOVA analysis.

		← column factor: architecture →																		
		G			HBA			HBR			LR			LB			HBM			
↑	row factor :	MMA	1	2	3	1	2	3	1	2	3	1	2	3	1	2	3	1	2	3
	hydrophobicity	BMA	1	2	3	1	2	3	1	2	3	1	2	3	1	2	3	1	2	3
↓		LMA	1	2	3	1	2	3	1	2	3	1	2	3	1	2	3	1	2	3
		interaction factor: comparison between column and row																		

The results of the ANOVA are summarised in **Table 5.7**. Three mean zeta potential values were obtained for each combination of architecture and hydrophobicity. In the ANOVA test the data are analysed for differences between architecture (the column factor), hydrophobicity (the row factor) and also for interaction between these two variables. This is illustrated in **Table 5.8**. The calculated F value is larger than F_{crit} for each source of variation. This means that the null hypothesis is rejected and there are significant differences between the results in terms of both hydrophobicity (i.e. whether methyl, butyl or lauryl methacrylate is used) and copolymer architecture. However, there is also interaction between the two factors which makes comparison between groups less clear. The Tukey post-hoc analysis was carried out to identify between which means the differences occur. The results of this are displayed graphically in **Figure 5.9**. Where no significant difference is indicated, any differences observed are within experimental error.

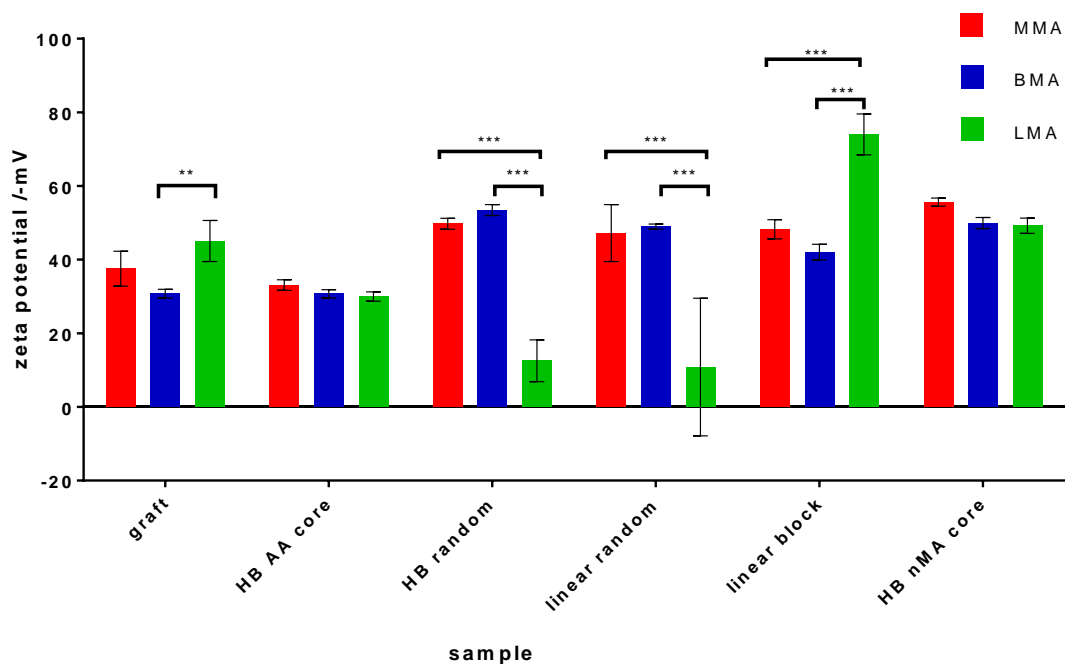


Figure 5.9. A graph of mean zeta potential values for the set of copolymers, showing the results of Tukey post-hoc analysis. Tie lines show significance level of comparisons between sets of copolymers: *** $P < 0.001$, ** $0.001 < P < 0.01$, * $0.01 < P < 0.05$, ns (not significant) $P \geq 0.05$. Here, only significant relationships between copolymers are shown on the graph.

5.3 Small Angle Neutron Scattering

Small Angle Neutron Scattering (SANS) is a powerful technique which can be applied to study the behaviour of materials on length scales between tens and hundreds of nanometres; hence it is suited to the study of soft matter systems such as polymers, colloids, surfactants and proteins. **Figure 5.10** shows the typical set-up for a SANS experiment. The detectors record scattering from the sample in terms of the number of scattered neutrons as a function of the wave vector, Q . The background scattering is then subtracted to yield reduced data representing scattering by the sample. Fitting mathematical models to the reduced data leads to the calculation of various parameters, which give information on bulk properties of the polymer such as the size, structure, dispersity and particle interaction.

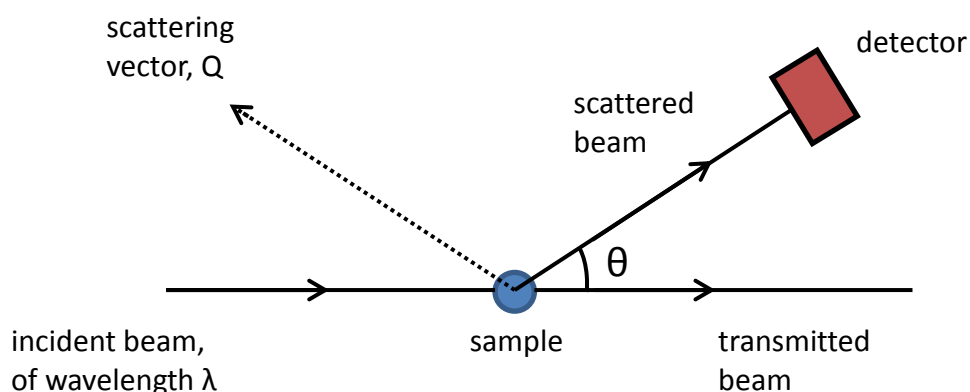


Figure 5.10. Typical set-up for a SANS experiment

SANS studies were carried out in two separate 48 hour beamtime allocations on the LoQ instrument at the ISIS facility. Due to time constraints, only 4 of the 6 sets of copolymers were studied: graft, HB block with alkyl methacrylate core, HB random and linear random. A series of five different solvent systems were chosen to investigate how the conformations of the copolymers changed in different solvency conditions. Deuterated THF (d-THF) is a good solvent for both poly(alkyl methacrylate) and poly(acrylic acid) blocks. D_2O , however, is a good solvent for PAA but a poor solvent for the PnMA blocks. The copolymers were studied in a 1:1 mixture of d-THF and D_2O , and also dispersed into D_2O . $CDCl_3$, on the other hand, is a good solvent for the PnMA blocks but a poor solvent for PAA. A 1:1 mixture of d-THF and $CDCl_3$ was used to

reverse the solvent selectivity compared to the d-THF:D₂O mixture. The final solvent was deuterated ethanol (d-EtOH), which was chosen to gain some information as to how the copolymers may behave in the ink formulation, which is primarily ethanol-based.

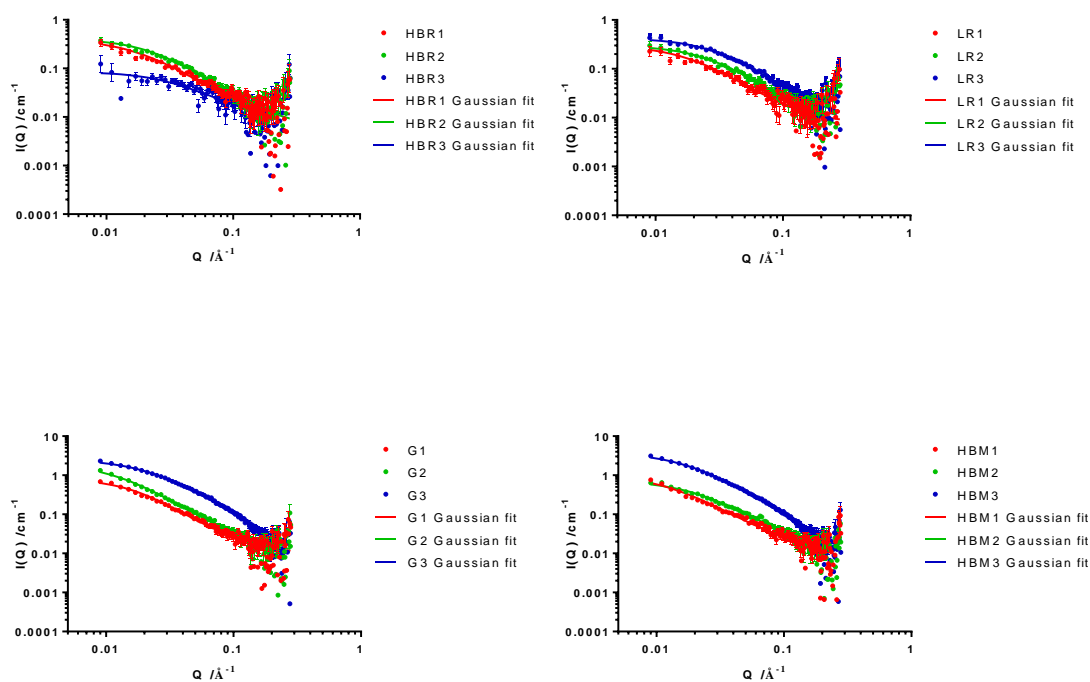


Figure 5.11 Scattering profiles for the reduced data obtained from P(nMA-AA) copolymers at 0.5% concentration in d-THF. Circles represent data points and solid lines represent optimal model fit. Error bars represent the standard error on each data point, but are not visible on some data points (at low Q due to small size of error bars, at high Q due to large size of error bars). (key: letters refer to architecture and distribution HBR = highly branched random, HBM = highly branched methacrylate core, G = graft and LR = linear random, numbers refer to methacrylate monomer 1 = MMA, 2 = BMA and 3 = LMA)

Figure 5.11 shows the scattering profiles obtained for the twelve copolymers in d-THF. SASView software was used to fit the scattering data to mathematical models. **Appendix 2** summarises the values of fitting parameters obtained from the fitting of

various models to the data whilst **Appendix 3** presents the model fits to the scattering data.

The best fit to this particular set of data was found using the ‘Poly_GaussCoil’ model, represented as solid lines on the graph. This provides an empirical form for the scattering from a disperse polymer chain in a good solvent, i.e. a Gaussian coil. The functional form for this model is given by **Equation 5.3**:^{203, 204}

$$I(Q) = scale \times \frac{2 \left[(1 + Ux)^{-\frac{1}{U}} + x - 1 \right]}{(1 + U)x^2} + bkg \quad \text{Equation 5.3}$$

$I(Q)$ represents the scattering intensity, bkg the background, x is the dimensionless chain dimension (**Equation 5.4**) and U is the Schultz-Zimm dispersion in the molecular weight distribution (**Equation 5.5**).

$$x = \frac{R_g^2 Q^2}{1 + 2U} \quad \text{Equation 5.4}$$

$$U = \frac{M_w}{M_n} - 1 \quad \text{Equation 5.5}$$

Additionally, R_g represents the radius of gyration of the polymer, Q the scattering vector, M_w the weight-average molecular weight and M_n the number-average molecular weight.

It would be expected for all of these materials to adopt a Gaussian coil conformation in d-THF as it is a good solvent for both blocks. The model provides values for parameters including R_g and dispersity. **Table 5.9** summarises the values of R_g and dispersity obtained. Full tables of calculated parameters are provided in **Appendix 2**. The R_g values obtained for these copolymers range between 50 to 150 Å (5 to 15 nm) which are typical for Gaussian coils. Larger values of dispersity were observed for both the linear and branched random materials compared to the graft and branched block copolymers. Dispersities were consistent within architecture and distribution groups (e.g. all three HBR copolymers had dispersities between 4.10 and 5.00 whilst all G copolymers had dispersities between 1.04 and 1.86).

Table 5.9. Selected Results of Model Fitting to SANS Data of P(nMA-AA) Copolymers in d-THF

sample	M_w/M_n	$R_g/\text{\AA}$
HBR1	5.00	87.4
HBR2	4.10	74.2
HBR3	4.96	50.5
LR1	5.00	90.4
LR2	5.00	64.5
LR3	2.75	57.8
G1	1.04	98.7
G2	1.70	148.0
G3	1.86	68.7
HBM1	3.11	145.0
HBM2	3.43	90.5
HBM3	3.00	106.1

The second solvent system was a 1:1 mixture of d-THF and D₂O, to investigate the effect of adding a block-selective solvent. As the solvency conditions change, it would be anticipated that the PAA segments would remain well-solvated whilst the PnMA segments would begin to collapse. **Figure 5.12** shows the scattering profiles for all twelve copolymers, with solid lines representing the model fits. The scattering intensity is much greater for these materials at low Q compared to the scattering in d-THF. This can indicate the presence of attractive interactions between particles causing larger particles or aggregates to form.

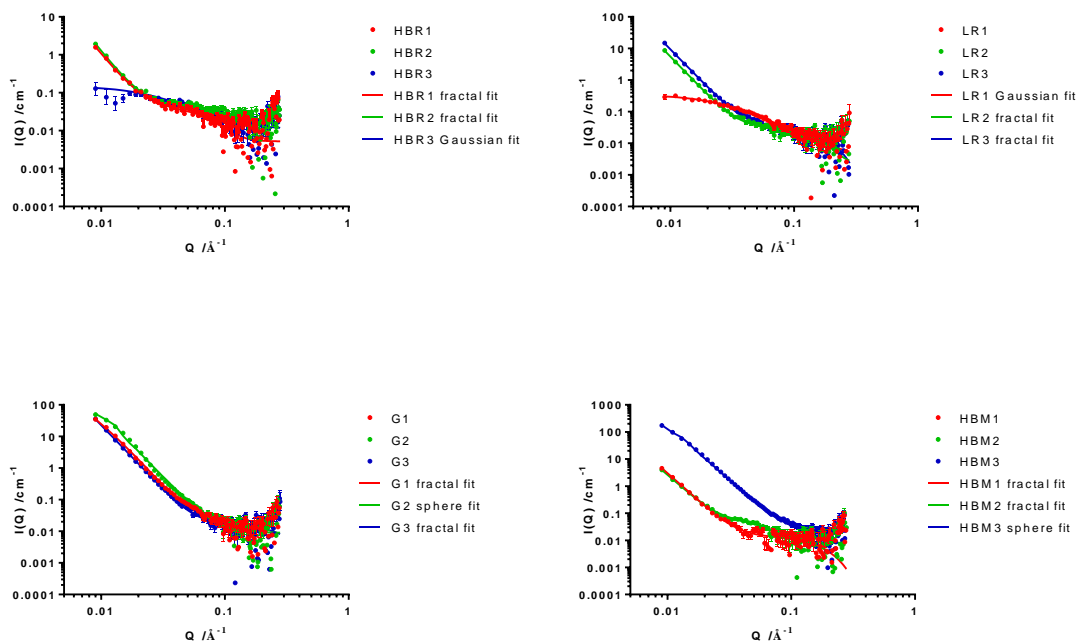


Figure 5.12. Scattering profiles for the reduced data obtained from P(nMA-AA) copolymers at 0.5% concentration in 1:1 d-THF:D₂O mixtures. Circles represent data points and solid lines represent optimal model fit. Error bars represent the standard error on each data point, but are not visible on some data points (at low Q due to small size of error bars, at high Q due to large size of error bars). (key: letters refer to architecture and distribution HBR = highly branched random, HBM = highly branched methacrylate core, G = graft and LR = linear random, numbers refer to methacrylate monomer 1 = MMA, 2 = BMA and 3 = LMA)

Differences between the behaviour of the copolymers due to both architecture and composition began to be seen in this solvent system. Whilst two copolymers, LR1 and HBR3, fitted best to the Poly_GaussCoil model indicating that they were still dissolved despite the D₂O addition, other models were found to best represent the rest of the data.

The first of these is the fractal model, which is used to calculate the scattering from fractal-like aggregates composed of spherical building blocks.²⁰⁵ **Equation 5.6** represents the overall scattering intensity, where $P(Q)$ is a function of the form factor, $F(Q)$, and $S(Q)$ is the structure factor, with bkg the background level.

$$I(Q) = P(Q)S(Q) + bkg \quad \text{Equation 5.6}$$

The form factor depends on the spatial distribution of the scattering lengths of the atoms in the sample, known as the contrast; hence the form factor $F(Q)$ is the Fourier transform of the contrast evaluated over the particle volume. If the particles are approximated to uniform spheres of SLD ρ , radius R_0 and volume V (given by **Equation 5.9** for a sphere), then $P(Q)$ can be represented by **Equation 5.7**. Here the function of $F(QR_0)$ is expanded in **Equation 5.8**.

$$P(Q) = scale \times V(\rho_{block} - \rho_{solvent})^2 F(QR_0)^2 \quad \text{Equation 5.7}$$

$$F(x) = \frac{3[\sin(x) - x \cos(x)]}{x^3} \quad \text{Equation 5.8}$$

$$V = \frac{4}{3}\pi R_0^3 \quad \text{Equation 5.9}$$

$S(Q)$, the structure factor, describes the spatial distribution of the individual scattering particles, through a Fourier transform of a pair correlation function. It is given by **Equation 5.10**, where D_f is the fractal dimension, Γ is the gamma function, and ξ is the correlation length. $S(Q)$ can be considered here as the form factor of a group of fractal objects distributed on a larger scale in space. The correlation length is introduced as a cutoff distance to describe how the pair correlation function behaves at large distances. It represents the distance above which the fractal law no longer applies to describe the mass distribution in the sample; in practice, it represents the size of the larger aggregate, such as the R_g of a branched polymer nearing gelation.^{206, 207}

$$S(Q) = 1 + \frac{D_f \Gamma(D_f - 1) \sin[(D_f - 1) \tan^{-1}(Q\xi)]}{\left[1 + \frac{1}{(Q\xi)^2}\right]^{\frac{(D_f-1)}{2}} (QR_0)^{D_f}} \quad \text{Equation 5.10}$$

The significant fitting parameters obtained from this model are the radius of the building blocks, the correlation length (representing the size of the larger aggregates), the scattering length density (SLD) of the polymer and the fractal dimension. The value of the fractal dimension indicates the type of fractal which is formed: D_f below 3

indicates mass fractals, which are formed by clustering of smaller particles, whereas D_f greater than 3 is characteristic of surface fractals, meaning particles with a rough ‘fractal’ surface. Different types of mass fractals are also indicated by D_f values, as demonstrated in **Figure 5.13** below.

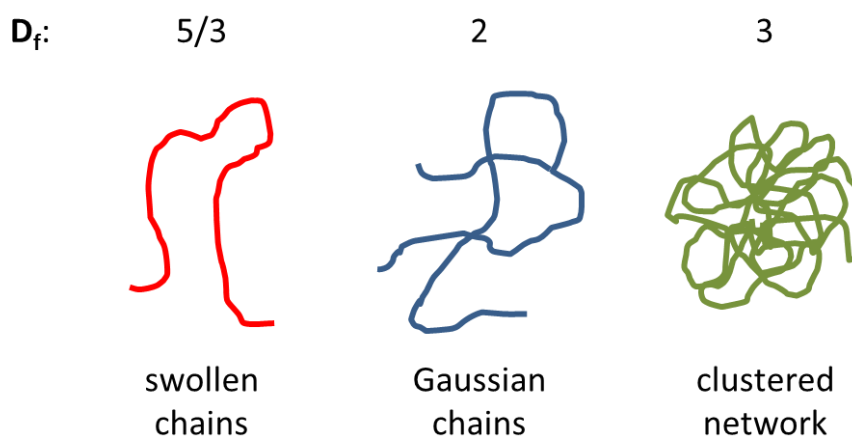


Figure 5.13. Schematic representation of the various fractal dimensions for mass fractal systems. Adapted from NIST Center for Neutron Research website.²⁰⁸

The second model which describes some of the d-THF:D₂O data is the sphere model.²⁰⁹ This provides the form factor, $P(Q)$, for a monodisperse spherical particle having a uniform SLD, as shown in **Equation 5.11**, where $\Delta\rho$ represents the difference in SLD between the solvent and the polymer (the contrast), R represents the radius of the sphere, bkg is the background level and V represents the volume of the scattering object; in this way the scale represents the volume fraction of the scatterer.

$$P(Q) = \frac{scale}{V} \left[\frac{3V(\Delta\rho)[\sin(QR) - QR \cos(QR)]}{(QR)^3} \right]^2 + bkg \quad \text{Equation 5.11}$$

The important parameters obtained from this model are the radius and the SLD of the sphere. **Table 5.10** summarises the results of the model fitting for each polymer, reporting the best model fit and the corresponding parameters obtained.

The majority of the data fitted best to the fractal model. This is thought to represent the polymer chains beginning to collapse and aggregate as the solvency conditions change. Following the addition of D₂O, the poly(alkyl methacrylate) chains will be less solvated and begin to collapse, but both the presence of d-THF and the fact that the poly(acrylic acid) segments remain well solvated prevents them from precipitating entirely. However, the chains begin to aggregate to minimise the interfacial energy and keep the hydrophobic PnMA segments away from the D₂O. The fractal dimensions of all of the data were very close to 3, indicating the formation of mass fractals in the configuration of clustered networks of small particles. The calculated radii of the building blocks are close to 20 Å (2 nm) representing the collapsed copolymers, whilst the size of the larger aggregates ranges from 200-350 Å (20-35 nm) for G1 and HBM2 and between 1000-1700 Å (100-170 nm) for LR2, LR3, G3, HBR1, HBR2 and HBM1. In the case of the G2 and HBM3 copolymers, the aggregation process has progressed further to the point of forming self-assembled structures, which are represented by the sphere model.

Table 5.10. Selected Results of Model Fitting to SANS Data of P(nMA-AA) Copolymers in 1:1 d-THF:D₂O Mixtures

sample	model	M_w/M_n	$R_g / \text{\AA}$	correlation length, $\xi / \text{\AA}$	fractal dimension	radius / \AA	SLD block / \AA^{-2}	radius / \AA	SLD sphere / \AA^{-2}
HBR1	fractal			1310.6	3.00	20.1	2.23×10^{-6}		
HBR2	fractal			1711.7	3.01	20.9	2.29×10^{-6}		
HBR3	Gaussian	5.00	65.2						
LR1	Gaussian	2.95	69.1						
LR2	fractal			1026.4	3.01	14.6	1.58×10^{-6}		
LR3	fractal			1292.4	3.00	11.4	1.41×10^{-6}		
G1	fractal			197.6	3.00	13.6	1.97×10^{-6}		
G2	sphere							443.0	3.54×10^{-6}
G3	fractal			1383.5	3.00	6.9	1.40×10^{-6}		
HBM1	fractal			1593.7	3.00	11.0	2.09×10^{-6}		
HBM2	fractal			347.2	3.05	17.7	2.00×10^{-6}		
HBM3	sphere							1236.9	1.67×10^{-6}

Figure 5.14 shows the scattering profiles obtained from the set of copolymers when dispersed into D₂O, following the same solvent switch procedure as outlined in section 5.2. As seen in the d-THF:D₂O mixture, the scattering intensity is large for these materials at low Q , indicating the presence of attractive interactions between particles causing large particles or aggregates to form. This is particularly noticeable for the graft copolymers, and HB P(LMA-*b*-AA).

There is also a noticeable increase in noise in this data set. This means that for the samples which exhibit low scattering, namely all three HBR samples and HBM1, the scattering is not clearly distinct from the background noise. As a result the data is more difficult to fit, and the model fits are not necessarily reliable but represent the best possible result.

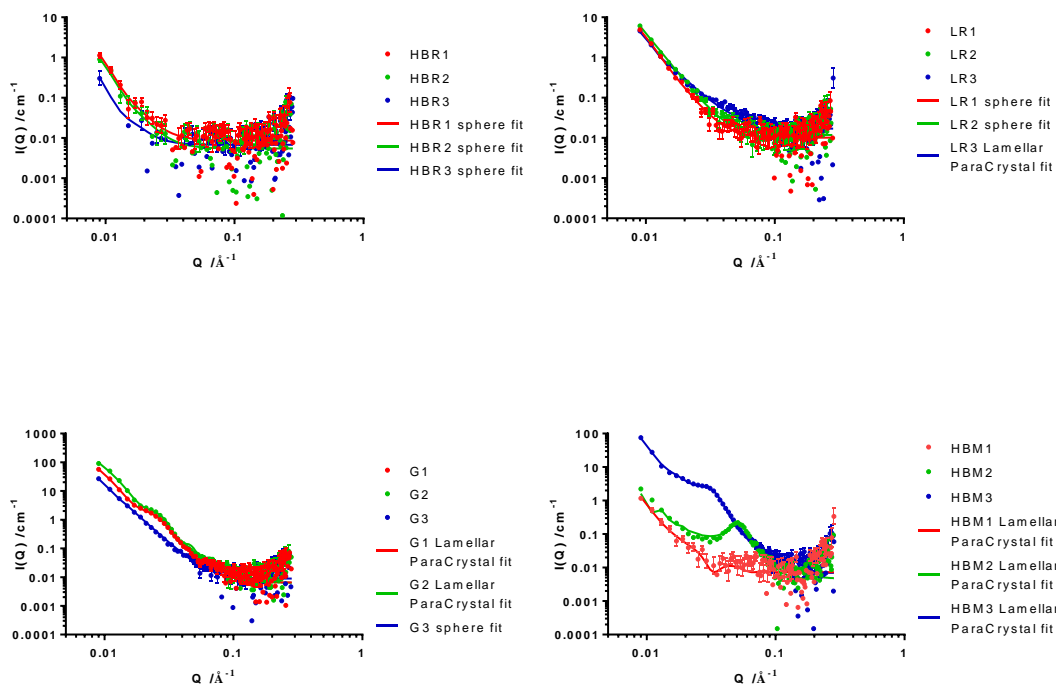


Figure 5.14. Scattering profiles for the reduced data obtained from P(nMA-AA) copolymers at 0.5% concentration in D₂O. Circles represent data points and solid lines represent optimal model fit. Error bars represent the standard error on each data point, but are not visible on some data points (at low Q due to small size of error bars, at high Q due to large size of error bars). (key: letters refer to architecture and distribution HBR = highly branched random, HBM = highly branched methacrylate core, G = graft and LR = linear random, numbers refer to methacrylate monomer 1 = MMA, 2 = BMA and 3 = LMA)

The overall scattering profiles appear similar for the same copolymers in d-THF:D₂O and D₂O. However, peaks are visible in some of the scattering profiles at medium Q . The most significant peak is seen in the scattering from HBM2, which appears to be a Bragg-like peak suggesting the presence of a multiple-layered structure. Less significant peaks were observed for LR3, G1, G2, HBM1 and HBM3.

The most suitable model to fit these data exhibiting peaks at medium Q was the Lamellar ParaCrystal model.²¹⁰ This is used to calculate the scattering from a stack of repeating lamellae, which is considered as a paracrystal to account for the repeat spacing. The model has also been used to model the scattering from multilamellar

vesicles. **Equation 5.12** is used to calculate the scattering, where $\Delta\rho$ represents the difference in SLD between the solvent and the polymer (the contrast), $Z_N(Q)$ represents the interference effects where more than one bilayer is present and Γ_m is the mass per area of the bilayer. In this application of the model, the scale factor is used instead of Γ_m and represents the volume fraction of the material forming the bilayer. $P_{bil}(Q)$ is the form factor of the bilayer, given by **Equation 5.13** in which it is approximated as the cross section of an infinite planar bilayer, where t represents the layer thickness.

$$I(Q) = 2\pi(\Delta\rho)^2\Gamma_m \frac{P_{bil}(Q)}{Q^2} Z_N(Q) \quad \text{Equation 5.12}$$

$$P_{bil}(Q) = \left(\sin \frac{\left(\frac{Qt}{2} \right)}{\frac{Qt}{2}} \right)^2 \quad \text{Equation 5.13}$$

Where there is a non-integer number of layers (N_L), **Equation 5.14** is used to calculate the value from a linear combination of the higher and lower values.

$$N_L = x_N N + (1 - x_N)(N + 1) \quad \text{Equation 5.14}$$

These six copolymers fitted to the Lamellar ParaCrystal model, suggesting a structure composed of layers with the hydrophobic PnMA on the inside to avoid the D₂O and PAA segments on the outer surfaces. The SLD values of the self-assembled structures are higher than those calculated for the copolymers alone, indicating the presence of D₂O within the particles. LR3, G1, HBM1 and HBM3 are composed of between two and three layers, hence the non-integer value, and G2 has between one and two layers. The most interesting case is that of the HBM2 copolymers which appears to have 10 layers. These are much thinner compared to those of the other copolymers. This particular material will be studied in more detail in Chapter 6.

The scattering profiles of the rest of the copolymers fitted well to the sphere model. **Table 5.11** summarises the important parameters obtained from the model fits. The particle sizes obtained agreed well with those determined through other techniques, as seen in **Figure 5.15**. The size by TEM, assessed through the use of ImageJ image analysis software to measure at least 100 particles in each case, is smaller than those measured by PALS and SANS for almost all materials. This is expected, however, as

TEM requires the particles to be dried onto grids before imaging whilst the other techniques are carried out in solution.

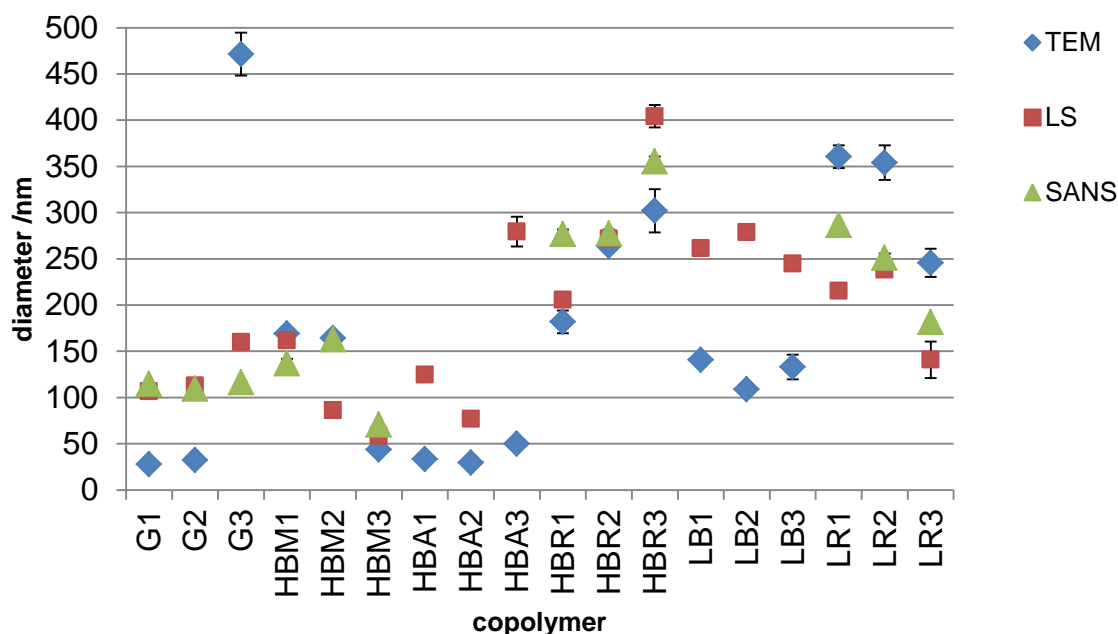


Figure 5.15. Comparison of particle sizes of P(nMA-AA) copolymers self-assembled in H₂O (D₂O for SANS) measured by: TEM (blue diamonds), PALS (red squares) and SANS (green triangles). Error bars represent the standard error on each data point, but are not visible on some data points. (key: letters refer to architecture and distribution HBR = highly branched random, HBM = highly branched methacrylate core, HBA = highly branched acrylic acid core, G = graft, numbers refer to methacrylate monomer 1 = MMA, 2 = BMA and 3 = LMA)

Table 5.11. Selected Results of Model Fitting to SANS Data of P(nMA-AA) Copolymers in D₂O

sample	model	radius /Å	SLD sphere /Å ⁻²	No. of layers	SLD layer /Å ⁻²	spacing /Å	thickness /Å
HBR1	sphere	1383.2	4.42 x10 ⁻⁶				
HBR2	sphere	1386.9	4.00 x10 ⁻⁶				
HBR3	sphere	1776.0	5.83 x10 ⁻⁶				
LR1	sphere	1432.4	3.61 x10 ⁻⁶				
LR2	sphere	1255.2	4.16 x10 ⁻⁶				
LR3	Lamellar ParaCrystal			2.10	3.77 x10 ⁻⁶	653.1	259.9
G1	Lamellar ParaCrystal			2.00	1.40 x10 ⁻⁶	169.6	171.6
G2	Lamellar ParaCrystal			1.61	1.81 x10 ⁻⁶	167.6	167.6
G3	sphere	582.12	2.35 x10 ⁻⁶				
HBM1	Lamellar ParaCrystal			2.44	3.71 x10 ⁻⁶	179.7	188.6
HBM2	Lamellar ParaCrystal			10.37	2.07 x10 ⁻⁶	114.6	42.3
HBM3	Lamellar ParaCrystal			2.60	2.29 x10 ⁻⁶	166.6	138.9

The next solvent system to be investigated was a 1:1 mixture of d-THF and CDCl_3 . This was intended as a reversal of the solvency conditions of d-THF: D_2O , as CDCl_3 is a good solvent for the PnMA segments but a poor solvent for PAA. The scattering profiles for this data set are shown in **Figure 5.16**.

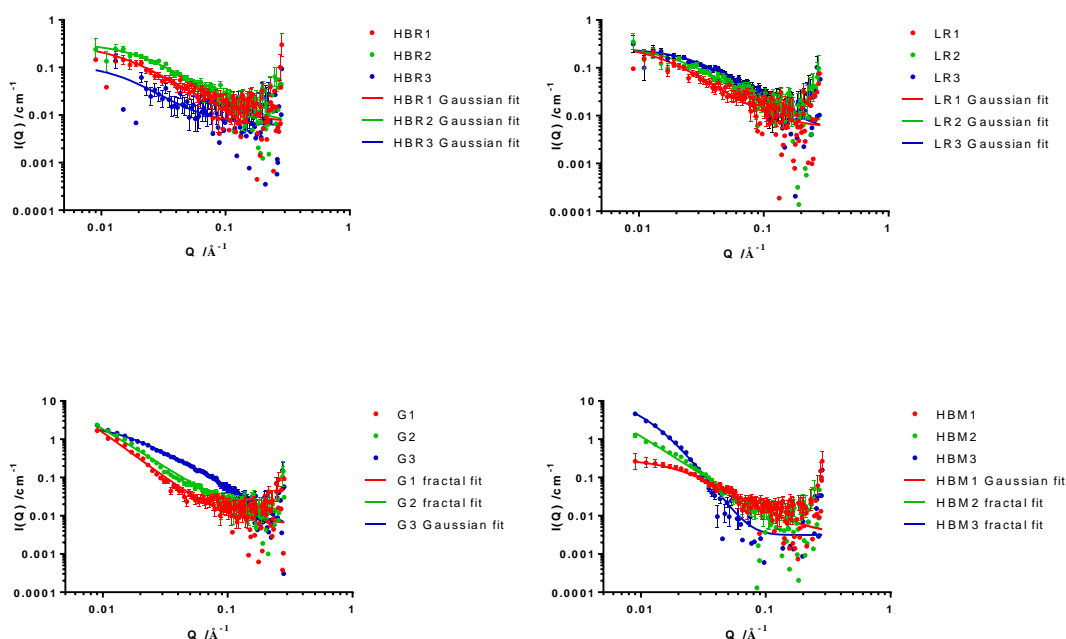


Figure 5.16. Scattering profiles for the reduced data obtained from P(nMA-AA) copolymers at 0.5% concentration in 1:1 d-THF: CDCl_3 mixtures. Circles represent data points and solid lines represent optimal model fit. Error bars represent the standard error on each data point, but are not visible on some data points (at low Q due to small size of error bars, at high Q due to large size of error bars). (key: letters refer to architecture and distribution HBR = highly branched random, HBM = highly branched methacrylate core, G = graft and LR = linear random, numbers refer to methacrylate monomer 1 = MMA, 2 = BMA and 3 = LMA)

The majority of the copolymers were found to remain as Gaussian coils following the addition of CDCl_3 to d-THF, including all branched and linear random materials in addition to G3 and HBM1. G1, G2, HBM2 and HBM3 on the other hand fitted best to the fractal model, indicating that these copolymers were beginning to

aggregate into larger structures as the solvency conditions changed. **Table 5.12** summarises the values of fitting parameters obtained from these models. The calculated values of the fractal dimension were between 2 and 3, indicating that the mass fractal structures formed are in transition from Gaussian chains to clustered networks of particles. The correlation lengths for these copolymers are smaller than those for the fractals formed in d-THF:D₂O, indicating a lesser degree of network formation. Additionally, the radii of the fractal building blocks are smaller.

Table 5.12. Selected Results of Model Fitting to SANS Data of P(nMA-AA) Copolymers in 1:1 d-THF:CDCl₃ Mixtures

sample	model	M_w/M_n	$R_g / \text{\AA}$	correlation length, $\xi / \text{\AA}$	fractal dimension	radius / \AA	SLD block / \AA^{-2}
HBR1	Gaussian	4.96	116.2				
HBR2	Gaussian	4.83	85.3				
HBR3	Gaussian	1.03	100.9				
LR1	Gaussian	1.56	101.2				
LR2	Gaussian	2.98	82.2				
LR3	Gaussian	2.00	56.7				
G1	fractal			328.1	2.36	4.9	3.19×10^{-6}
G2	fractal			499.7	2.03	4.0	1.56×10^{-6}
G3	Gaussian	2.48	116.8				
HBM1	Gaussian	1.67	86.5				
HBM2	fractal			364.7	2.10	5.0	4.34×10^{-6}
HBM3	fractal			102.7	3.01	3.8	2.31×10^{-6}

Finally, the behaviour of the copolymers in d-EtOH was investigated, since the ink formulations tested later in Chapter 8 are primarily ethanol-based. The copolymers were dispersed into d-EtOH from THF using the same solvent switch method as employed for dispersion into D₂O. Only the BMA versions of the copolymers were used for SANS, as these were the materials used in printing studies. **Figure 5.17** shows the scattering profiles for this set of copolymers.

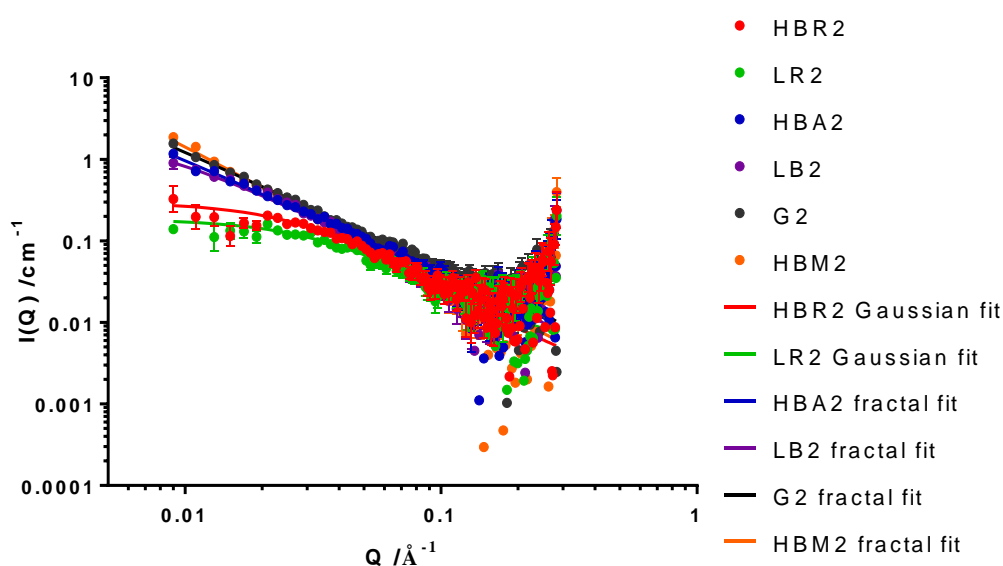


Figure 5.17. Scattering profiles for the reduced data obtained from P(BMA-AA) copolymers at 0.5% concentration in d-EtOH. Circles represent data points and solid lines represent optimal model fit. Error bars represent the standard error on each data point, but are not visible on some data points (at low Q due to small size of error bars, at high Q due to large size of error bars). (key: letters refer to architecture and distribution HBR = highly branched random, HBM = highly branched methacrylate core, G = graft, LR = linear random, HBA = highly branched acrylic acid core and LB = linear block, numbers refer to methacrylate monomer, 2 = BMA)

In this solvent system, the scattering of the copolymers differed strongly according to their monomer sequence distribution. The scattering of both random

copolymers, HBR2 and LR2, was best represented by the Gaussian model, indicating that they remained dissolved in d-EtOH. However, the other four copolymers having segmented structures, G2, HBM2, HBA2, and LB2, displayed higher scattering intensities which were found to be best fitted by the fractal model. This indicated that these copolymers have a tendency to begin aggregating into larger structures in d-EtOH. This could have significance for the formulation of inks, as the formation of aggregates in the ink prior to or during the printing process could lead to nozzle clogging and consequently a decrease in print quality. The values of the fitting parameters obtained from these models are summarised in **Table 5.13**. Here, the fractal dimensions are close to $5/3$ which is the standard value for swollen polymer chains, showing that the fractal aggregates are composed of aggregated swollen chains instead of clustered networks.

Table 5.13. Selected Results of Model Fitting to SANS Data of P(BMA-AA) Copolymers in d-EtOH

sample	model	M_w/M_n	$R_g/\text{\AA}$	correlation length, $\xi/\text{\AA}$	fractal dimension	radius / \AA	SLD block / \AA^{-2}
HBR2	Gaussian	2.38	56.0				
LR2	Gaussian	3.99	48.5				
G2	fractal			499.9	1.49	6.0	1.40×10^{-6}
HBM2	fractal			599.2	1.72	4.2	1.60×10^{-6}
HBA2	fractal			499.9	1.48	5.7	1.47×10^{-6}
LB2	fractal			166.1	1.57	5.3	1.40×10^{-6}

Table 5.14. Summary of SANS Results: Comparison of Models for P(nMA-AA) Copolymers in each Solvent System

sample	d-THF	1:1 d-THF:D ₂ O	D ₂ O	1:1 d-THF:CDCl ₃	d-EtOH
HBR1	Gaussian	fractal	sphere	Gaussian	
HBR2	Gaussian	fractal	sphere	Gaussian	Gaussian
HBR3	Gaussian	Gaussian	sphere	Gaussian	
LR1	Gaussian	Gaussian	sphere	Gaussian	
LR2	Gaussian	fractal	sphere	Gaussian	Gaussian
LR3	Gaussian	fractal	Lamellar ParaCrystal	Gaussian	
G1	Gaussian	fractal	Lamellar ParaCrystal	fractal	
G2	Gaussian	sphere	Lamellar ParaCrystal	fractal	fractal
G3	Gaussian	fractal	sphere	Gaussian	
HBM1	Gaussian	fractal	Lamellar ParaCrystal	Gaussian	
HBM2	Gaussian	fractal	Lamellar ParaCrystal	fractal	fractal
HBM3	Gaussian	sphere	Lamellar ParaCrystal	fractal	
LB2					fractal
HBA2					fractal

Table 5.14 summarises the results of the model fits for the SANS data of each copolymer in each solvent system. This allows identification of trends within the data. In d-THF all copolymers are well solvated and therefore form Gaussian coils, since both PAA and PnMA segments experience a good solvent environment. In the other four solvent systems, changes in self-assembly behaviour are observed for different copolymers. Overall, the random and segmented copolymers exhibit different responses to solvent environment. This is seen most clearly in d-EtOH, in which the two random copolymers form Gaussian coils whilst the four segmented copolymers form fractal aggregates. The trend is less evident in the other solvent systems but still present: for example, in D₂O all the random copolymers form spheres whilst the segmented

copolymers form multilamellar micelles, with the notable exceptions of LR3 and G3. These two copolymers, however, are among the exceptions from the 1:1 PnMA:PAA molar ratio, with G3 having no detectable PAA and LR3 having much more PAA than PLMA (1.7:1.0), which may explain why they behave differently to the rest of the materials with equivalent structure. For the most part, the segmented structures show more response to the solvent system, meaning that they are quicker to form self-assembled structures, whereas the random copolymers respond less: either by remaining as Gaussian coils or by forming less organised self-assembled structures, such as spheres instead of multilamellar structures. This is due to structural differences in the copolymers. In the segmented copolymers the separate blocks are able to move and respond more independently to the solvent conditions, whereas in the random copolymers the PAA and PnMA segments are distributed randomly and unable to move independently, therefore it is much more difficult for them to aggregate together.

5.4 Conclusions

The poly(alkyl methacrylate-acrylic acid) copolymers were dispersed into water, a block-selective solvent for the hydrophilic block, using the solvent switch method starting from THF. A combination of TEM, PALS (including particle sizing and zeta potential measurements) and SANS was used to study the self-assembly behaviour of the materials. Differences in the self-assembled structures formed were observed due to architecture, monomer distribution and also the hydrophobicity of the alkyl methacrylate monomer. Larger, smooth spherical micelles were observed for the random materials in both branched and linear architectures. The block and graft copolymers, on the other hand, formed a greater range of structures including aggregates, spherical micelles and more unusual structures such as lamellar 'onion' micelles.

Small angle neutron scattering was used to study the copolymer behaviour in a range of different solvent systems. In d-THF, a good solvent for both blocks, all the data fitted to the Gaussian coil model indicating that the copolymers were well solvated. Differences between the copolymers were observed in the other solvent systems. Following the addition of D₂O to form 1:1 d-THF:D₂O mixtures, the majority of copolymers were represented by a fractal model as the chains began to aggregate and form clustered networks, whilst a couple of materials either remained Gaussian coils or aggregated further to form spheres. All copolymers formed self-assembled structures in

D₂O. Most scattering profiles fitted well to the sphere model whilst some notable examples exhibited lamellar behaviour similar to that of multi-lamellar vesicles. When CDCl₃, a hydrophobic block-selective solvent, was added to d-THF in a 1:1 mixture, the copolymers primarily remained as Gaussian coils with four materials beginning to aggregate into fractals. D-EtOH was also studied to simulate the solvent base used for the printing ink formulation. The behaviour of the copolymers was found to vary according to monomer sequence distribution: both branched and linear random copolymers were well-solvated as Gaussian coils whilst the block and graft copolymers formed fractal aggregates of swollen chains.

6. Formation of Onion Micelles from the Self-Assembly of HB P(BMA-*b*-AA) in Water

In this chapter, we show that the branched P(BMA-*b*-AA) copolymer forms lamellar ‘onion’ micelles. The mechanism of formation of these unusual structures is investigated. These micelles exhibit a temperature response which can be used to encapsulate and release Rhodamine B, a model compound.

6.1 Introduction

The self-assembly of amphiphilic block copolymers in solution has led to the formation of many aggregates with interesting morphologies including spherical micelles, vesicles, rods, tubes and lamellae.^{195, 211-214} For linear amphiphilic block copolymers in a block selective solvent, variation of copolymer morphology from spheres to worms to vesicles can be observed. It has been proposed that there exists a packing parameter, P , which can control the type of morphology formed. This concept was introduced to rationalise surfactant self-assembly²¹⁵ and was later extended to include the self-assembly of diblock copolymers.²¹⁶ A short stabiliser (hydrophilic) block results in a low steric barrier to micelle fusion and therefore a drive to achieve greater stability through the formation of larger structures, whereas long stabiliser blocks provide effective steric stabilisation, removing the drive for micelle fusion.²¹⁷

The most widely studied of these supramolecular aggregates are micelles, which can be classified into simple and complex micelles. Simple micelles, called primary micelles by Eisenberg,²¹⁸ are formed by the primary aggregation of block copolymers in a block-selective solvent due to microphase separation. Complex micelles, however, are larger in size with a more complicated structure.^{196, 219} These are large compound micelles (LCMs) formed from the secondary aggregation of primary micelles.

Large micelles have also been reported from the self-assembly of dendrimers and highly branched (HB) copolymers in solution. Branching within copolymer molecules leads to an overall globular structure. This results in the existence of different mechanisms of self-assembly compared to linear block copolymers.²⁰¹ HB copolymers tend to form unimolecular micelles in solution, which undergo secondary aggregation into multimicelle aggregates (MMAs).¹⁹⁹

Self-organised precipitation (SORP) involves the evaporation of a good solvent from a mixture of both good and poor solvents, allowing the formation of well-developed separation structures in block copolymer nanoparticles. The kinetically-preferred morphology is formed on removal of solvent from the disordered solvent-containing nanoparticles.²²⁰ Thus, the evaporation of a good solvent from a good-poor solvent mixture results in the trapping of kinetic structures.²²¹ These in-plane structured micelles are metastable and locked in a kinetically trapped nonergodic state of dispersion (i.e. a local equilibrium) which is stabilised by glassy domains within the polymer. It was found that further annealing of the structures, either by the action of heat or solvent, led to formation of the thermodynamically preferred morphology.²²²

6.2 Self-Assembly of HB P(nMA-*b*-AA) Copolymers in Water

As shown in Section 5.2, the three HB P(nMA-*b*-AA) copolymers self-assemble into very different structures when dispersed into water. Spherical micelles with a rough appearance to the particle surface are formed from the HB P(MMA-*b*-AA) copolymer. The BMA analogue, however, forms lamellar ‘onion’ micelles. **Figure 6.1** shows a larger TEM image of these structures. The HB P(LMA-*b*-AA) copolymer forms much smaller particles which are more elliptical in shape and have a dimple in the centre. These results clearly demonstrate the strong effect that changing the alkyl group on the methacrylate monomer has on the self-assembly behaviour, as the architecture, degree of branching and molecular weights were kept as constant as possible and could not account for the differences in self-assembled structures observed. Further experiments were therefore carried out on this set of copolymers to investigate the unusual behaviour observed.

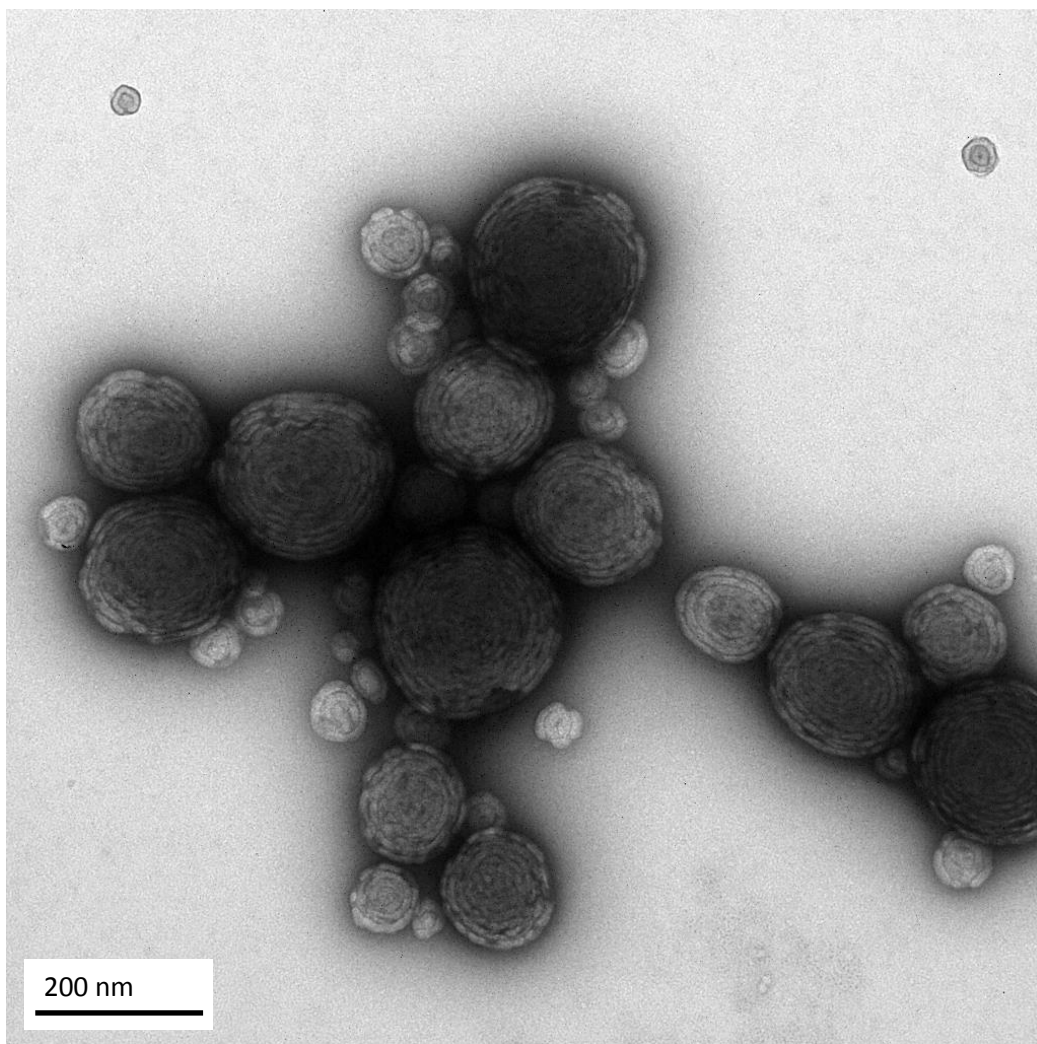


Figure 6.1. TEM image of HB P(BMA-*b*-AA) self-assembled into onion micelles in water, negatively stained with uranyl formate.

SEM was used to investigate whether the onion micelles had flat disc-like structures or three-dimensional spherical structures. SEM is used to study the surface of the sample whereas TEM can enable visualisation of the internal structure. A TEM grid to which a stained HB P(BMA-*b*-AA) dispersion was adsorbed was sputter-coated with Au and used for SEM imaging to allow direct comparison between the TEM and SEM images. The SEM images in **Figure 6.2** show that the onion micelles are in fact spherical, and the lamellar structure as shown by TEM is a series of internal concentric shells.

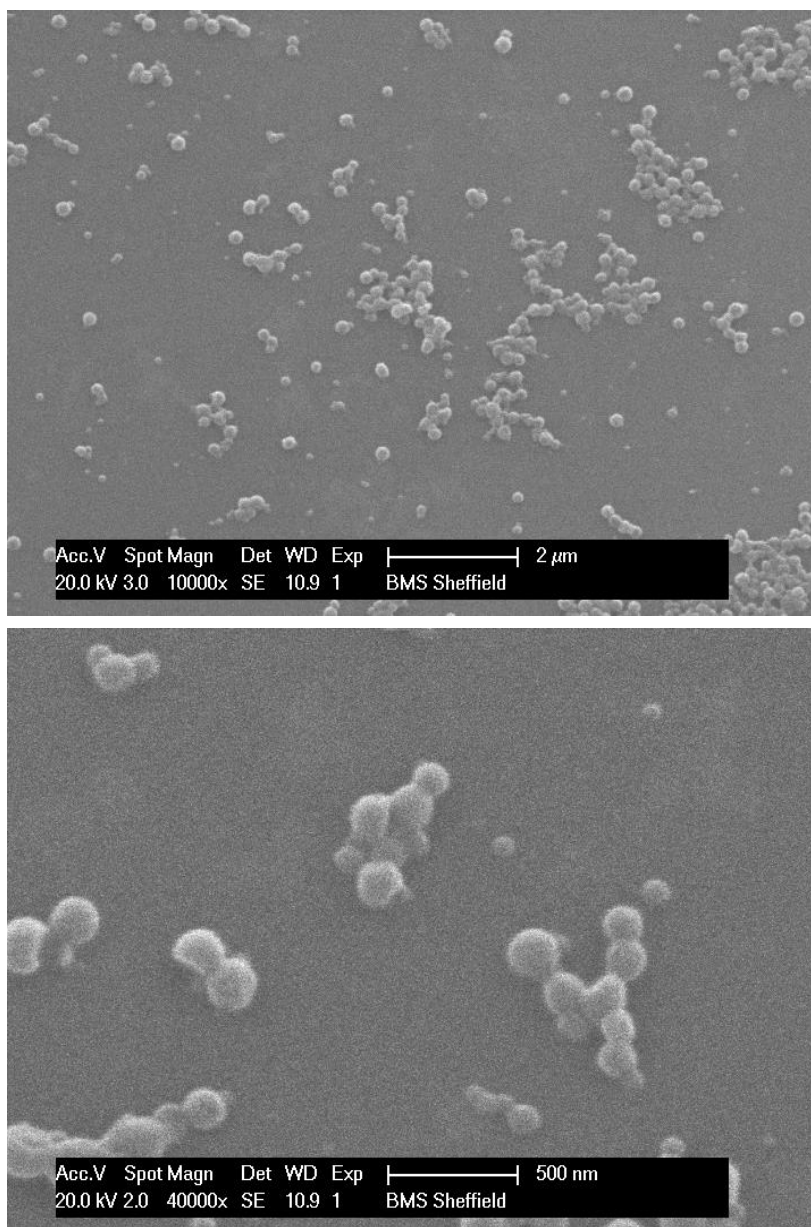


Figure 6.2. SEM images of the spheres formed by HB P(BMA-*b*-AA). A TEM grid with adsorbed HB P(BMA-*b*-AA), stained with uranyl formate, was sputter-coated with Au and imaged by SEM

SANS was used to study dispersions of the copolymers in D₂O. Diverse scattering profiles were obtained for the three samples, as seen in **Figure 6.3**. A clear Bragg peak was observed for the HB P(BMA-*b*-AA) sample which is characteristic of a multilayered structure. The simple relation **Equation 6.1**:

$$Q = \frac{2\pi}{d} \quad \text{Equation 6.1}$$

can be used to predict the layer spacing. Using the Q value of the Bragg peak an average spacing of 12 nm is predicted for HB P(BMA-*b*-AA). Despite the apparent differences in the profiles, the scattering of all three copolymers fitted to a Lamellar ParaCrystal model.²¹⁰ **Table 6.1** summarises the values of the fitting parameters obtained from the model. It must be noted that due to the greater amount of noise in the scattering of the HBM1 particles, the model fit is much less reliable than those of the other copolymers and therefore the parameters in **Table 6.1** are subject to a large degree of error.

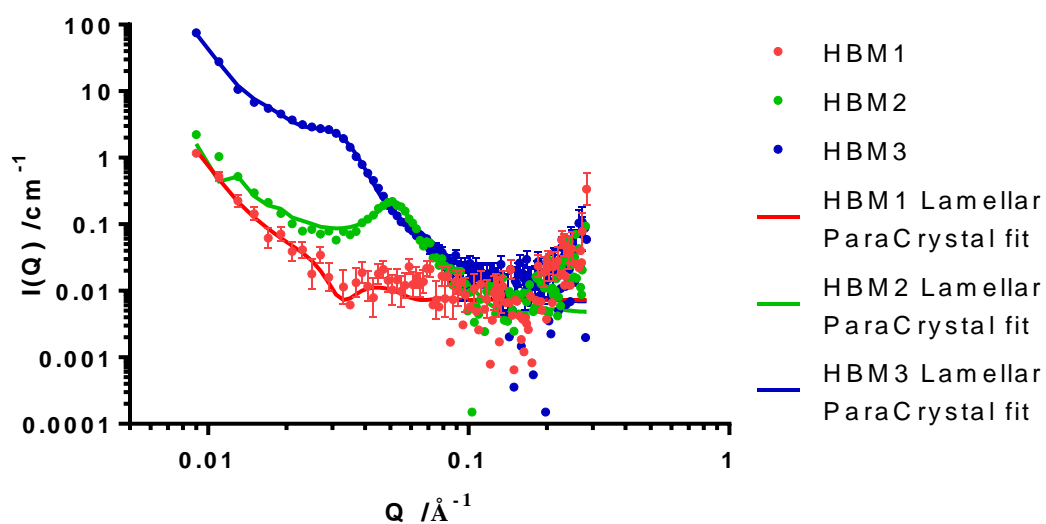


Figure 6.3. SANS scattering profiles of $I(Q)$ against Q for the reduced data obtained from HB P(*n*MA-*b*-AA) copolymers dispersed in D₂O at 0.5% w/v (HBM1: HB P(MMA-*b*-AA), HBM2: HB P(BMA-*b*-AA), HBM3: HB P(LMA-*b*-AA)). Solid line shows fits to Lamellar ParaCrystal Model for each copolymer.

Table 6.1 Summary of Values Obtained for Fitting Parameters from Model Fit to HB P(nMA-*b*-AA) SANS Data

Model Parameter	HBM1	HBM2	HBM3
Number of layers	2.44	10.37	2.60
Dispersity of spacing	0.25	0.22	0.24
SLD layers /Å ⁻²	3.71 x 10 ⁻⁶	2.07 x 10 ⁻⁶	2.29 x 10 ⁻⁶
Spacing /Å	179.7	114.6	166.6
Thickness /Å	188.6	42.3	138.9

The model fit gives a layer spacing for HBM2 of 11.4 nm, which is very close to the spacing obtained from the Bragg peak, and demonstrates some associated dispersity which can be observed in the TEM images. The model suggests an average of ten layers which also seems to agree with the TEM results. The scattering length density (SLD) of the layers is approximately $2.07 \times 10^{-6} \text{ \AA}^{-2}$. This shows that there is water within the onion structure as the calculated SLD for the copolymer is $1.4 \times 10^{-6} \text{ \AA}^{-2}$.

Interestingly, lamellar structures were also indicated for HBM1 and HBM3, but with much fewer layers. The results suggest a mixture of bi- and tri-layered micelles, with much thicker layers than calculated for HBM2. Increased values of SLD again indicate the presence of D₂O within the micelle structure.

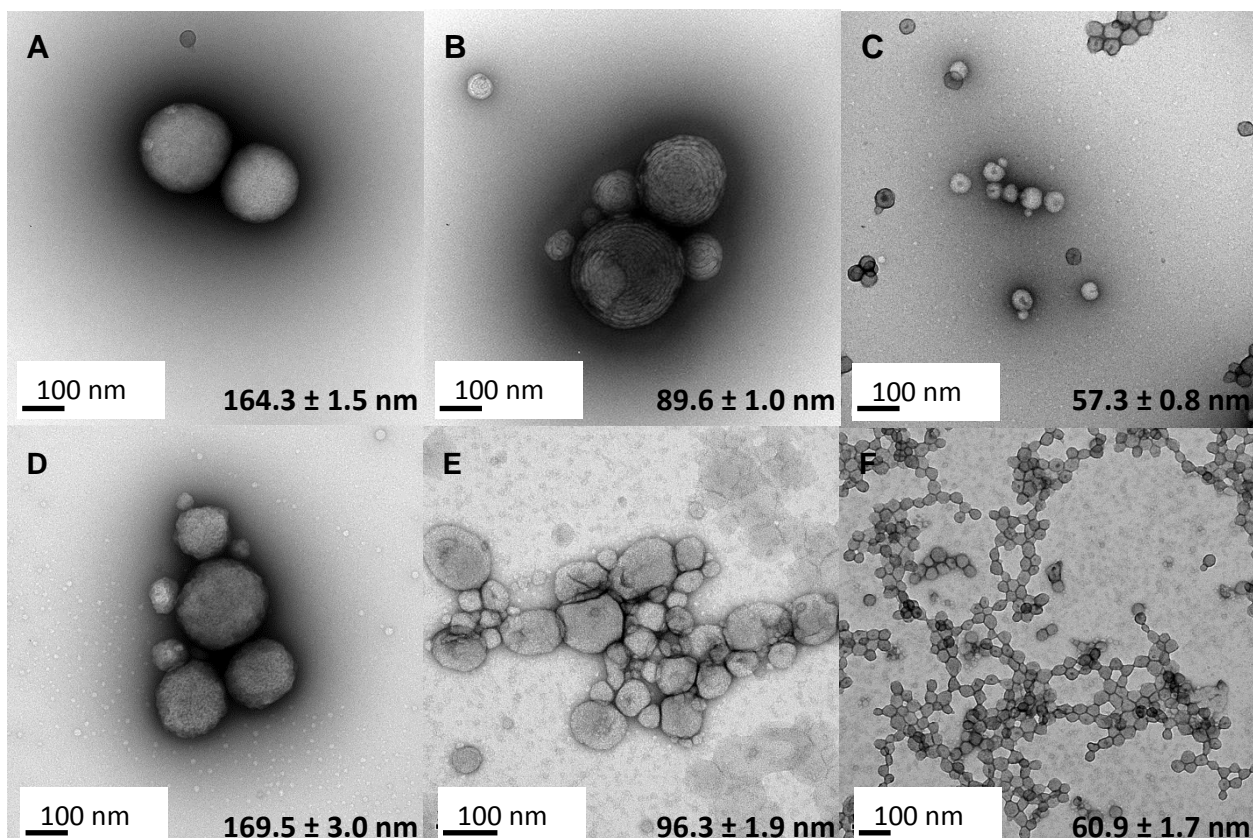


Figure 6.4. Representative TEM images of copolymers A: HB P(MMA-*b*-AA), B: HB P(BMA-*b*-AA) and C: HB P(LMA-*b*-AA) self-assembled in water and D: HB P(MMA-*b*-AA), E: HB P(BMA-*b*-AA) and F: HB P(LMA-*b*-AA) following annealing at 45°C for 12 hours. Samples were stained with uranyl formate. Inset text displays the results of particle sizing measurements.

Annealing was carried out on the dispersions to investigate whether the self-assembled structures responded to temperature. Sample tubes containing copolymer dispersion in water were sealed and immersed in an oil bath heated to 45°C for 12 hours. Samples were removed and imaged by TEM before and after the annealing period, as shown in **Figure 6.4**. Particle sizing measurements were also performed. The HB P(MMA-*b*-AA) and HB P(LMA-*b*-AA) structures underwent a small increase in size and associated error, and their shapes appeared to become slightly more irregular. The HB P(BMA-*b*-AA) micelles also underwent a small increase in particle size and the error increased. More significantly, the lamellar structure was no longer present, with a more vesicle-like structure observed.

A second study was carried out to investigate the time-dependence of the annealing process. A sample of onion micelles in water was heated at 40 °C and samples were removed and analysed by TEM during the annealing process. **Figure 6.5** shows some of the images taken at time points of 8, 14, 17 and 20 hours.

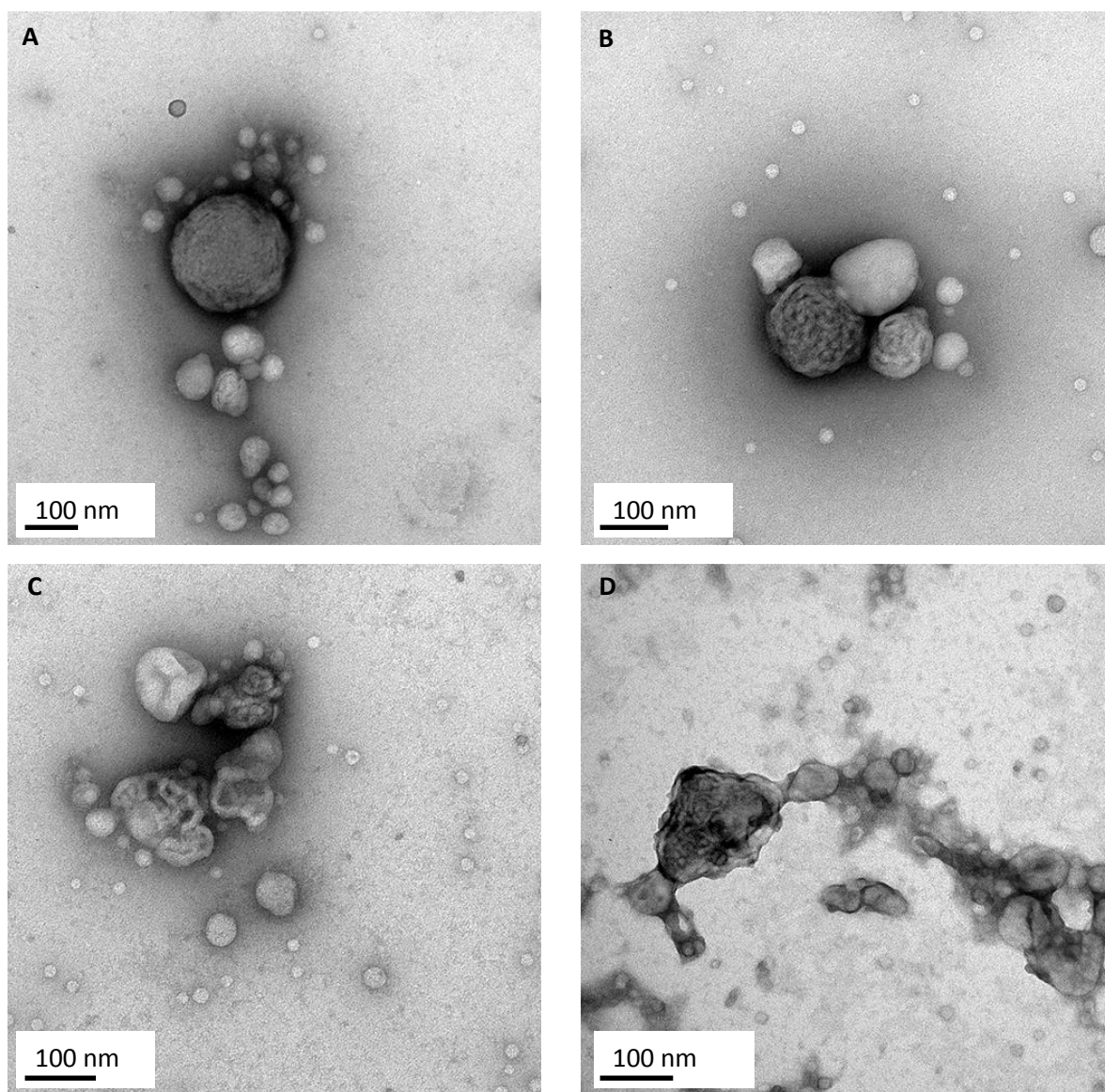


Figure 6.5. Representative TEM images of HB P(BMA-*b*-AA) onion micelles self-assembled in water following annealing at 40 °C after A) 8 h, B) 14 h, C) 17 h and D) 20 h. Samples were negatively stained with uranyl formate. Onion micelles are still seen after 8 h (A) but reorganisation begins to be observed by 14 h (B) and is evident by 17 h (C). Vesicle-like structures are observed after 20 h of annealing (D).

Lamellar structure was still observed in the images taken following eight hours of annealing. By 14 hours, however, some evidence of unravelling and reorganisation was seen, with some of the structures no longer having visible layers. A much greater degree of unravelling of the onion structures was observed in the sample taken after 17 hours of annealing, with some structures having a more vesicle-like appearance. The final image shows the structures after 20 hours of heating. The majority of structures observed adopted a vesicle-like structure with no visible lamellar structures, although a few lamellar domains were observed such as the one seen in the image in **Figure 6.5**. These results show that the annealing process does occur gradually over a period of time, although the mechanism of the annealing process of these onion micelles and how the transition occurs from an ordered lamellar structure to a disordered vesicle-like structure remains unclear.

The pH response of the micelles was also investigated. Dispersions were prepared in buffer solutions at pH 4, 7 and 10, with NaCl added as necessary to maintain constant ionic strength. **Figure 6.6** shows TEM images of each dispersion at each pH, and **Figure 6.7** shows the particle sizing data represented graphically.

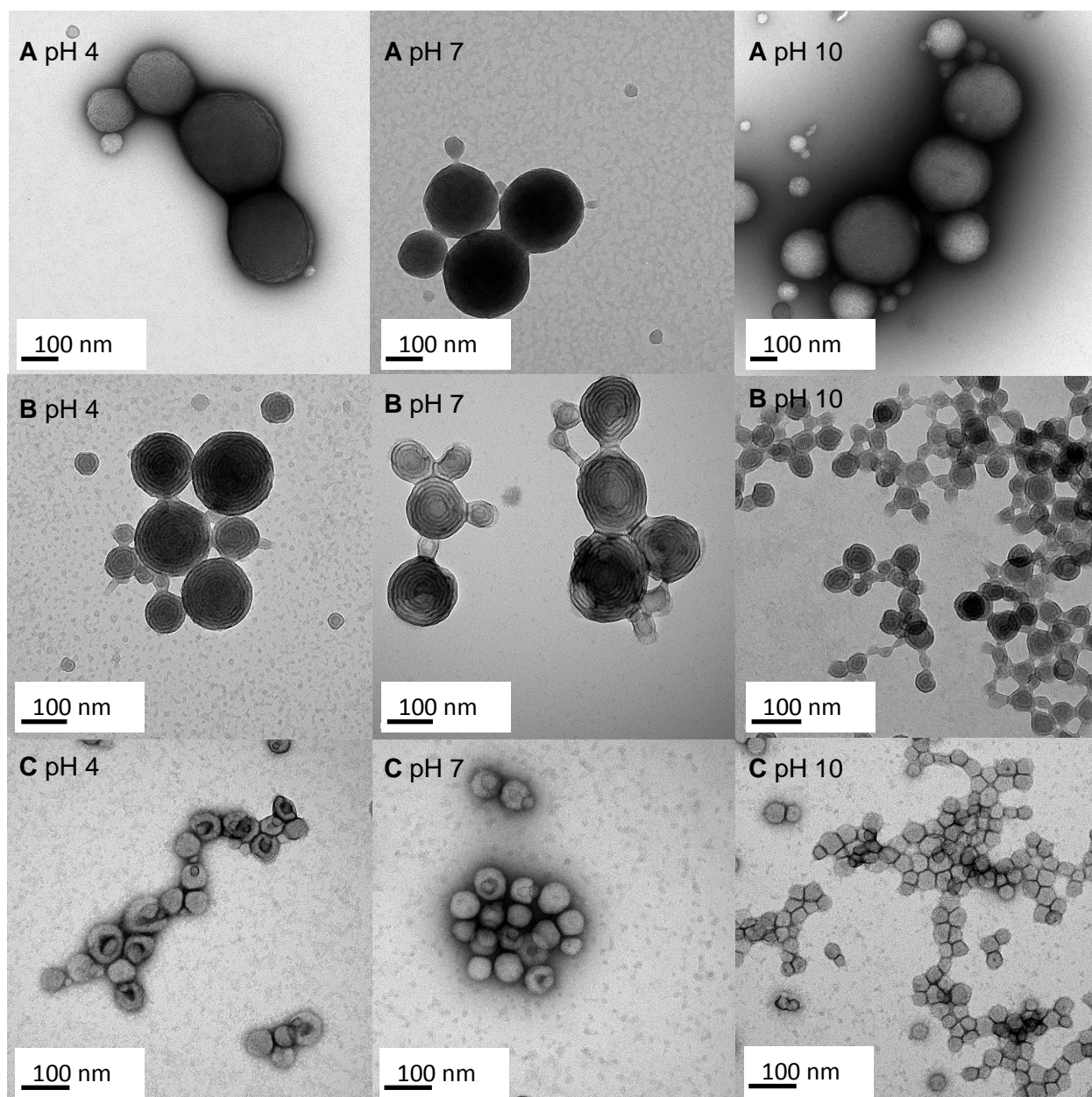


Figure 6.6. Representative TEM images of copolymers A: HB P(MMA-*b*-AA), B: HB P(BMA-*b*-AA) and C: HB P(LMA-*b*-AA) self-assembled in water at different pH values: pH4, pH7 and pH 10. Samples are stained with uranyl formate. Samples were prepared by Joseph Ferner during his undergraduate summer placement.

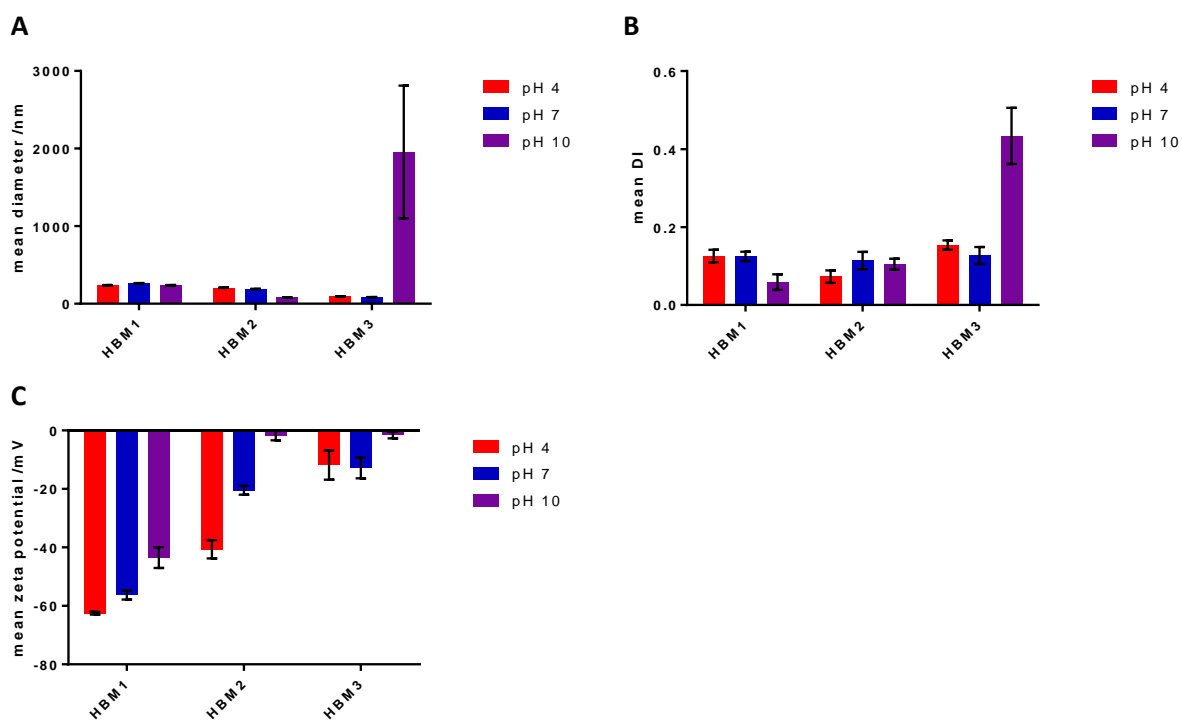


Figure 6.7. Results of PALS measurements of copolymers HBM1: HB P(MMA-*b*-AA), HBM2: HB P(BMA-*b*-AA) and HBM3: HB P(LMA-*b*-AA) self-assembled in water at different pH values: pH4 (red), pH7 (blue) and pH 10 (purple). Graph A represents mean diameters, Graph B represents mean dispersity indices, and Graph C represents mean zeta potential values. Samples were prepared by Joseph Ferner during his undergraduate summer placement.

The self-assembled structures of all three copolymers appear to be stable at both pH 4 and pH 7, but the HBM2 and HBM3 dispersions become unstable at pH 10 when the acrylic acid groups are fully ionised. For HBM1 a slight increase in size and decrease in zeta potential from pH 4 to pH 7 are observed but the dispersion stability is maintained. At pH 10 the HBM1 particle results are close to those at pH 4, with similar particle size and appearance and the zeta potential, although decreased by almost 20 mV, still represents a stable colloid. The mean particle sizes decreased slightly for HBM2 and HBM3 from pH 4 to pH 7. The HBM2 zeta potential decreased by 20 mV, falling below the stable colloidal threshold, while the zeta potential of the HBM3 dispersion remained close to -12 mV which demonstrates that it is the least stable of the

three copolymers. At pH 10 the HBM2 particles are much smaller, although they still possess a lamellar structure. The zeta potential is much reduced indicating a loss of stability. Conversely, the mean diameter obtained from PALS for HBM3 is very large. This is due to the presence of large aggregates of the smaller micelles, which can be seen to be aggregating in the TEM image. The zeta potential identifies a corresponding loss of colloidal stability.

It is, however, counterintuitive that the zeta potential should become less negative from pH 4 through to pH 10. At pH 4 the acrylic acid should be mostly protonated, whilst at pH 7, above the pKa of approximately 5, the acid groups are mostly ionised and expected to be almost fully ionised at pH 10. The zeta potential would be expected to become correspondingly more negative as pH increases. This could be possibly be explained by aggregation of the particles as they obtain more negative charge, which would act to screen the charges from the electrode. Some evidence for this is observed in the TEM images.

These results indicate that there is some pH response for the HBM2 and HBM3 copolymers in that they lose stability at high pH as the PAA segments become ionised. This is not observed for the HBM1 copolymer however. This variation is possibly due to the difference in hydrophobicity between the methyl, butyl and lauryl groups on the alkyl methacrylate. As MMA is the least hydrophobic, there is less of a difference in the hydrophobic/hydrophilic balance when the hydrophilic segment is ionised.

The stability of the onion micelles under ambient conditions was also investigated. A sample of HB P(BMA-*b*-AA) dispersed in water was prepared and analysed by TEM and PALS to confirm that onion micelles were formed. This sample was then kept on the lab bench at room temperature for a period of 5 weeks and subsequently re-analysed. **Figure 6.8** shows TEM images of the sample before and after storage. It is clear that the lamellar structure remains intact during this period, although some aggregation may have occurred, though this may be due to drying effects during TEM grid preparation. These results suggest that despite the kinetically trapped nature of the onion structures, they are stable at room temperature.

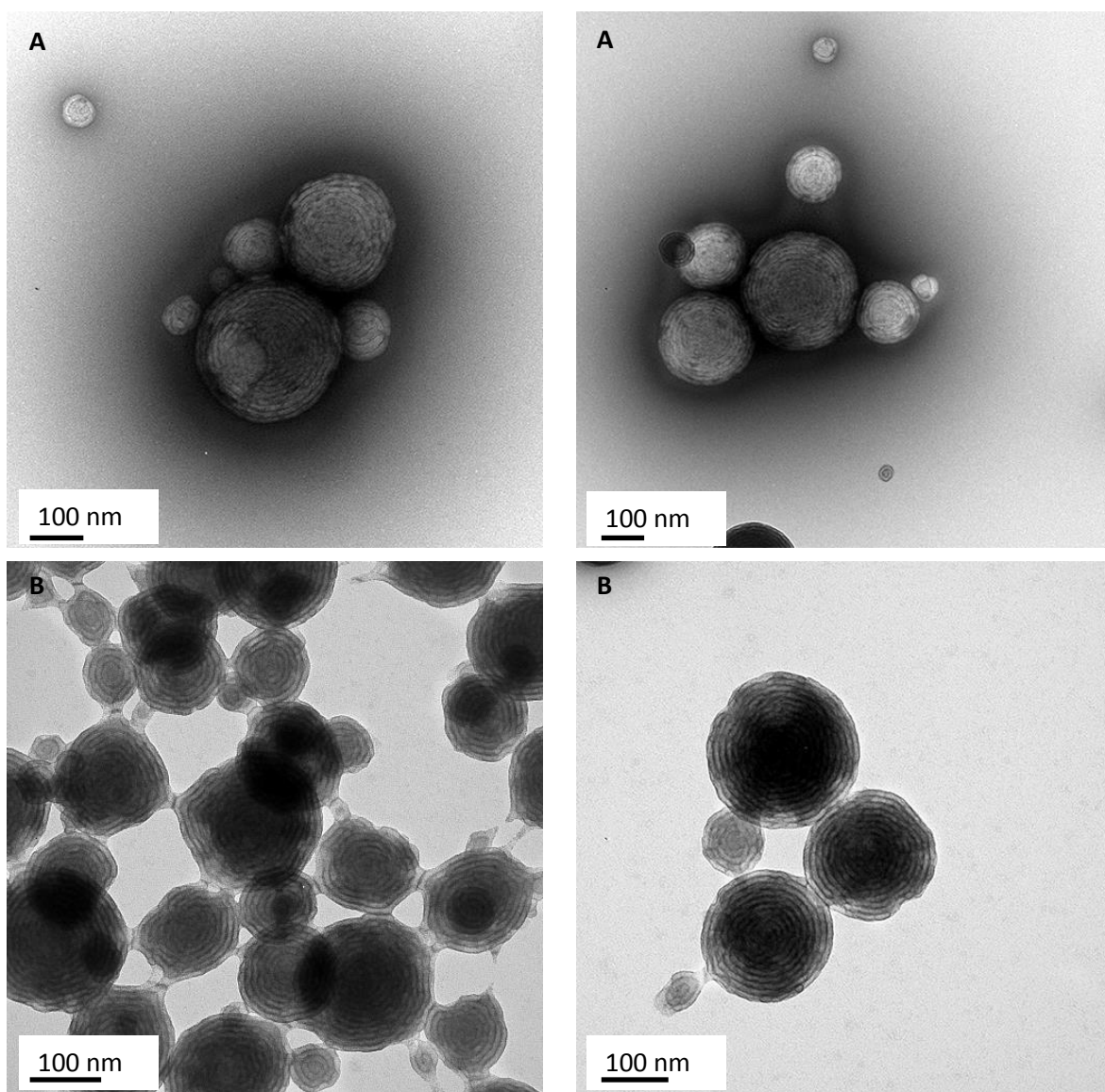


Figure 6.8 TEM images of onion micelles formed from HB P(BMA-*b*-AA) dispersed in water A) immediately following preparation and B) after 5 weeks storage at ambient conditions. Although there is a slight increase in size after five weeks storage, there are no significant differences between the structures and so it can be concluded that they are stable under ambient conditions.

Table 6.2 Results of PALS Analysis of the Onion Micelles formed from HB P(BMA-*b*-AA) Dispersed in Water Immediately Following Preparation ($t = 0$) and After 5 Weeks Storage in Ambient Conditions ($t = 5$ weeks)

storage time	mean diameter /nm	mean dispersity
$t = 0$	82.5 ± 0.7	0.10 ± 0.02
$t = 5$ weeks	210.8 ± 1.2	0.14 ± 0.01

One interesting aspect of the onion micelle formation is the mechanism by which they are formed. Several experiments were carried out to aid in determining this. The first of these was the investigation of the effect of the rate of block-selective solvent addition to the copolymer solution. This was added using a syringe pump to ensure a constant addition rate, which meant that the rate could be easily varied. Five different water addition rates were selected: 0.05, 0.10, 0.20, 0.50 and 1.00 ml min⁻¹, and dispersions prepared at each rate were analysed by TEM and PALS. **Figure 6.9** shows example TEM images of onion micelles prepared at each addition rate. The thicknesses of the lamellae within the onions were measured using ImageJ image analysis software and are represented graphically in **Figure 6.10**.

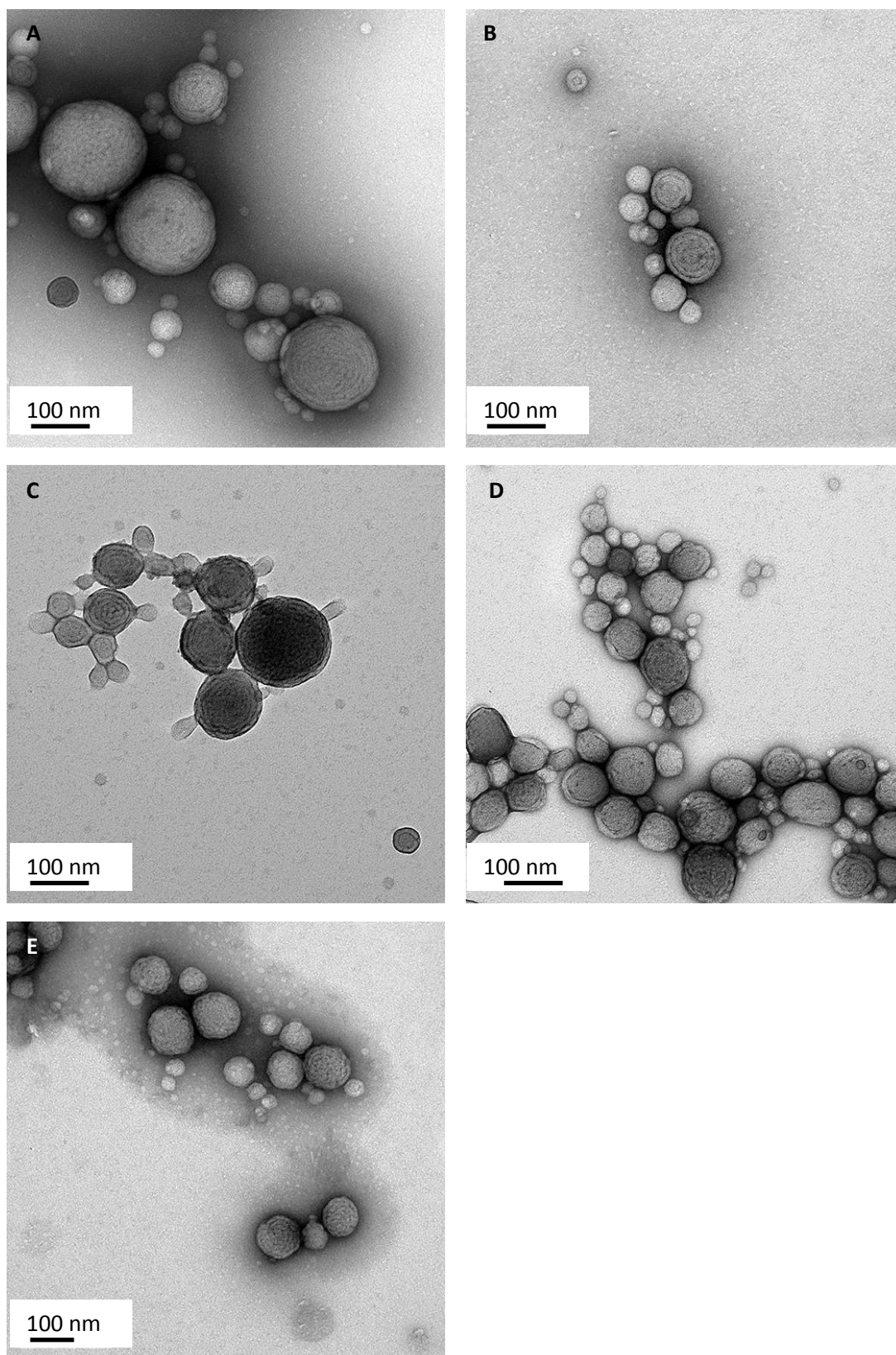


Figure 6.9. Representative TEM images of HB P(BMA-*b*-AA) copolymer self-assembled in water at different rates of water addition: A) 0.05, B) 0.10, C) 0.20, D) 0.50 and E) 1.00 ml min⁻¹. Samples are stained with uranyl formate. Lamellar structure is observed in each image.

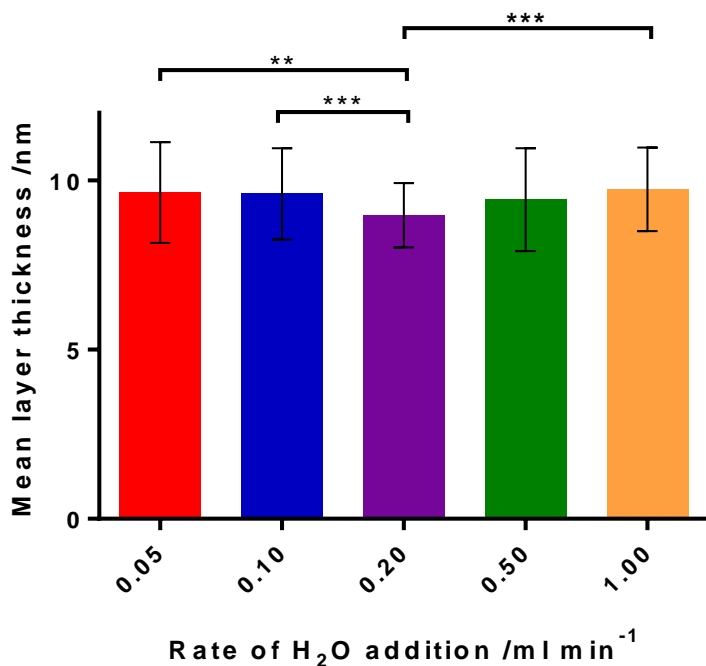


Figure 6.10. Graph of mean layer thickness of onion micelles, as calculated from TEM images using ImageJ software, at different rates of water addition to HB P(BMA-*b*-AA) copolymer solution in THF. Error bars represent standard deviation. Tie lines show significance level of comparisons between sets of copolymers: *** $P < 0.001$, ** $0.001 < P < 0.01$, * $0.01 < P < 0.5$, ns (not significant) $P \geq 0.05$. Here, only significant relationships between copolymers are shown on the graph.

A one-way ANOVA was carried out on these data to determine whether there are statistically significant differences between the means of the different addition rates. The rationale behind the test and the method are fully explained in **Appendix 1. Tables 6.3** and **6.4** summarise the results for this set of data. The calculated F value is larger than F_{crit} but only by a small margin, and the R^2 value, which gives a measure of the goodness of fit of the linear regression model, is 0.05 which is very low. This suggests that we cannot be confident that the observed differences between the measured layer thicknesses at different rates of water addition are actually due to the change in rate. A Tukey post-hoc analysis was carried out to identify where the significant differences lie.

These are indicated on the graph in **Figure 6.10**. It was concluded that the rate of water addition did not control the structure of the onion micelles.

Table 6.3. Summary Data for Mean Layer Thickness of Onion Micelles at Different Rates of Water Addition used for One-Way ANOVA

addition rate /ml min ⁻¹	N (count)	mean layer thickness /nm	standard deviation /nm
0.05	113	9.64	1.49
0.10	100	9.90	1.35
0.20	100	8.97	0.95
0.50	108	9.43	1.52
1.00	104	9.74	1.24

Table 6.4. One-Way ANOVA Results for Mean Layer Thickness of Onion Micelles at Different Rates of Water Addition

F	F _{crit}	P	P<0.05?	R ²
7.15	2.45	<0.001	Y	0.05

It was theorised that the evaporation step was the driving force for the formation of the onion micelles. In order to test this, the micelle preparation procedure was carried out as usual but instead of allowing the THF to evaporate once the water was added, the solution was injected into a dialysis cassette and the THF removed by dialysis against water. After 24 hours, the dispersion was removed from the cassette and imaged by TEM; **Figure 6.11** shows some of the images. Instead of onion micelles, many small spherical micelles are formed. The mean diameter of these micelles is 18 ± 4 nm. This is comparable to the diameter of the individual layers of the onion micelles formed when the THF is evaporated. Some coalescence of small spheres is observed; they appear to form a worm-like structure which is beginning to curve, and in the final image what looks like an onion micelle in the process of formation is seen. These results suggest that the evaporation step is a significant part of the process of onion micelle formation from this copolymer.

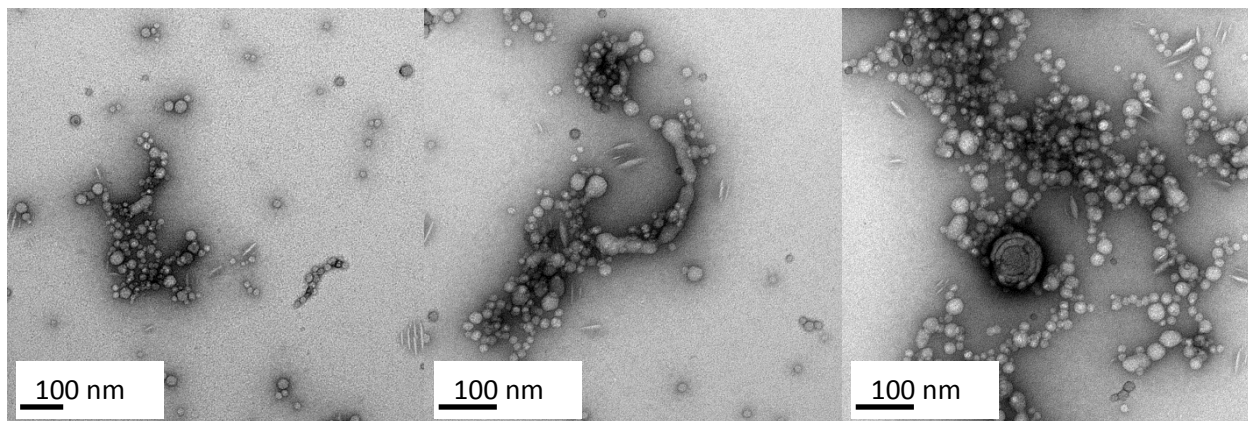


Figure 6.11. Representative TEM images of HB P(BMA-*b*-AA) copolymer self-assembled in water. Following water addition, samples were dialysed against water for 24 hours to remove residual THF, instead of the evaporation step. Samples were stained with uranyl formate. Predominantly small spherical micelles are observed, with some evidence of coalescence into worm-like structures.

A study was carried out in order to check that a significant amount of water was not lost during the evaporation of THF from the solution. This would result in the polymer being present at a higher concentration in the dispersion than intended, meaning that theories concerning dilute solution behaviour may not be applicable. This was tested through monitoring the water loss through mass balance, with the THF loss monitored by ^1H NMR. It was found that 11.5% of the water was lost in the time taken for all of the THF to evaporate. This resulted in a final polymer concentration of 0.56% w/v, which is only a discrepancy of 12% from the assumed concentration of 0.50% w/v and therefore we can consider the dispersion to be dilute.

Another aspect to be considered when attempting to elucidate the mechanism of onion micelle formation is the time-dependence of the process. For example, do we see nucleation from the centre of a micelle, suggesting a gradual self-assembly process, or does assembly occur at a certain concentration (ie. when a certain proportion of THF has evaporated)? In order to investigate this, the standard onion micelle preparation procedure was carried out and once all the water had been added, samples of the

dispersion were removed every fifteen minutes and studied by TEM. **Figure 6.12** shows the results of the study.

Irregular flocs were formed in the initial stages, as seen in images A to C. 40 minutes after water addition was complete, what appear to be large aggregates of small worm-like structures were observed. The first onion-like structures were observed after 60 minutes, but most appear to be in the process of completion; for example the structure in image E where a lamellae appears to be not yet coiled into the onion. After 75 minutes, well-defined onion micelles were observed throughout the sample. Some aggregated 'floc' is also seen. Discrete micelles continued to be observed at the later time points, in addition to some which appear to be still in the process of forming, as well as very small spheres and worm-like structures. Some structures which are more vesicle-like in appearance are observed in the later stages of the experiment. The results of the study appear to suggest that the formation of onion micelles is time-dependent, which is compatible with the concept of onion formation being a kinetic process. However the mechanism of formation remains not fully understood.

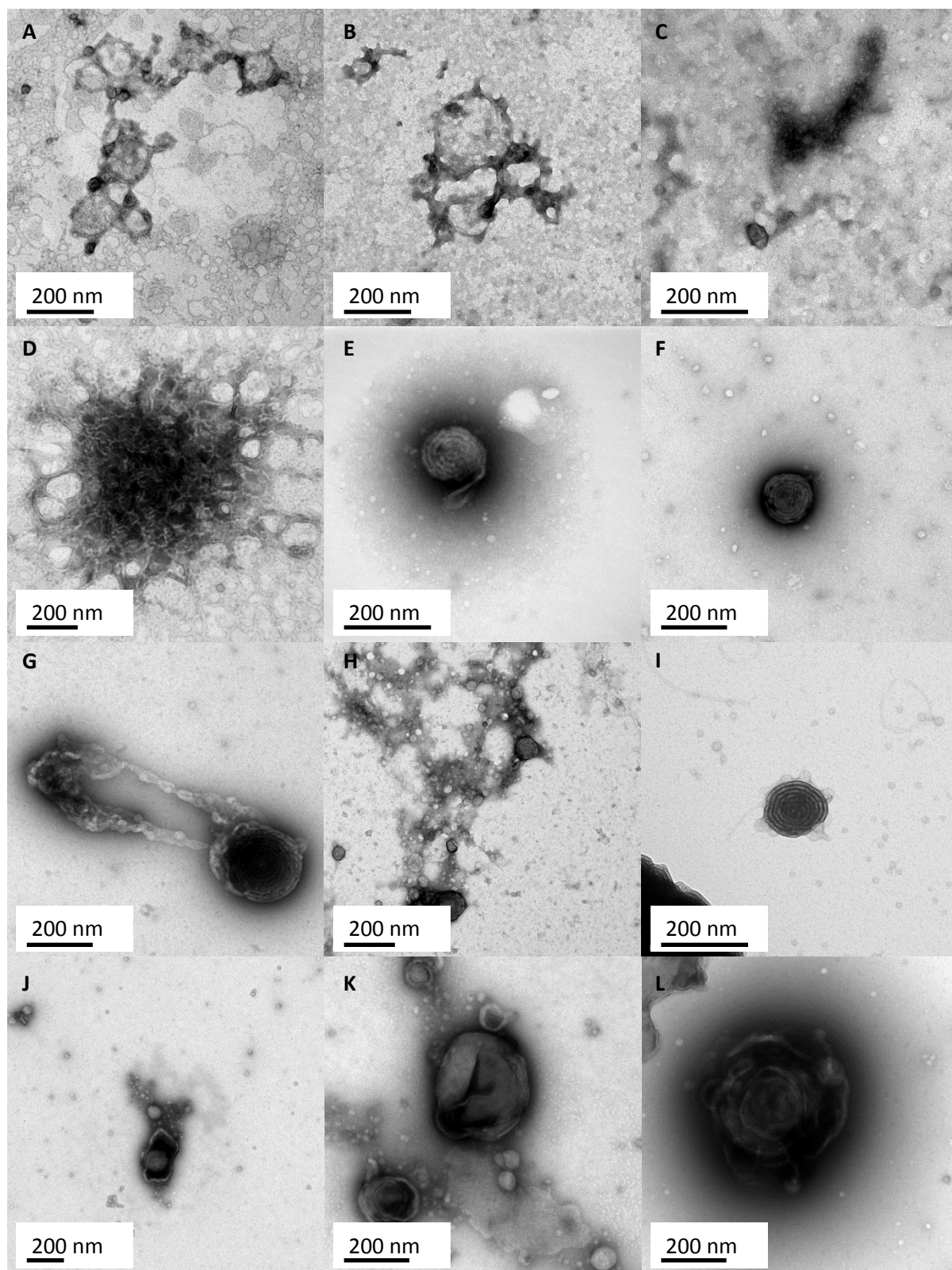


Figure 6.12 Representative TEM images of HB P(BMA-*b*-AA) copolymer self-assembled in water, showing the evolution of self-assembly following water addition to copolymer in THF solution. Samples were removed at regular intervals of 15 minutes and analysed by TEM: A) $t = 0$, B) $t = 15$ min, C) $t = 30$ min, D) $t = 45$ min, E) $t = 60$

min, F) $t = 75$ min, G) $t = 90$ min, H) $t = 105$ min, I) $t = 120$ min, J) $t = 135$ min, K) $t = 150$ min, and L) $t = 165$ min. Samples were stained with uranyl formate.

The ratio of hydrophilic to hydrophobic segments in a block copolymer is known to play an important role in self-assembly. Consequently, the ratio of methacrylate to acrylic acid in these copolymers was expected to affect their self-assembly behaviour. To test this theory, HB P(nMA-*b*-AA) copolymers with varying ratios of BMA to AA were synthesised by Natalie Paul, an undergraduate student carrying out a summer project. Five different polymers were prepared in all, with BMA:AA ratios of 0.5:1.0, 0.75:1.0, 1.0:1.0, 1.5:1.0 and 2.0:1.0. Dispersions in water were prepared and imaged by TEM; **Figure 6.13** shows the images obtained.

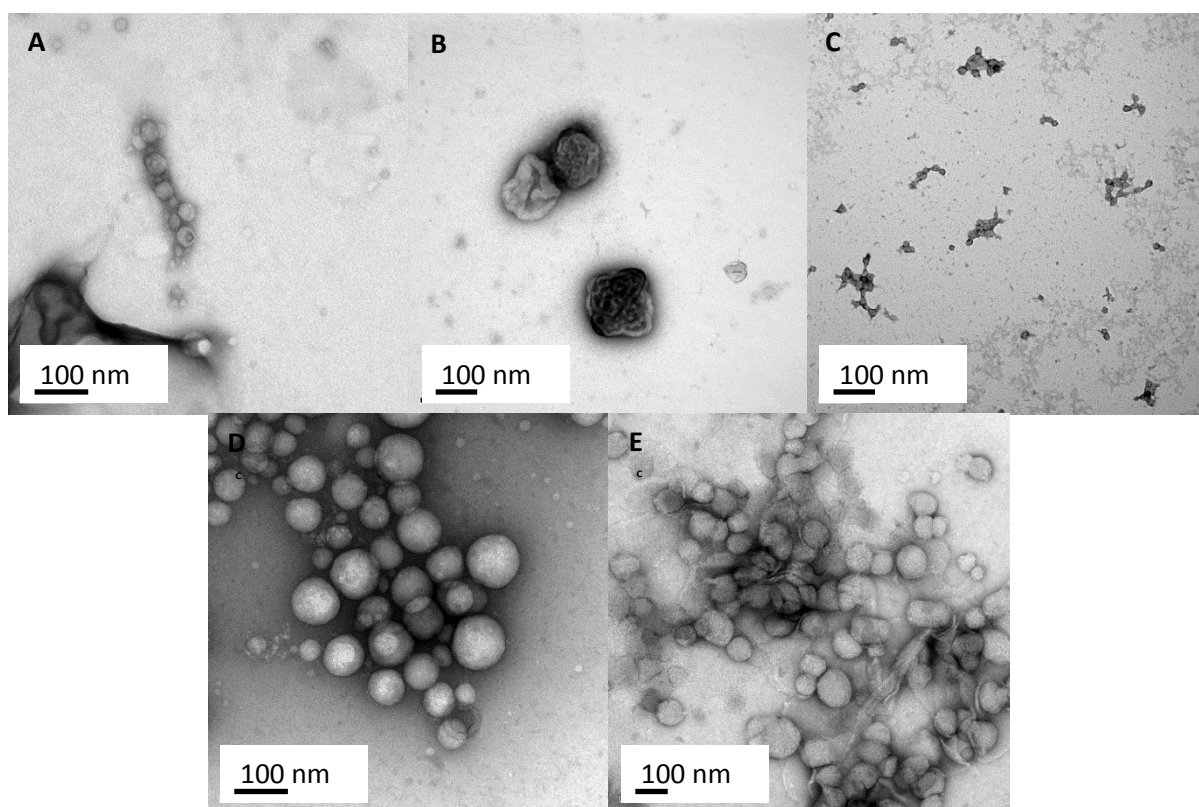


Figure 6.13 Representative TEM images of HB P(BMA-*b*-AA) copolymers with varying ratios of BMA to AA self-assembled in water: A) 0.5:1.0, B) 0.75:1.0, C) 1.0:1.0, D) 1.5:1.0, E) 2.0:1.0. Samples were stained with uranyl formate.

The results seen in **Figure 6.13** confirm that the ratio of hydrophobic to hydrophilic monomer within these copolymers has a significant effect on their self-assembly behaviour. Large spheres are seen when less AA is present relative to the amount of BMA, whereas very small spheres are formed where copolymers contain more AA relative to BMA. This is consistent with the work of Warren et al.²¹⁷ who found that a longer hydrophilic ‘stabiliser’ block meant that the steric energy barrier was too high to allow micelle fusion, whilst a shorter stabiliser block leads to more favourable micelle fusion. In the case of linear block copolymers, this leads to the formation of fibres or ‘worms’ when the stabiliser block is shorter. In this case, when there is less AA the small unimolecular micelles fuse to form more energetically favourable large compound micelles, whereas when more AA is present it can adequately stabilise the smaller micelles. Onion micelles are observed at only one ratio, 0.75:1.0 PBMA:PAA, indicating the presence of a ‘sweet spot’ where onion micelle formation is favourable.

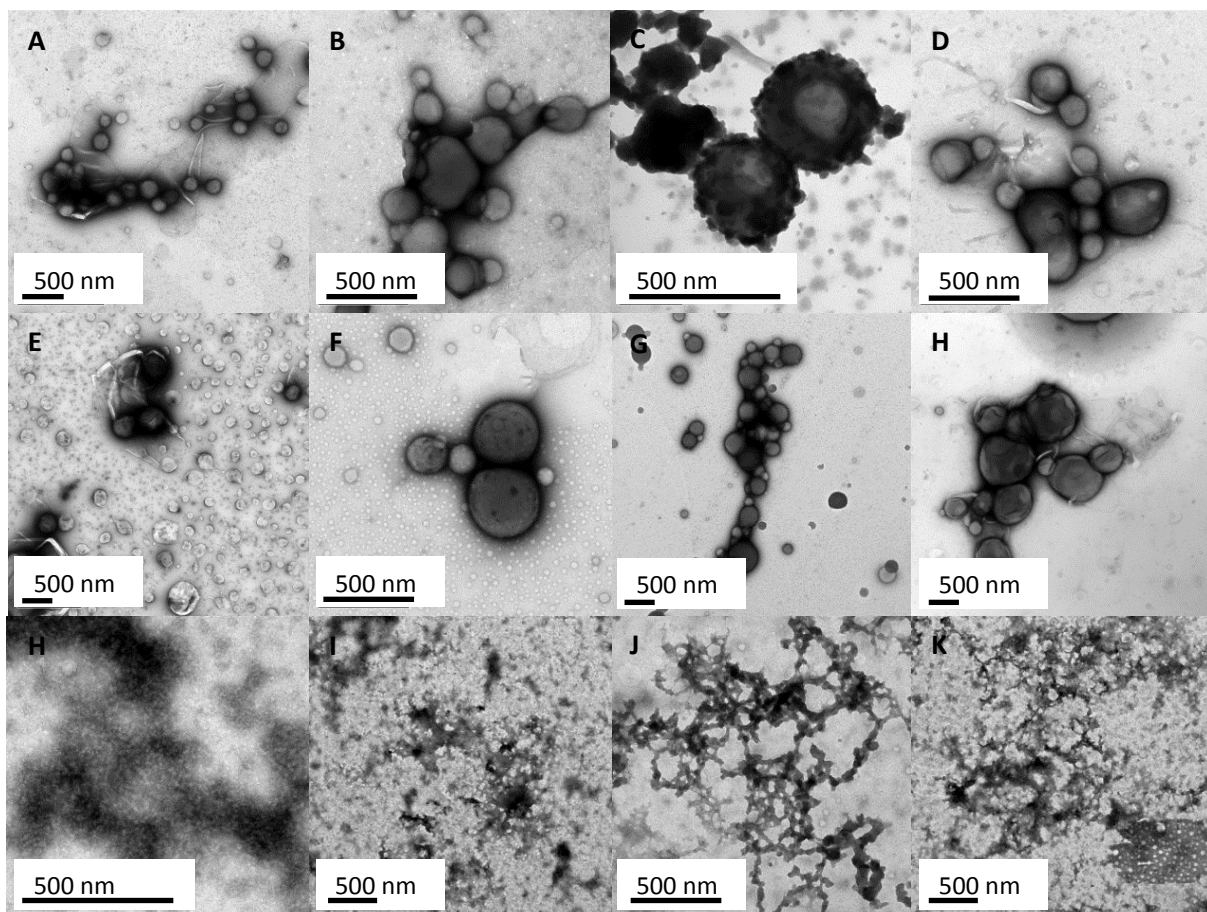


Figure 6.14 Representative TEM images of HB P(nMA-*co*-AA) copolymers self-assembled in buffer solutions at different pH values: HB P(MMA-*co*-AA) A) pH 1, B) pH 4, C) pH 7, D) pH 10, HB P(BMA-*co*-AA) E) pH 1, F) pH 4, G) pH 7, H) pH 10, HB P(LMA-*co*-AA) I) pH 1, J) pH 4, K) pH 7, L) pH 10. Samples were stained with uranyl formate. Samples were prepared by Joseph Ferner during his undergraduate summer placement.

The effect of pH on the formation of the other HB copolymers was also studied. Dispersions of each MMA, BMA and LMA version of HB P(AA-*b*-nMA) and HB P(nMA-*co*-AA) were prepared in buffer solutions at pH values of 1, 4, 7 and 10, with NaCl added where necessary to keep the ionic strength constant. The results of TEM imaging for the branched random copolymers are shown in **Figure 6.14** and for the branched block copolymers with PAA core in **Figure 6.15**. Onion micelles are not observed for either structure, indicating that the architecture is important for onion formation. The random copolymer forms large smooth micelles at intermediate pH, and

are less stable at both high and low pH. The HB P(LMA-*co*-AA) copolymer formed aggregated structures at all pH values. However the block copolymer with PAA core and PnMA side chains was found to form interesting structures. The presence of the hydrophilic core and hydrophobic side chains seemed to encourage the formation of raspberry-like structures (seen in images C, D, F, G and H). These were more stable at pH 7 and 10.

These results suggest that the segmentation of the hydrophobic and hydrophilic parts of branched copolymers induces the formation of more unusual self-assembled structures, whilst branched copolymers with a random distribution of hydrophilic and hydrophobic monomers tend to form larger spherical 'compound' micelles.

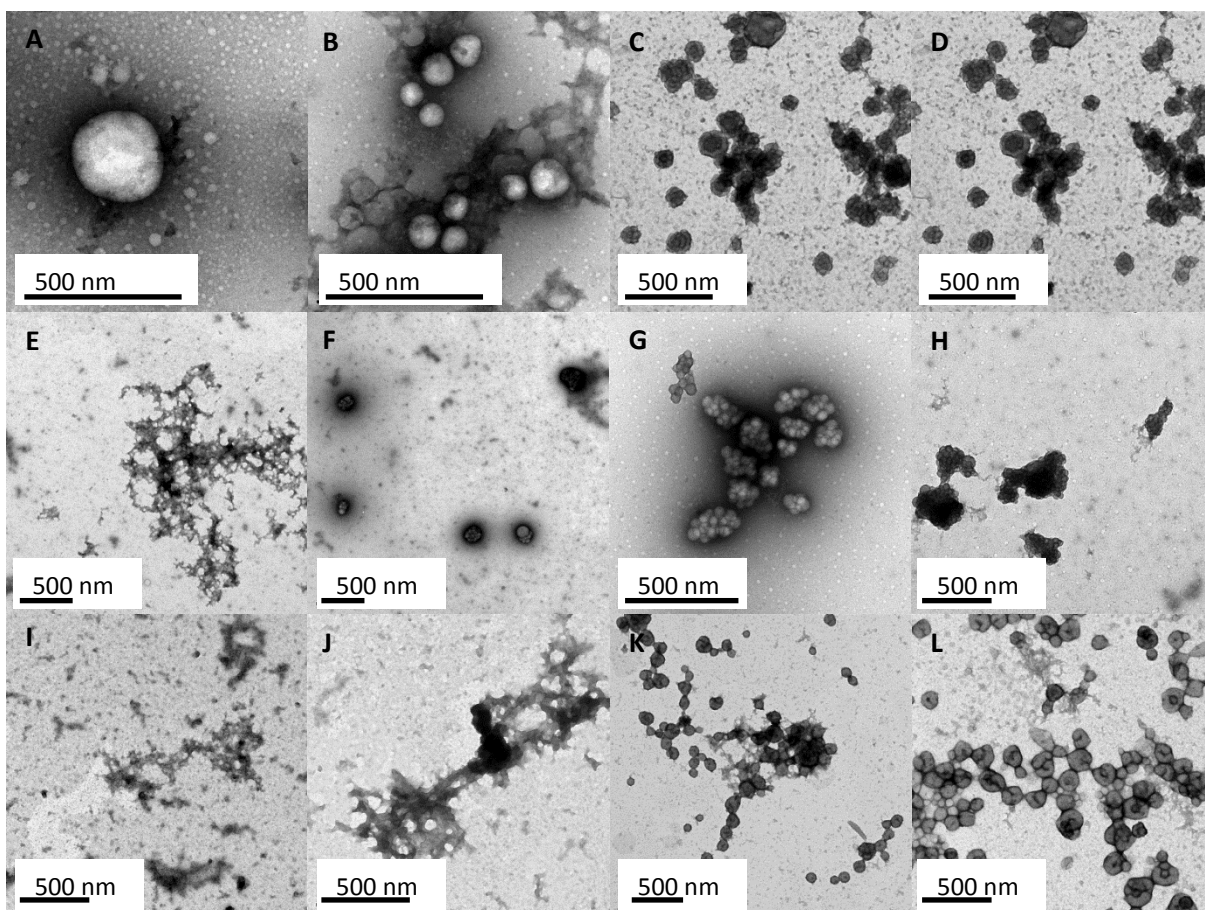


Figure 6.15 Representative TEM images of HB P(AA-*b*-nMA) copolymers self-assembled in buffer solutions at different pH values: HB P(AA-*b*-MMA) A) pH 1, B) pH 4, C) pH 7, D) pH 10, HB P(AA-*b*-BMA) E) pH 1, F) pH 4, G) pH 7, H) pH 10, HB P(AA-*b*-LMA) I) pH 1, J) pH 4, K) pH 7, L) pH 10. Samples were stained with uranyl formate. Samples were prepared by Joseph Ferner during his undergraduate summer placement.

6.3 Discussion of the Formation of Onion Micelles

The formation of onion micelles occurs due to the packing and coalescence of small unimolecular micellar spheres. The self-assembly process is driven by minimisation of interfacial energy. At this ratio of hydrophilic PAA to hydrophobic PBMA segments, the stabilising hydrophilic block is not long enough to confer sufficient steric stabilisation and hence the barrier to micelle fusion is low.

THF is a good solvent for both PAA and PBMA, so the copolymers are initially present as random coils in solution, as the SANS data confirm. Water, however, is a

good solvent for PAA and a poor solvent for PBMA (meaning it is a traditional block-selective solvent for amphiphilic block copolymer self-assembly). As the water is added and THF begins to evaporate, PAA becomes more soluble and PBMA becomes less soluble. The PBMA segments are driven inside the micelle to minimise the contact with water, with PAA on the outside acting to stabilise the micelles. It is proposed that the presence of some remaining THF in the mixture promotes the hydrogen bonding between PAA segments rather than the occurrence of hydrogen bonding between PAA and water. Particle coalescence leads to the formation of lamellar phases. Curvature is induced in an attempt to reduce the PBMA contact with water and increase the PAA contacts. Lamellae align into spherical particles following the curvature of the initial spheres. Hydrogen bonding of PAA to PAA in adjacent shells (lamellae) minimises the presence of PAA-water interactions.

The slow evaporation of THF from the THF-water solvent mixture allows time for the structural rearrangement to occur, followed by kinetic trapping of the onion structure once the evaporation is complete. This renders the onions metastable at room temperature. This is analogous to the SORP process where particles containing different kinetically trapped morphologies are prepared from block copolymers via the evaporation of good solvent from good/poor solvent mixtures. Yabu et al.²²¹ outlined the evolution of these structures from random coils in the good solvent, to nucleation of initial chains and adsorption of further copolymers as solvent quality decreases with evaporation of the good solvent, followed by eventual precipitation into nanoparticles dispersed in the poor solvent. Yabu et al. found that the provision of thermal energy to the system during the annealing process allows a more thermodynamically favourable structure to form. This appears to explain the behaviour of these HB P(BMA-*b*-AA) onion micelles also.

6.4 Release Studies from HB P(nMA-*b*-AA) Micelles

The interesting structures created by these branched P(BMA-*b*-AA) copolymers and their temperature-responsive behaviour may well have utility in encapsulation and release. This is an important form of technology used in applications such as drug delivery, cosmetics, foods and agriculture, and in the petrochemical industry, and involves the encapsulation of a target compound followed by release at a controlled rate

in response to some kind of trigger. Rhodamine B was chosen as the model compound to be used in the release studies. The structure of Rhodamine B is shown in **Figure 6.16** below. Since PAA acquires a negative charge when the acid group becomes ionised, a positively charged compound was chosen to promote binding. Additionally, Rhodamine B is a conjugated molecule and therefore its release can be easily monitored by UV-vis spectroscopy.

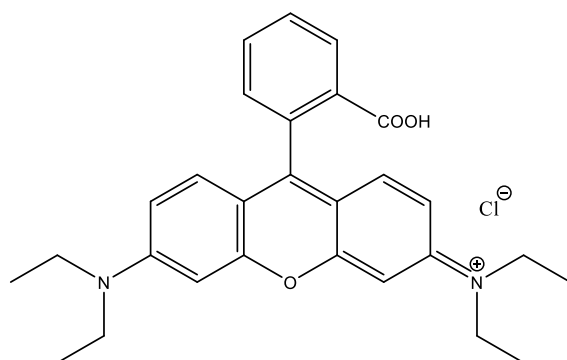


Figure 6.16. Chemical structure of Rhodamine B

The standard micelle preparation procedure was performed with Rhodamine B added to the water. This meant that when the onion micelles formed, Rhodamine B would be encapsulated inside them. The dispersions were then exhaustively dialysed against water at room temperature to remove any unbound Rhodamine B. Once no more Rhodamine B could be detected in the dialysate, the dialysis cassettes were placed into water heated at 40 °C, samples were taken at regular intervals and Rhodamine B release was monitored. A calibration was carried out to enable the concentration of Rhodamine B in water to be calculated. **Figure 6.17** shows the release profiles of the experiment, which was repeated three times. These proof-of-concept studies represent the amount of Rhodamine B released in the form of concentration; however it would be advantageous to study the percentage of total release, where the amount of compound encapsulated is measured before release to enable this to be calculated.

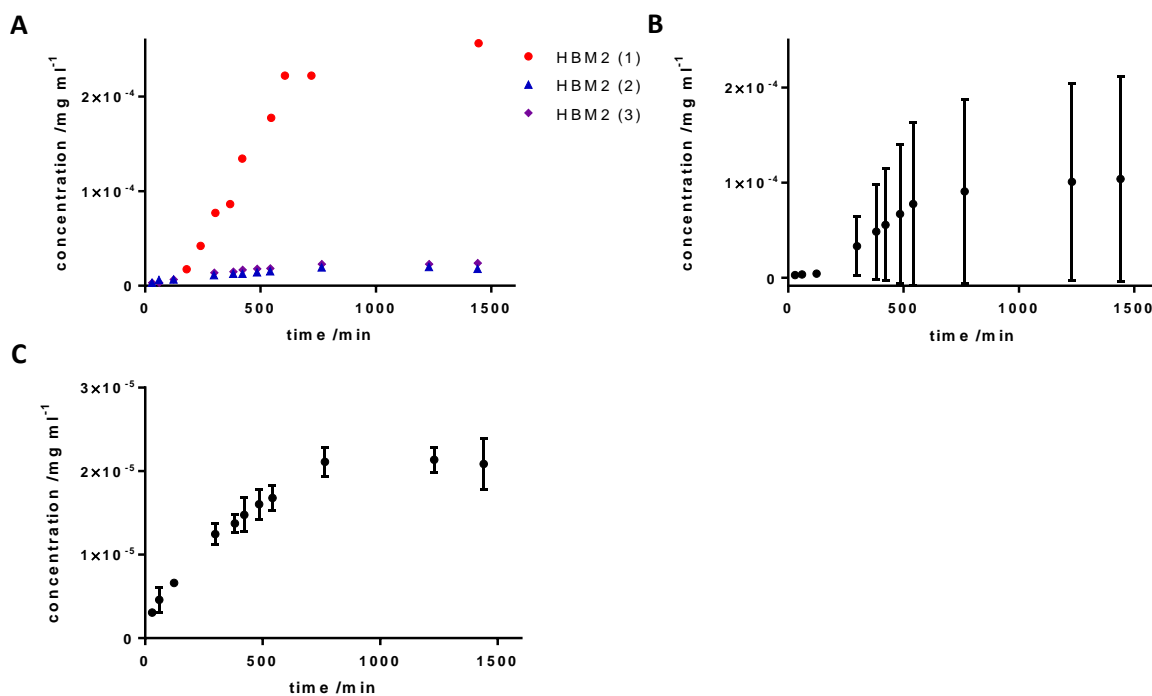


Figure 6.17. Release profiles of encapsulated Rhodamine B from HB P(BMA-*b*-AA) onion micelles monitored by UV-vis spectroscopy. Graph A shows the data from the three separate repeats of the experiment, Graph B shows the mean result from all three data sets with error bars representing standard deviation and Graph C shows the mean result from the second and third data sets with error bars representing standard deviation

Graph A in **Figure 6.17** shows the three separate release profiles whilst Graph B shows the release from the three experiments combined to give a mean value. The error bars show that the standard deviation is very large after the first few data points ($t > 250$ min), as the discrepancy between the first experiment and the other two is so large. This difference can be explained as the first time the experiment was carried out, the 40 °C water was contained in a beaker with tin foil acting as a lid; this did not control evaporation well and therefore over the period of the release experiment a reasonable volume of water would have been lost through evaporation. This would artificially increase the detected concentration of Rhodamine B in the water. The methodology was improved for the second and third experiments by using a sealed wide-necked Duran bottle to hold the water, thereby preventing the loss of water due to evaporation and leading to more accurate results. Consequently, only the second and third experiments are considered in the following analysis. Graph C in **Figure 6.17** shows the mean of the

second and third experiments and the data have substantially smaller error bars than Graph B.

It had been hypothesised that a burst release profile might have been observed as Rhodamine B was released from each layer of the onion micelle, but this was not seen. Initial release was very slow for approximately the first 120 minutes, after which point release appeared to be steady until a plateau was reached. It is possible the rate-limiting step could be the reorganisation of the layers, which occurs over the first few hours, after which point the trapped Rhodamine B is able to be released.

The same experiment was carried out on the HB P(MMA-*b*-AA) and HB P(LMA-*b*-AA) samples to compare their behaviour to that of HB P(BMA-*b*-AA). Both demonstrated similar release profiles to each other, which were different to those of the BMA onion micelles. The release profiles show fast initial release with no induction period, followed by a gradual slowing of release rate over time. Less overall Rhodamine B release was observed as less was able to be encapsulated within the micelles, since there are no layers present within the structures, and therefore more release of unbound compound was seen at room temperature. More Rhodamine B was able to be encapsulated within and released from HB P(MMA-*b*-AA) than HB P(LMA-*b*-AA). This could be because HB P(MMA-*b*-AA) forms larger micelles than the LMA analogue meaning more Rhodamine B can be contained inside them.

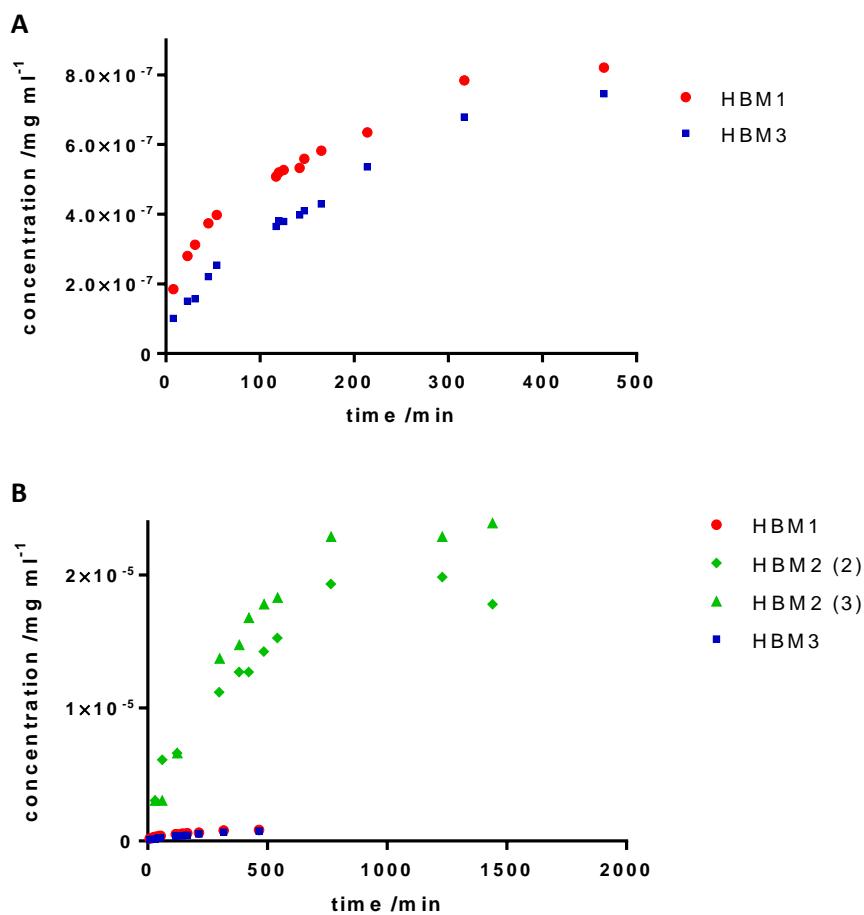


Figure 6.18. A) Release profiles of encapsulated Rhodamine B from HB P(MMA-*b*-AA) (HBM1, red) and HB P(LMA-*b*-AA) (HBM3, blue) micelles monitored by UV-vis spectroscopy and B) Comparison of release profiles of encapsulated Rhodamine B from HB P(MMA-*b*-AA) (HBM1, red), HB P(BMA-*b*-AA) (HBM2, green) and HB P(LMA-*b*-AA) (HBM3, blue) micelles

Equation 6.2 presents Fick's law of diffusion, where j_i is the diffusional flux, D is the diffusion coefficient, c_i is the concentration and x is the position. It states that the flux goes from regions of high concentration to regions of low concentration with magnitude proportional to the concentration gradient.

$$j_i = -D_{ip} \frac{dc_i}{dx} \quad \text{Equation 6.2}$$

Ritger and Peppas used this as the basis to derive the generalised **Equation 6.3**, where M_t is the concentration at time t , M_∞ is the concentration as time approaches infinity, k is a constant which incorporates characteristics of the system and the released compound, and n is a diffusional exponent.²²³

$$\frac{M_t}{M_\infty} = kt^n \quad \text{Equation 6.3}$$

The diffusional exponent is indicative of the mechanism of transport of the compound. An n value of 0.50 indicates that release is purely controlled by Fickian diffusion, whereas n greater than 0.50 demonstrates non-Fickian release behaviour. This equation is valid for the first 60 per cent of the fractional release. **Figure 6.19** shows the results of fitting this equation to the release data obtained for the different HB P(nMA-*b*-AA) copolymers.

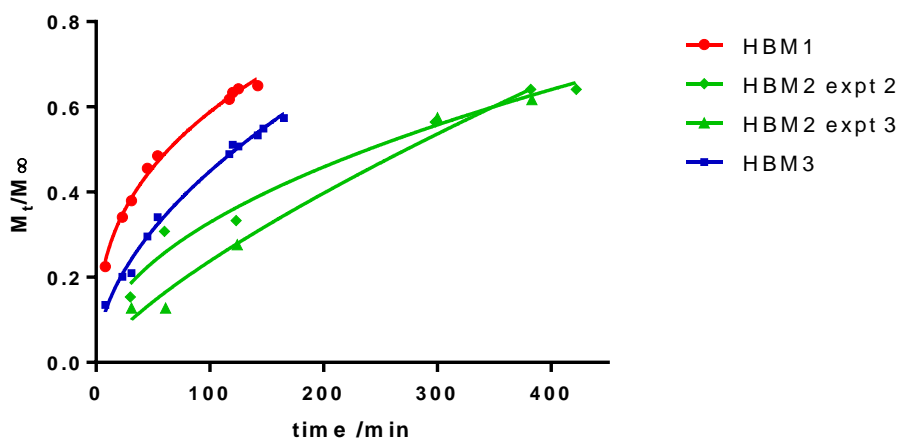


Figure 6.19. Graph of the results of fitting Ritger and Peppas' equation²²³ to data for the release of Rhodamine B from HB P(nMA-*b*-AA) micelles

Table 6.5 summarises the results obtained from the model fits. HBM3 has $n \approx 0.50$ indicating Fickian-diffusion controlled release. HBM1 has $n < 0.50$ which suggests

that something might be inhibiting the release so that it is slower than diffusion. For the HBM2 experiments, $n \geq 0.50$, suggesting that release from the onion micelles is faster than pure diffusion control. R^2 values are large for all samples, indicating good fits to the data. The results of the HBM2 experiments have much larger standard error values than those of the HBM1 and HBM3.

Table 6.5. Summary of Results of the Fitting of Ritger and Peppas' equation to Data for the Release of Rhodamine B from HB P(nMA-*b*-AA) Micelles

sample	k	n	SE on n	R ²
HBM1	9.21×10^{-8}	0.36	0.011	0.995
HBM2 expt 2	1.48×10^{-9}	0.48	0.048	0.976
HBM2 expt 3	3.92×10^{-10}	0.74	0.084	0.981
HBM3	2.96×10^{-8}	0.53	0.021	0.992

6.5 Conclusions

Here the self-assembly of the HB block P(nMA-*b*-AA) copolymers in water was studied in more detail. SEM was used to show that the HB P(BMA-*b*-AA) onion particles had a spherical 3D structure, which confirmed that the lamellar structure seen on the TEM images is internal. The lamellar structure was confirmed by the SANS data which fitted to a lamellar paracrystal model, with the parameters obtained from the fit in agreement with observations made by TEM. Annealing the sample at 45 °C for 24 hours was found to remove the lamellar structure, whilst no change was observed when the same procedure was carried out on the MMA and LMA analogues. Closer study of the annealing process seemed to suggest that the 'denaturing' of the onions is gradual, indicating a time-dependence. Dispersions of all three copolymers were prepared in buffer solutions at different pH values and studied by TEM and PALS. All three formed the most stable dispersions at pH 4 and 7, whilst both HB P(BMA-*b*-AA) and HB P(LMA-*b*-AA) were unstable at pH 10. The onion particles were found to be stable when stored at room temperature over a period of five weeks.

Several experiments were carried out to aid with elucidating the mechanism by which the onion micelles form. The rate of water addition to the copolymer solution was

investigated but found to have no statistically significant effect on onion formation. The evaporation of THF, however, was found to play an important role as when this step was omitted, small spheres were formed instead. The time-dependence of the onion formation was studied by TEM. Well-defined onions were formed 75 minutes after the addition of water was complete. The process appeared to be gradual; although the mechanism of formation remained unclear, the results did suggest a time-dependence. It was found that the ratio of BMA to AA within the polymer does affect the self-assembly behaviour. Onion micelles were only formed at one ratio, while small or large spheres were formed at the other ratios depending on the degree of steric stabilisation. The effect of pH on the other branched structures, HB block with PAA core and HB random, was studied. It was found that neither architecture formed onion micelles, but the HB P(AA-*b*-BMA) polymer formed raspberries. This suggested that architecture as well as composition influences self-assembly behaviour.

Finally, the onion micelles were investigated as delivery systems. Rhodamine B was used as a model compound, which was encapsulated within the micelles and released when they were heated. The release was monitored by UV-visible spectroscopy. The same experiment was carried out on the MMA, BMA and LMA copolymers. A much greater amount of Rhodamine B was released from the BMA polymer. This was also the only polymer to display an induction period in the release profile, possibly due to the reorganisation of the layers prior to release. Fitting of the release data to Ritger and Peppas' equation for release indicates that the MMA and LMA polymers display release behaviour that is under diffusion control, or slightly slower, whereas release from the BMA onions is faster than diffusion control.

7. Surface Properties and Adhesion Behaviour

The behaviour of the copolymers at surfaces is investigated by measuring the contact angles of probe solvents on polyolefin substrates coated with polymer. This allows calculation of surface energies of each coated substrate. Additionally, AFM force spectroscopy is tested as a technique for assessing copolymer adhesion behaviour.

7.1 Introduction

To aid with understanding how the copolymer materials behave during printing, both their solution properties, as explored in Chapter 5, and their surface activity need to be understood. The performance of materials in many applications depends on not only their bulk properties but also their microstructure at the surface and their behaviour at interfaces.

The surface of a polymer material cannot be considered as unchangeable and rigid, since there is always a response of polymer chains to their environment or to applied stimuli.²²⁴ This response can include changing the location and/or conformation of side chains, backbone, pendant groups, segments, or end groups.²²⁵ The major responses that occur are governed by surface energies, polymer chain entropy and a variety of specific segmental interactions. The surface energy in particular has a major role in the response due to the inherent tendency of a system to minimise the interfacial energy between a polymer surface and its environment.

As outlined in Chapter 1, the surface energy of a material can be considered as an adhesive parameter which characterises its affinity to other materials. Contact angle measurements can be used to calculate the surface energy of a solid. The amount of work required to separate two bodies adhering to each other, designated L and S in **Figure 7.1**, called the work of adhesion, is represented by **Equation 7.1**, where E_{adh} is the total energy change (work) of adhesion, γ_L is the surface energy of the liquid, γ_S is the surface energy of the solid and γ_{LS} is the surface energy of the liquid-solid interface:

$$E_{adh} = \gamma_L + \gamma_S - \gamma_{LS} \quad \text{Equation 7.1}$$

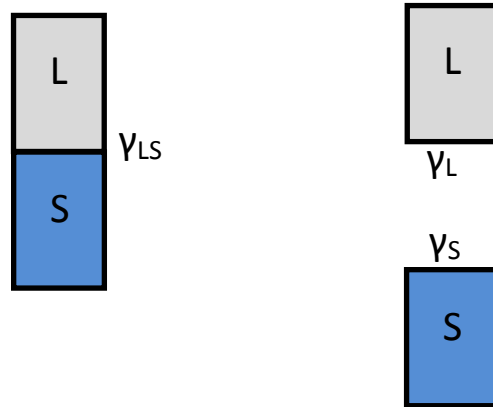


Figure 7.1. Schematic diagram to represent the work of adhesion

If the body L is a liquid drop and the body S is a solid substrate then the contact angle, θ , of the liquid drop at the surface of the substrate is determined by the Young equation, **Equation 7.2**:

$$\cos \theta = \frac{\gamma_S - \gamma_{LS}}{\gamma_L} \quad \text{Equation 7.2}$$

Combining these equations results in **Equation 7.3**:

$$E_{adh} = \gamma_L + \gamma_S - \gamma_{LS} = \gamma_L(1 + \cos \theta) \quad \text{Equation 7.3}$$

The applicability of contact angle measurements for evaluating surface energy is based on the thermodynamic argument that a non-homogeneous interfacial region between two surfaces in contact can be approximated by a Gibbs dividing surface at equilibrium. When the position of this dividing surface is chosen appropriately, a functional relationship can be formed between the three surface tension terms, and this can provide an equation of state:²²⁶

$$\gamma_{LS} = f(\gamma_L, \gamma_S) \quad \text{Equation 7.4}$$

Once the equation of state has been established, γ_S can be calculated from the measured contact angle of a test liquid with a known surface tension by solving **Equation 7.5** for γ_S :

$$\gamma_S - f(\gamma_L, \gamma_S) = \gamma_L \cos \theta \quad \text{Equation 7.5}$$

The mathematical form of the equation of state differs depending on the model used and the associated assumptions made. Different models have been proposed by van Oss and Good,²²⁷ Fowkes,²²⁸ Owens and Wendt,²²⁹ Kloubek,²³⁰ Wu,²³¹ Li and Neumann,²³² and Schultz et al.,²³³ among others.

The surface tension can be partitioned into dispersive and polar components. This requires the inclusion of extra terms in the equation. **Equation 7.6** is attributed to Fowkes, Owen and Wendt, and employs a geometric mean polar correction to account for the presence of polar forces in addition to dispersive forces.

$$\gamma_{LS} = \gamma_L + \gamma_S - 2 \left[\sqrt{\gamma_L^d \gamma_S^d} - \sqrt{\gamma_L^p \gamma_S^p} \right] \quad \text{Equation 7.6}$$

When **Equation 7.6** is chosen as the equation of state, the final result is **Equation 7.7**.

$$\gamma_L(1 + \cos \theta) = 2 \left[\sqrt{\gamma_L^d \gamma_S^d} - \sqrt{\gamma_L^p \gamma_S^p} \right] \quad \text{Equation 7.7}$$

Equation 7.7 can be used to determine the polar and dispersive components of the surface energy of a solid based on the contact angle results for two different liquids. If liquids with known surface tension are chosen then γ_L is known and $\cos \theta$ is measured, allowing the remaining two parameters, γ_S^D and γ_S^P to be calculated. The requirements for the two probe liquids are that one has only dispersive parts, whereas the other has both dispersive and polar parts; this allows for simultaneous equations to be solved to find γ_S^D and γ_S^P .

7.2 Surface Analysis by Contact Angle Measurements

Contact angles were measured using the sessile drop technique coupled with digital image analysis to study how the amphiphilic copolymers behaved when on the surface of polyolefin substrates. **Figure 7.2** shows a schematic diagram of the experimental setup. Two substrates were chosen, PP and also PMMA, which although not a polyolefin is used extensively in industry and therefore is of interest.

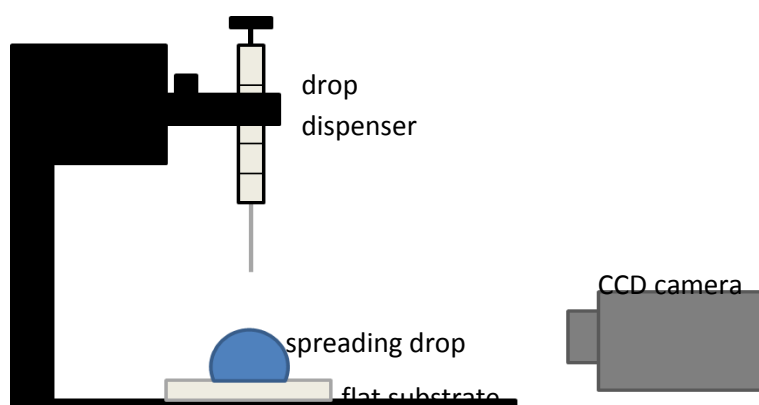


Figure 7.2. Schematic diagram of sessile drop technique for contact angle measurement.

Contact angle measurements can be subject to several sources of error. Steps were taken in this work to minimise these by: recording at least five stable measurements for each sample; monitoring the temperature and humidity in the laboratory where the experiment was carried out and working under similar conditions as far as possible; buying high quality substrates to minimise surface roughness; and thoroughly cleaning substrates before use by washing with IPA and allowing to dry, and removing any dust with compressed air.

Cleaned substrates were coated with layers of amphiphilic copolymer by using K bars to perform drawdowns of polymer solutions in THF. Coatings of 54 μm thickness were applied onto each substrate. Firstly ATR-FTIR was carried out to verify that the substrates were adequately coated. **Figure 7.3** shows an example result for one substrate. The black trace represents the FTIR spectrum for bare PP whilst the blue trace represents PP coated with a 54 μm layer of P(BMA-*b*-AA). The chemical structures are included to demonstrate the differences in functional groups between the two. There are two main differences between the two spectra, the first of which is the appearance of a

very broad O-H stretch from $3600\text{--}2400\text{ cm}^{-1}$, overlapping the C-H absorptions. This is characteristic of a carboxylic acid group. Secondly a large C=O stretch appears at around 1700 cm^{-1} . Neither of these functional groups is present in PP. This confirms that the substrate has been successfully coated, and similar results were seen for all coated substrates.

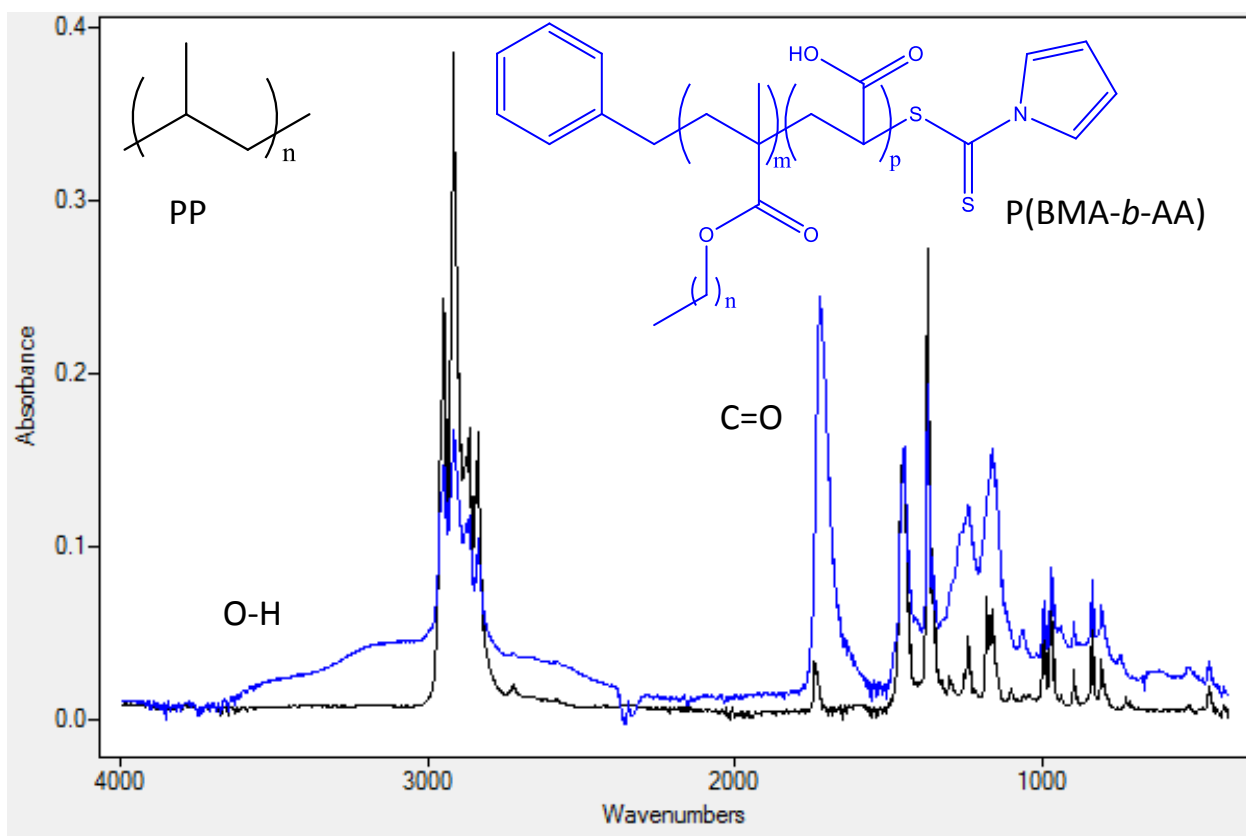


Figure 7.3. Overlaid ATR-FTIR spectra of a) (black trace) bare PP substrate and b) (blue trace) PP substrate coated with $54\ \mu\text{m}$ layer of P(BMA-*b*-AA). The O-H stretch and C=O stretch are labelled. The chemical structures of PP and P(BMA-*b*-AA) are included to illustrate the functional groups present in the molecules.

The two probe solvents chosen for the experiment were α -bromonaphthalene (BN), which is fully dispersive (non-polar), and ethylene glycol (EG), which has both dispersive and polar parts. **Figure 7.4** shows the chemical structures of both compounds.

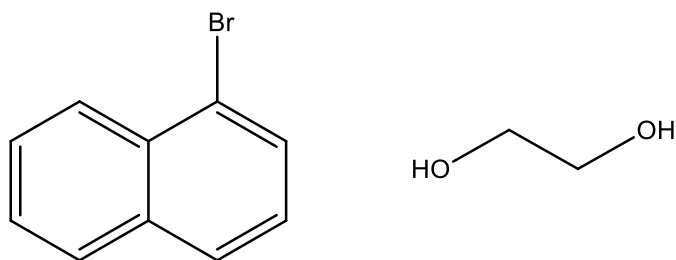


Figure 7.4. Chemical structures of the two probe solvents, α -bromonaphthalene and ethylene glycol

Contact angles were measured using both probe solvents on both PP and PMMA substrates. Solvent droplets were deposited on the coated substrates and images were recorded using a digital camera system, with multiple frames being recorded over time for each droplet. The Young-Laplace equation was fitted to the droplets to give contact angle values. Mean contact angles were calculated by including only the frames where the drop had reached equilibrium. **Table 7.1** and **Figure 7.5** show the results for the PP substrates, while **Table 7.2** shows the results of the ANOVA analysis. On the graph the red bars represent the contact angles measured for EG while the blue bars represent the data for BN. The error bars represent the 95% confidence interval for each sample, as calculated from **Equation 7.8**, where \bar{x} represents the sample mean, t_{n-1} the t value for $n-1$ degrees of freedom, s the sample standard deviation and n the sample size.

$$CI = \bar{x} \pm t_{n-1} \times \frac{s}{\sqrt{n}} \quad \text{Equation 7.8}$$

Statistical analysis was employed to determine whether the differences observed between the contact angle results of the substrates coated with different copolymers or the inks containing different formulations were statistically significant. The method chosen was the one-way ANOVA, or one-way analysis of variance. This test compares the means between independent groups and determines whether any of the means are significantly different from each other. The procedure for this test is explained in **Appendix 1**. Tukey post-hoc analysis is then carried out to determine where the differences lie.

The data measured using EG as probe show that there are only small differences in contact angle between the bare PP substrate, the Dianal MB2594 polymer and the amphiphilic copolymers with block architectures: P(BMA-*b*-AA), P(BMA-*co*-VBC-*g*-AA) and HB P(AA-*b*-BMA). These differences are however statistically significant, except for these between the bare PP and the HBA-coated PP. The two random copolymers, P(BMA-*co*-AA) and HB P(BMA-*co*-AA), exhibit very different behaviour, however. Much lower contact angles were measured on these coatings, meaning that the substrates are much more wetted by EG. This indicates that these surfaces are more polar than those of the other coated substrates.

When BN is the probe, greater differences are observed between the bare substrate and the block copolymers, whilst the results for the Dianal MB2594 and the random copolymers are more like those of the bare PP. Again, all differences between copolymers are statistically significant, with the exception of the LB and G coatings. The contact angles for all substrates show that BN is far more wetting than EG, suggesting that all coated substrates have more non-polar than polar parts exposed.

Table 7.1. Results of Contact Angle Measurements on PP Substrates, either Bare or Coated with P(BMA-*b*-AA), P(BMA-*co*-VBC-*g*-AA), P(BMA-*co*-AA), HB P(BMA-*b*-AA), HB P(AA-*b*-BMA) and Dianal MB2594

coating	probe solvent	contact angle /°	standard deviation /°	95% CI /°
bare	EG	77.8	1.48	0.24
LB		72.4	2.98	0.38
G		67.6	2.53	0.36
LR		28.0	3.28	1.88
HBR		39.3	7.13	1.51
HBA		78.6	3.46	0.52
Dianal		74.8	4.67	0.66
MB2594				
bare	BN	35.3	1.57	0.31
LB		10.2	0.35	0.19
G		11.1	1.91	0.44
LR		39.1	2.15	0.30
HBR		44.8	4.45	0.63
HBA		10.3	5.36	0.91
Dianal		35.5	4.30	1.23
MB2594				

(key: letters refer to architecture and distribution LB = linear block, G = graft, LR = linear random, HBR = highly branched random, HBA = highly branched acrylic acid core)

Table 7.2. Results of ANOVA Analysis of Contact Angle Measurements of Probe Solvents on PP Substrates Coated with Copolymers

Probe solvent	F	F _{crit}	P	P<0.05?	R ²
EG	4470	2.18	<0.0001	Y	0.992
BN	13300	2.18	<0.0001	Y	0.998

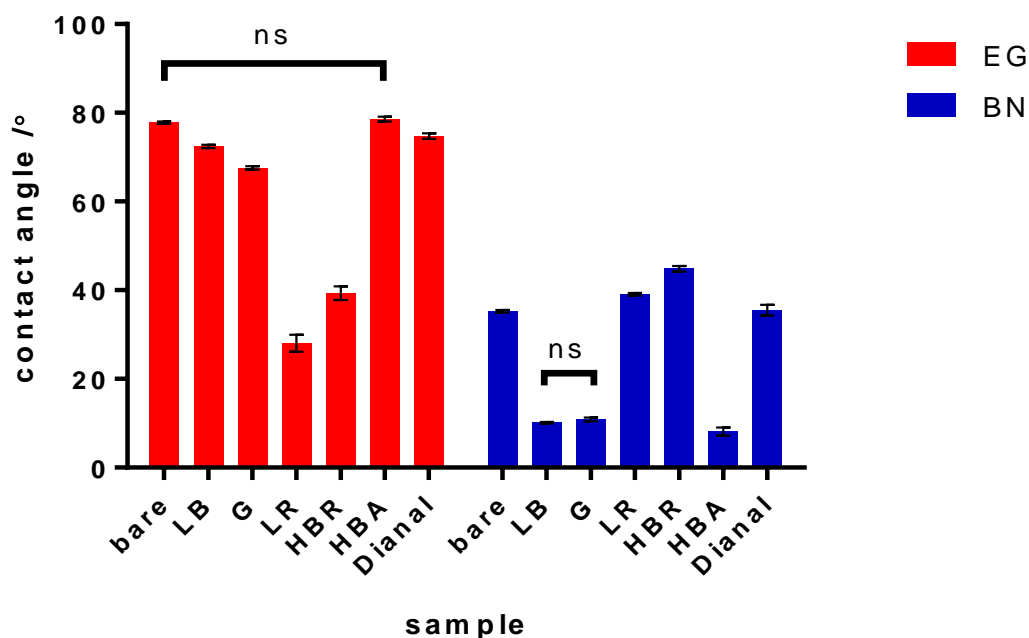


Figure 7.5. Results of contact angle measurements on PP substrates: bare PP, PP coated with P(BMA-*b*-AA), P(BMA-*co*-VBC-*g*-AA), P(BMA-*co*-AA), HB P(BMA-*b*-AA), HB P(AA-*b*-BMA) and Dianal MB2594. Red bars show contact angles measured using ethylene glycol as probe solvent and blue bars show contact angles measured using α -bromonaphthalene. Tie lines show significance level of comparisons between sets of copolymers: *** $P < 0.001$, ** $0.001 < P < 0.01$, * $0.01 < P < 0.5$, ns (not significant) $P \geq 0.05$. Here, only not significant relationships between copolymers are shown on the graph, as all other comparisons returned $P < 0.001$. (key: letters refer to architecture and distribution LB = linear block, G = graft, LR = linear random, HBR = highly branched random, HBA = highly branched acrylic acid core)

Table 7.3 and **Figure 7.6** show the results for the same experiment carried out on the coated PMMA substrates, while **Table 7.4** shows the results of the ANOVA analysis. The results are very similar to those for the coated PP substrates. This is not particularly surprising, as the coating thickness of 54 μm is quite large, meaning that the surface of the copolymer is well separated from, and therefore not influenced by, the substrate. Any differences observed between the two sets of coated substrates may be due to variation in their surface roughness. Draw downs using K bars do not provide perfectly uniform coatings and it is likely that industrial grade plastics may have had some difference in surface roughness even before coatings were applied.

The differences between the results of each coating are statistically significant, with the exception of the HBA and Dianal MB2594 coatings with EG as probe. The main difference from the PP substrates is that the contact angles for EG on the block and Dianal MB2594 polymers are slightly higher than those for the bare substrate, whilst the difference between the contact angles of the bare substrate and the random copolymers is even larger. The measured contact angles for BN on coated PMMA substrates are similar to those measured for BN on the coated PP substrates. The major exception is the Dianal MB2594 polymer which has a much lower angle of 9.3° on PMMA compared to 35.5° on PP. The coated substrate is much more wetted on PMMA than PP, indicating that non-polar components are interacting with the non-polar BN solvent.

Table 7.3. Results of Contact Angle Measurements on PMMA Substrates, either Bare or Coated with P(BMA-*b*-AA), P(BMA-*co*-VBC-*g*-AA), P(BMA-*co*-AA), HB P(BMA-*b*-AA), HB P(AA-*b*-BMA) and Dianal MB2594

coating	probe solvent	contact angle /°	standard deviation /°	95% CI /°
bare	EG	58.7	2.80	0.30
LB		66.8	0.85	0.10
G		73.0	1.41	0.23
LR		15.6	0.89	0.06
HBR		16.2	1.92	0.55
HBA		64.7	0.52	0.08
Dianal MB2594		64.5	0.34	0.05
bare	BN	23.9	1.20	0.23
LB		13.0	0.61	0.21
G		10.0	2.23	0.51
LR		37.9	1.43	0.21
HBR		32.8	1.46	0.19
HBA		7.6	0.88	0.19
Dianal MB2594		9.3	1.18	0.30

(key: letters refer to architecture and distribution LB = linear block, G = graft, LR = linear random, HBR = highly branched random, HBA = highly branched acrylic acid core)

Table 7.4. Results of ANOVA Analysis of Contact Angle Measurements of Probe Solvents on PMMA Substrates Coated with Copolymers

Probe solvent	F	F _{crit}	P	P<0.05?	R ²
EG	276000	2.18	<0.0001	Y	0.999
BN	19400	2.18	<0.0001	Y	0.998

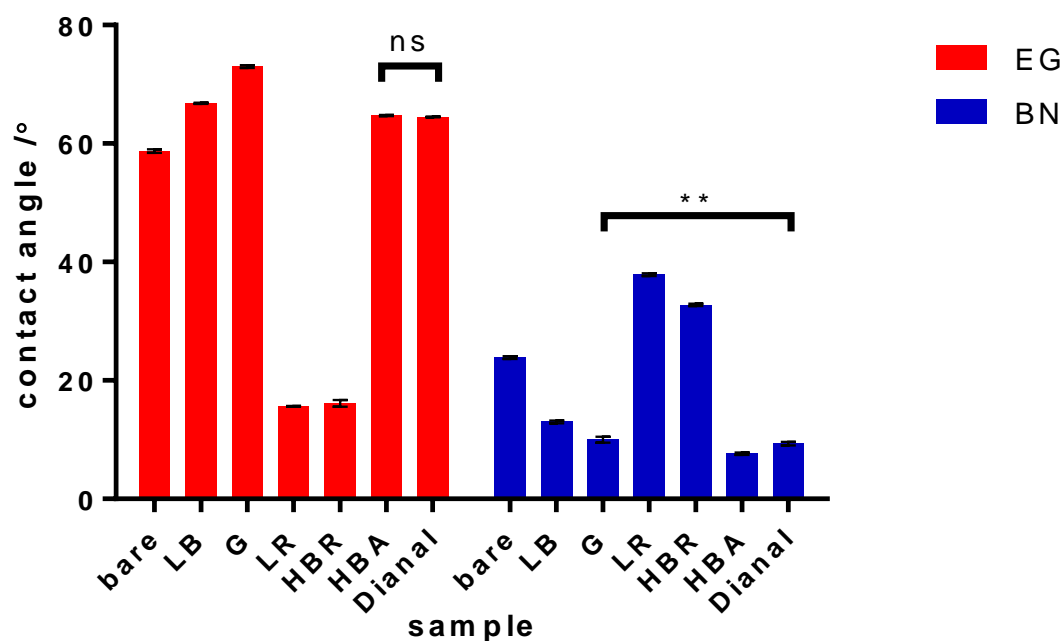


Figure 7.6. Results of contact angle measurements on PMMA substrates: bare PMMA, PMMA coated with P(BMA-*b*-AA), P(BMA-*co*-VBC-*g*-AA), P(BMA-*co*-AA), HB P(BMA-*b*-AA), HB P(AA-*b*-BMA) and Dianal MB2594. Red bars show contact angles measured using ethylene glycol as probe solvent and blue bars show contact angles measured using α -bromonaphthalene. Tie lines show significance level of comparisons between sets of copolymers: *** $P < 0.001$, ** $0.001 < P < 0.01$, * $0.01 < P < 0.5$, ns (not significant) $P \geq 0.05$. Here, only two relationships between copolymers are shown on the graph, as all other comparisons returned $P < 0.001$. (key: letters refer to architecture and distribution LB = linear block, G = graft, LR = linear random, HBR = highly branched random, HBA = highly branched acrylic acid core)

Surface energies of the different coated substrates were then calculated using **Equation 7.7**. This allowed calculation of the surface energy due to both dispersive and polar parts, in addition to the overall surface energy. The results for the coatings on the PP substrates are summarised in **Table 7.5** and represented graphically in **Figure 7.7**, with the blue parts representing the dispersive components and the red parts representing the polar parts. It is clear that there is a larger polar component to the surface energies of the P(BMA-*co*-AA) and HB P(BMA-*co*-AA) coatings. The overall surface energies are larger for the amphiphilic copolymers compared to the Dianal MB2594 polymer and the uncoated PP substrate.

Table 7.5. Calculated Surface Energies from Contact Angle Measurements on PP Substrates, either Bare or Coated with P(BMA-*b*-AA), P(BMA-*co*-VBC-*g*-AA), P(BMA-*co*-AA), HB P(BMA-*b*-AA), HB P(AA-*b*-BMA) and Dianal MB2594.

coating	$\gamma_{\text{tot}}/\text{mN/m}$	$\gamma_{\text{d}}/\text{mN/m}$	$\gamma_{\text{p}}/\text{mN/m}$	% polarity
bare	37.30	36.65	0.65	1.74
LB	44.70	43.71	0.99	2.22
G	44.35	35.01	9.33	21.04
LR	43.87	43.57	0.30	0.69
HBR	46.30	43.69	2.61	5.63
HBA	39.89	32.48	7.41	18.59
Dianal MB2594	36.69	36.44	0.25	0.69

(key: letters refer to architecture and distribution LB = linear block, G = graft, LR = linear random, HBR = highly branched random, HBA = highly branched acrylic acid core)

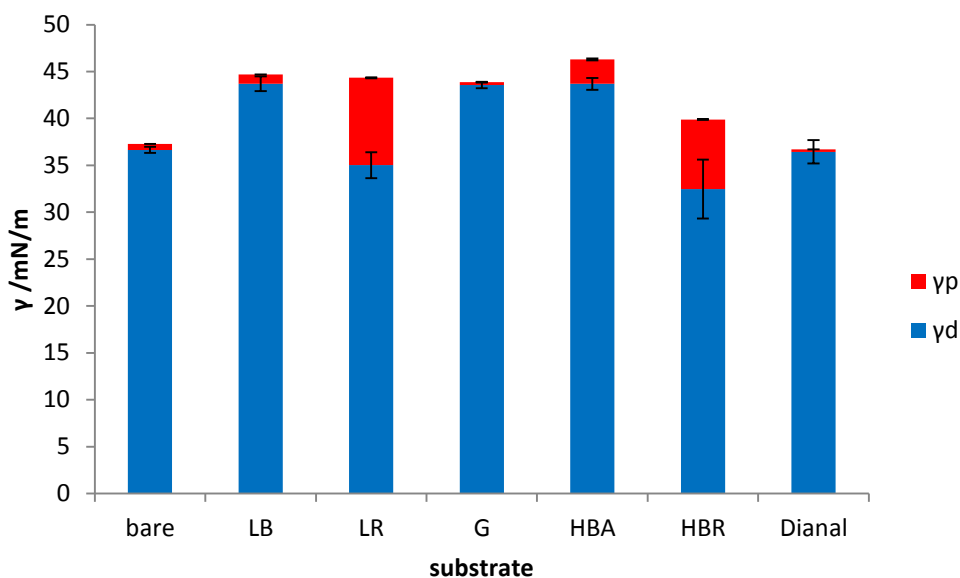


Figure 7.7. Calculated surface energy from contact angle measurements of coated PP substrates: bare PP, PP coated with P(BMA-*b*-AA), P(BMA-*co*-VBC-*g*-AA), P(BMA-*co*-AA), HB P(BMA-*b*-AA), HB P(AA-*b*-BMA) and Dianal MB2594. Blue bars represent the surface energy due to dispersive parts of the polymer and red bars represent the surface energy due to polar parts. Error bars are estimated from the percentage errors on the contact angle data from which surface energies are calculated.

The surface energies of the coatings on PMMA substrates are summarised in **Table 7.6** and represented graphically in **Figure 7.8**. The overall surface energies are slightly larger on PMMA than on PP substrates. Less polar contributions are seen for the bare substrate, Dianal MB2594, and block and graft copolymer coatings. The random copolymers again have comparatively large polar contributions. The percentage polarity of each coating was calculated for each substrate, PP and PMMA, by comparing the ratio of the polar contribution to the overall surface energy. These results are shown graphically in **Figure 7.9**. The blue bars represent the data for coatings on PP and the red bars represent the data for coatings on PMMA. Similar trends are seen on both substrates for the most part. The graft and Dianal MB2594 coatings both display very low polarity, even less than the bare substrates. The linear block polymer coating is slightly more polar than the bare PP and PMMA. The HB P(AA-*b*-BMA) polymer is the only coating which displayed a substantial difference in polarity between substrates, with 5.6% polarity on PP but only 0.3% polarity on PMMA, which mirrors the polarity

difference of the bare substrates. In contrast the linear and branched random polymers had a much higher percentage polarity, with 21.0% and 25.0% on PP and PMMA respectively for LR and 18.6% and 21.6% polarity for HBR.

These differences in polarity when coated on the substrates are caused by the difference in sequence distribution of the PAA and methacrylate segments within the copolymers. In the block and graft copolymers, the PAA and methacrylate blocks are separate and are therefore able to move independently in order to minimise the energy at the interface. In the random copolymers however, the PAA and methacrylate units are randomly distributed and therefore mixed together. As a result, they are unable to move independently to minimise energy and therefore both polar and dispersive parts are present on the coating surface.

Table 7.6. Calculated Surface Energies from Contact Angle Measurements on PMMA Substrates, either Bare or Coated with P(BMA-*b*-AA), P(BMA-*co*-VBC-*g*-AA), P(BMA-*co*-AA), HB P(BMA-*b*-AA), HB P(AA-*b*-BMA) and Dianal MB2594.

coating	γ_{tot} /mN/m	γ_{d} /mN/m	γ_{p} /mN/m	% polarity
bare	40.85	40.69	0.16	0.40
LB	44.82	43.73	1.10	2.45
G	47.39	35.54	11.86	25.01
LR	43.48	43.27	0.21	0.47
HBR	44.12	44.01	0.11	0.26
HBA	47.97	37.61	10.35	21.58
Dianal MB2594	43.91	43.82	0.01	0.21

(key: letters refer to architecture and distribution LB = linear block, G = graft, LR = linear random, HBR = highly branched random, HBA = highly branched acrylic acid core)

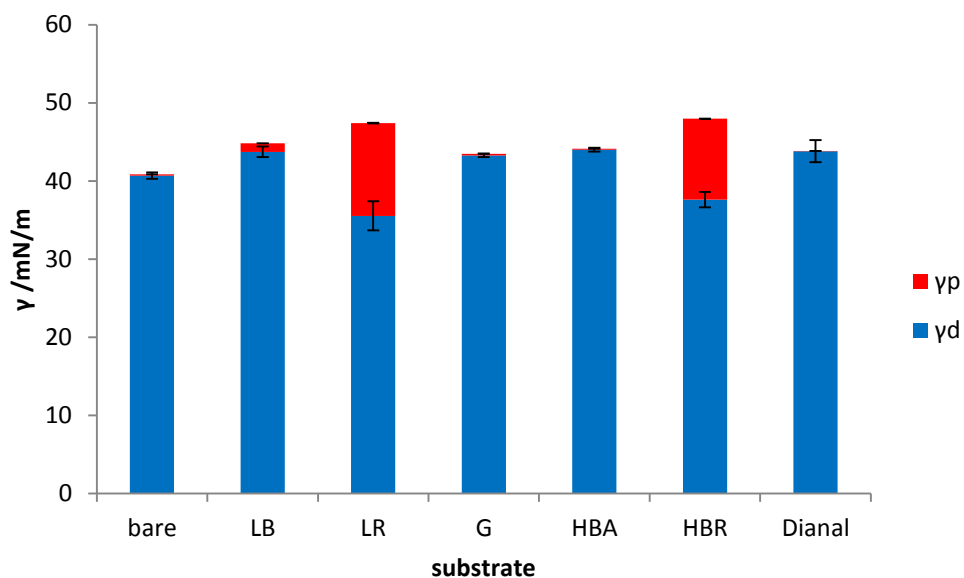


Figure 7.8. Calculated surface energy from contact angle measurements of coated PMMA substrates: bare PMMA, PMMA coated with P(BMA-*b*-AA), P(BMA-*co*-VBC-*g*-AA), P(BMA-*co*-AA), HB P(BMA-*b*-AA), HB P(AA-*b*-BMA) and Dianal MB2594. Blue bars represent the surface energy due to dispersive parts of the polymer and red bars represent the surface energy due to polar parts. Error bars are estimated from the percentage errors on the contact angle data from which surface energies are calculated.

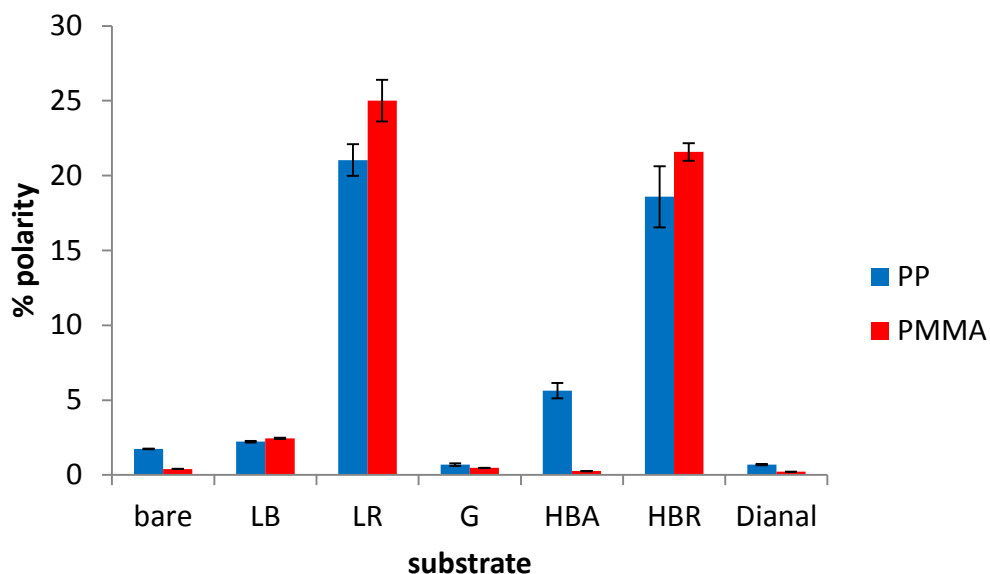


Figure 7.9. Percentage polarity calculated from ratio of surface energy due to polar parts to total surface energy of coatings on PP and PMMA substrates: bare substrate, substrate coated with P(BMA-*b*-AA), P(BMA-*co*-VBC-*g*-AA), P(BMA-*co*-AA), HB P(BMA-*b*-AA), HB P(AA-*b*-BMA) and Dianal MB2594. Blue bars represent the percentage polarity of coatings on PP and red bars represent the percentage polarity of coatings on PMMA.

A second study was carried out to investigate whether differences could be observed between the amphiphilic copolymers if they were formulated into inks and their contact angles on a polyolefin substrate were measured. The details of the ink formulations are explained in Section 8.3 of Chapter 8. Inks were made containing the graft, linear block, linear random and HB random at 0.5% concentration w/w, in addition to one containing Dianal MB2594 as in the standard formulation for the BK107 ink. The base solvent for the ink was also tested, as well as a formulation containing the base solvent and the surfactants. Comparison of these formulations allowed investigation of whether firstly adding surfactant to the solvent base, and also adding the different polymers to the solvent and surfactant, had an effect on the overall wetting behaviour of the droplet on a substrate. PP was chosen as the polyolefin substrate to test.

Table 7.7. Results of contact angle measurements on PP substrates: base solvent, base solvent with surfactants, ink with: Dianal MB2594, P(BMA-co-VBC-g-AA), P(BMA-b-AA), P(BMA-co-AA), and HB P(BMA-co-AA).

formulation	mean contact angle /°	standard deviation /°	95% CI /°
base solvent	30.8	1.85	0.29
base solvent + surfactant	32.0	3.80	0.55
Dianal MB2594	27.2	2.18	0.38
G	28.2	2.13	0.41
LB	21.8	1.90	0.39
LR	22.6	3.08	0.75
HBR	25.1	1.45	0.33

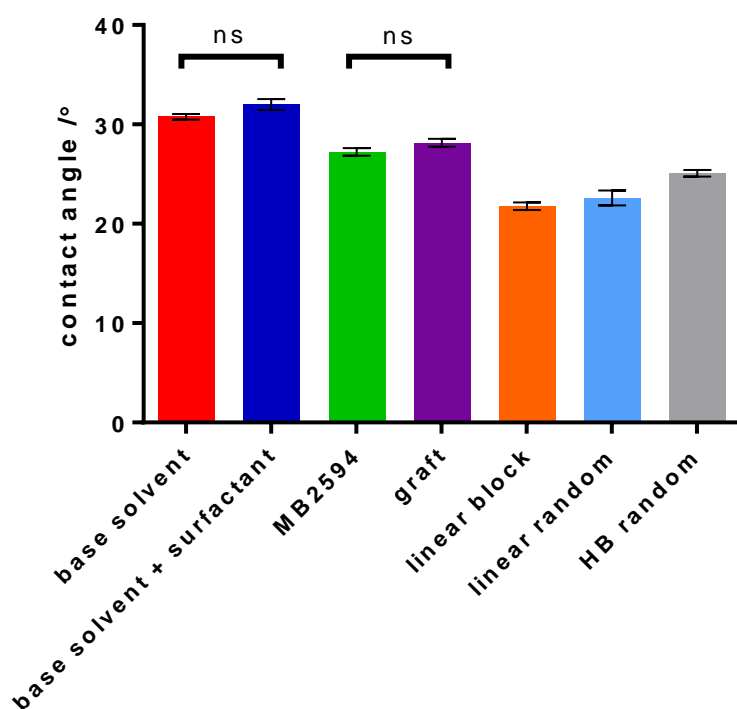


Figure 7.10. Results of contact angle measurements on PP substrates: base solvent, base solvent with surfactants, ink with: Dianal MB2594, P(BMA-co-VBC-g-AA), P(BMA-b-AA), P(BMA-co-AA), and HB P(BMA-co-AA). Tie lines show significance level of comparisons between sets of copolymers: *** $P < 0.001$, ** $0.001 < P < 0.01$, * $0.01 < P < 0.05$, ns (not significant) $P \geq 0.05$. Here, only not significant relationships between copolymers are shown on the graph, as all other comparisons returned $P < 0.001$.

Table 7.7 and **Figure 7.10** show the results of this study. The error bars on the graph represent the 95% confidence interval for each sample. There is evidence of significant difference between the mean contact angles of the different inks due to the different formulations, as seen in **Table 7.8**. Although, the calculated R^2 for this data is 0.881, indicating that there is some uncertainty in the model fit. A Tukey post-hoc analysis found significant differences between all inks, except between the base solvent and the base solvent containing surfactant, and between the MB2594 and graft inks. The polymer additives act to reduce the contact angle. The lowest contact angles are seen for the inks containing the linear block and random copolymers, meaning that the inks wet better on the PP substrate.

Table 7.8. Results of ANOVA Analysis of Contact Angle Measurements of Inks Containing Copolymers on PP substrates

F	F _{crit}	P	P<0.05?	R ²
195	2.18	<0.0001	Y	0.881

7.3 AFM Force Spectroscopy

Atomic Force Microscopy is a powerful technique for surface analysis. The Atomic Force Microscope (AFM) consists of a sharp tip at the end of a cantilever spring. This is supported by a piezoelectric crystal which varies the lateral and vertical position of the cantilever with respect to the sample surface. Optical detection of the deflection of the cantilever allows probing of the interaction between the tip and the surface.

The forces acting between the tip and the sample are caused by steric repulsion in addition to van der Waals, electrostatic and specific chemical binding interactions.²³⁴ Local variations in these forces as the tip scans the sample surface provide the basis for different contrasts in the acquired images. Different scanning modes such as contact and tapping modes have been developed and optimised for the scanning of various specific surface properties. These include chemistry,^{235, 236} viscoelasticity²³⁷ and surface charge.^{238, 239}

The AFM is not only used for topographical imaging of solid surfaces at high resolution. It can also be used to measure force-distance curves, known as force curves. These give valuable information such as elasticity, hardness, surface charge densities and adhesion.²⁴⁰ This is possible since any force exerted on the cantilever causes the laser beam reflecting off the back of the cantilever to be deflected. Assuming a simple relationship between force and deflection, namely Hooke's law, allows the force to be deduced from the deflection and the cantilever spring constant.²⁴¹ This force spectroscopy technique has been widely used in studies of interaction forces of both synthetic polymers^{240, 242} and biological molecules.^{243, 244}

AFM force spectroscopy has been widely applied to polymers and other macromolecules in experiments investigating the entropic and enthalpic elasticity of a single polymer chain,²⁴⁵ the interaction between macromolecules and small molecules,²⁴⁶ force induced conformational transitions²⁴⁷ and the interfacial conformation and desorption force of macromolecules,²⁴⁸ among many others. Force spectroscopy has also been used to measure the adhesion behaviour of polymers.^{249, 250}

Using an AFM in contact mode to make force measurements on a substrate provides a quantitative indication of the adhesiveness of a material through measuring the adhesion force between the tip and the substrate. An experiment was carried out to investigate whether this method would be suitable for assessing differences in adhesion behaviour between different copolymers. In this study, a silicon wafer was spincoated with the polymer from solution and the adhesion between the polymer and a standard silicon nitride AFM tip was measured. This was performed on a set of polymer brushes at different stages in the graft copolymer synthesis: a P(LMA-*co*-VBC) backbone, a functionalised P(LMA-*co*-VBC) backbone and a P(LMA-*co*-VBC-*g*-AA) graft copolymer.

One hundred measurements were performed over a 300 nm x 300 nm square location on each coated substrate, and then another hundred in a second location on each, giving a force curve for each measurement. The measurements record the pull off force in V, which is converted to adhesion force in nN by multiplying the pull off force by the deflection sensitivity, which is measured during the original experiment, and then multiplying by the cantilever spring constant.

The distributions of adhesion forces which are obtained are then displayed as histograms with the forces grouped into bins. The histograms for each sample can then be compared to determine how the force distributions have changed after each step in the synthesis. Below in **Figure 7.11** the data obtained from the experiment is presented.

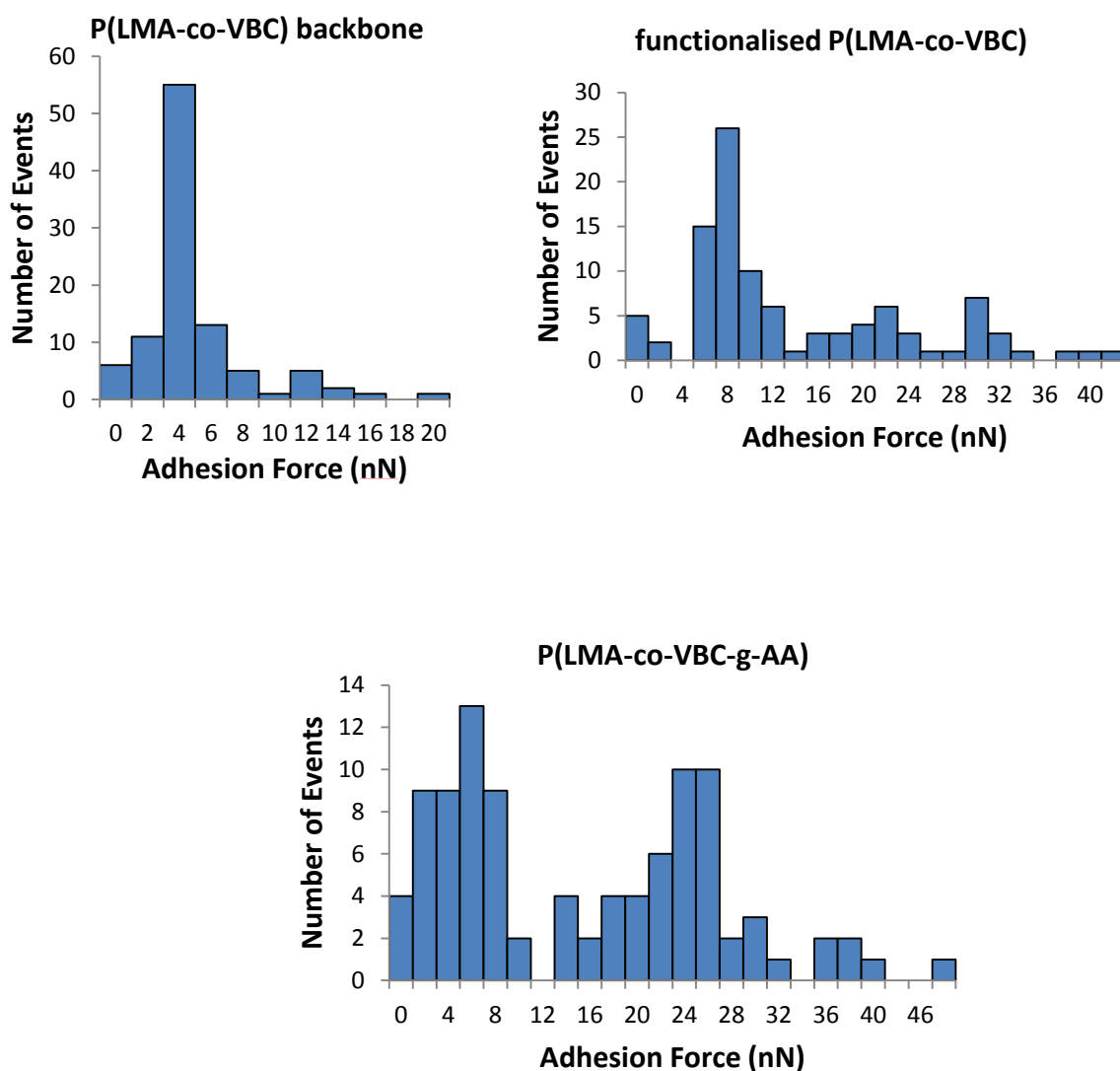


Figure 7.11. Histograms of force measurement data showing the number of events recorded at each adhesion force for a P(LMA-co-VBC) backbone, the same P(LMA-co-VBC) backbone after functionalisation, and then the same backbone after grafting reaction to produce P(LMA-co-VBC-g-AA) graft copolymer

From these histograms it can be seen that there is a clear difference in the force distributions of the backbone and the functionalised backbone. The largest force observed for the backbone falls within the 20 nN bin whereas after functionalisation the strongest force observed was as high as 40 nN. The peak of the distribution also shifts to a greater force after functionalisation. These results indicate that the polymer becomes more adhesive to the tip after it has been functionalised.

Differences can also be observed between the force distributions of the functionalised backbone and the graft copolymer. There are a greater number of events with a greater adhesion force, and the maximum force observed is also larger. A peak is still seen at low force however, similar to that seen in the functionalised backbone. This suggests a bimodal distribution with a peak at low force, around 6 nN, caused by areas of the polymer where grafts have not grown from the backbone, and then a second peak at larger forces, around 25 nN, due to sites where some grafting has occurred making the polymer more adhesive.

A more precise method of comparing the different distributed data sets is non-parametric (i.e. for use with non-continuous data from populations with distributions which are not normal) statistical analysis. The appropriate test to use is the Mann-Whitney U Test, which is a non-parametric statistical test that compares two samples of data and tests the null hypothesis that they originate from the same population. The assumption in this test is that the samples to be compared are from distributions that are not normal but they are similar. The test provides a P value; under the null hypothesis $P = 0.5$, meaning the samples are from the same population, whereas under the alternative hypothesis $P \neq 0.5$, with a 95% confidence interval of $P=0.05$.

Table 7.9 Results of Mann-Whitney U Test carried out on Force Measurement Data of one Backbone, Functionalised Backbone and Brush

Backbone vs. Functionalised Backbone	Functionalised Backbone vs. Brush
P<0.0001	P=0.4443

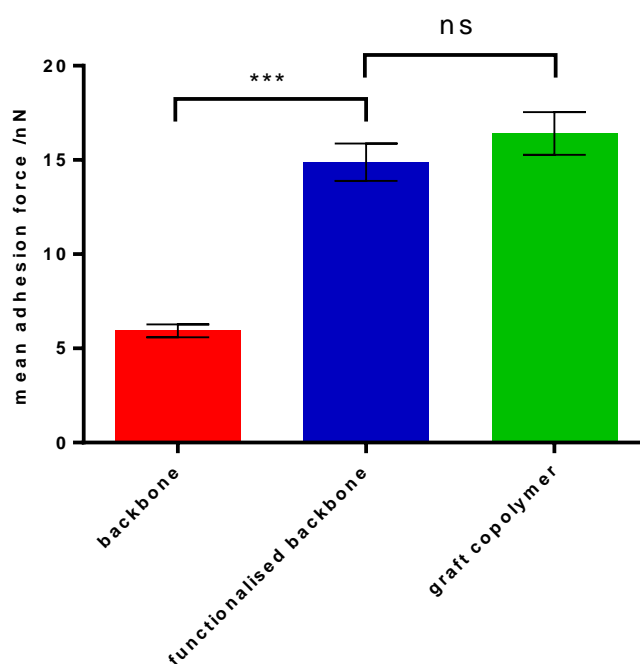


Figure 7.12. Comparison of the mean adhesion forces for the P(LMA-*co*-VBC) backbone, functionalised P(LMA-*co*-VBC) backbone and P(LMA-*co*-VBC-*g*-AA) copolymer following grafting. The results of the Mann-Whitney U Test are displayed using tie lines to show the significance level of comparisons between copolymers: *** $P < 0.001$, ** $0.001 < P < 0.01$, * $0.01 < P < 0.5$, ns (not significant) $P \geq 0.05$.

Table 7.9 shows that the P value for the comparison of the initial backbone and the functionalised backbone is extremely small. This means that the two samples did not come from the same population, confirming what was observed from the histograms that the adhesion forces did increase on functionalisation. However the P value obtained from the comparison between the functionalised backbone and the brush is close to 0.5 which indicates that there is no significant difference between the two samples. These results are displayed graphically in **Figure 7.12**. In experimental terms, and taking the histogram distribution into consideration, this suggests that some grafting has occurred in some places on the polymer backbone, but not to a great enough extent to make the overall populations significantly different. The data thus clearly show that functionalisation with the dithioate group increased the coating's adhesion to silicon nitride. This is perhaps not surprising but is a new result.

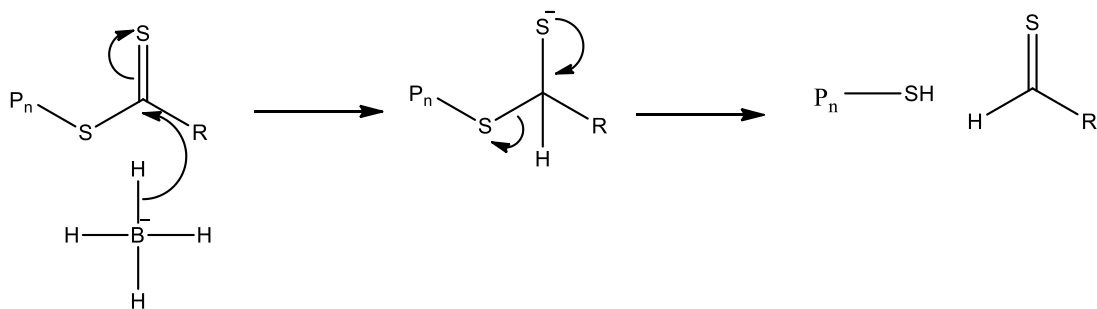
This technique, in conjunction with a statistical analysis method to confirm apparent trends in the data, yields useful information on the differences in adhesion behaviour between a set of copolymer materials. It could be extended by using single-molecule force spectroscopy which involves coating an AFM tip with a single molecule of copolymer and measuring its adhesion with a range of substrates. In this way the differences in adhesion between different copolymers and substrates could be studied, simulating conditions experienced by the copolymer additives during and after printing.

7.4 Method for Removal of RAFT End Groups

In order for single-molecule force spectroscopy to be feasible, the copolymers need to be strongly bonded to the tips. It is well known and frequently exploited that thiol groups adhere to gold.²⁵¹ Therefore, if the tips can be coated in gold and if the copolymers possess thiol end groups, the copolymers can be bonded to the tips.

The copolymer materials have pyrrole dithioester groups at the chain ends originating from the RAFT agent. These can be converted to other useful functionalities. This has been demonstrated by Perrier et al.⁶⁵ who published a method of removing the thiocarbonyl-thio end groups from a range of methacrylate, acrylate, acrylamide, and styrenyl polymers through heating with an excess of free radical initiator. Choice of initiator allows the introduction of different functionalities onto the chain ends, and the RAFT agent is recovered. Boyer et al.²⁵² later converted dithioester and trithiocarbonate end groups to pyridyl disulfide (PDS) functionalities via aminolysis in the presence of 2,2'-dithiopyridine yielding protected thiol groups, avoiding side reactions such as disulfide coupling which have been observed previously.^{253, 254}

An alternative way to convert dithioester groups to thiols is by reduction with a borohydride reducing agent. **Scheme 7.1** shows the mechanism for this reaction. Polymer-supported borohydride reagents are commercially available and provide a simple and clean method to carry out reduction chemistry.



Scheme 7.1 Mechanism for the reduction of RAFT dithioester end groups to thiol groups using a borohydride reducing agent

Linear samples of PBMA prepared by RAFT polymerisation were used to test the proposed method. Two different polymer-supported borohydride reagents, Amberlite IRA-400 and Amberlite A26 were used to see if there was a difference in their activity. The reaction procedure was extremely facile, requiring simply that the borohydride-functionalised resins were added to solutions of pyrrole-ended polymer and agitated under ambient conditions for a period of twenty four hours. Following precipitation after the reaction was complete, it was clear that the RAFT dithioester groups had been removed as the appearance of the polymer had changed dramatically from a yellow amorphous solid to a more powdery white polymer. ^1H NMR confirmed that the reaction was successful as no pyrrole protons were observed in the spectra. This shows that either of the Amberlite reagents can be used to easily convert dithioester groups to thiols. This method should be able to be applied to the copolymer materials to introduce thiol groups at the chain ends allowing them to be used for single-molecule AFM studies.

7.5 Conclusions

PP and PMMA substrates were coated with copolymer layers. ATR-FTIR was used to confirm coating. Contact angles were measured using the sessile drop method, with BN and EG chosen as probe solvents. This allowed the calculation of surface energies due to the polar and dispersive parts to the copolymer, as well as the total surface energy. The main findings were that the amphiphilic copolymer coatings gave higher overall surface energies compared to the bare substrates and those coated with

Dianal MB2594 polymer. A much larger polar component was observed for both the branched and linear random copolymers when compared to the block and graft materials. Contact angles were also measured on uncoated PP substrates using ink formulations containing the copolymers as additives as the probe. A relatively small range of contact angles was observed, but statistical analysis using a one-way ANOVA confirmed that there are significant differences between the inks depending on the copolymer additive.

Also, AFM force spectroscopy was tested as a method to study changes in the adhesion behaviour of different copolymers and was found to detect structural changes in graft P(LMA-*co*-VBC-*g*-AA) copolymers during the functionalisation and grafting process. A statistical analysis method was found to allow comparison of force data from polymer samples and confirm whether differences were present. To allow extension of the technology to the use of single-molecule force spectroscopy, a method was developed to reduce the RAFT dithioester end groups remaining in the copolymers to thiols, to enable adhesion to gold-coated AFM cantilevers.

8. Materials Testing for Printing Applications

Finally, the poly(butyl methacrylate-acrylic acid) copolymers are formulated into inks and these are tested in printing applications using both thermal inkjet and piezoelectric inkjet printers. The adhesion behaviour is investigated using the standard industry testing methods.

8.1 Introduction

The main aim of this section of work is to investigate the suitability of the amphiphilic poly(alkyl methacrylate-acrylic acid) copolymers for inkjet printing and to examine their effectiveness as an additive in a commercial ink formulation to improve adhesion to low energy substrates.

There are several objectives for this work in the form of questions to be investigated:

- can the amphiphilic copolymer materials be incorporated into ink formulations?
- can these inks be jetted?
- can they be printed onto polyolefin substrates?
- can the adhesion performance of the copolymers be assessed?

8.2 Synthesis of Copolymers for Printing

A new set of copolymers were needed to test their performance in printing applications as larger quantities of material were required. The copolymers containing BMA were chosen as the most suitable set to assess the printer performance of these novel materials. This balanced the desire for greater hydrophobicity of the oleophilic segment with ease of processability and scale-up to larger quantities. The LMA copolymers made the synthetic procedures more difficult due to both the long alkyl chain causing steric hindrance, as was particularly observed for the graft copolymers, and also due to the low T_g of PLMA rendering the polymers very sticky at room temperature and therefore hard to manipulate.

P(BMA-AA) copolymers were synthesised in each of the six combinations of architecture and monomer distribution: graft, HB block with PAA core, HB block with PBMA core, HB random, linear block, and linear random. **Table 8.1** summarises the

results of these polymerisations, which were designed to yield similar results to the previously synthesised copolymers which are reported in Chapters 3 and 4. Conversions were calculated from ^1H NMR integrals for the addition of the second block for this type of copolymer. Conversions of each monomer were also calculated for the random copolymers. The table also includes the molecular weight data for Dianal MB2594. This is an acrylic polymer which is employed as an adhesion-promoting additive in ink formulations, including the ink which the copolymers will be tested in. Therefore Dianal MB2594 will be used to compare the performance of the copolymers.

Table 8.1. Results of Syntheses of Poly(Butyl Methacrylate-Acrylic Acid) Copolymers for use in Printing Studies

sample	conversion / mol % (monomer)	yield / % mass recovery	DB ^a	molar composition BMA:AA ^a	M _n /g mol ⁻¹ ^b	M _w /g mol ⁻¹ ^b	Đ ^b
P(BMA- <i>co</i> - VBC- <i>g</i> -AA)	30 (AA)	20	0.09	15.3:1	19000	32200	1.67
HB P(BMA- <i>b</i> - AA)	52 (AA)	33	0.14	12.9:1	24000	65900	2.74
HB P(AA- <i>b</i> -BMA)	90 (BMA)	68	0.37	1.27:1	13400	41200	3.08
HB P(BMA- <i>co</i> - AA)	65 (AA), 97 (BMA)	76	0.26	1.87:1	9600	28700	2.98
P(BMA- <i>b</i> - AA)	94 (AA)	70	-	0.63:1	22800	87600	3.84
P(BMA- <i>co</i> - AA)	81 (AA), 98 (BMA)	94	-	1.40:1	44400	85700	1.93
Dianal MB2594	-	-	-	-	6800	11900	1.80

^a determined by ^1H NMR ^b determined by GPC (THF, PMMA standards)

The resulting copolymers were similar to those synthesised previously, with M_n values reasonably close to the target value of 20000 g mol⁻¹, with the exception of the linear P(BMA-*co*-AA) random copolymer which had a molar mass of twice the target. The dispersities were as expected except for the linear P(BMA-*b*-AA) block material which had a large dispersity for a linear copolymer. This could be due to either the

occurrence of branching within the polymer during the addition of PAA, or an artefact of either the methylation process or conformational changes in the GPC solvent. Alternatively, the broad dispersity could be a result of the switch in kinetics from the polymerisation of alkyl methacrylates to that of acrylic acid. This does however allow good comparison with the branched materials as the dispersities are comparable. The calculated values for the degrees of branching (DB) were similar to those determined in Chapter 4, which were generally in the range 0.10-0.30. Lower PAA contents were detected in the P(BMA-*co*-VBC-*g*-AA) graft and HB P(BMA-*b*-AA) block copolymers as these achieved only a low conversion and consequently a low yield. The Dianal MB2594 polymer has much lower molecular weight than the copolymers, while the dispersity suggests either a linear polymer or one with a low degree of branching.

8.3 Copolymers in Ink Formulations

The printing performance of these copolymer materials was assessed at Domino UK Ltd. The copolymers were applied as an additive to the ink, as set by the initial objective of this project. The ink was chosen to have an organic solvent base due to the solubility of the P(BMA-AA) copolymers. An ethanol-based Domino ink of BK107 was selected as a model formulation due to previous studies which demonstrated that the materials were soluble in this particular solvent base. This consists of a mixture of denatured ethanol, 1-methoxy-2-propanol, and Highsol P. The ink formulation also contains a black dye for the visual identification of the printed code as well as several additives to improve flow and surface active properties. The standard binder in BK107 is the low molecular weight and acid functional styrene/acrylic resin, Dianal MB2594. This is present at 0.5% concentration by mass to facilitate adhesion without any detriment to the jetting performance from the printhead. In the test formulations this was replaced by the amphiphilic copolymers with the material being present at both 0.5% and 1.0% copolymer concentration by mass. These fluids were compared directly to some 'control' inks containing the standard Dianal polymer at the same concentrations. Each ink was filtered through a 1 μm PTFE filter before use to remove any large particulates.

8.3.1 Viscometry of Copolymer Inks

An Anton Paar AMVn rolling ball viscometer was used to measure the dynamic viscosities of the ink formulations according to the Hoesppler's falling ball technique, which obtains a measure of viscosity through measuring the time taken for a stainless steel ball to roll down a capillary containing the sample fluid. The angle of the capillary can be varied, which in turn varies the time taken for the ball to roll the length of the capillary as the gravitational force is opposed by the buoyancy and viscous forces of the liquid. The calculation requires the densities of the samples to be known, which were measured on an Anton Paar DM38 density meter and displayed in **Table 8.2**.

Table 8.2. Results of Density Measurements for BK107 Ink Solutions containing Copolymer as Additive

Polymer	density of ink with 0.5% polymer / g ccm ⁻¹	density of ink with 1.0% polymer / g ccm ⁻¹	density difference between 0.5% and 1.0% polymer concentration
HB P(BMA- <i>b</i> -AA)	0.8956	0.8990	0.0034
P(BMA- <i>co</i> -VBC- <i>g</i> - AA)	0.8951	0.8978	0.0027
HB P(BMA- <i>co</i> -AA)	0.8961	0.8971	0.0010
HB P(AA- <i>b</i> -BMA)	0.8965	0.8988	0.0023
P(BMA- <i>b</i> -AA)	0.8967	0.8976	0.0009
P(BMA- <i>co</i> -AA)	0.8959	0.8968	0.0009
Dianal MB2594	0.8966	0.8967	0.0001

The densities of all the ink formulations are quite similar with a range of only 0.0039 g ccm⁻¹ between the lowest and highest viscosities of both polymer concentration inks. This is not surprising as the polymer is present at low concentrations in the overall formulation, even at 1% mass. However, increasing the polymer concentration does cause a small increase in density for all inks, as would be expected. The difference between the inks with 0.5% and 1.0% polymer concentration are much larger for the branched and graft materials than the linear copolymers and the standard

formulation. Of the branched materials, the smallest increase in density is seen for the HB random copolymer. This material behaves more similarly to the linear copolymers. The Dianal polymer in the standard formulation has a density increase of only 0.0001 g cm^{-1} when the concentration is increased from 0.5 to 1.0%, demonstrating that it has less effect on the overall density of the ink than the other copolymers.

Figure 8.1 and **Figure 8.2** demonstrate the viscosities of the inks with 0.5% and 1% polymer content respectively, and are plotted on the same scale so the differences between the two are clear. An increase in viscosity is seen in all samples as the concentration of polymer in the ink is increased, as expected. Greater differences between the samples are observed at 1.0% polymer concentration, as the polymer begins to have more influence on the overall properties of the ink. At both concentrations, the ink containing Dianal MB2594 has the lowest viscosity whilst the linear random copolymer has the highest.

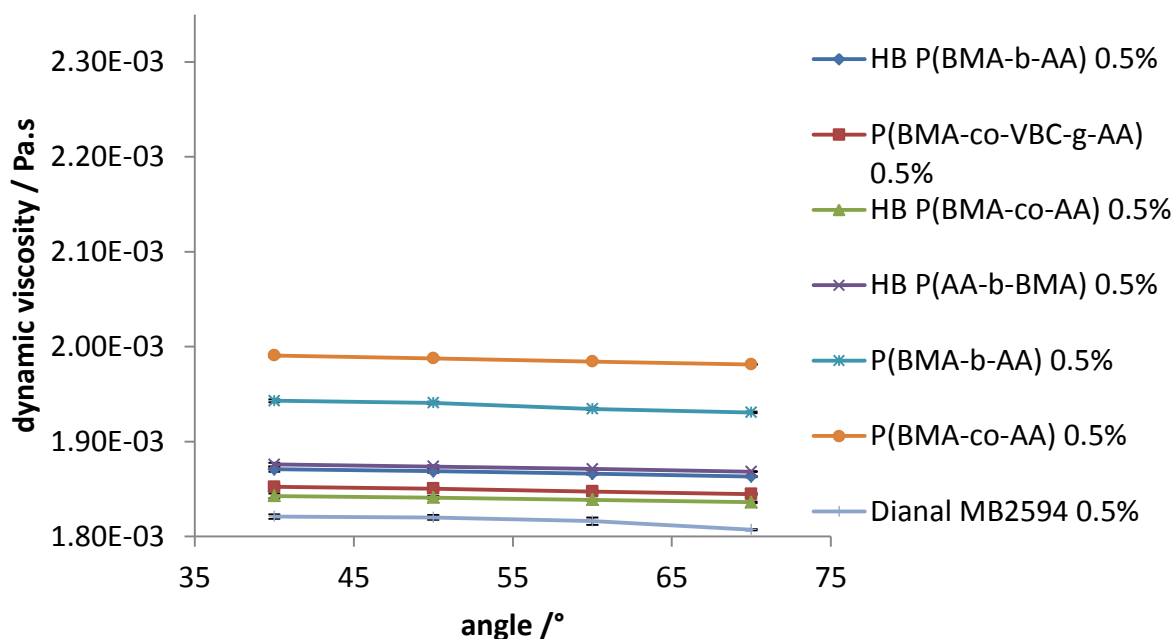


Figure 8.1. Dynamic viscosity measurements of inks with BK107 formulation containing copolymers at 0.5% concentration measured on an Anton Paar rolling ball viscometer. Error bars represent the standard errors but in most cases are smaller than the data points and thus not visible.

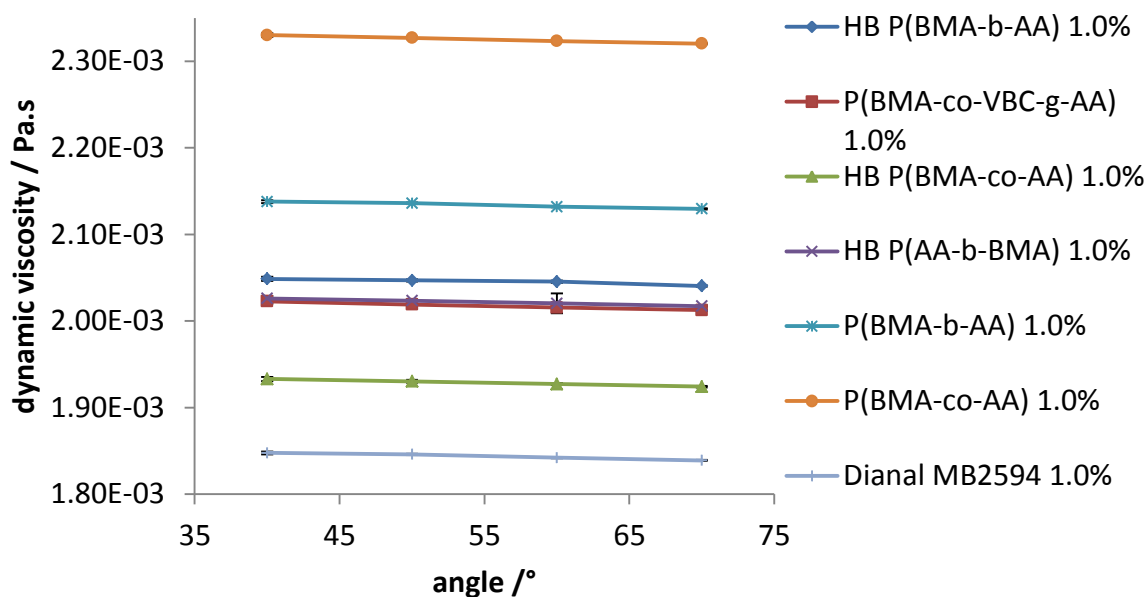


Figure 8.2. Dynamic viscosity measurements of inks with BK107 formulation containing copolymers at 1.0% concentration measured on an Anton Paar rolling ball viscometer. Error bars represent the standard errors but in most cases are smaller than the data points and thus not visible.

Statistical analysis was performed on this data to determine whether there were significant differences between samples, using the two-way ANOVA with a significance level of 0.05. This is used to analyse variance in data sets where there are two independent variables; in this case the angle of shear and the polymer in the ink. **Appendix 1** explains the test in more detail. The results for the 0.5% inks are summarised in **Table 8.3** and for the 1.0% inks in **Table 8.4**. The findings for the 0.5% ink are that there are significant differences between inks according to both the shear angles and the copolymer in the ink, but that there are no interactions between the two variables. A Tukey post-hoc analysis of the results indicated that the only data where no significant difference was observed was between the HBA and HBM inks, and HBR and G inks at each shear angle, and also at the lowest angle of shear there was no significant difference between G and HBM. These results are illustrated on the graph in **Figure 8.3**. In the case of the inks with 1.0% polymer content, much larger differences between variables were observed, indicated by much larger F values. Significant

differences were found between shear angles and samples, but also an interaction between the two variables was observed. Tukey post-hoc analysis showed that difference was observed between all copolymers and shear angles except for between the G, HBM and HBA copolymers. These results are illustrated on the graph in **Figure 8.4**.

Table 8.3. Statistical Analysis of Viscometry Data for Inks Containing 0.5% w/w Polymer Using the Two-way ANOVA

Source of variation	F	F _{crit}	P	P<0.05?
Interaction	0.574	1.84	0.9114	N
Shear Angle	12.8	2.76	<0.0001	Y
Sample	2240	2.25	<0.0001	Y

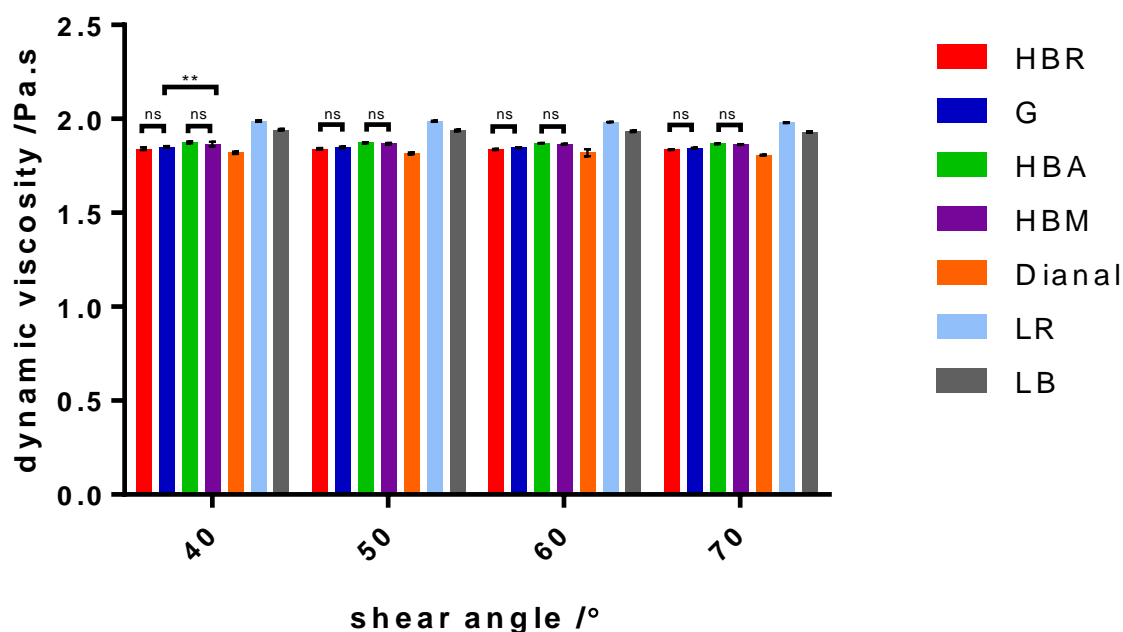


Figure 8.3. Bar chart showing the dynamic viscosity measurements of inks with BK107 formulation containing copolymers at 0.5% concentration. Error bars represent the standard errors. Tie lines show significance level of comparisons between sets of copolymers: *** P<0.001, ** 0.001<P<0.01, * 0.01<P<0.05, ns (not significant) P ≥ 0.05. Here, only not significant relationships between copolymers are shown on the graph, as all other comparisons returned P<0.001.

Table 8.4. Statistical Analysis of Viscometry Data for Inks Containing 1.0% w/w Polymer Using the Two-way ANOVA

Source of variation	F	F _{crit}	P	P<0.05?
Interaction	7.16	1.84	<0.0001	Y
Shear Angle	49.3	2.76	<0.0001	Y
Sample	25700	2.25	<0.0001	Y

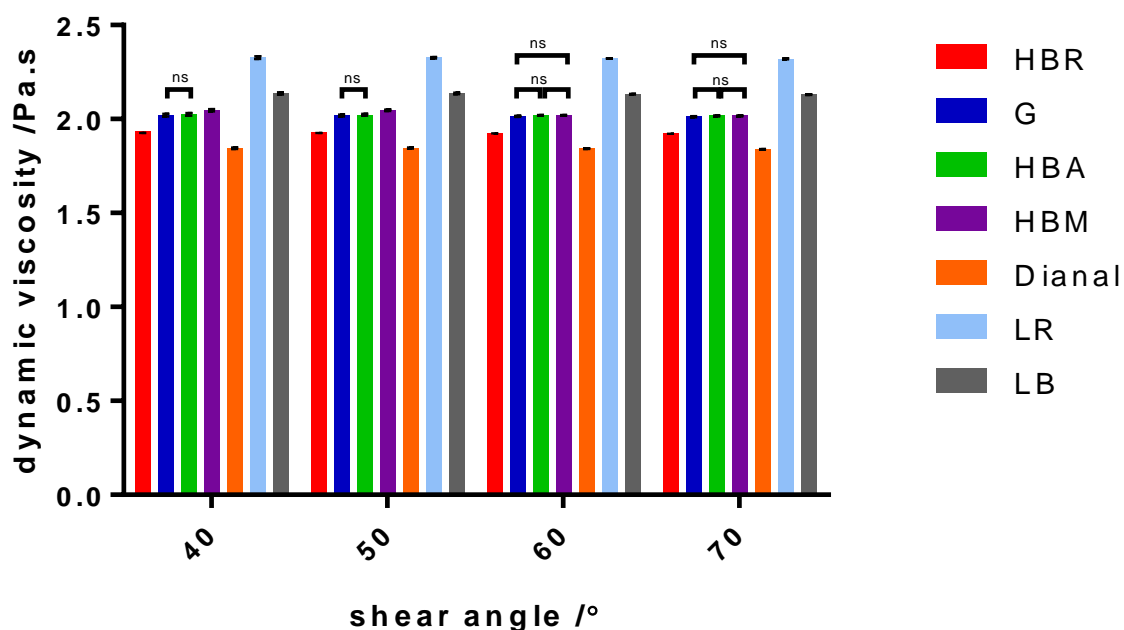


Figure 8.4. Bar chart showing the dynamic viscosity measurements of inks with BK107 formulation containing copolymers at 1.0% concentration. Error bars represent the standard errors. Tie lines show significance level of comparisons between sets of copolymers: *** $P < 0.001$, ** $0.001 < P < 0.01$, * $0.01 < P < 0.05$, ns (not significant) $P \geq 0.05$. Here, only not significant relationships between copolymers are shown on the graph, as all other comparisons returned $P < 0.001$.

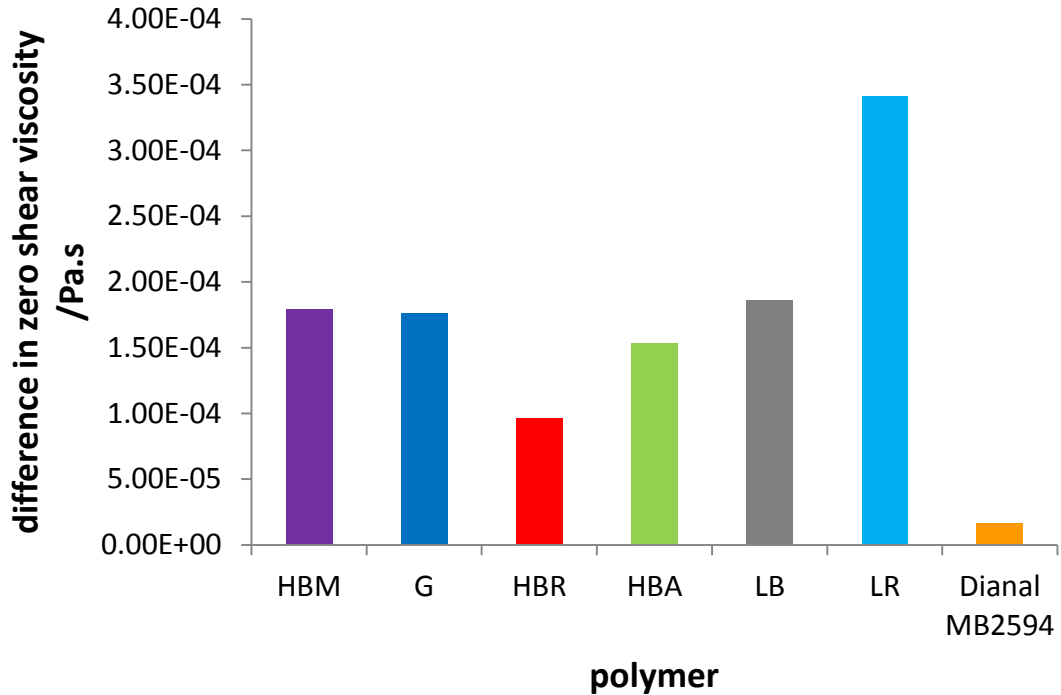


Figure 8.5. Bar chart showing the difference in zero shear viscosity (dynamic viscosity extrapolated to zero shear) between BK107 ink formulations containing copolymers at 0.5 % and 1.0% concentrations

Figure 8.5 shows the differences between the zero shear viscosities at the two concentrations displayed as a bar chart. The zero shear viscosity is found by extrapolating the dynamic viscosity data for each sample to zero. The amphiphilic copolymers and the Dialal MB2594 polymer behave very differently. A very small increase in viscosity of 1.60×10^{-5} Pa.s is observed for the Dialal MB2594, while more substantial increases are seen for the other materials. The highest increases are seen for the linear random copolymer, at 3.41×10^{-4} Pa.s, and the linear block copolymer, at 1.86×10^{-4} Pa.s. The viscosity differences are very similar for the HB block copolymer with PBMA core and for the graft copolymer, with an observed increase of close to 1.80×10^{-4} Pa.s. The HB block copolymer with PAA core displayed very similar behaviour, with a viscosity increase of 1.53×10^{-4} Pa.s, which is 2×10^{-5} Pa.s less than the other two samples. However an interesting result is that the HB random copolymer demonstrates a much lower increase in viscosity of 9.60×10^{-5} Pa.s as the polymer concentration is doubled. Although higher than the Dialal MB2594, this is much lower

than for the other copolymers. This means that at a given viscosity more HB P(BMA-*co*-AA) could be present compared to the other copolymers.

This is significant in printing applications as a balance must be found between additive concentration and ink properties, such as viscosity, which allows maximum additive performance whilst still retaining the ink properties that allow it to print. If the copolymer does improve the adhesion behaviour of the ink, then it would be an advantage to be able to increase the mass loading in the formulation whilst retaining the same viscosity. These differences in viscosity can be related to the molecular weight, polymer conformation, structure and solubility of the polymeric system; hence cannot be explained by a single factor.

8.4 Thermal Inkjet Printing with Domino G Series

The Domino G Series is a commercial thermal inkjet printer that operates with two rows of 150 nozzles using HP45 ink cartridges. Cartridges were filled with each of the eight ink formulations to be tested, as pictured in **Figure 8.6**. Once complete, a vacuum system was used to remove remaining air from the cartridges, as printing can be disrupted if cartridges are not sufficiently purged. A nozzle firing program was applied to fire a single row of nozzles in an “ABC” pattern and the heating waveform was the same as used for the BK107 ink.



Figure 8.6. Cartridges filled with BK107 ink formulations for use on the G Series printer

8.4.1 Decap Time

Knowledge of the decap time is an important performance criterion for a drop-on-demand printhead, such as the HP45. Decap time is the time from the point at which the cartridge cap is removed and the nozzles are uncovered that the nozzles can remain dormant and then still fire a drop without loss of print quality. To study this, each cartridge was used to print a sample barcode at specific time intervals after the cartridge is decapped. These intervals were at the time of initial print ($t=0$) then at ten seconds, one minute, five minutes, twenty minutes and thirty five minutes after the initial print. **Figure 8.7** shows the results for one sample, HB P(BMA-*co*-AA), at 0.5% polymer concentration.



Figure 8.7. Prints of sample barcode using BK107 ink with 0.5% HB P(BMA-*co*-AA) copolymer at time intervals: $t = 0$, 10 s, 1 min, 5 min, 20 min, and 35 min to study decap time

For this cartridge containing the HB random copolymer the print quality was maintained over the test period. However the other inks with 0.5% polymer content did show a difference in print quality over time, as seen in **Figure 8.8** with the HB block copolymer. A poor initial print is observed, with banding visible within the image and

an uneven border on the left side of the barcode square. This is improved after 10 seconds, although some unevenness can be observed along the border, and after 1 minute a good print is obtained with no further change seen up to the end of the test. The same result was observed for all the other inks with the 0.5% polymer content.

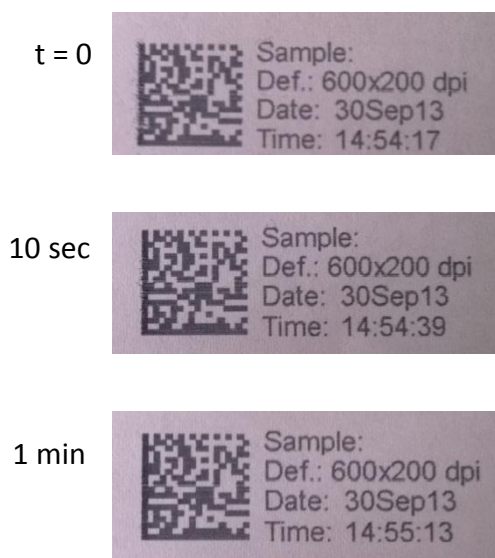


Figure 8.8. Prints of sample barcode using BK107 ink with 0.5% HB P(BMA-*b*-AA) copolymer at time intervals $t=0$, 10 s, and 1 min, to study decap time

The decap test was repeated with the inks containing 1.0% of copolymer in the formulation. Different results were seen for these inks compared to the 0.5% formulations, with all seven behaving similarly to each other. **Figure 8.9** shows the results for the HB P(BMA-*co*-AA) ink.



Figure 8.9. Prints of sample barcode using BK107 ink with 1.0% HB P(BMA-*co*-AA) copolymer at time intervals $t = 0, 10 \text{ s}, 1 \text{ min}, 5 \text{ min}, 20 \text{ min},$ and 35 min to study decap time

The 1% inks showed improvement in print quality over a longer time period than the 0.5% inks. Severe banding was seen in the initial prints, with gradual improvement seen up until the 35 minute print. This indicates that increasing the copolymer concentration does have an effect on the decap time of the ink.

Decap time is related to the volatility of the ‘vehicle’ or solvent; as the solvent evaporates the non-volatile components of the ink can precipitate out of solution and deposit around the nozzle. This leads to nozzle blocking, which is what reduces the print quality and must be fixed before printing can continue. Polymeric surfactants can be used to aid longer decap times by keeping the ink components in the fluid for a longer time before deposition.

The print quality of the standard inks was maintained until the decap time when the print quality decreased. It is an unusual feature of Domino’s BK107 inks that the initial print is of lower quality and then the print improves with time since the nozzles were exposed. Following this improvement it is expected that standard decap behaviour

would be observed if the study was continued for a longer time period, meaning that print quality would begin to decrease at a certain time.

8.4.2 Adhesion Testing

A series of 2D barcodes were printed onto polyolefin substrates to enable testing of the adhesion behaviour of the inks. Polypropylene (PP), high density polyethylene (HDPE) and low density polyethylene (LDPE) substrates were prepared by cleaning with ethanol and drying before use. The surface energies of these substrates are 30.1 mN/m for PP, 35.7 mN/m for HDPE and 33.7 mN/m for LDPE.²⁵⁵ **Figure 8.10** shows the 2D barcode consisting of four squares printed onto a sample substrate. Four sets of barcodes were printed to allow one to be used for each different aspect of the standard adhesion test and all were dried at room temperature for 24 hours prior to testing.

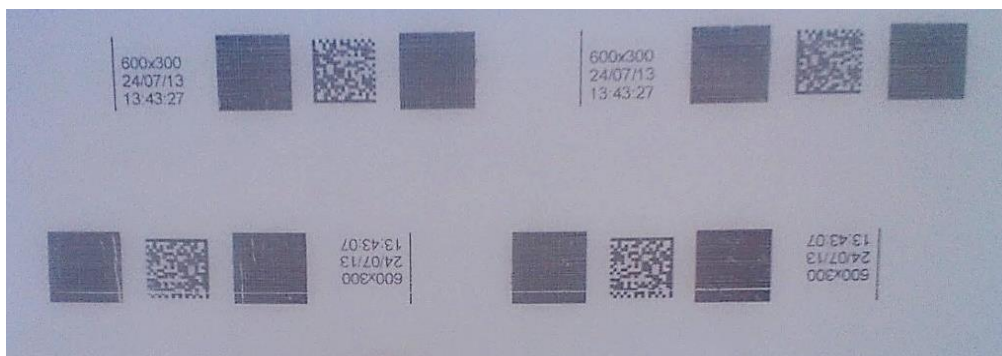
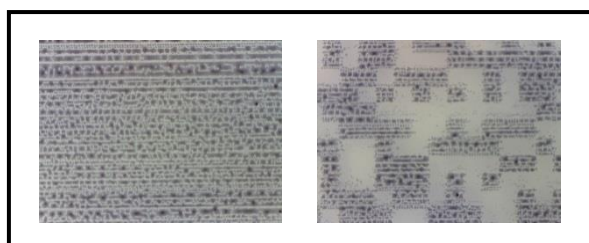


Figure 8.10. Sample 2D barcode pattern printed onto polyolefin substrate

The standard adhesion test used in industry has four aspects. Two types of tape are applied; a 610 tape (standard Sellotape) and 810 tape (Scotch Magic tape). A strip of each tape is adhered over a four square barcode and then peeled off to see how much material, if any, is removed. The third test is to scratch one of the barcode squares with a HB graded pencil and see how easily ink is removed, and the final test is to do the same with a fingernail. These tests are somewhat subjective, however, as they are qualitative in nature and it is difficult to accurately compare results for different samples, hence the motivation for AFM force spectroscopy as a possible alternative technique. Nevertheless the standard test was carried out on all of the copolymer inks,

except for the ones containing HB P(BMA-*b*-AA) which would not print well enough to allow the tests to be carried out at either 0.5% or 1.0% concentration. Possible reasons for this will be discussed later in Section 8.5.2.

Table 8.5 summarises the adhesion test results for the inks with a 0.5% w/w polymer content, and **Table 8.6** summarises the results for a 1.0% w/w polymer content. Additionally, a handheld USB microscope was used to image the test squares before and after the adhesion tests were performed. This allowed a closer observation of the effect of the adhesion tests on the printed substrates. **Figure 8.11** shows the results for one ink.



nail



810 tape



HB
pencil



610 tape



Figure 8.11. Images of 2D barcode squares printed with 0.5% HB P(AA-*b*-BMA) ink on PP substrate before adhesion testing (squares in box) and after testing. Images were taken with a USB digital microscope with 10x - 40x zoom.

Table 8.5. Results of Adhesion Testing using Standard Test for BK107 Ink Solutions containing Copolymer as Additive at 0.5% w/w.

(Tape test results record what printed material was visible on the lifted tapes. Pencil and nail scratch tests record the ease of removing printed material from the substrate, on the scale easy-medium-hard with intermediate levels where required.)

polymer	substrate	610 tape	810 tape	HB pencil	nail
HB P(AA- <i>b</i> -BMA) 0.5%	LDPE	nothing visible	nothing visible	easy-med.	easy-med.
	HDPE	nothing visible	nothing visible	Easy	easy-med.
	PP	nothing visible	faint lines from 2 squares	Hard	hard
P(BMA- <i>co</i> -VBC- <i>g</i> - AA) 0.5%	LDPE	nothing visible	lines from one square	Easy	med.
	HDPE	nothing visible	one spot	med.	med.-hard
	PP	nothing visible	faint 3 squares	Easy	hard
HB P(BMA- <i>co</i> -AA) 0.5%	LDPE	one square	nothing visible	med.	med.-hard
	HDPE	nothing visible	nothing visible	Easy	easy-med.
	PP	nothing visible	lines from 2 squares	med.	hard
P(BMA- <i>b</i> - AA) 0.5%	LDPE	nothing visible	nothing visible	med.-hard	med.
	HDPE	nothing visible	nothing visible	med.	easy
	PP	2 squares almost complete	small line	can't scratch	hard
P(BMA- <i>co</i> -AA) 0.5%	LDPE	nothing visible	nothing visible	med.-hard	med.
	HDPE	few spots	nothing visible	Easy	easy
	PP	faint partial 2 squares	faint square and line	Hard	hard
Dianal MB2594 0.5%	LDPE	nothing visible	nothing visible	easy-med.	easy-med.
	HDPE	nothing visible	faint square	easy-med.	easy
	PP	3 partial squares	4 partial squares	Hard	hard

Table 8.6. Results of Adhesion Testing using Standard Test for BK107 Ink Solutions containing Copolymer as Additive at 1.0% w/w. (Tape test results record what printed material was visible on the lifted tapes. Pencil and nail scratch tests record the ease of removing printed material from the substrate, on the scale easy-medium-hard with intermediate levels where required).

polymer	substrate	610 tape	810 tape	HB pencil	nail
HB P(AA- <i>b</i> -BMA) 1.0%	LDPE	nothing visible	few dots	Hard	hard
	HDPE	few dots	few dots	Hard	med.
	PP	nothing visible	2 lines	can't scratch	hard
P(BMA- <i>co</i> - VBC- <i>g</i> - AA) 1.0%	LDPE	nothing visible	one partial line	med.	med.
	HDPE	nothing visible	nothing visible	med.	med.
	PP	nothing visible	several lines	can't scratch	hard
HB P(BMA- <i>co</i> - AA) 1.0%	LDPE	nothing visible	few dots	med.	med.
	HDPE	few dots	few dots	med.	easy-med.
	PP	1 almost complete square, 1 partial square	3 partial lines	can't scratch	hard
P(BMA- <i>b</i> - AA) 1.0%	LDPE	nothing visible	nothing visible	med.	med.
	HDPE	nothing visible	nothing visible	med.	easy
	PP	4 almost complete squares	3 partial squares	can't scratch	hard
P(BMA- <i>co</i> - AA) 1.0%	LDPE	nothing visible	nothing visible	med.-hard	med.
	HDPE	faint smudges	nothing visible	Easy	easy
	PP	4 almost complete squares	4 partial squares	can't scratch	hard
Dianal MB2594 1.0%	LDPE	nothing visible	nothing visible	med.	med.
	HDPE	nothing visible	nothing visible	easy-med.	easy
	PP	4 almost complete squares	2 almost complete squares, 2 faint squares	Hard	hard

In **Figure 8.11** no difference can be seen between the untested squares and those that were tape-tested. However, scratches where ink has been removed can be clearly seen on the squares which were scratch-tested with the pencil and the fingernail. This was the case for all the inks with 0.5% polymer concentration, with good resistance to the tape test evident as very little material was seen on the tapes, and in many cases none at all, whereas the scratch resistance was much lower. Almost all samples could be scratched with both nail and pencil. The results were reversed for the inks with 1.0% polymer content, which were much harder to scratch. In several cases no material could be removed even when strong pressure was applied. However, the tape tests were able to remove material in more cases.

Differences in adhesion behaviour were observed between the different substrates as well. Results for inks printed on PP were in general different to those for inks printed on LDPE and HDPE, which tended to behave similarly to each other. Inks printed on PP were generally harder to scratch, but performed worse than those on LDPE and HDPE in the tape tests at both 0.5% and 1.0% polymer content. One significant result was that all inks with 1.0% polymer performed well in the scratch test when printed on PP, with all proving completely scratch resistant to the pencil test and very difficult to scratch with a fingernail.

Variation was also observed between the different polymers. For the inks with 0.5% polymer content, the branched copolymers demonstrated better resistance to the tape tests, whilst the linear materials had better scratch resistance. The ink containing the Dianal MB2594 polymer behaved similarly to the linear copolymers, but performed slightly worse in the tape tests with more material being removed. This is possibly a result of the lower molecular weight of the Dianal polymer. The same trends between branched and linear copolymers were observed in the inks with 1.0% copolymer in the tape tests, with the branched polymers performing better. The ink with 1.0% w/w of Dianal MB2594 showed the worst performance when printed on PP, with almost all printed material being removed by the tapes. However the results of the scratch tests were similar for all inks.

These results suggest that varying the copolymer additive in the ink formulations does affect their adhesion behaviour when printed onto polyolefin substrates. Differences are apparent between the branched and linear copolymers, and an alternate

behaviour is observed for inks printed on LDPE and HDPE in comparison to PP. Additionally, increasing the copolymer content of the inks appears to have a definite effect on their adhesion behaviour. Greater copolymer content appears to improve scratch resistance while having a slight adverse effect on surface adhesion.

However, one issue with these adhesion tests is that they are not necessarily testing what is intended, namely the strength of the adhesion force between the substrate and the printed material. When a piece of tape is adhered to the printed substrate and peeled, printed material will be removed if the adhesion strength of tape to printed material is stronger than that of printed material to substrate. This could explain why the inks with 0.5% polymer concentration show good scratch resistance but material can be removed with tape, as there is good adhesion with the substrate but also good adhesion with the tape. If adhesive behaviour was poor then material may not be lifted with the tape as it may not adhere to the tape. This is one reason why an alternative adhesion testing method is being sought in the form of AFM, as explored in Chapter 7.

8.4.3 Jet Xpert

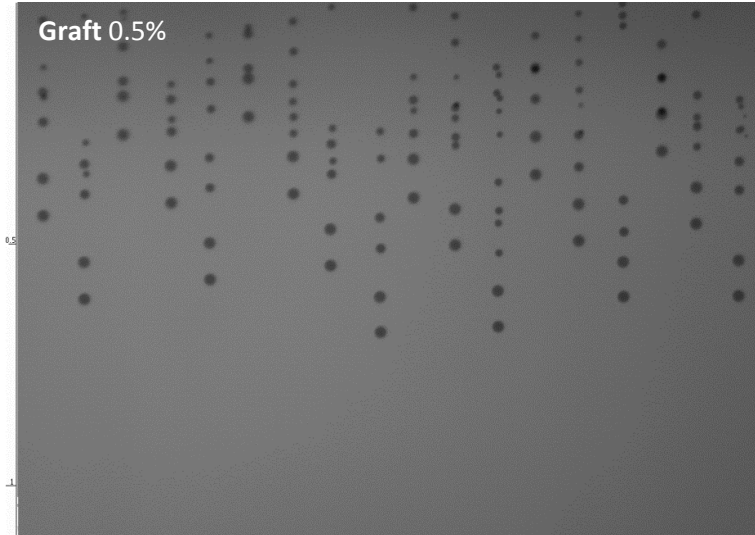
A Jet Xpert imaging system was used to view the ink drops in-flight. The system has two cameras, one angled to view the drop curtain to allow ‘time in flight’ droplet analysis (drop velocity and break-up) and one angled to view the nozzle plate (nozzle firing and wetting). **Figure 8. 12** shows images of the drop curtain for some of the inks with 0.5% polymer content: Dianal MB2594, graft, HB random, linear block and linear random, and also the Dianal MB2594 ink with 1.0% polymer content. The images are taken while the cartridge is in constant operation in an ‘ABC’ nozzle firing pattern. Clear differences are observed in the jetting behaviour of the formulations. The Dianal MB2594 0.5% and graft 0.5% inks performed well, with regular drops in the ‘drop curtain’. Fewer drops are seen for the HB random 0.5% ink, and slightly more irregularity is observed to indicate a nozzle blocking issue and/or the influence of viscosity. The images of the linear block and linear random 0.5% inks demonstrate that these inks have a problem with nozzle blocking; as a result few nozzles are able to fire jets. The Dianal MB2594 ink with 1.0% polymer content has more visible instability in the jets, suggesting that higher polymer content has a negative effect on the jetting behaviour.

Dianal MB2594 0.5%



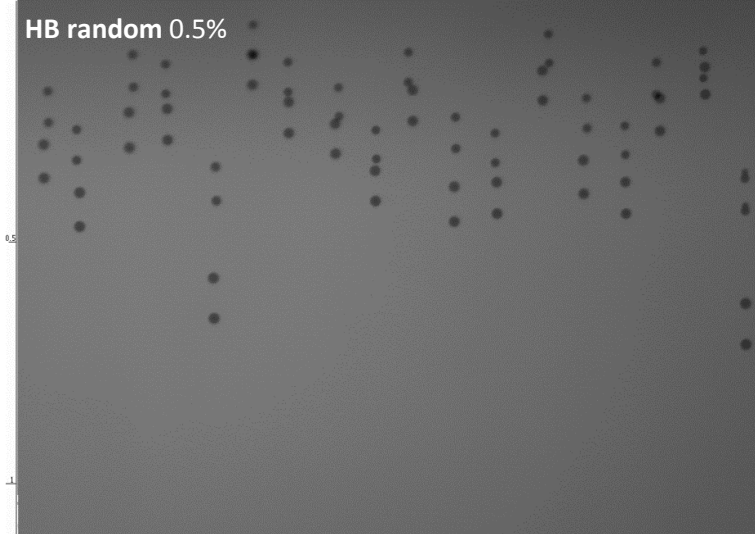
delay1 = 60.05 us, delay2 = 30.05 us, pw = 625 ns, shutter = 5.0 ms, LED = 80, External freq. 1.0 pixel = 0.00151 mm, #strokes = 1

Graft 0.5%



delay1 = 100.05 us, delay2 = 10.05 us, pw = 625 ns, shutter = 5.0 ms, LED = 80, External freq. 1.0 pixel = 0.00151 mm, #strokes = 1

HB random 0.5%



delay1 = 200.05 us, delay2 = 20.05 us, pw = 625 ns, shutter = 5.0 ms, LED = 80, External freq. 1.0 pixel = 0.00151 mm, #strokes = 1

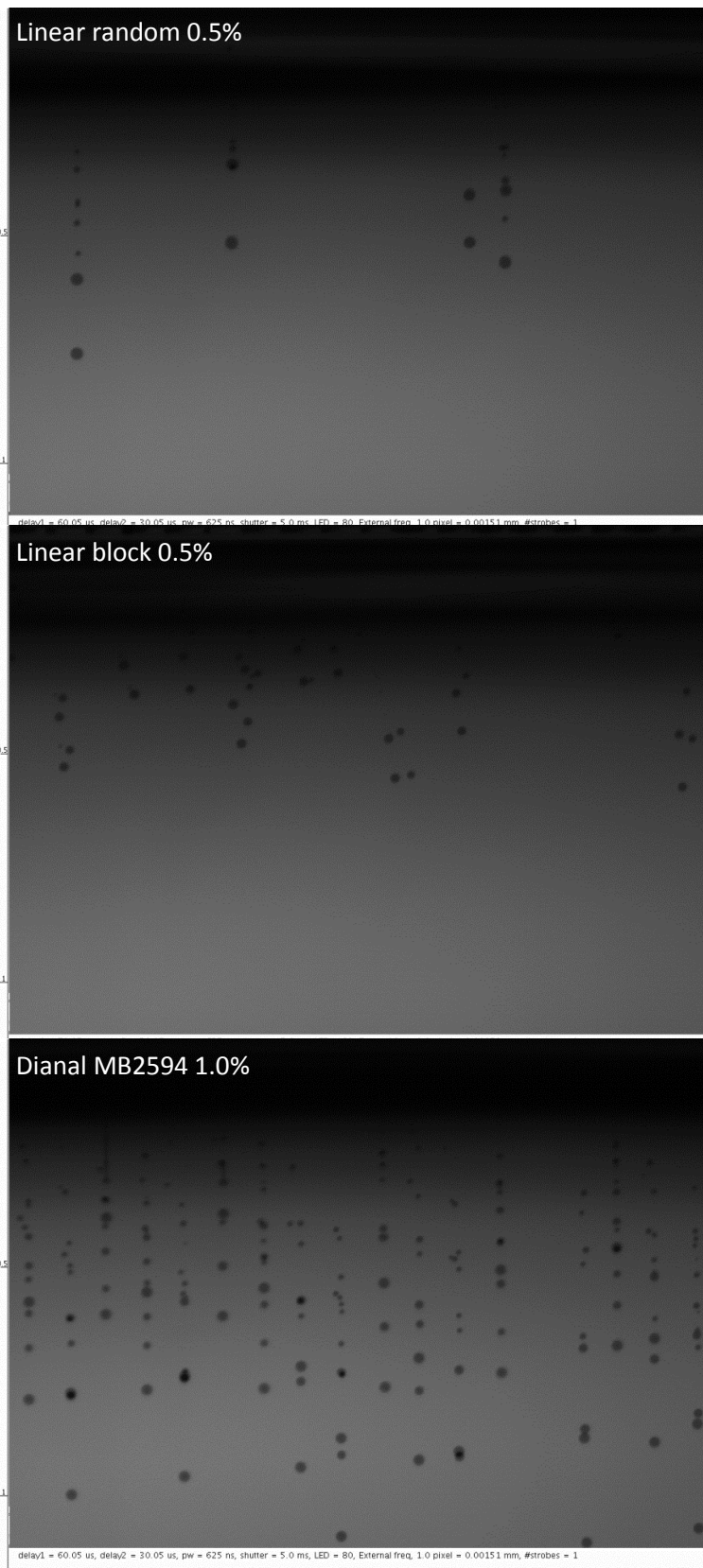
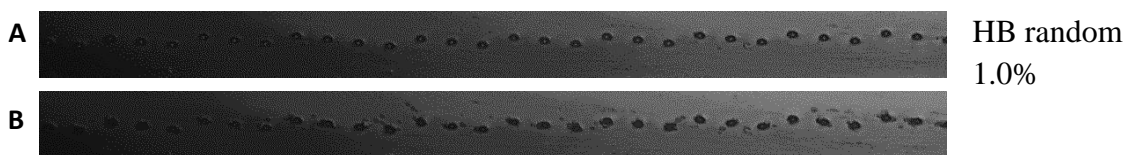
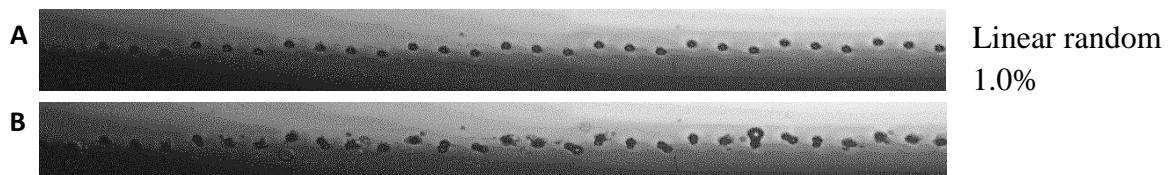
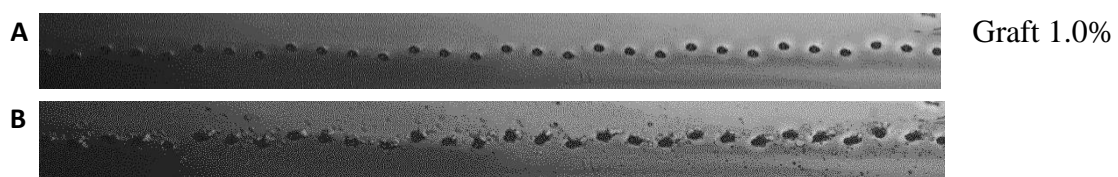
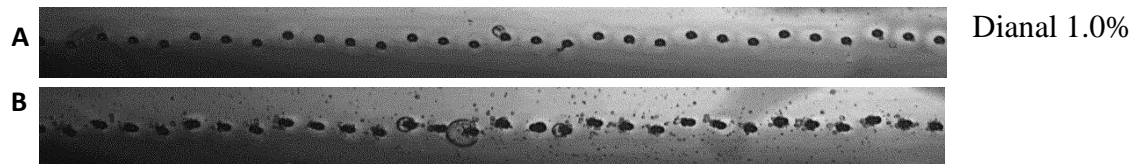
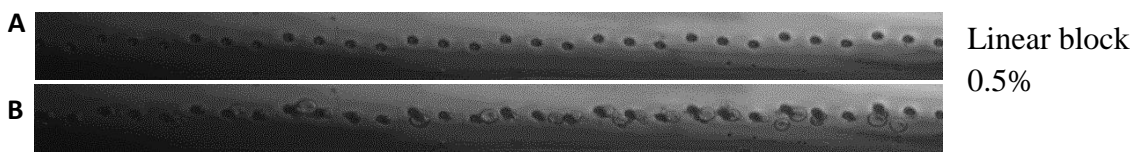
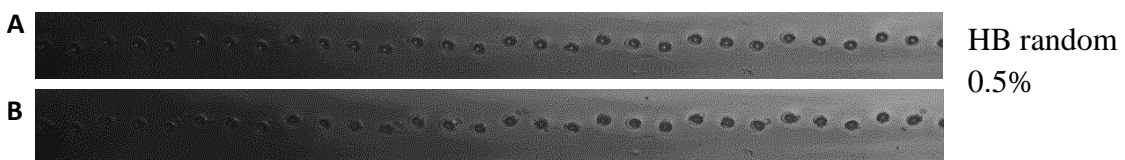
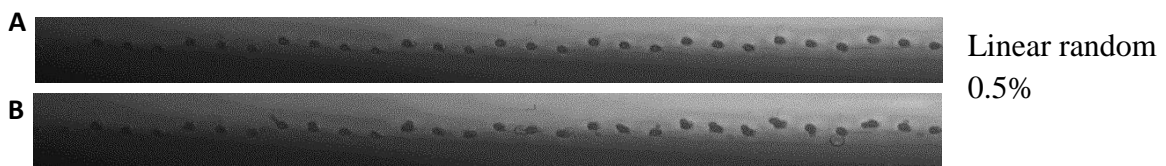
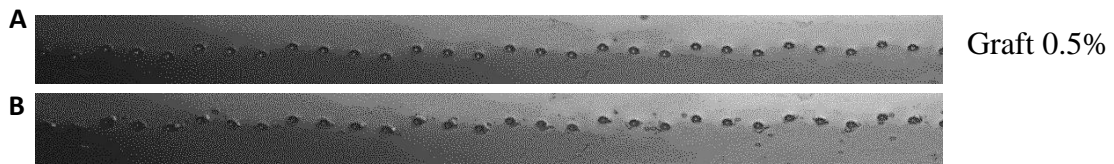
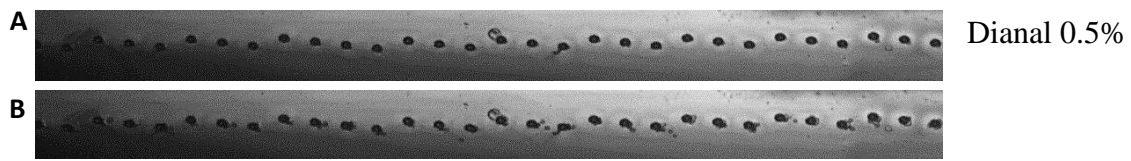


Figure 8.12. Images of drop curtain recorded while ink is jetting on JetXpert imaging system. A good result would be a curtain of evenly spaced, stable jets with regular droplets.



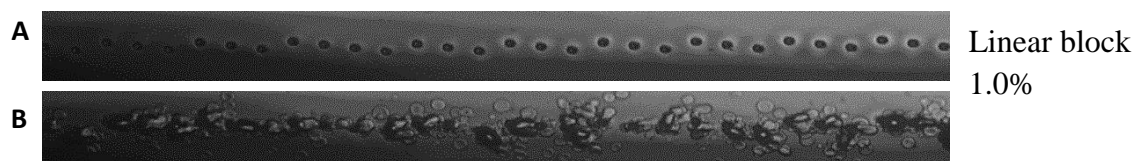


Figure 8.13. Images of nozzle plate at a) $t= 0$ and b) $t= 2$ min recorded while ink is jetting on Jet Xpert imaging system. A good result would be minimal spotting on the nozzle plate and no ink pooling around the nozzles.

Figure 8.13 comprises the images from the camera angled onto the nozzle plate. Images were taken before printing was started ($t= 0$) and after two minutes of continuous jetting ($t= 2$ min). Some depositing on the nozzle plate is seen for the inks with 0.5% polymer content. Pooling of ink around the nozzles can be observed for the linear random 0.5% ink and to a greater degree for the linear block 0.5% ink. This explains why poor jetting was seen for these two inks.

This was also carried out for the inks with increased 1.0% polymer content. A greater degree of depositing occurred on the nozzle plate for all inks to highlight the higher polymer concentration of polymer may have more of a destabilising effect on this particular formulation. This is most severe for the linear block 1.0% ink where a large amount of ink is visible around each nozzle, preventing the nozzles from being able to fire, as seen with the drop “curtain” image in **Figure 8.12**.

These results are difficult to rationalise as the ink performance in terms of the number of satellites formed, the drop velocity, the degree of dusting on the nozzle plate and the degree of nozzle blocking are influenced by many factors including: ink viscosity; deposition leading to narrowing of the nozzle aperture; deposition on the heater elements; chemical interactions between the ink components; and solubility. Nevertheless these results do seem to scale with the viscosities of the inks (as presented in Figure 8.1) at least to some degree: the inks containing the linear copolymers had the highest viscosities and experienced problems with nozzle blocking leading to very poor printing performance, especially at 1.0% w/w which had the highest viscosities of all. The Dianal MB2594 inks had the lowest measured viscosities. The ink with 0.5%

polymer was found to jet well although it appears there are many satellite drops, whilst greater instability was seen at 1.0% concentration. This could be due to these inks behaving as low viscosity Newtonian fluids and breaking into a range of droplet sizes due to Rayleigh-Taylor instabilities.²⁵⁶

8.5 Drop on Demand Printing with Fujifilm Dimatix

Further printing tests were carried out using a Fujifilm Dimatix printer, pictured in **Figure 8.14**. This is a drop on demand printer with piezoelectric actuation that is specially designed for research use, allowing the precise deposition of fluid materials on a substrate. The print head takes disposable cartridges which require less than 2 ml of fluid, making them well suited to optimisation studies with small volumes of formulation.

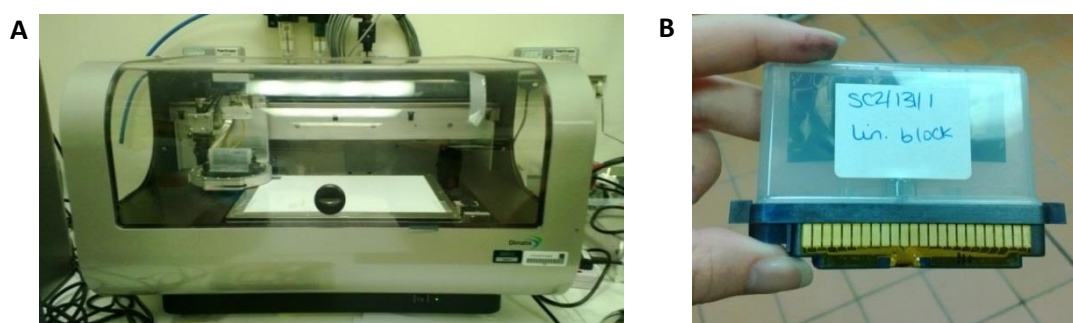


Figure 8.14. a) Fujifilm Dimatix DMP2831 DOD printer and b) Dimatix cartridge

A major advantage of the Dimatix is that a number of print settings can be varied to test printing performance under different conditions. The Dimatix comes programmed with default settings which are recommended for a ‘model fluid’ with a viscosity of 0.01 Pa.s and surface tension of 0.03 N m⁻¹. These settings consist of a firing voltage (the voltage applied to each nozzle to achieve ejection of an ink drop) of 16 V, a cartridge temperature of 30 °C and a throw distance (height of print head above platen on which substrate is placed, therefore the distance ink drops travel) of 1 mm.

Initially these settings were used to print a test image with each of the 0.5% and 1.0% ink formulations onto standard A4 paper. The print qualities were poor, as would be expected since these inks are known to have viscosities in the range $1.80 \times 10^{-3} - 2.35 \times 10^{-3}$ Pa.s which is much lower than the recommended values for the model fluid.



Figure 8.15. Example of poor print quality seen when using the default print settings to print onto A4 paper

8.5.1 Print Setting Optimisation

In order to improve the printing of the inks, the print settings needed to be optimised. The three settings which have most effect on the printing results are the firing voltage, the cartridge temperature and the throw distance. Therefore one ink was chosen, the one containing HB P(BMA-*b*-AA) at 0.5% by mass, and each setting was varied in turn to obtain the optimum settings.

Firstly the firing voltage was varied. The more viscous the fluid to be jetted, the higher the firing voltage required, as more energy is needed to force the ink out of the print head. The inks containing the amphiphilic copolymer materials are much less viscous than the model fluid so an optimum firing voltage of lower than the recommended 16 V would be expected. **Figure 8.16** shows the results of the voltage optimisation.

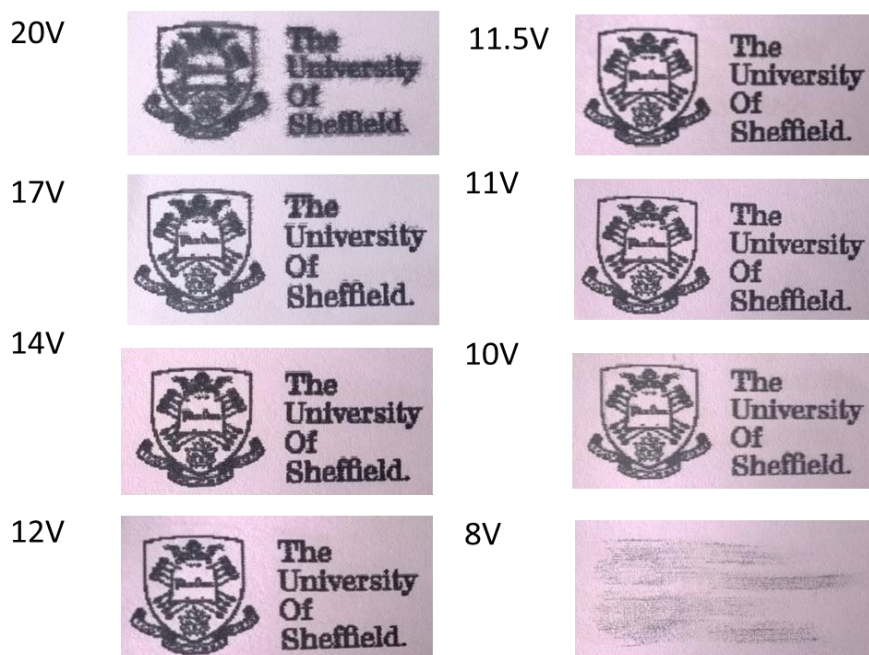


Figure 8.16. Results of firing voltage optimisation using HB P(BMA-*b*-AA) 0.5% ink printed onto A4 paper with fixed cartridge temperature of 30 °C and a print height of 1 mm

11.5 V was chosen as the optimum firing voltage as this gave the best print. Print quality was judged both visually and through examination with the USB microscope which allowed closer inspection. Good print quality in this case means that the print has no visible banding, no uneven edges to printed objects and no visible satellite drops. At 20 V, the highest voltage tested, the print was blurred and unclear with many satellite drops around the edges of the objects and shadowing underneath, as the drops were ejected with too much force. The opposite effect was seen at 8 V, the lowest voltage tested, with only a faint impression of the image being printed. This demonstrates that the ink drops did not receive a firing pulse with enough energy to eject them from the nozzle.

The firing voltage was therefore fixed to 11.5 V and the other variables were investigated, the results of which are shown in **Figure 8.17**. The next variable to test was the throw distance, or print height. This was initially set at 1.5 mm, and then reduced to 1.0 mm, 0.5 mm, and 0.3 mm. The 1.5 mm print was the poorest with more satellite drops observed. These were reduced as the throw distance was decreased until

0.3 mm where some blurring and ink transfer was observed from the substrate being too close to the printhead. The 0.5 mm value was selected as the optimum setting for the throw distance, and the effect of cartridge temperature was then studied.

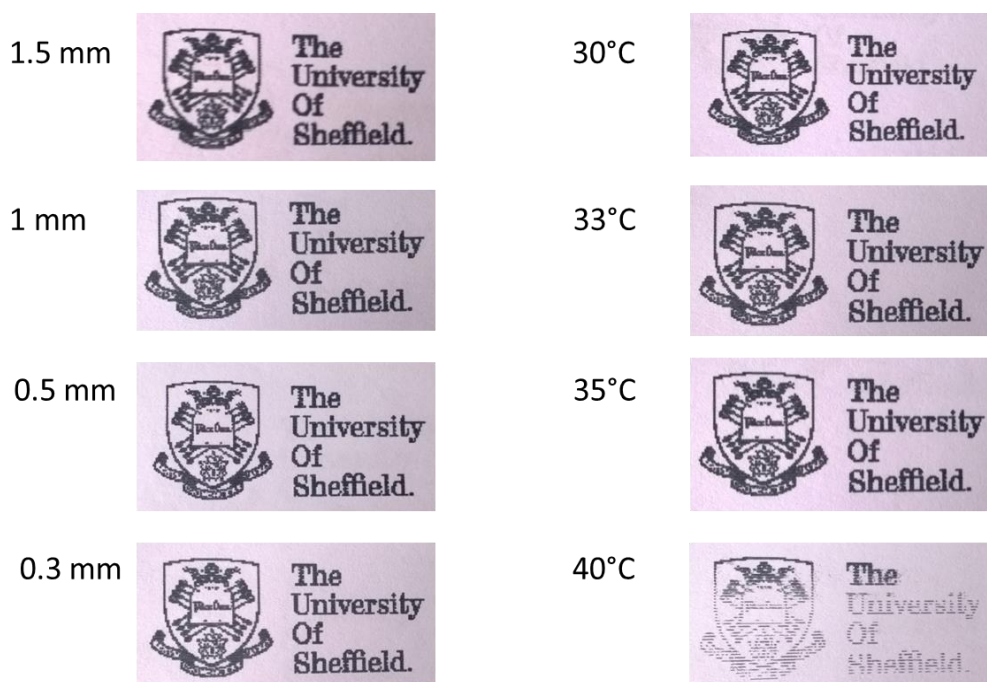


Figure 8.17. Results of throw distance and cartridge temperature optimisation using HB P(BMA-*b*-AA) 0.5% ink printed onto A4 paper with fixed firing voltage 11.5V

The temperature was varied over the range 30 to 40 °C. Little difference in print quality was observed until 40 °C where a large degree of banding was seen and the print became very faint, showing that the cartridge is unable to print when the temperature is too high. This is as a result of the viscosity decreasing as the temperature is increased; once the lower viscosity limit is reached the printer will be unable to fire. 33 °C was chosen as the optimum temperature, completing a new set of printing parameters for the HB P(BMA-*b*-AA) 0.5% ink. These settings were applied to the other inks with both 0.5% and 1.0% polymer contents and found to print well with all of them. This shows that the different polymers in the inks and the associated variations in viscosity are not large enough to have any significant effect on their printing behaviour.

8.5.2 Printing onto Substrates

Once optimised printing settings were obtained, each of the inks was printed onto polyolefin substrates (PP, HDPE and LDPE), as performed using the G Series printer. Good prints were achieved for all of the inks at both concentrations of polymer. **Figure 8.18** shows the printed images on the three different substrates for the ink with HB P(BMA-*b*-AA) at 1.0% concentration by mass. The print is lighter on PP compared to LDPE and HDPE but the features of the image are still clearly visible.

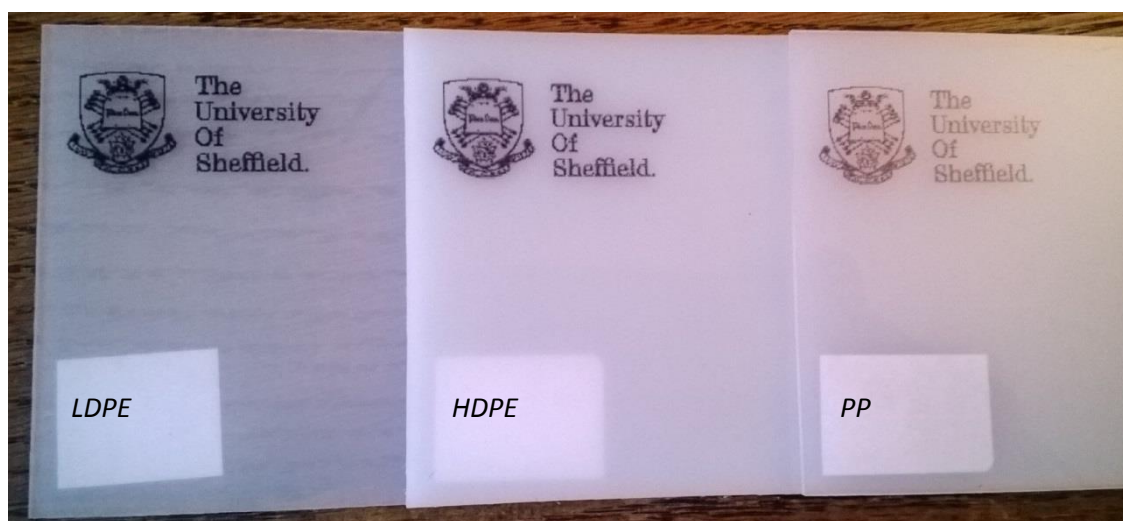


Figure 8.18. Results of printing onto polyolefin substrates using HB P(BMA-*b*-AA) 1.0% ink with optimised print settings

The two inks containing the HB P(BMA-*b*-AA) copolymer stopped jetting on the G Series printer, whereas good prints were achieved using the Dimatix. This can be explained by the difference in printing technologies employed in the two printers, as the G Series is a TIJ printer whereas the Dimatix is a PIJ. Therefore the G Series has to heat the ink whereas the Dimatix only uses pressure to eject ink droplets. The effect of heat on these polymers in solution is unknown but it could explain why they stop jetting. It is possible that some kind of aggregation is happening which is blocking the nozzles and preventing droplet ejection.

In addition, print quality is improved by the ability of the Dimatix to allow variable print settings so that a suitable configuration can be found. The G Series printer on the other hand has fixed settings depending on the energy file applied, which in turn

is chosen depending on the type of ink being used. For the BK107 ethanol-based ink the energy file has a firing pulse of 8.4V. Although this much lower voltage appears a possible explanation for the difference in printing performance, this is not directly comparable to the firing pulse of the Dimatix as other parameters are different between the two printers, in addition to the printing mechanism itself. Others factors which affect performance are the nozzle size and printhead design features such as the cavity dimensions and ejection velocity. These are unknown for the Dimatix printer as it is not Domino technology.

The full set of inks were also printed onto glass slides, which gave good prints under the optimised conditions despite glass having a much higher surface energy than the polyolefin substrates; the surface energy of glass is reported as being within the range 43-113 mN/m.²⁵⁷ Following drying of the printed substrates in an oven at 40 °C for an hour, the standard adhesion tests were carried out. No visible material was removed in the tape tests and the print was strongly scratch resistant. This would be expected as adhesion to glass is greater due to the higher surface energy.

8.5.3 Printing Polymer Solutions

Although interesting results were obtained from the printing tests using the copolymers as additives to the ink formulations, it was important to also study the behaviour of the copolymers when printed in isolation. The HB P(BMA-*co*-AA) copolymer was dissolved in the BK107 base solvent mixture to prepare samples at a range of concentrations, 1, 3 and 5% w/w, to investigate the effect of concentration on printing. Solutions of a second copolymer, the HB P(AA-*b*-BMA) copolymer, were prepared at 3.8% concentration in different mixtures of the BK107 base solvent mixture and 1,2-hexanediol (HD). HD is a higher molecular weight glycol with a viscosity of 6.37×10^{-2} Pa.s at 25 °C. This high viscosity means that the addition of small amounts of HD to a solution can result in an increase of overall viscosity without large changes in overall properties. The HB P(AA-*b*-BMA) solutions were prepared in mass ratios of 1:1 and 3:1 BK107:HD in addition to a control solution with no HD.

8.5.3.1 Viscometry

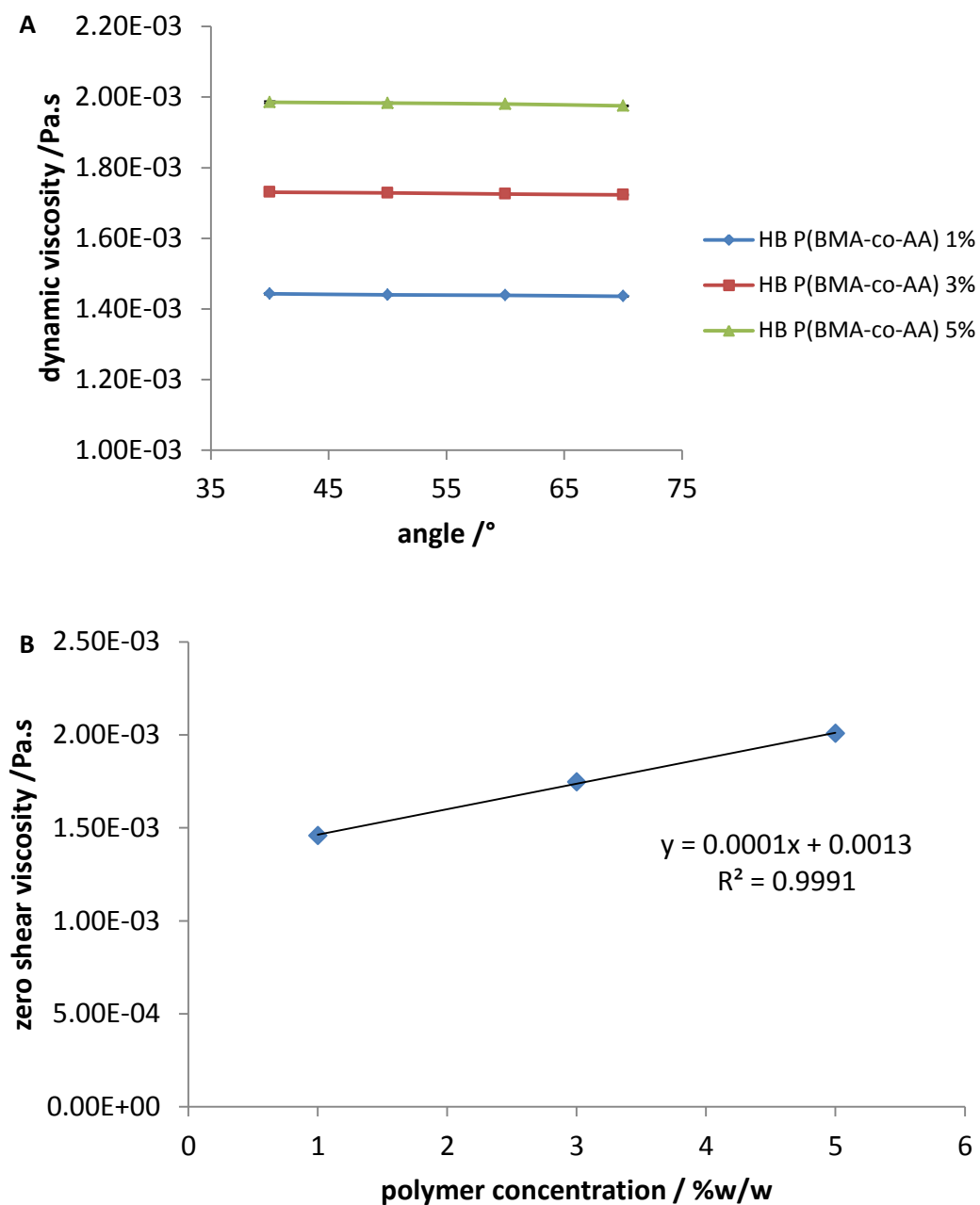


Figure 8.19. a) Dynamic viscosity measurements of HB P(BMA-co-AA) copolymer in solution (BK107 solvent mixture) at 1.0, 3.0 and 5.0% concentration by mass measured on an Anton Paar rolling ball viscometer, error bars represent the standard errors but in most cases are smaller than the data points and thus not visible.

and b) Comparison of dynamic viscosities at different concentrations of HB P(BMA-co-AA) copolymer demonstrating a linear relationship between the variables.

Figure 8.19 demonstrates that the dynamic viscosity of the solutions varies linearly ($R^2 = 0.999$) with the concentration of polymer, as would be expected. **Figure 8.20** shows that at a constant polymer concentration the amount of added HD as viscosity modifier has a large effect on the dynamic viscosity of the solution. An increase in the content of HD from 25% to 50% by mass resulted in an increase in viscosity of greater than 3×10^{-3} Pa.s, from 3.87×10^{-3} to 7.55×10^{-3} Pa.s. This is an increase of 95%.

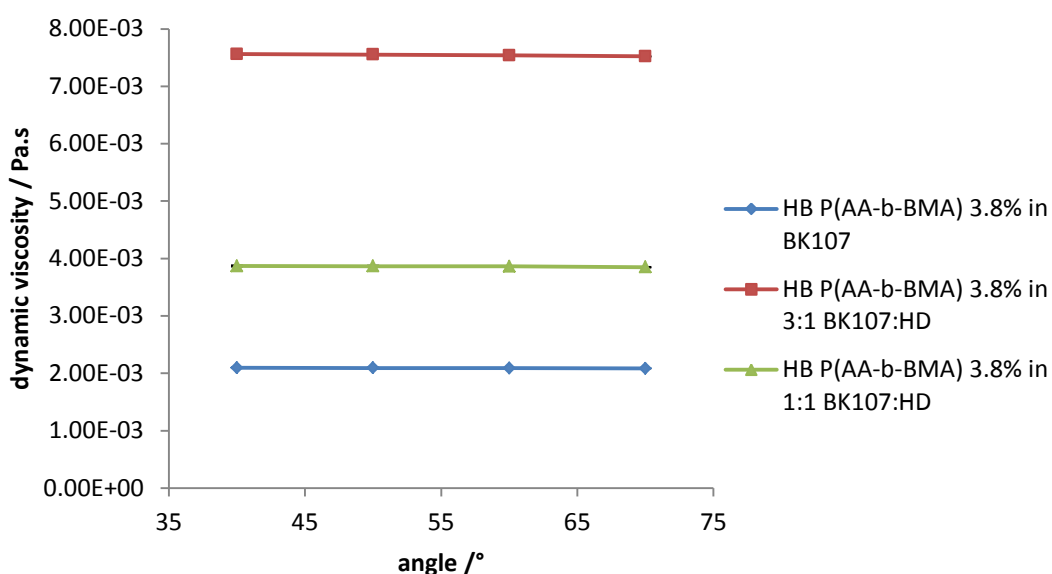


Figure 8.20. Dynamic viscosity measurements of HB P(AA-*b*-BMA) copolymer at 3.8% concentration in BK107 solvent mixture and 3:1 and 1:1 mass ratios of BK107 solvent:1,2-hexanediol (HD) measured on an Anton Paar rolling ball viscometer. Error bars represent the standard errors but in most cases are smaller than the data points and thus not visible.

8.5.3.2 Printing Tests

Initial printing tests with the Dimatix demonstrated that it was very difficult to see the printed images and therefore assess the quality of printing as the solutions appeared colourless when printed. The prints were tested for fluorescence as the RAFT end groups remaining in the polymer structure contain aromatic groups which could act as fluorophores. However these were not present in adequate number and therefore no fluorescence was observed. As a result a 5% w/w solution of the black dye used in the BK107 ink in the necessary solvent was prepared, and two drops of this solution were added to each cartridge. This resulted in a lightly coloured solution which was visible when printed onto the substrates, whilst containing dye at low concentration with the aim of not affecting the overall behaviour of the system.

All six of these polymer 'inks' were printed onto both HDPE and glass substrates, with examples being shown in **Figure 8.21**.

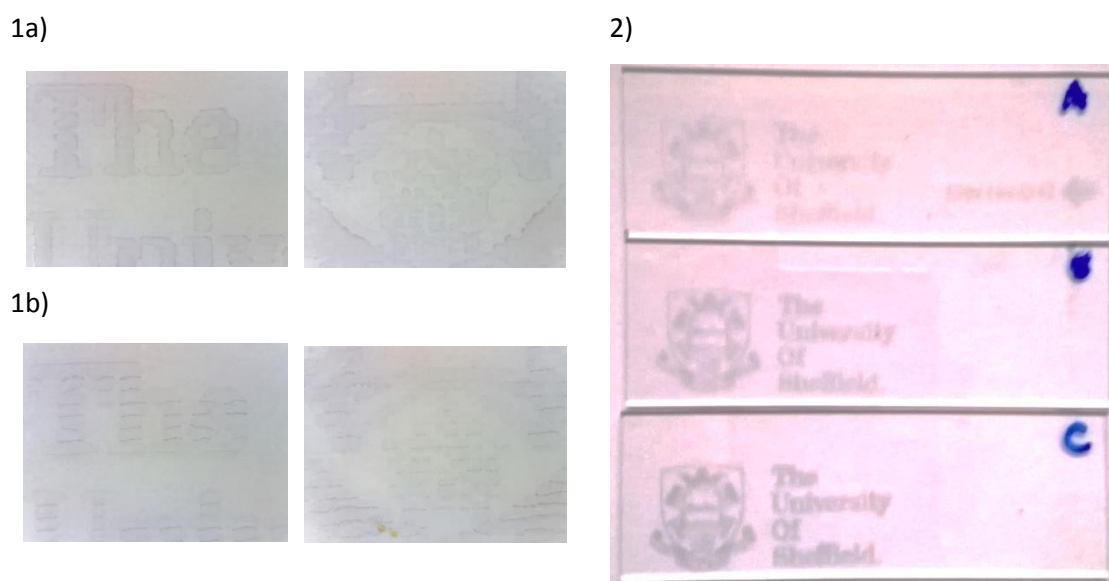


Figure 8.21. Results of printing with copolymer 'ink' 1a) HB P(AA-*b*-BMA) 3.8% in 3:1 BK107:HD and b) HB P(AA-*b*-BMA) 5% in BK107 printed onto HDPE substrate, 2) **A**: HB P(BMA-*co*-AA) 1% in BK107, **B**: HB P(BMA-*co*-AA) 3% in BK107 and **C**: HB P(BMA-*co*-AA) 5% in BK107 printed onto glass

For the HB P(AA-*b*-BMA) inks a better print was obtained with the more viscous ink, with less banding observed in the images and a more even distribution of

colourant. The differences were not as clear in the prints of the HB P(BMA-*co*-AA) inks although the printed image appeared to be darker the higher the concentration of polymer in the ink. Tape tests performed on the samples did not remove any visible material, and the printed images could not be scratched.

Table 8.7. Comparison of Viscosity Measurements with Determined Optimal Firing Voltage for Solutions of HB P(BMA-*co*-AA) and HB P(AA-*b*-BMA) Copolymer in BK107 Solvent Mixture

Sample	viscosity /Pa.s	firing voltage /V
HB P(BMA- <i>co</i> -AA) 1%	1.44×10^{-3}	10.0
HB P(BMA- <i>co</i> -AA) 3%	1.73×10^{-3}	10.5
HB P(BMA- <i>co</i> -AA) 5%	1.98×10^{-3}	11.5
HB P(AA- <i>b</i> -BMA) 3.8%	2.09×10^{-3}	11.0
HB P(AA- <i>b</i> -BMA) 3.8% 3:1 BK107:HD	3.86×10^{-3}	14.0
HB P(AA- <i>b</i> -BMA) 3.8% 1:1 BK107:HD	7.54×10^{-3}	22.0

The optimal firing voltage was determined for each of the polymer ‘inks’. The results, shown in **Table 8.7**, are as expected, with a directly proportional relationship between viscosity and firing voltage: the higher the viscosity, the higher the firing voltage necessary to achieve the best print. Small variation in firing voltage is seen for the HB P(BMA-*co*-AA) inks as the increase in polymer concentration causes only a small increase in viscosity. The HB P(AA-*b*-BMA) inks show a large increase in the firing voltage needed as the HD content is increased. This is due to the magnitude of the increase in viscosity of the ink.

8.6 Summary

Test	HBR	G	HBA	HBM	LR	LB	Dianal MB2594
Viscometry	2 nd lowest viscosity at 0.5% and 1.0%, 2 nd lowest increase from 0.5% to 1.0%	medium viscosity at 0.5% and 1.0%, medium increase			highest viscosity at 0.5% and 1.0%, biggest increase	2 nd highest viscosity at 0.5% and 1.0%, medium increase	lowest viscosity at 0.5% and 1.0%, v.low increase (low MW)
Decap Time (TIJ)	0.5%: print quality maintained	0.5%: poor initial print, good from 1 min onwards					
	1.0%: v.poor initial print, gradual improvement up to 35 min						
Adhesion Testing (TIJ)	better tape test performance than linear, worse scratch resistance			couldn't be tested, would not print	perform worse than branched in tape test, better scratch resistance		worst performer in tape test (low MW), OK scratch resistance
Jet Xpert (TIJ)	some irregularity and nozzle blocking	regular drop curtain	was not tested	couldn't be tested, would not print	nozzle blocking, doesn't fire (high viscosity)		regular drop curtain (0.5%), less stable at 1.0%
	little pooling seen (0.5%), slightly more (1.0%)	little pooling around nozzles (0.5%), more at 1.0%			pooling around nozzles, worst for LB (0.5%), even worse at 1.0%		slight pooling (0.5%), increased at 1.0%
Print Setting Optimisation (DOD)	same settings required for all inks at 0.5% and 1.0%						
Printing on Substrates (DOD)	good prints for all at 0.5% and 1.0% on PP, LDPE, HDPE and glass using optimised settings						

8.7 Conclusions

Larger scale syntheses of the amphiphilic poly(butyl methacrylate-acrylic acid) copolymers were carried out to enable testing of the materials for their intended application in inkjet printing. These were successful, with molecular weights close to the target value of 20000 g mol^{-1} . These copolymers were incorporated into ethanol-based ink formulations at compositions of 0.5% and 1.0% by mass, and inks containing the standard Dianal MB2594 polymer were prepared for comparison. The results of the ink testing are summarised in **Section 8.6**. Density and viscosity were measured to allow comparison of the fluid properties of the inks. Statistical analysis showed significant differences between the viscosities of different inks, with increased viscosity observed at the higher concentration of polymer. The smallest increase in viscosity was seen for Dianal MB2594 whilst the linear copolymers caused the largest increase. Interestingly, HBR produced a relatively small increase in viscosity compared to the other copolymers.

The jetting of the inks was then tested on both a TIJ and a DOD printing system. The decap time of filled cartridges was investigated on the TIJ printer; the HBR-containing ink was found to behave best at 0.5% w/w whilst all gave the same results at 1.0%. A Jet Xpert system was used to visualise both the drop curtain and the nozzle plate during printing. Poor performance was observed for the LB and LR inks, and the HBM ink which ceased firing altogether. Better jetting was seen for the other inks containing branched polymers. The inks were printed onto polyolefin substrates and the standard industry adhesion tests were performed. The inks containing branched polymers gave better results in the tape test but displayed poor scratch resistance, whilst the opposite case was observed for the linear copolymers. The Dianal MB2594 gave the worst results in the tape test, although scratch resistance was adequate.

The DOD printer allowed the variation of print settings involving firing voltage, print height and cartridge temperature. Setting optimisation was performed and found to be the same for all inks at both 0.5% and 1.0% w/w. Printing was carried out onto polyolefin and glass substrates, and good performance was achieved for all inks at both concentrations.

Finally, solutions of HBR in the solvent base were used to investigate the effect of copolymer concentration, and solutions of HBA in the solvent base with added HD

were used to investigate the effect of tailoring the solution viscosity. Viscometric testing revealed a linear increase in viscosity as the polymer concentration increased, whilst adding HD was found to have a large effect on viscosity, with a 95% increase in viscosity observed when HD content was increased from 25% to 50% by mass. The solutions were printed onto both HDPE and glass using a DOD printer. The more viscous solutions were found to give the best prints. Adhesion testing was carried out and all solutions were found to be scratch resistant with no visible material removed by the tape test either.

9. Conclusions and Future Work

9.1 Conclusions

This project was concerned with the design and synthesis of amphiphilic copolymers for use as adhesion-promoting additives for printing ink. Adhesion would be improved through interaction between the hydrophobic segment and the polyolefin substrate, and between the hydrophilic segment and the dye or pigment particles, to form an adhesive bridge between dye and substrate. Poly(acrylic acid) was selected to form the hydrophilic segments, and poly(alkyl methacrylate) was chosen to form the hydrophobic segments. Methyl, butyl, and lauryl methacrylates were employed thereby allowing variation of the hydrophobicity of this block. These materials were prepared having equivalent monomer composition but in a range of architectures: graft, branched, and linear. Both block and random monomer distributions were also incorporated. These variations allowed investigation of the effect of copolymer structure on their material properties, and additionally their performance in printing applications.

The first approach involved the synthesis of graft copolymers using a grafting-from route where alkyl methacrylate was copolymerised with VBC to produce linear hydrophobic backbones with methylene chloride branch points. These branch points were then functionalised with pyrrole-1-carbodithioic acid through substitution of the chlorine atoms with dithioester groups, creating in-situ RAFT agents from which poly(acrylic acid) grafts could be grown. Initially, degrees of functionalisation were poor, due to the insolubility of the base in the reaction solvent. This problem was solved by employing a heterogeneous reaction system with the use of phase transfer catalysis to promote transport of the reagents across the interface. This improved the functionalisation step and allowed graft copolymers to be synthesised. Methyl, butyl and lauryl methacrylate analogues were produced, with graft copolymer found to be the major fraction in each case despite the presence of PAA homopolymer. Grafting proved less efficient for the P(LMA-*co*-VBC-*g*-AA) copolymer. This was found to be due to the steric effect of the long alkyl chain, since an alternative synthetic route with *t*-butyl acrylate also proved unsuccessful. Synthesis of a hexyl methacrylate analogue showed evidence of reduced grafting efficiency, suggesting the beginning of a steric effect at alkyl chain lengths of six carbon atoms or more.

Poly(acrylic acid-alkyl methacrylate) copolymers were then produced in branched architectures using a RAFT agent that possesses both dithioester and vinyl functional groups, allowing two sites for polymerisation. A one-pot reaction led to the formation of random copolymers, whilst sequential monomer addition produced first a macro-chain transfer agent followed by chain extension to add the second block. Linear copolymers were also produced in block and random monomer sequence distributions using a variation on the same synthetic route using a different RAFT agent. This has the same structure as the branching RAFT agent but without the vinyl functional group, thereby eliminating the branching step. Molar masses of 20000 g mol^{-1} were targeted to fit the constraints of ink formulations, with PAA:PnMA molar ratios of 1:1. Broad molecular weight distributions were observed by GPC, particularly for the branched copolymers, but overall the majority of the molecular weight distribution fell within the desired range. The majority of PAA:PnMA ratios were close to the target values, although some variation was again present. ^{13}C NMR was used to confirm the monomer sequence distribution through examination of the distribution of peaks in the carbonyl region. GPC with viscometric detection was used to determine the Mark-Houwink parameters of each copolymer, which give a measure of polymer branching. Values of α were below 0.5 for the branched materials and greater than 0.6 for the linear copolymers, as expected. The graft copolymers exhibited α values between those of these groups. This is in accordance with the structure of a graft copolymer which is intermediate between linear and branched.

These amphiphilic copolymers were dispersed into water from THF using the solvent switch method. TEM, PALS and SANS were all used to characterise the dispersions. As water is a block-selective solvent for PAA, the copolymers were found to self-assemble into macromolecular structures. The size and morphology of these structures varied according to architecture, monomer sequence distribution and also the hydrophobicity of the methacrylate block. It was found that segmented structures are not necessary for self-assembly, as the random copolymers formed smooth spheres, which were larger than those formed from the segmented copolymers. SANS was used to study the solution behaviour of the copolymers in a range of solvent systems. In d-THF, a good solvent for both blocks, all copolymers were found to adopt a Gaussian coil conformation. The addition of D_2O to form a 1:1 d-THF: D_2O mixture led to the beginning of the formation of self-assembled structures. The majority of copolymers

formed fractal aggregates as the solvency conditions became poorer for the methacrylate blocks. When dispersed into D₂O, all copolymers self-assembled into macromolecular structures. For most copolymers the scattering fitted best to the sphere model, whilst multi-lamellar micelles were observed for several copolymers, primarily those with segmented structures. A reversal of solvency conditions was created by using a 1:1 mixture of d-THF and CDCl₃, a selective solvent for the methacrylate block. Most of the copolymers remained as Gaussian coils, although fractal aggregates were observed for some of the segmented copolymers. The butyl methacrylate copolymers were also studied in d-EtOH to replicate the printing solvent. The random copolymers formed Gaussian coils, in contrast to the segmented copolymers which all formed fractal aggregates suggesting they may be more prone to nozzle clogging.

The branched block copolymers with PnMA core and PAA outer were chosen for further study due to their interesting self-assembly behaviour. The BMA analogue formed particularly unusual onion micelles. These were shown by SEM to be spherical in nature, with TEM allowing visualisation of the internal lamellar structure. These were found to exhibit a temperature response, with the lamellar structure removed by heating; the MMA and LMA analogues on the other hand did not respond to temperature. The encapsulation and release behaviour of all three copolymers was investigated using Rhodamine B as a model compound whose release could be monitored by UV-vis spectroscopy. Substantially more Rhodamine B was released from the HB P(BMA-*b*-AA) copolymer. Several experiments were carried out to aid in determining the formation mechanism of the onion micelles. The formation is proposed to occur due to the packing and coalescence of small unimolecular micellar spheres, driven by the need to minimise interfacial energy. This is enabled by the slow evaporation of the good solvent, THF, from the THF:H₂O good:poor solvent system allowing time for the structural rearrangement followed by kinetic trapping of a non-equilibrium structure.

The copolymers were then studied as coatings on polyolefin substrates using the sessile drop method to measure contact angles. This allowed subsequent calculation of surface energies for each copolymer, in the form of overall surface energy and also the surface energies due to polar and dispersive parts of the materials. When compared to the bare substrates and the standard Dianal MB2594 polymer, the amphiphilic copolymers were found to provide higher overall surface energies. Interestingly, the

branched and linear random copolymers provided a much larger polar component on the surface of the coated substrate compared to the copolymers with segmented structures. This suggests that these materials could provide greater adhesion to ink as the polar groups would be present on the surface for the dye or pigment to adsorb to. Inks containing the copolymers were also used as probe solvents to measure contact angles on uncoated PP substrates. Statistically significant differences were seen between inks depending on the copolymer in the formulation, although the overall variation in contact angle was small. AFM force spectroscopy was tested as a method for measuring changes in the adhesion behaviour of different copolymers. It was found to detect structural changes in graft P(LMA-co-VBC-g-AA) copolymers during the functionalisation and grafting process. A method for converting the dithioester end groups originating from the RAFT process into thiols was developed to allow use of single molecule force spectroscopy by adhering thiol-ended polymers to gold-coated cantilevers.

Finally, the butyl methacrylate copolymers were tested in printing applications. Larger scale syntheses of the materials were carried out successfully. The materials, in addition to Dianal MB2594 as a standard, were incorporated into ethanol-based ink formulations at both 0.5 and 1.0% by mass. Jetting of the inks was tested on both a TIJ printer, (including study of decap time, Jet Xpert imaging and adhesion testing), and a DOD printer (with print setting optimisation being carried out). Subsequently, solutions of HBR in the solvent base were used to investigate the effect of copolymer concentration, and solutions of HBA in the solvent base with added HD were used to investigate the effect of tailoring the solution viscosity. Poor jetting performance was observed for the LB and LR inks, and the HBM ink which ceased firing altogether. The other inks containing branched polymers jetted much better. In terms of adhesion testing, the inks containing branched polymers gave better results in the tape test but displayed poor scratch resistance, whilst the opposite case was observed for the linear copolymers. The Dianal MB2594 gave the worst results in the tape test, although scratch resistance was adequate. For the polymer-only solutions, more viscous solutions were found to give the best prints, although all solutions were found to be both scratch and tape test resistant.

Overall, when the complete results of the project are considered, the branched random copolymer would appear to be the best candidate for an adhesion-promoting

additive for use in printing ink for several reasons. The synthetic route for these copolymers is simpler than for the block and graft materials, as the random materials can be produced in a one-pot reaction. The molar masses for these copolymers are also closer to the desired range to suit printing applications compared to the other materials, indicating better control over the polymerisation. SANS showed that the random copolymers remained dissolved in d-EtOH while the segmented copolymers formed fractal aggregates. This indicates that problems with nozzle clogging are less likely for inks containing random copolymers. The contact angle results suggest that the random materials also provide more polar groups on the surface when coated onto a polyolefin substrate, suggesting better adhesion to dye or pigments deposited from an ink. Finally, the inks containing branched copolymers were found to jet better than those containing linear copolymers. For this reason, the branched random copolymer would be recommended over the linear analogue.

9.2 Future Work

There are several aspects where ongoing research into these amphiphilic poly(alkyl methacrylate-co-acrylic acid) copolymers would be beneficial.

The use of statistical modelling of triads in NMR spectra could be used to expand and develop the empirical method of identifying block or random monomer sequence distribution into a qualitative method of determining both the monomer sequence distribution and the tacticity of block copolymers. Additionally, calculation of the reactivity ratios would indicate whether the copolymers tend towards block or random distributions; it would be interesting to observe the differences between the methyl, butyl and lauryl methacrylate monomers and investigate whether the reactivity ratios are affected by the copolymer architecture.

More investigation using GPC with viscometric detection is required to confirm whether the unusual results obtained for the comparison of contraction factor with molecular weight are accurate. The data could be improved if it were possible to obtain alternative linear analogues for the branched and graft materials with identical molecular weight distributions, although clearly this is not trivial. If triple detection GPC were available with the additional capability for light scattering, more information about the branching of the copolymers could be obtained, for example using branching

models to calculate the branching number of each copolymer. Additionally, measurement of the dn/dc increment would aid in improving calculations, as dn/dc is known to vary across the molecular weight distribution for copolymers.

The full power of SANS could be employed to gain more information about the behaviour of the copolymers in solution through the use of contrast matching. If one block was selectively deuterated and the other remained hydrogenated, the individual behaviour of the blocks could be studied. This may be particularly useful in the case of the onion micelles. Furthermore, neutron reflectivity could be used to investigate the structure of the copolymers when applied as a thin film on a substrate.

There is much potential for continuation and expansion of the onion micelle self-assembly work. Further study is needed to fully explain how and why the onion micelles are driven to form. This fundamental understanding would aid the application of the technology. Following the use of Rhodamine B in proof-of-concept studies, the release of other compounds can be investigated. In the printing field, there is a possibility of encapsulating fragrance or dye within the micelle which could then be printed onto a substrate and the substance released on heating of the substrate. In order for this to be feasible, the behaviour of the micelles as a coating would need to be investigated. Additionally, the thermal behaviour of the onions would need to be studied. A simple test of this would be thermogravimetric analysis (TGA).

The system could be applied to the encapsulation and release of other active compounds such as drugs or other biomedical substances. It would be advantageous to incorporate a pH response into the system in addition to temperature response. Another thing to consider if the system proved to have commercial potential would be to investigate whether a polymerisation-induced self-assembly (PISA) approach would be possible to enable a one-pot synthesis of onion micelles from the starting macro-CTA. This would reduce the need for time-consuming post-polymerisation processing steps.

AFM experiments could be instrumental in explaining the adhesion results of the copolymers to polyolefin substrates at a molecular level. An AFM cantilever can be coated with a layer of gold to allow the adhesion of a single molecule of thiol-ended copolymer. The adhesion of this single molecule to a range of substrates can then be measured. It is hoped this will prove a reproducible test of copolymer adhesion to substrates, although AFM is an expensive technique which requires in-depth training for

the user and is therefore unlikely to become a routine industrial analysis technique. Nonetheless it should allow screening of potential adhesion-promoting additives before the formulation stage.

10. Experimental

10.1 Materials

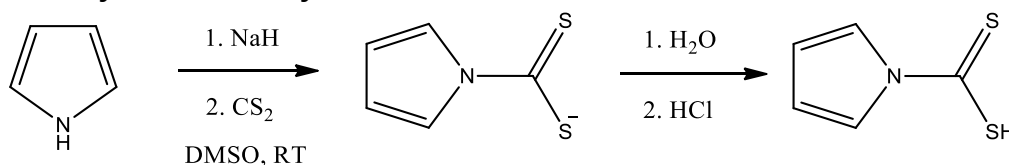
Sodium hydride (60% in mineral oil dispersion, Aldrich), carbon disulphide (99+%, Aldrich), 4-vinylbenzyl chloride (90%, Aldrich), benzyl bromide (98%, Aldrich), 4,4'-azobis (4-cyanovaleric acid) (ACVA, $\geq 98\%$, Aldrich), methanol (Fisher), acetone (Fisher), diethyl ether (Fisher), hexane (Fisher), chloroform (Fisher), 1,4-dioxane (Aldrich, sure-seal, anhydrous 99.8%), dimethyl sulfoxide (DMSO, Aldrich, sure-seal anhydrous 99.9%), dichloromethane (Fisher), petroleum ether 40-60 (Fisher), caesium carbonate (99%, Aldrich), potassium iodide (99%, Aldrich), hexadecyl trimethyl ammonium bromide (HTAB, 99%, Aldrich), hexadecyl trimethyl ammonium chloride (HTAC, 98%, Fluka), tetrabutyl ammonium bromide (TBAB, 99%, Aldrich), tetrabutyl ammonium chloride (TBAC, 99%, Fluka), Amberlyst IRA-400-supported borohydride (Aldrich), Amberlite A26-supported borohydride (Aldrich), trimethylsilyl diazomethane (2.0 M in hexanes, Aldrich) and Rhodamine B (fluorescence grade, Aldrich) were used as purchased.

Pyrrole (99%, Aldrich) was distilled over calcium hydride (95%, Aldrich) under reduced pressure to give a colourless liquid. Acrylic acid (99%, Aldrich) was distilled under reduced pressure to remove inhibitors. AIBN (97%, BDH Laboratory Supplies) was recrystallized from methanol. Deionised water was obtained from a Millipore (Milli-Q) purification system at a resistivity of $18.2 \Omega \cdot \text{cm}^{-1}$.

Toluene and dimethyl formamide (DMF) were obtained from the Grubb's dry solvent system.

MEHQ inhibitors were removed from methyl methacrylate (99%, Aldrich), n-butyl methacrylate (99%, Aldrich), hexyl methacrylate (97%, VWR), lauryl methacrylate (96%, Lancaster), and t-butyl acrylate (98%, Aldrich) by running through a column packed with inhibitor remover (Aldrich).

10.2 Synthesis of Pyrrole-1-carbodithioic Acid



Pyrrole (2.00 g) was added dropwise over 20 minutes to a rapidly stirring suspension of sodium hydride (0.720 g, 29.8 mmol) in DMSO (40 ml). The solution was stirred at

room temperature for 30 minutes then cooled to 0°C using an ice bath. Carbon disulphide (2.27 g, 29.8 mmol) was added dropwise over 20 minutes to create an orange-brown solution. This was stirred at room temperature for 30 minutes and then cooled to 0 °C. 1 mol dm⁻³ HCl was added dropwise to pH 2 to form a yellow precipitate. The suspension was filtered and the solids washed with deionised water (3x 25 ml). The product was finally dried in vacuo at room temperature for 24 hours to give 3.84 g (90 %) of a dark orange solid.

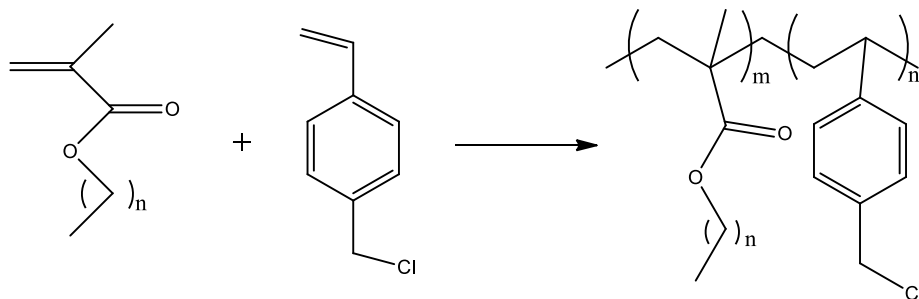
¹H NMR (CDCl₃, 400 MHz) δ/ppm: 6.46 (t, 2H, N(CH)₂-(CH)₂), 7.78 (t, 2H, N(=CH)₂).

¹³C NMR (CDCl₃, 100 MHz) δ/ppm: 115.46 (2C, N(CH)₂-(CH)₂), 121.96 (2C, N(=CH)₂), 191.85 (1C, -C(=S)SH)

Calculated for C₅H₅NS₂: C, 41.93; H, 3.52; N, 9.78; S, 44.77. Found: C, 44.76; H, 3.90; N, 8.72; S, 40.02.

EI MS m/z: 143 (calculated 143)

10.3 Free Radical Copolymerisation of Alkyl Methacrylate and 4-Vinylbenzyl Chloride to form P(nMA-co-VBC) Copolymer Backbone



Alkyl methacrylate monomer (methyl, butyl or lauryl), 4-vinylbenzyl chloride, ACVA and toluene were mixed together in the desired ratio and the resulting solution was freeze-pump-thawed on a vacuum line (10⁻³ mbar, three cycles) then flame-sealed and heated in a thermostated water bath at 60 °C for up to 36 h to undergo polymerisation. Products were precipitated into rapidly stirring ice cold methanol. The methanol was removed by decanting and the polymer was dried in vacuo at room temperature for 24 hours. The procedure was repeated once more to remove any traces of residual monomer, giving polymer products as clear adhesive solids.

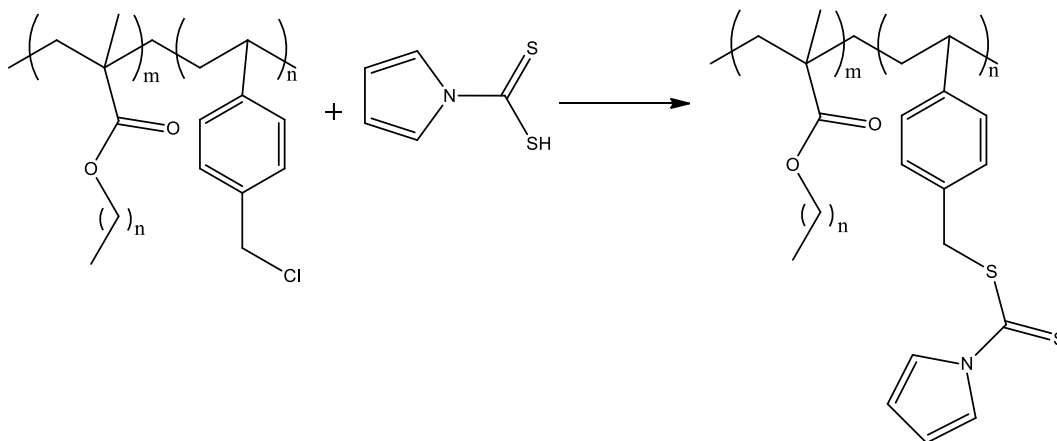
P(MMA-co-VBC): $^1\text{H NMR}$ (CDCl_3 , 400 MHz) δ/ppm : 0.95 (d, $J = 69.43$ Hz, 3H, $-\text{CH}_3$), 1.90 (br, 2H, $-\text{CH}_2\text{C}(\text{CH}_3)(\text{C}=\text{O})\text{OCH}_3$), 3.62 (br, 2H, $\text{C}(\text{O})\text{OCH}_3$), 4.55 (br, 1H, CHAr), 7.02 (br, 2H, Ar), 7.21 (br, 2H, Ar)

P(BMA-co-VBC): $^1\text{H NMR}$ (CDCl_3 , 400 MHz) δ/ppm : 0.89 (s, 3H, $-\text{CH}_3$), 1.00 (br, 3H, $-(\text{CH}_2)_3\text{CH}_3$), 1.42 (br, 2H, $-(\text{CH}_2)\text{CH}_3$), 1.62 (br, 2H, $-(\text{CH}_2\text{CH}_2\text{CH}_3)$), 1.92 (br, 2H, $-\text{CH}_2\text{C}(\text{CH}_3)(\text{C}=\text{O})\text{O}(\text{CH}_2)_3\text{CH}_3$), 3.96 (br, 2H, $\text{C}(\text{O})\text{OCH}_2$), 4.55 (br, 1H, CHAr), 7.02 (br, 2H, Ar), 7.21 (br, 2H, Ar)

P(HMA-co-VBC): $^1\text{H NMR}$ (CDCl_3 , 400 MHz) δ/ppm : 0.89 (br, 3H, $-\text{CH}_3$), 1.00 (br, 3H, $-(\text{CH}_2)_5\text{CH}_3$), 1.42 (br, 6H, $-(\text{CH}_2)_3\text{CH}_3$), 1.62 (br, 2H, $-(\text{CH}_2(\text{CH}_2)_3\text{CH}_3)$), 1.92 (br, 2H, $-\text{CH}_2\text{C}(\text{CH}_3)(\text{C}=\text{O})\text{O}(\text{CH}_2)_5\text{CH}_3$), 3.94 (br, 2H, $\text{C}(\text{O})\text{OCH}_2$), 4.55 (br, 1H, CHAr), 7.02 (br, 2H, Ar), 7.21 (br, 2H, Ar)

P(LMA-co-VBC): $^1\text{H NMR}$ (CDCl_3 , 400 MHz) δ/ppm : 0.91 (br, 3H, $-(\text{CH}_2)_3\text{CH}_3$), 1.02 (br, 3H, $-\text{CH}_3$), 1.39 (br, 2H, $-(\text{CH}_2)_9\text{CH}_3$), 1.61 (br, 2H, $-(\text{CH}_2(\text{CH}_2)_9\text{CH}_3)$), 1.89 (br, 2H, $-\text{CH}_2\text{C}(\text{CH}_3)(\text{C}=\text{O})\text{O}(\text{CH}_2)_3\text{CH}_3$), 3.93 (br, 2H, $\text{C}(\text{O})\text{OCH}_2$), 4.55 (br, 1H, CHAr), 7.02 (br, 2H, Ar), 7.21 (br, 2H, Ar)

10.4 Functionalisation of P(LMA-co-VBC) Linear Copolymers with Pyrrole-1-Carbodithioic Acid

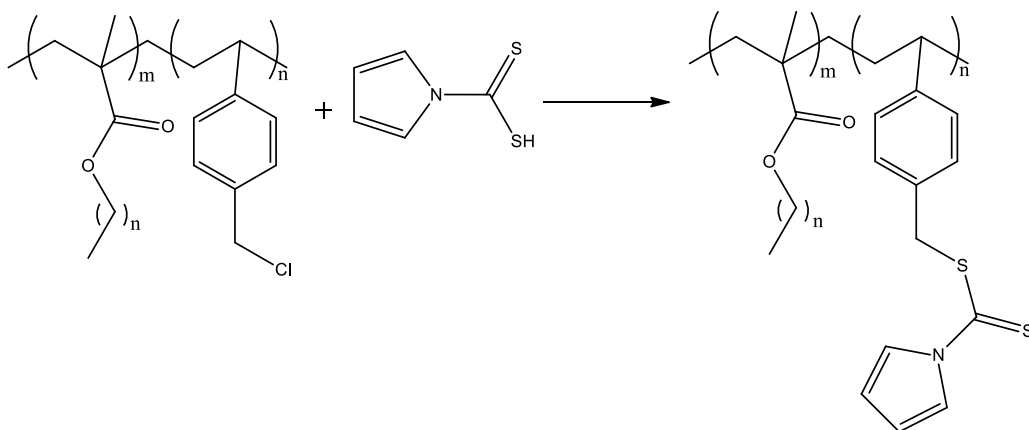


Linear P(LMA-co-VBC) copolymers (500 mg) were dissolved in the required solvent (50 ml). Potassium iodide (0.0780 g, 0.468 mmol) was added, followed by caesium carbonate (0.903 g, 4.68 mmol) and the suspension stirred under a nitrogen atmosphere at room temperature. Pyrrole-1-carbodithioic acid (0.0800 g, 0.562 mmol) was finally added and stirring continued for an appropriate length of time, resulting in a dark brown solution. The mixture was then centrifuged (3000 rpm, 5 minutes) and decanted from

the Cs_2CO_3 residue. The solvent was removed and the reaction mixture washed with acetone (2x 10 ml) and methanol (2x 10 ml) to give the linear polymer as a brown adhesive solid.

P(LMA-co-VBC): ^1H NMR (CDCl_3 , 400 MHz) δ/ppm : : 0.91 (br, 3H, $-(\text{CH}_2)_3\text{CH}_3$), 1.02 (br, 3H, $-\text{CH}_3$), 1.39 (br, 2H, $-(\text{CH}_2)_9\text{CH}_3$), 1.61 (br, 2H, $-(\text{CH}_2(\text{CH}_2)_9\text{CH}_3)$), 1.89 (br, 2H, $-\text{CH}_2\text{C}(\text{CH}_3)(\text{C}(\text{=O})\text{O}(\text{CH}_2)_3\text{CH}_3-$), 3.93 (br, 2H, $\text{C}(\text{=O})\text{OCH}_2-$), 4.55 (br, 1H, CHAr), 6.46 (br, 2H, $\text{N}(\text{CH})_2-(\text{CH})_2$), 7.02 (br, 2H, Ar), 7.21 (br, 2H, Ar), 7.72 (br, 2H, $\text{N}(\text{=CH})_2$)

10.5 Functionalisation of P(nMA-co-VBC) Linear Copolymers with Pyrrole-1-Carbodithioic Acid using Phase Transfer Catalysis



The appropriate phase transfer catalyst (5 mg) was added directly into a three-necked round bottom flask which was then flushed with nitrogen. Linear P(nMA-co-VBC) (500 mg) and pyrrole-1-carbodithioic acid (0.0800 g, 0.562 mmol) were dissolved in toluene (50 ml). This solution was then flushed with nitrogen and injected into the reaction vessel. Potassium iodide (0.0780 g, 0.468 mmol) and caesium carbonate (0.903 g, 4.68 mmol) were dissolved in deionised water (30 ml) and injected following flushing with nitrogen. The resulting mixture was stirred under a nitrogen atmosphere at room temperature for the required length of time. The mixture was then separated into the organic and aqueous layers and the organic layer was retained. The solvent was removed and the reaction mixture washed with acetone (2x 10ml) and methanol (2x 10ml). This was then re-dissolved in a minimum amount of DCM and re-precipitated into rapidly stirring ice cold methanol to give the linear polymer as a brown adhesive solid.

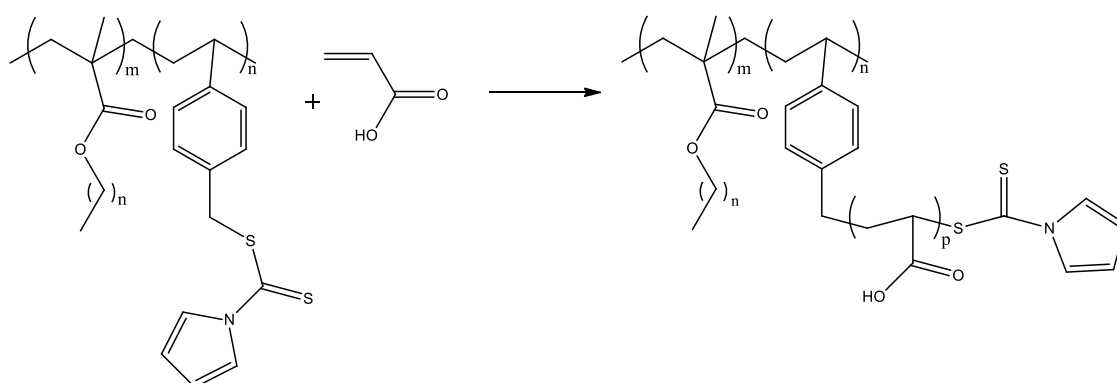
P(MMA-co-VBC): ^1H NMR (CDCl_3 , 400 MHz) δ/ppm : 0.95 (d, $J=69.43$ Hz, 3H, $-\text{CH}_3$), 1.90 (br, 2H, $-\text{CH}_2\text{C}(\text{CH}_3)(\text{C}=\text{O})\text{OCH}_3$), 3.62 (br, 2H, $\text{C}(\text{O})\text{OCH}_3$), 4.55 (br, 1H, CHAr), 6.46 (br, 2H, $\text{N}(\text{CH})_2-(\text{CH})_2$), 7.02 (br, 2H, Ar), 7.21 (br, 2H, Ar), 7.72 (br, 2H, $\text{N}(\text{=CH})_2$)

P(BMA-co-VBC): ^1H NMR (CDCl_3 , 400 MHz) δ/ppm : 0.89 (s, 3H, $-\text{CH}_3$), 1.00 (br, 3H, $-(\text{CH}_2)_3\text{CH}_3$), 1.42 (br, 2H, $-(\text{CH}_2)\text{CH}_3$), 1.62 (br, 2H, $-(\text{CH}_2\text{CH}_2\text{CH}_3)$), 1.92 (br, 2H, $-\text{CH}_2\text{C}(\text{CH}_3)(\text{C}=\text{O})\text{O}(\text{CH}_2)_3\text{CH}_3-$), 3.96 (br, 2H, $\text{C}(\text{O})\text{OCH}_2-$), 4.55 (br, 1H, CHAr), 6.46 (br, 2H, $\text{N}(\text{CH})_2-(\text{CH})_2$), 7.02 (br, 2H, Ar), 7.21 (br, 2H, Ar), 7.72 (br, 2H, $\text{N}(\text{=CH})_2$)

P(HMA-co-VBC): ^1H NMR (CDCl_3 , 400 MHz) δ/ppm : : 0.89 (br, 3H, $-\text{CH}_3$), 1.00 (br, 3H, $-(\text{CH}_2)_5\text{CH}_3$), 1.42 (br, 6H, $-(\text{CH}_2)_3\text{CH}_3$), 1.62 (br, 2H, $-(\text{CH}_2(\text{CH}_2)_3\text{CH}_3)$), 1.92 (br, 2H, $-\text{CH}_2\text{C}(\text{CH}_3)(\text{C}=\text{O})\text{O}(\text{CH}_2)_5\text{CH}_3$), 3.94 (br, 2H, $\text{C}(\text{O})\text{OCH}_2-$), 4.55 (br, 1H, CHAr), 6.34 (m, 2H, Ar), 7.02 (br, 2H, Ar), 7.21 (br, 2H, Ar), 7.73 (br, 2H, Ar)

P(LMA-co-VBC): ^1H NMR (CDCl_3 , 400 MHz) δ/ppm : : 0.91 (br, 3H, $-(\text{CH}_2)_3\text{CH}_3$), 1.02 (br, 3H, $-\text{CH}_3$), 1.39 (br, 2H, $-(\text{CH}_2)_9\text{CH}_3$), 1.61 (br, 2H, $-(\text{CH}_2(\text{CH}_2)_9\text{CH}_3)$), 1.89 (br, 2H, $-\text{CH}_2\text{C}(\text{CH}_3)(\text{C}=\text{O})\text{O}(\text{CH}_2)_3\text{CH}_3-$), 3.93 (br, 2H, $\text{C}(\text{O})\text{OCH}_2-$), 4.55 (br, 1H, CHAr), 6.46 (br, 2H, $\text{N}(\text{CH})_2-(\text{CH})_2$), 7.02 (br, 2H, Ar), 7.21 (br, 2H, Ar), 7.72 (br, 2H, $\text{N}(\text{=CH})_2$)

10.6 Grafting of Acrylic Acid onto P(nMA-co-VBC) Backbones via RAFT Polymerisation to form P(nMA-co-VBC-g-AA) Graft Copolymer



Functionalised P(nMA-co-VBC) backbone was dissolved in toluene then the desired amounts of ACVA or AIBN and acrylic acid were added. The resulting solution was freeze-pump-thawed on a vacuum line (10^{-3} mbar, three cycles) then flame-sealed and heated in a thermostated water bath at $60\text{ }^\circ\text{C}$ for up to 40 h to undergo polymerisation. The products were then precipitated into rapidly stirring ice-cold petroleum ether. The

non-solvent was removed by decanting and the polymer was dried in vacuo at room temperature for 24 h, giving polymer products as brown adhesive solids.

P(MMA-co-VBC-g-AA): ^1H NMR (1:1 CDCl_3 : $\text{DMSO}-d^6$, 400 MHz) δ /ppm: 0.94-0.66 (br, 3H, $-\text{CH}_3$), 1.32-0.95 (br, 2H, $-\text{CH}_2\text{C}(\text{CH}_3)(\text{C}(\text{=O})\text{OCH}_3)$), 1.86 (br, 2H, $-\text{CH}_2\text{CHCOOH}$), 3.52 (br, 2H, $\text{C}(\text{=O})\text{OCH}_3$), 4.57 (br, 2H, $-\text{CH}_2\text{Ar}$ -), 6.34 (br, 2H, Ar), 7.12 (d, Hz, 1H), 7.67 (br, 2H, Ar), 11.87 (s, 1H, $-\text{COOH}$)

^{13}C NMR (1:1 CDCl_3 : $\text{DMSO}-d^6$, 100 MHz) δ /ppm: 18.86 (1C, $-\text{CH}_3$), 44.40 (1C, $-\text{CHC}(\text{=O})\text{OH}$), 51.82 (1C, $-\text{C}(\text{=O})\text{OCH}_3$), 176.30 (1C, $-\text{C}(\text{=O})\text{OH}$), 177.46 (1C, $-\text{C}(\text{=O})\text{CH}_3$)

P(BMA-co-VBC-g-AA): ^1H NMR (1:1 CDCl_3 : $\text{DMSO}-d^6$, 400 MHz) δ /ppm: 0.89 (s, 3H, $-\text{CH}_3$), 1.00 (br, 3H, $-(\text{CH}_2)_3\text{CH}_3$), 1.42 (br, 2H, $-(\text{CH}_2)\text{CH}_3$), 1.62 (br, 2H, $-(\text{CH}_2\text{CH}_2\text{CH}_3)$), 1.92 (br, 4H, $-\text{CH}_2\text{C}(\text{CH}_3)(\text{C}(\text{=O})\text{O}(\text{CH}_2)_3\text{CH}_3$ - and $-\text{CH}_2\text{CHCOOH}$), 3.96 (br, 2H, $\text{C}(\text{=O})\text{OCH}_2$ -), 4.57 (br, 2H, $-\text{CH}_2\text{Ar}$ -), 6.34 (br, 2H, Ar), 7.12 (d, Hz, 1H), 7.67 (br, 2H, Ar), 11.96 (s, 1H, $-\text{COOH}$)

^{13}C NMR (1:1 CDCl_3 : $\text{DMSO}-d^6$, 100 MHz) δ /ppm: 13.82 (1C, $-(\text{CH}_2)_3\text{CH}_3$), 19.31 (1C, $-(\text{CH}_2)_2\text{CH}_2\text{CH}_3$), 30.20 (1C, $-\text{CH}_2\text{CH}_2\text{CH}_2\text{CH}_3$), 44.57 (1C, $-\text{CHC}(\text{=O})\text{OH}$), 64.54 (1C, $\text{CH}_2(\text{CH}_2)_2\text{CH}_3$), 176.30 (1C, $-\text{C}(\text{=O})\text{OH}$), 177.06 (1C, $-\text{C}(\text{=O})(\text{CH}_2)_3\text{CH}_3$)

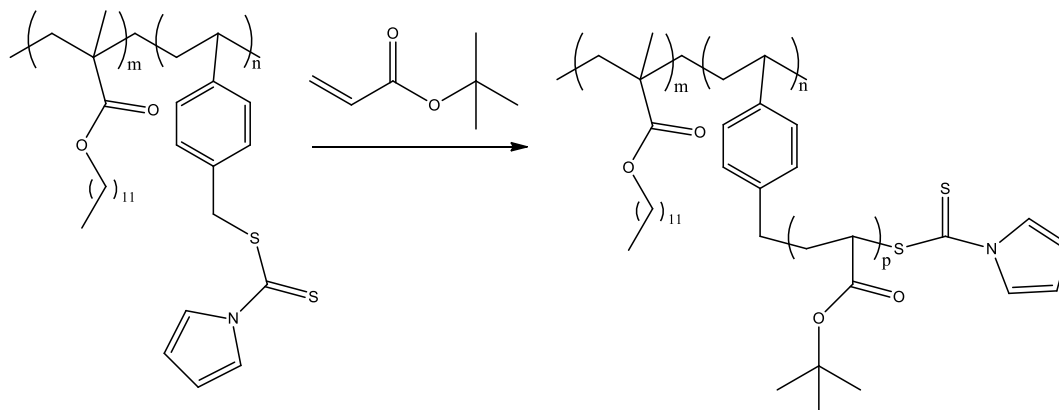
P(HMA-co-VBC-g-AA): ^1H NMR (1:1 CDCl_3 : $\text{DMSO}-d^6$, 400 MHz) δ /ppm: 0.89 (br, 3H, $-\text{CH}_3$), 1.00 (br, 3H, $-(\text{CH}_2)_5\text{CH}_3$), 1.42 (br, 6H, $-(\text{CH}_2)_3\text{CH}_3$), 1.62 (br, 2H, $-(\text{CH}_2(\text{CH}_2)_3\text{CH}_3)$), 1.92 (br, 2H, $-\text{CH}_2\text{C}(\text{CH}_3)(\text{C}(\text{=O})\text{O}(\text{CH}_2)_5\text{CH}_3$ and $-\text{CH}_2\text{CHCOOH}$), 3.94 (br, 2H, $\text{C}(\text{=O})\text{OCH}_2$ -), 4.55 (br, 1H, CHAr), 6.34 (m, 2H, Ar), 7.02 (br, 2H, Ar), 7.21 (br, 2H, Ar), 7.73 (br, 2H, Ar)

^{13}C NMR (1:1 CDCl_3 : $\text{DMSO}-d^6$, 100 MHz) δ /ppm: 14.10 (1C, $-(\text{CH}_2)_{11}\text{CH}_3$), 22.45 (1C, $-(\text{CH}_2)_{10}\text{CH}_2\text{CH}_3$), 25.70 (3C, $-(\text{CH}_2)_6(\text{CH}_2)_3(\text{CH}_2)_2\text{CH}_3$), 28.07 (5C, $-\text{CH}_2(\text{CH}_2)_5(\text{CH}_2)_5\text{CH}_3$), 31.34 (1C, $-\text{CH}_2\text{CH}_2\text{CH}_3$), 44.59 (1C, $-\text{CHC}(\text{=O})\text{OH}$), 64.81 (1C, $-\text{C}(\text{=O})\text{OCH}_2$ -), 176.30 (1C, $-\text{C}(\text{=O})\text{OH}$), 177.07 (1C, $-\text{C}(\text{=O})(\text{CH}_2)_3\text{CH}_3$)

P(LMA-co-VBC-g-AA) ^1H NMR (1:1 CDCl_3 : $\text{DMSO}-d^6$, 400 MHz) δ /ppm: : 0.91 (br, 3H, $-(\text{CH}_2)_3\text{CH}_3$), 1.02 (br, 3H, $-\text{CH}_3$), 1.39 (br, 2H, $-(\text{CH}_2)_9\text{CH}_3$), 1.61 (br, 2H, $-(\text{CH}_2(\text{CH}_2)_9\text{CH}_3)$), 1.89 (br, 2H, $-\text{CH}_2\text{C}(\text{CH}_3)(\text{C}(\text{=O})\text{O}(\text{CH}_2)_3\text{CH}_3$ -), 3.93 (br, 2H, $\text{C}(\text{=O})\text{OCH}_2$ -), 4.55 (br, 1H, CHAr), 6.46 (br, 2H, $\text{N}(\text{CH})_2-(\text{CH})_2$), 7.02 (br, 2H, Ar), 7.21 (br, 2H, Ar), 7.72 (br, 2H, $\text{N}(\text{=CH})_2$)

^{13}C NMR (1:1 CDCl_3 : $\text{DMSO}-d^6$, 100 MHz) δ /ppm: 13.79 (1C, $-\text{CH}_3$), 14.26 (1C, $-(\text{CH}_2)_{11}\text{CH}_3$), 22.63 (1C, $-(\text{CH}_2)_{10}\text{CH}_2\text{CH}_3$), 29.27 (3C, $-(\text{CH}_2)_6(\text{CH}_2)_3(\text{CH}_2)_2\text{CH}_3$), 29.62 (5C, $-\text{CH}_2(\text{CH}_2)_5(\text{CH}_2)_5\text{CH}_3$), 31.86 (1C, $-\text{CH}_2\text{CH}_2\text{CH}_3$)

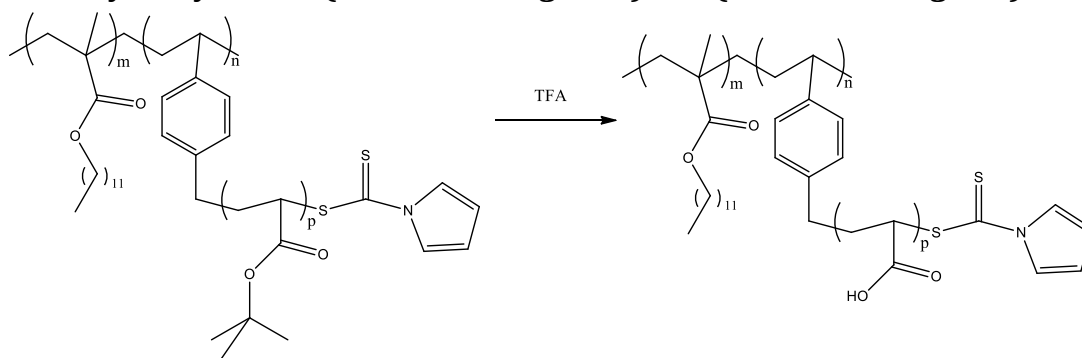
10.7 Grafting of t-Butyl Acrylate onto P(LMA-co-VBC) Backbones via RAFT Polymerisation to form P(LMA-co-VBC-g-tBA) Graft Copolymers



Functionalised P(LMA-co-VBC) backbone was dissolved in toluene then the desired amounts of ACVA or AIBN and t-butyl acrylate were added. The resulting solution was freeze-pump-thawed on a vacuum line (10^{-3} mbar, three cycles) then flame-sealed and heated in a thermostated water bath at $60\text{ }^\circ\text{C}$ for up to 40 h to undergo polymerisation. The products were then precipitated into rapidly stirring ice cold methanol. The non-solvent was removed by decanting and the polymer was dried in vacuo at room temperature for 24 h, giving polymer products as brown adhesive solids.

P(LMA-co-VBC-g-tBA) ^1H NMR (1:1 CDCl_3 : $\text{DMSO}-d^6$, 400 MHz) δ /ppm: : 0.91 (br, 3H, $-(\text{CH}_2)_3\text{CH}_3$), 1.02 (br, 3H, $-\text{CH}_3$), 1.39 (br, 2H, $-(\text{CH}_2)_9\text{CH}_3$), 1.61 (br, 2H, $-(\text{CH}_2(\text{CH}_2)_9\text{CH}_3)$), 1.89 (br, 2H, $-\text{CH}_2\text{C}(\text{CH}_3)(\text{C}=\text{O})\text{O}(\text{CH}_2)_3\text{CH}_3-$), 3.93 (br, 2H, $\text{C}(\text{O})\text{OCH}_2-$), 4.55 (br, 1H, CHAr), 6.46 (br, 2H, $\text{N}(\text{CH}_2)_2-(\text{CH})_2$), 7.02 (br, 2H, Ar), 7.21 (br, 2H, Ar), 7.72 (br, 2H, $\text{N}(\text{=CH})_2$)

10.8 Hydrolysis of P(LMA-co-VBC-g-tBA) to P(LMA-co-VBC-g-AA)

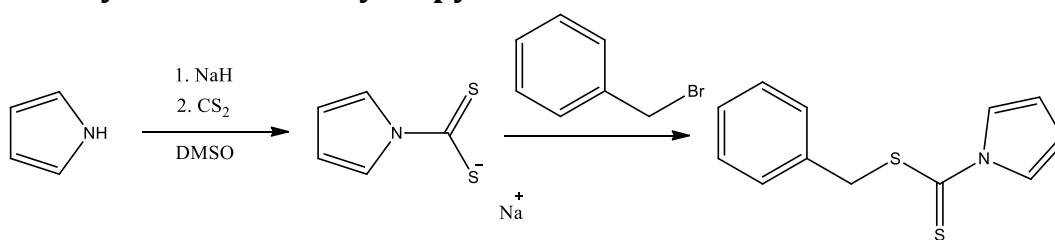


P(LMA-co-VBC-g-tBA) (0.500 g) was dissolved in DCM (40 ml) and 1.5 ml TFA added. The mixture was stirred for 48 hours at room temperature. The mixture was then washed with H₂O and the organic layer retained. The solvent was then removed to give the polymer product as a brown adhesive solid.

P(LMA-co-VBC-g-AA) ¹H NMR (1:1 CDCl₃:DMSO-*d*⁶, 400 MHz) δ/ppm: : 0.91 (br, 3H, -(CH₂)₃CH₃), 1.02 (br, 3H, -CH₃), 1.39 (br, 2H, -(CH₂)₉CH₃), 1.61 (br, 2H, -(CH₂(CH₂)₉CH₃), 1.89 (br, 2H, -CH₂C(CH₃)(C(=O)O(CH₂)₃CH₃-), 3.93 (br, 2H, C(=O)OCH₂-), 4.55 (br, 1H, CHAr), 6.46 (br, 2H, N(CH)₂-(CH)₂), 7.02 (br, 2H, Ar), 7.21 (br, 2H, Ar), 7.72 (br, 2H, N(=CH)₂)

¹³C NMR (1:1 CDCl₃:DMSO-*d*⁶, 100 MHz) δ/ppm: 13.79 (1C, -CH₃), 14.26 (1C, -(CH₂)₁₁CH₃), 22.63 (1C, -(CH₂)₁₀CH₂CH₃), 29.27 (3C, -(CH₂)₆(CH₂)₃(CH₂)₂CH₃), 29.62 (5C, -CH₂(CH₂)₅(CH₂)₅CH₃), 31.86 (1C, -CH₂CH₂CH₃)

10.9 Synthesis of Benzyl-1-pyrrolocarbodithioate



Pyrrole (5.00 g, 74.53 mmol) was added dropwise over 20 minutes to a rapidly stirring suspension of sodium hydride (1.790 g, 74.53 mmol) in DMSO (80 ml). The solution was stirred at room temperature for 30 minutes then cooled to 5 °C using an ice bath. Carbon disulphide (5.670 g, 74.53 mmol) was added dropwise over 20 minutes to form an orange-brown solution. This was stirred at room temperature for 30 minutes and then benzyl bromide (12.69 g, 74.53 mmol) was added dropwise and the solution was stirred overnight at room temperature. The mixture was extracted using distilled water (80 ml)

and diethyl ether (80 ml), and the aqueous layer washed with ether (160 ml) until all the organic product was extracted. The organic layer was dried over MgSO_4 , which was then removed by gravity filtration. The solvent was removed from the mixture by rotary evaporation giving the crude product as a black liquid. This was then purified by flash column chromatography on silica using hexane as the solvent. The yellow phase was collected and the solvent removed by rotary evaporation to give 5.780 g (33 %) of a yellow oil. The air sensitive product was stored under nitrogen at $-18\text{ }^\circ\text{C}$.

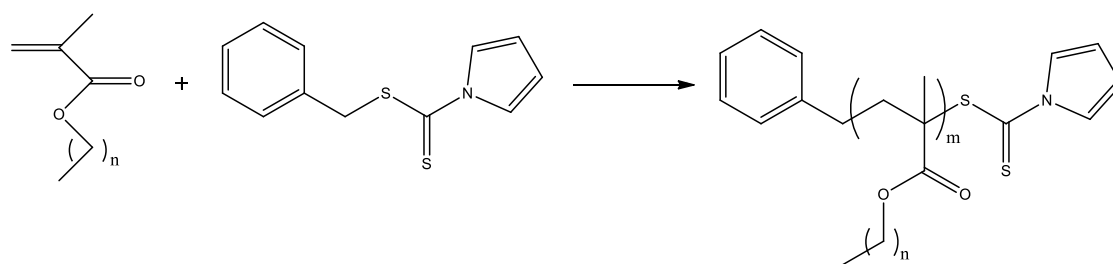
^1H NMR (CDCl_3 , 400 MHz) δ /ppm: 4.64 (s, 2H, $-\text{C}(=\text{S})-\text{S}-\text{CH}_2-$), 6.36 (s, 2H, Ar), 7.37 (m, 4H, Ar), 7.74 (s, 2H, Ar)

^{13}C NMR (CDCl_3 , 100 MHz,) δ /ppm: 41.76 (1C, $\text{CH}_2-\text{S}(\text{C}=\text{S})-$), 114.24 (2C, $\text{N}(\text{CH})_2-(\text{CH})_2$), 120.69 (2C, $\text{N}(\text{=CH})_2$), 127.99 (1C, Ar), 128.80 (2C, Ar), 129.43 (2C, Ar), 199.37 (1C, $-\text{C}(=\text{S})\text{S}-$)

Calculated for $\text{C}_{12}\text{H}_{11}\text{NS}_2$: C, 61.76; H, 4.75; N, 6.00; S, 27.48. Found: C, 61.42; H, 4.49; N, 5.72; S, 27.18.

EI MS m/z : 233 (calculated 233)

10.10 RAFT Polymerisation of Alkyl Methacrylates using Benzyl-1-pyrrolicarbodithioate to form Linear P(nMA) Macro-Chain Transfer Agent



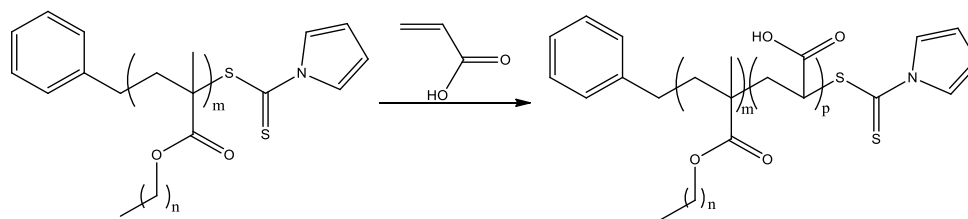
Each alkyl methacrylate monomer (methyl, butyl, or lauryl), benzyl-1-pyrrolicarbodithioate, ACVA and dioxane were mixed together in the desired ratio until the solid initiator had dissolved. The resulting solution was freeze-pump-thawed on a vacuum line (10^{-3} mbar, three cycles) then flame-sealed and heated in a thermostated water bath at $60\text{ }^\circ\text{C}$ for up to 24 h to undergo polymerisation. The products were then precipitated into rapidly stirring ice-cold methanol. The non-solvent was removed by decanting and the polymer was dried in vacuo at room temperature for 24 h, giving polymer products as yellow powdery or amorphous solids.

PMMA: $^1\text{H NMR}$ (CDCl_3 , 400 MHz) δ/ppm : 0.95 (d, $J=69.43$ Hz, 3H, $-\text{CH}_3$), 1.90 (br, 2H, $-\text{CH}_2\text{C}(\text{CH}_3)(\text{C}(\text{=O})\text{OCH}_3)$), 3.62 (br, 2H, $\text{C}(\text{=O})\text{OCH}_3$), 6.36 (m, 2H, Ar), 7.17-7.44 (br, 4H, Ar), 7.69 (br, 2H, Ar)

PBMA: $^1\text{H NMR}$ (CDCl_3 , 400 MHz) δ/ppm : : 0.89 (s, 3H, $-\text{CH}_3$), 1.00 (br, 3H, $-(\text{CH}_2)_3\text{CH}_3$), 1.42 (br, 2H, $-(\text{CH}_2)\text{CH}_3$), 1.62 (br, 2H, $-(\text{CH}_2\text{CH}_2\text{CH}_3)$), 1.92 (br, 2H, $-\text{CH}_2\text{C}(\text{CH}_3)(\text{C}(\text{=O})\text{O}(\text{CH}_2)_3\text{CH}_3-$), 3.96 (br, 2H, $\text{C}(\text{=O})\text{OCH}_2-$), 4.63 (br, 1H, CHAr), 6.34 (m, 2H, Ar), 7.30-7.45 (br, 4H, Ar), 7.72 (br, 2H, Ar)

PLMA: $^1\text{H NMR}$ (CDCl_3 , 400 MHz) δ/ppm : 0.91 (br, 3H, $-\text{CH}_3$), 1.00 (br, 3H, $-(\text{CH}_2)_{11}\text{CH}_3$), 1.42 (br, 18H, $-(\text{CH}_2)_9\text{CH}_3$), 1.62 (br, 2H, $-(\text{CH}_2(\text{CH}_2)_9\text{CH}_3)$), 1.92 (br, 2H, $-\text{CH}_2\text{C}(\text{CH}_3)(\text{C}(\text{=O})\text{O}(\text{CH}_2)_{11}\text{CH}_3)$), 3.94 (br, 2H, $\text{C}(\text{=O})\text{OCH}_2-$), 6.37 (m, 2H, Ar), 7.30-7.45 (br, 4H, Ar), 7.67 (br, 2H, Ar)

10.11 Synthesis of Linear P(nMA-*b*-AA) Block Copolymers via RAFT Polymerisation of P(nMA) Macro-Chain Transfer Agent and Acrylic Acid



Linear P(nMA) macro-CTA (methyl, butyl or lauryl) was dissolved in dioxane then the desired amounts of ACVA and acrylic acid were added. The resulting solution was freeze-pump-thawed on a vacuum line (10^{-3} mbar, three cycles) then flame-sealed and heated in a thermostated water bath at $60\text{ }^\circ\text{C}$ for up to 40 h to undergo polymerization. The products were then precipitated into rapidly stirring ice-cold petroleum ether. The non-solvent was removed by decanting and the polymer was dried in vacuo at room temperature for 24 h, giving polymer products as pale yellow powdery solids.

P(MMA-*b*-AA): $^1\text{H NMR}$ (1:1 CDCl_3 : $\text{DMSO}-d_6$, 400 MHz) δ/ppm : 0.94-0.66 (br, 3H, $-\text{CH}_3$), 1.32-0.95 (br, 2H, $-\text{CH}_2\text{C}(\text{CH}_3)(\text{C}(\text{=O})\text{OCH}_3)$), 1.86 (br, 2H, $-\text{CH}_2\text{CHCOOH}$), 3.52 (br, 2H, $\text{C}(\text{=O})\text{OCH}_3$), 4.57 (br, 2H, $-\text{CH}_2\text{Ar}-$), 6.34 (br, 2H, Ar), 7.30-7.45 (br, 4H, Ar), 7.67 (br, 2H, Ar), 11.87 (s, 1H, $-\text{COOH}$)

^{13}C NMR (1:1 CDCl_3 : $\text{DMSO}-d^6$, 100 MHz) δ /ppm: 18.82 (1C, $-\text{CH}_3$), 44.42 (1C, $-\text{CHC}(=\text{O})\text{OH}$), 51.77 (1C, $-\text{C}(=\text{O})\text{OCH}_3$), 176.55 (1C, $-\text{C}(=\text{O})\text{OH}$), 177.50 (1C, $-\text{C}(=\text{O})\text{OCH}_3$)

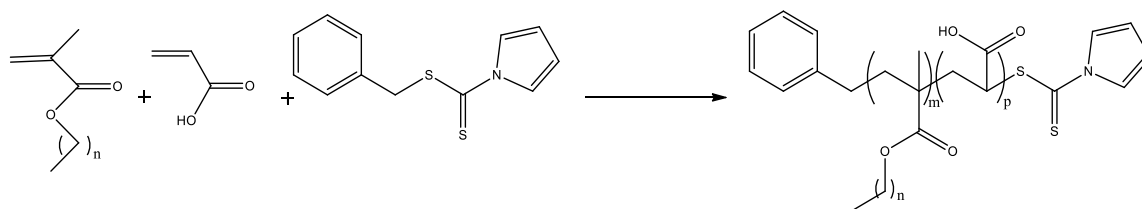
P(BMA-*b*-AA): ^1H NMR (1:1 CDCl_3 : $\text{DMSO}-d^6$, 400 MHz) δ /ppm: 0.89 (s, 3H, $-\text{CH}_3$), 1.00 (br, 3H, $-(\text{CH}_2)_3\text{CH}_3$), 1.42 (br, 2H, $-(\text{CH}_2)\text{CH}_3$), 1.62 (br, 2H, $-(\text{CH}_2\text{CH}_2\text{CH}_3)$), 1.92 (br, 4H, $-\text{CH}_2\text{C}(\text{CH}_3)(\text{C}(=\text{O})\text{O}(\text{CH}_2)_3\text{CH}_3-$ and $-\text{CH}_2\text{CHCOOH}$), 3.96 (br, 2H, $\text{C}(=\text{O})\text{OCH}_2-$), 4.57 (br, 2H, $-\text{CH}_2\text{Ar}-$), 6.34 (br, 2H, Ar), 7.30-7.45 (br, 4H, Ar), 7.67 (br, 2H, Ar), 11.96 (s, 1H, $-\text{COOH}$)

^{13}C NMR (1:1 CDCl_3 : $\text{DMSO}-d^6$, 100 MHz) δ /ppm: 13.77 (1C, $-(\text{CH}_2)_3\text{CH}_3$), 19.29 (1C, $-(\text{CH}_2)_2\text{CH}_2\text{CH}_3$), 30.19 (1C, $-\text{CH}_2\text{CH}_2\text{CH}_2\text{CH}_3$), 44.60 (1C, $-\text{CHC}(=\text{O})\text{OH}$), 64.59 (1C, $-\text{C}(=\text{O})\text{OCH}_2-$), 176.28 (1C, $-\text{C}(=\text{O})\text{OH}$), 177.16 (1C, $-\text{C}(=\text{O})\text{O}(\text{CH}_2)_3\text{CH}_3$)

P(LMA-*b*-AA): ^1H NMR (1:1 CDCl_3 : $\text{DMSO}-d^6$, 400 MHz) δ /ppm: 0.91 (br, 3H, $-\text{CH}_3$), 1.00 (br, 3H, $-(\text{CH}_2)_{11}\text{CH}_3$), 1.42 (br, 18H, $-(\text{CH}_2)_9\text{CH}_3$), 1.62 (br, 2H, $-(\text{CH}_2(\text{CH}_2)_9\text{CH}_3)$), 1.92 (br, 2H, $-\text{CH}_2\text{C}(\text{CH}_3)(\text{C}(=\text{O})\text{O}(\text{CH}_2)_{11}\text{CH}_3$ and $-\text{CH}_2\text{CHCOOH}$), 3.94 (br, 2H, $\text{C}(=\text{O})\text{OCH}_2-$), 4.59 (br, 2H, $-\text{CH}_2\text{Ar}-$), 6.34 (br, 2H, Ar), 7.30-7.45 (br, 4H, Ar), 7.67 (br, 2H, Ar), 11.94 (s, 1H, $-\text{COOH}$)

^{13}C NMR (1:1 CDCl_3 : $\text{DMSO}-d^6$, 100 MHz) δ /ppm: 14.18 (1C, $-(\text{CH}_2)_{11}\text{CH}_3$), 22.62 (1C, $-(\text{CH}_2)_{10}\text{CH}_2\text{CH}_3$), 29.29 (3C, $-(\text{CH}_2)_6(\text{CH}_2)_3(\text{CH}_2)_2\text{CH}_3$), 29.61 (5C, $-\text{CH}_2(\text{CH}_2)_5(\text{CH}_2)_5\text{CH}_3$), 31.87 (1C, $-\text{CH}_2\text{CH}_2\text{CH}_3$), 64.69 (1C, $-\text{C}(=\text{O})\text{OCH}_2-$), 176.28 (1C, $-\text{C}(=\text{O})\text{OH}$), 177.41 (1C, $-\text{C}(=\text{O})\text{O}(\text{CH}_2)_{11}\text{CH}_3$)

10.12 RAFT polymerisation of Alkyl Methacrylates and Acrylic Acid using Benzyl-1-pyrrolicarbodithioate to form Linear Random P(nMA-*co*-AA) Copolymer



Each alkyl methacrylate monomer (methyl, butyl and lauryl), benzyl-1-pyrrole carbodithioate, ACVA and dioxane were mixed together in the desired ratio until the solid initiator had dissolved. The resulting solution was freeze-pump-thawed on a vacuum line (10^{-3} mbar, three cycles) then flame-sealed and heated in a thermostated

water bath at 60 °C for up to 24 h to undergo polymerisation. The products were then precipitated into rapidly stirring ice-cold petroleum ether. The non-solvent was removed by decanting and the polymer was dried in vacuo at room temperature for 24 h, giving polymer products as yellow powdery or amorphous solids.

P(MMA-co-AA): ^1H NMR (1:1 CDCl_3 : $\text{DMSO}-d^6$, 400 MHz) δ /ppm: 0.94-0.66 (br, 3H, $-\text{CH}_3$), 1.32-0.95 (br, 2H, $-\text{CH}_2\text{C}(\text{CH}_3)(\text{C}(\text{=O})\text{OCH}_3)$), 1.86 (br, 2H, $-\text{CH}_2\text{CHCOOH}$), 3.52 (br, 2H, $\text{C}(\text{=O})\text{OCH}_3$), 4.57 (br, 2H, $-\text{CH}_2\text{Ar}$ -), 6.34 (br, 2H, Ar), 7.30-7.45 (br, 4H, Ar), 7.67 (br, 2H, Ar), 11.87 (s, 1H, $-\text{COOH}$)

^{13}C NMR (1:1 CDCl_3 : $\text{DMSO}-d^6$, 100 MHz) δ /ppm: 22.77 (1C, $-\text{CH}_3$), 44.36 (1C, $-\text{CHC}(\text{=O})\text{OH}$), 51.75 (1C, $-\text{C}(\text{=O})\text{OCH}_3$), 176.88 (1C, $-\text{C}(\text{=O})\text{OH}$), 177.26 (1C, $-\text{C}(\text{=O})\text{OCH}_3$)

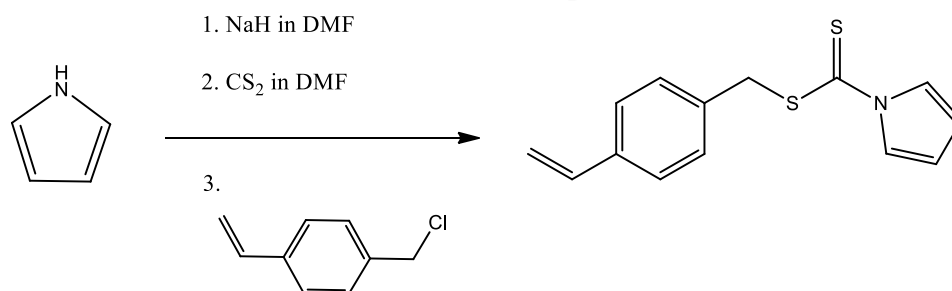
P(BMA-co-AA): ^1H NMR (1:1 CDCl_3 : $\text{DMSO}-d^6$, 400 MHz) δ /ppm: 0.89 (s, 3H, $-\text{CH}_3$), 1.00 (br, 3H, $-(\text{CH}_2)_3\text{CH}_3$), 1.42 (br, 2H, $-(\text{CH}_2)\text{CH}_3$), 1.62 (br, 2H, $-(\text{CH}_2\text{CH}_2\text{CH}_3)$), 1.92 (br, 4H, $-\text{CH}_2\text{C}(\text{CH}_3)(\text{C}(\text{=O})\text{O}(\text{CH}_2)_3\text{CH}_3$ - and $-\text{CH}_2\text{CHCOOH}$), 3.96 (br, 2H, $\text{C}(\text{=O})\text{OCH}_2$ -), 4.57 (br, 2H, $-\text{CH}_2\text{Ar}$ -), 6.34 (br, 2H, Ar), 7.30-7.45 (br, 4H, Ar), 7.67 (br, 2H, Ar), 11.96 (s, 1H, $-\text{COOH}$)

^{13}C NMR (1:1 CDCl_3 : $\text{DMSO}-d^6$, 100 MHz) δ /ppm: 13.91 (1C, $-(\text{CH}_2)_3\text{CH}_3$), 19.24 (1C, $-(\text{CH}_2)_2\text{CH}_2\text{CH}_3$), 30.36 (1C, $-\text{CH}_2\text{CH}_2\text{CH}_2\text{CH}_3$), 44.66 (1C, $-\text{CHC}(\text{=O})\text{OH}$), 64.34 (1C, $-\text{C}(\text{=O})\text{OCH}_2$ -), 176.17 (1C, $-\text{C}(\text{=O})\text{OH}$), 177.41 (1C, $-\text{C}(\text{=O})\text{O}(\text{CH}_2)_3\text{CH}_3$)

P(LMA-co-AA): ^1H NMR (1:1 CDCl_3 : $\text{DMSO}-d^6$, 400 MHz) δ /ppm: 0.91 (br, 3H, $-\text{CH}_3$), 1.00 (br, 3H, $-(\text{CH}_2)_{11}\text{CH}_3$), 1.42 (br, 18H, $-(\text{CH}_2)_9\text{CH}_3$), 1.62 (br, 2H, $-(\text{CH}_2(\text{CH}_2)_9\text{CH}_3)$), 1.92 (br, 2H, $-\text{CH}_2\text{C}(\text{CH}_3)(\text{C}(\text{=O})\text{O}(\text{CH}_2)_{11}\text{CH}_3$ and $-\text{CH}_2\text{CHCOOH}$), 3.94 (br, 2H, $\text{C}(\text{=O})\text{OCH}_2$ -), 4.59 (br, 2H, $-\text{CH}_2\text{Ar}$ -), 6.34 (br, 2H, Ar), 7.30-7.45 (br, 4H, Ar), 7.67 (br, 2H, Ar), 11.94 (s, 1H, $-\text{COOH}$)

^{13}C NMR (1:1 CDCl_3 : $\text{DMSO}-d^6$, 100 MHz) δ /ppm: 14.25 (1C, $-(\text{CH}_2)_{11}\text{CH}_3$), 22.58 (1C, $-(\text{CH}_2)_{10}\text{CH}_2\text{CH}_3$), 29.25 (3C, $-(\text{CH}_2)_6(\text{CH}_2)_3(\text{CH}_2)_2\text{CH}_3$), 29.56 (5C, $-\text{CH}_2(\text{CH}_2)_5(\text{CH}_2)_5\text{CH}_3$), 31.82 (1C, $-\text{CH}_2\text{CH}_2\text{CH}_3$), 64.69 (1C, $-\text{C}(\text{=O})\text{OCH}_2$ -), 176.19 (1C, $-\text{C}(\text{=O})\text{OH}$), 177.18 (1C, $-\text{C}(\text{=O})\text{O}(\text{CH}_2)_{11}\text{CH}_3$)

10.13 Synthesis of 4-Vinylbenzyl-1-pyrrolecabdithioate



Pyrrole (5.00 g) and DMF (10 ml) were added dropwise over 30 minutes to a rapidly stirring suspension of sodium hydride (2.98 g) in DMF (80 ml) to produce a yellow foam. The solution was stirred at room temperature for 30 minutes then cooled to 0 °C using an ice bath. Carbon disulphide (5.68 g, 4.50 ml) and DMF (10 ml) were added dropwise over 10 minutes to create a dark red solution. This was stirred at room temperature for 30 minutes and then cooled to 0 °C. 4-vinylbenzyl chloride (11.37 g, 10.50 ml) and DMF (10 ml) were then added dropwise over 20 minutes. The brown solution was stirred overnight at room temperature.

The solution product was placed in a separating funnel with diethyl ether (80 ml) and distilled water (80 ml). The organic layer was recovered and the aqueous layer was extracted with diethyl ether (3 x 160 ml). The organic extracts were combined and dried over magnesium sulphate, before gravity filtration. The solvent was then removed by rotary evaporation to give a brown oil.

The oil was purified by flash chromatography, with a column of 6cm diameter, using 100% hexane as the eluent. The desired fractions were identified by thin layer chromatography (TLC) and combined, then the solvent was removed by rotary evaporation to give 5.93 g of a bright yellow oil. The air sensitive product was stored under nitrogen at -18 °C.

R_f (silica, hexane): 0.14.

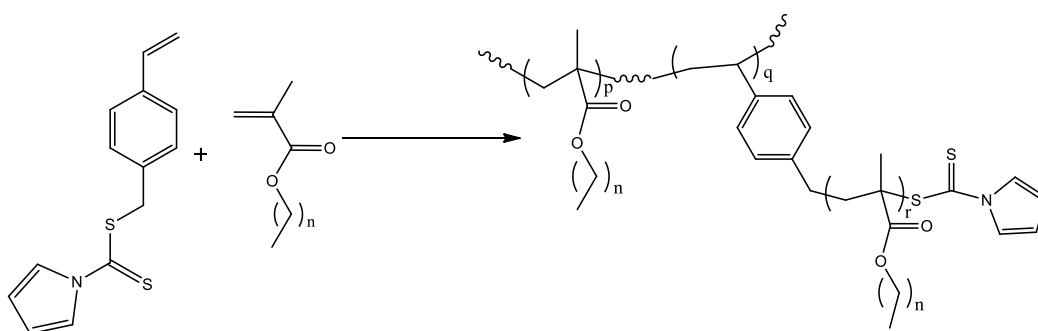
¹H NMR (CDCl₃, 250 MHz) δ/ppm: 4.60 (s, 1H, -C(=S)-S-CH₂-), 5.28 (d, J = 10.93 Hz, 1H, -CH=CHH), 5.76 (d, J = 17.60 Hz, 1H, -CH=CHH), 6.34 (t, J = 2.43 Hz, 2H, Ar), 6.71 (dd, J = 17.60, 10.88 Hz, 1H, -CH=CH₂), 7.38 (m, 4H, Ar), 7.72 (t, J = 2.37 Hz, 2H, Ar)

^{13}C NMR (CDCl_3 , 63 MHz) δ /ppm: 40.94 (1C, $-\text{C}(=\text{S})-\text{S}-\text{CH}_2-$), 113.69 (2C, Ar), 113.83 (1C, $\text{CH}_2=\text{CH}-$), 120.10 (2C, Ar), 126.00 (2C, Ar), 129.06 (2C, Ar), 133.96 (1C, Ar), 135.65 (1C, $-\text{CH}=\text{CH}_2$), 199.27 (1C, $-\text{C}(=\text{S})\text{S}-$)

Calculated for $\text{C}_{14}\text{H}_{13}\text{NS}_2$: C, 64.83; H, 5.05; N, 5.40; S, 24.72. Found: C, 64.35; H, 5.13; N, 4.99; S, 22.50.

EI MS m/z : 259 (calculated 259)

10.14 RAFT polymerisation of Alkyl Methacrylates using 4-Vinylbenzyl-1-pyrrolicarbodithioate to form Highly Branched P(nMA) Macro-Chain Transfer Agent



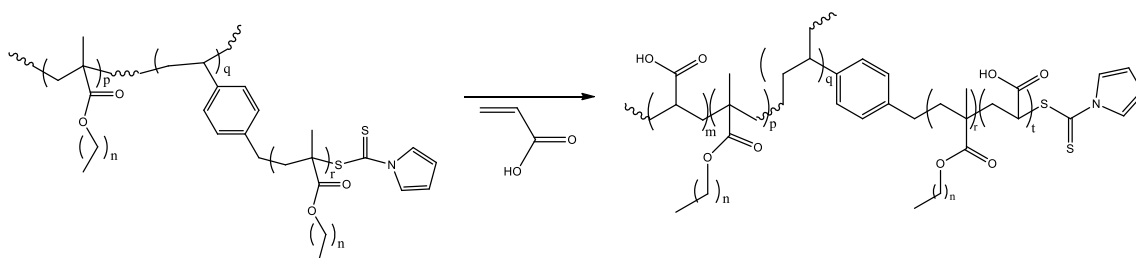
Each alkyl methacrylate monomer (methyl, butyl and lauryl), 4-vinylbenzyl-1-pyrrolicarbodithioate, ACVA and dioxane were mixed together in the desired ratio until the solid initiator had dissolved. The resulting solution was freeze-pump-thawed on a vacuum line (10^{-3} mbar, three cycles) then flame-sealed and heated in a thermostated water bath at 60°C for up to 24 h to undergo polymerisation. The products were then precipitated into rapidly stirring ice-cold methanol. The non-solvent was removed by decanting and the polymer was dried in vacuo at room temperature for 24 h, giving polymer products as yellow amorphous solids.

PMMA: ^1H NMR (CDCl_3 , 400 MHz) δ /ppm: 0.95 (d, $J=69.43$ Hz, 3H, $-\text{CH}_3$), 1.90 (br, 2H, $-\text{CH}_2\text{C}(\text{CH}_3)(\text{C}(\text{O})\text{OCH}_3)$), 3.62 (br, 2H, $\text{C}(\text{O})\text{OCH}_3$), 6.36 (m, 2H, Ar), 7.17-7.44 (br, 4H, Ar), 7.69 (br, 2H, Ar)

PBMA: ^1H NMR (CDCl_3 , 400 MHz) δ /ppm: : 0.89 (s, 3H, $-\text{CH}_3$), 1.00 (br, 3H, $-(\text{CH}_2)_3\text{CH}_3$), 1.42 (br, 2H, $-(\text{CH}_2)\text{CH}_3$), 1.62 (br, 2H, $-(\text{CH}_2\text{CH}_2\text{CH}_3)$), 1.92 (br, 2H, $-\text{CH}_2\text{C}(\text{CH}_3)(\text{C}(\text{O})\text{O}(\text{CH}_2)_3\text{CH}_3-$), 3.96 (br, 2H, $\text{C}(\text{O})\text{OCH}_2-$), 4.63 (br, 1H, CHAr), 6.34 (m, 2H, Ar), 7.30-7.45 (br, 4H, Ar), 7.72 (br, 2H, Ar)

PLMA: ^1H NMR (CDCl_3 , 400 MHz) δ/ppm : 0.91 (br, 3H, $-\text{CH}_3$), 1.00 (br, 3H, $-(\text{CH}_2)_{11}\text{CH}_3$), 1.42 (br, 18H, $-(\text{CH}_2)_9\text{CH}_3$), 1.62 (br, 2H, $-(\text{CH}_2(\text{CH}_2)_9\text{CH}_3)$), 1.92 (br, 2H, $-\text{CH}_2\text{C}(\text{CH}_3)(\text{C}=\text{O})\text{O}(\text{CH}_2)_{11}\text{CH}_3$), 3.94 (br, 2H, $\text{C}(\text{O})\text{OCH}_2-$), 6.37 (m, 2H, Ar), 7.30-7.45 (br, 4H, Ar), 7.67 (br, 2H, Ar)

10.15 Synthesis of HB P(nMA-*b*-AA) Block Copolymers via RAFT Polymerisation of HB P(nMA) Macro-Chain Transfer Agent and Acrylic Acid



HB P(nMA) macro-CTA (methyl, butyl or lauryl) was dissolved in dioxane then the desired amounts of ACVA and acrylic acid were added. The resulting solution was freeze-pump-thawed on a vacuum line (10^{-3} mbar, three cycles) then flame-sealed and heated in a thermostated water bath at 60°C for up to 40 h to undergo polymerisation. The products were then precipitated into rapidly stirring ice-cold petroleum ether. The non-solvent was removed by decanting and the polymer was dried in vacuo at room temperature for 24 h, giving polymer products as pale yellow powdery solids.

HB P(MMA-*b*-AA): ^1H NMR (1:1 CDCl_3 : $\text{DMSO}-d^6$, 400 MHz) δ/ppm : 0.94-0.66 (br, 3H, $-\text{CH}_3$), 1.32-0.95 (br, 2H, $-\text{CH}_2\text{C}(\text{CH}_3)(\text{C}=\text{O})\text{OCH}_3$), 1.86 (br, 2H, $-\text{CH}_2\text{CHCOOH}$), 3.52 (br, 2H, $\text{C}(\text{O})\text{OCH}_3$), 4.57 (br, 2H, $-\text{CH}_2\text{Ar}-$), 6.34 (br, 2H, Ar), 7.30-7.45 (br, 4H, Ar), 7.67 (br, 2H, Ar), 11.87 (s, 1H, $-\text{COOH}$)

^{13}C NMR (1:1 CDCl_3 : $\text{DMSO}-d^6$, 100 MHz) δ/ppm : 22.78 (1C, $-\text{CH}_3$), 44.40 (1C, $-\text{CHC}(\text{O})\text{OH}$), 51.84 (1C, $-\text{C}(\text{O})\text{OCH}_3$), 176.37 (1C, $-\text{C}(\text{O})\text{OH}$), 177.47 (1C, $-\text{C}(\text{O})\text{OCH}_3$)

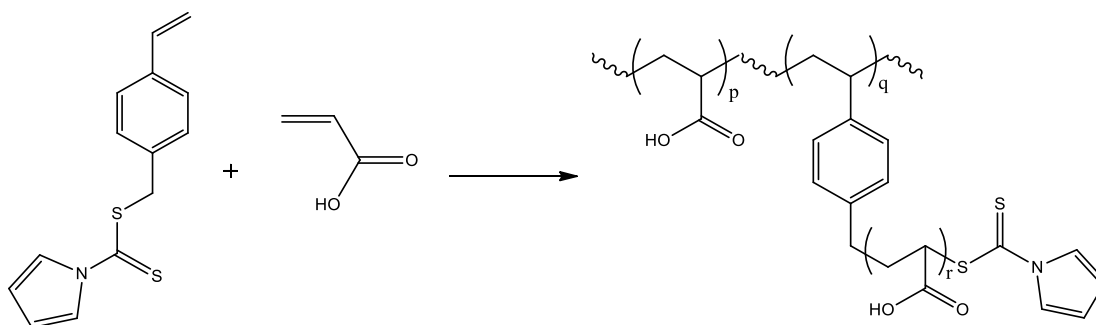
HB P(BMA-*b*-AA): ^1H NMR (1:1 CDCl_3 : $\text{DMSO}-d^6$, 400 MHz) δ/ppm : 0.89 (s, 3H, $-\text{CH}_3$), 1.00 (br, 3H, $-(\text{CH}_2)_3\text{CH}_3$), 1.42 (br, 2H, $-(\text{CH}_2)\text{CH}_3$), 1.62 (br, 2H, $-(\text{CH}_2\text{CH}_2\text{CH}_3)$), 1.92 (br, 4H, $-\text{CH}_2\text{C}(\text{CH}_3)(\text{C}=\text{O})\text{O}(\text{CH}_2)_3\text{CH}_3-$ and $-\text{CH}_2\text{CHCOOH}$), 3.96 (br, 2H, $\text{C}(\text{O})\text{OCH}_2-$), 4.57 (br, 2H, $-\text{CH}_2\text{Ar}-$), 6.34 (br, 2H, Ar), 7.30-7.45 (br, 4H, Ar), 7.67 (br, 2H, Ar), 11.96 (s, 1H, $-\text{COOH}$)

^{13}C NMR (1:1 CDCl_3 : $\text{DMSO-}d^6$, 100 MHz) δ /ppm: 13.75 (1C, $-(\text{CH}_2)_3\text{CH}_3$), 19.28 (1C, $-(\text{CH}_2)_2\text{CH}_2\text{CH}_3$), 30.16 (1C, $-\text{CH}_2\text{CH}_2\text{CH}_2\text{CH}_3$), 44.60 (1C, $-\text{CHC}(=\text{O})\text{OH}$), 64.58 (1C, $-\text{C}(=\text{O})\text{OCH}_2-$), 176.37 (1C, $-\text{C}(=\text{O})\text{OH}$), 177.52 (1C, $-\text{C}(=\text{O})\text{O}(\text{CH}_2)_3\text{CH}_3$)

HB P(LMA-*b*-AA): ^1H NMR (1:1 CDCl_3 : $\text{DMSO-}d^6$, 400 MHz) δ /ppm: 0.91 (br, 3H, $-\text{CH}_3$), 1.00 (br, 3H, $-(\text{CH}_2)_{11}\text{CH}_3$), 1.42 (br, 18H, $-(\text{CH}_2)_9\text{CH}_3$), 1.62 (br, 2H, $-(\text{CH}_2(\text{CH}_2)_9\text{CH}_3)$), 1.92 (br, 2H, $-\text{CH}_2\text{C}(\text{CH}_3)(\text{C}(=\text{O})\text{O}(\text{CH}_2)_{11}\text{CH}_3$ and $-\text{CH}_2\text{CHCOOH}$), 3.94 (br, 2H, $\text{C}(=\text{O})\text{OCH}_2-$), 4.59 (br, 2H, $-\text{CH}_2\text{Ar}-$), 6.34 (br, 2H, Ar), 7.30-7.45 (br, 4H, Ar), 7.67 (br, 2H, Ar), 11.94 (s, 1H, $-\text{COOH}$)

^{13}C NMR (1:1 CDCl_3 : $\text{DMSO-}d^6$, 100 MHz) δ /ppm: 14.18 (1C, $-(\text{CH}_2)_{11}\text{CH}_3$), 22.62 (1C, $-(\text{CH}_2)_{10}\text{CH}_2\text{CH}_3$), 29.29 (3C, $-(\text{CH}_2)_6(\text{CH}_2)_3(\text{CH}_2)_2\text{CH}_3$), 29.61 (5C, $-\text{CH}_2(\text{CH}_2)_5(\text{CH}_2)_5\text{CH}_3$), 31.87 (1C, $-\text{CH}_2\text{CH}_2\text{CH}_3$), 64.69 (1C, $-\text{C}(=\text{O})\text{OCH}_2-$), 176.28 (1C, $-\text{C}(=\text{O})\text{OH}$), 177.41 (1C, $-\text{C}(=\text{O})\text{O}(\text{CH}_2)_{11}\text{CH}_3$)

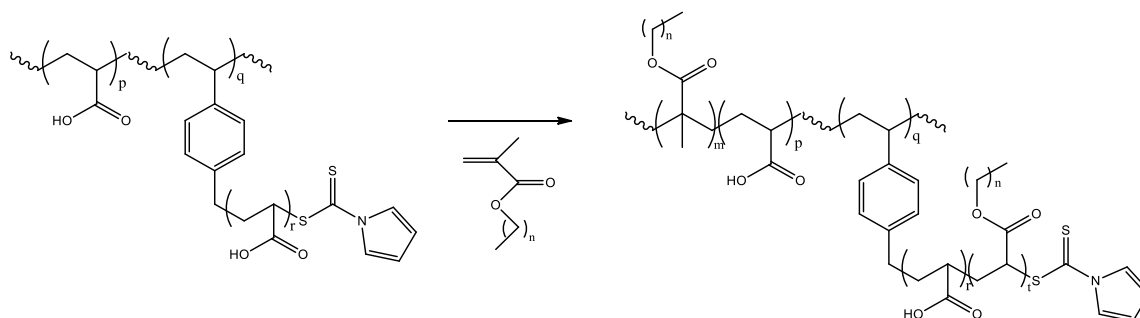
10.16 RAFT Polymerisation of Acrylic Acid using 4-Vinylbenzyl-1-pyrrolicarbodithioate to form HB PAA Macro-Chain Transfer Agent



Acrylic acid, 4-vinylbenzyl-1-pyrrolicarbodithioate, ACVA and dioxane were mixed together in the desired ratio until the solid initiator had dissolved. The resulting solution was freeze-pump-thawed on a vacuum line (10^{-3} mbar, three cycles) then flame-sealed and heated in a thermostated water bath at $60\text{ }^\circ\text{C}$ for up to 24 h to undergo polymerisation. The products were then precipitated into rapidly stirring ice-cold diethyl ether. The non-solvent was removed by decanting and the polymer was dried in vacuo at room temperature for 24 h, giving polymer products as yellow amorphous solids.

^1H NMR (400 MHz, $\text{DMSO-}d^6$) δ /ppm: 1.63 (br, 2H, $-\text{CH}_2\text{CHCOOH}$), 2.22 (br, 1H, $-\text{CHCOOH}$), 4.60 (br, 2H, $-\text{CH}_2\text{Ar}-$), 6.46 (br, 2H, Ar), 7.20 (br, 4H, Ar), 7.75 (br, 2H, Ar), 12.32 (s, 1H, $-\text{COOH}$)

10.17 Synthesis of HB P(AA-*b*-nMA) Block Copolymers via RAFT Polymerisation of HB PAA Macro-Chain Transfer Agent and Alkyl Methacrylates



HB PAA macro-CTA was dissolved in dioxane then the desired amounts of ACVA and methacrylate monomer (methyl, butyl or lauryl) were added. The resulting solution was freeze-pump-thawed on a vacuum line (10^{-3} mbar, three cycles) then flame-sealed and heated in a thermostated water bath at 60 °C for up to 40 h to undergo polymerisation. The products were then precipitated into rapidly stirring ice-cold petroleum ether. The non-solvent was removed by decanting and the polymer was dried in vacuo at room temperature for 24 h, giving polymer products as pale yellow powdery solids.

HB P(AA-*b*-MMA): ^1H NMR (1:1 CDCl_3 :DMSO- d^6 , 400 MHz) δ /ppm: 0.94-0.66 (br, 3H, $-\text{CH}_3$), 1.32-0.95 (br, 2H, $-\text{CH}_2\text{C}(\text{CH}_3)(\text{C}=\text{O})\text{OCH}_3$), 1.86 (br, 2H, $-\text{CH}_2\text{CHCOOH}$), 3.52 (br, 2H, $\text{C}(\text{O})\text{OCH}_3$), 4.57 (br, 2H, $-\text{CH}_2\text{Ar}-$), 6.34 (br, 2H, Ar), 7.30-7.45 (br, 4H, Ar), 7.67 (br, 2H, Ar), 11.87 (s, 1H, $-\text{COOH}$)

^{13}C NMR (1:1 CDCl_3 :DMSO- d^6 , 100 MHz) δ /ppm: 18.82 (1C, $-\text{CH}_3$), 44.41 (1C, $-\text{CHC}(\text{O})\text{OH}$), 51.80 (1C, $-\text{C}(\text{O})\text{OCH}_3$), 176.55 (1C, $-\text{C}(\text{O})\text{OH}$), 177.49 (1C, $-\text{C}(\text{O})\text{OCH}_3$)

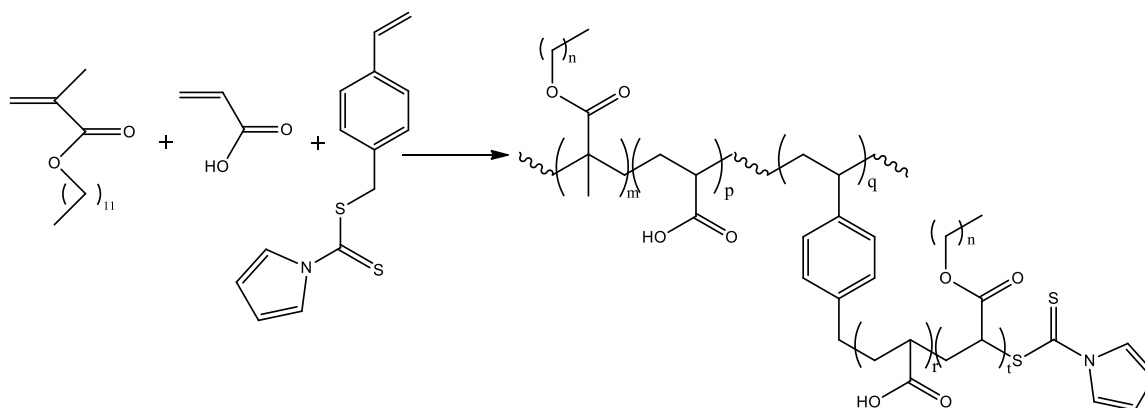
HB P(AA-*b*-BMA): ^1H NMR (1:1 CDCl_3 :DMSO- d^6 , 400 MHz) δ /ppm: 0.89 (s, 3H, $-\text{CH}_3$), 1.00 (br, 3H, $-(\text{CH}_2)_3\text{CH}_3$), 1.42 (br, 2H, $-(\text{CH}_2)\text{CH}_3$), 1.62 (br, 2H, $-(\text{CH}_2\text{CH}_2\text{CH}_3)$), 1.92 (br, 4H, $-\text{CH}_2\text{C}(\text{CH}_3)(\text{C}=\text{O})\text{O}(\text{CH}_2)_3\text{CH}_3-$ and $-\text{CH}_2\text{CHCOOH}$), 3.96 (br, 2H, $\text{C}(\text{O})\text{OCH}_2-$), 4.57 (br, 2H, $-\text{CH}_2\text{Ar}-$), 6.34 (br, 2H, Ar), 7.30-7.45 (br, 4H, Ar), 7.67 (br, 2H, Ar), 11.96 (s, 1H, $-\text{COOH}$)

^{13}C NMR (1:1 CDCl_3 :DMSO- d^6 , 100 MHz) δ /ppm: 13.77 (1C, $-(\text{CH}_2)_3\text{CH}_3$), 19.29 (1C, $-(\text{CH}_2)_2\text{CH}_2\text{CH}_3$), 30.19 (1C, $-\text{CH}_2\text{CH}_2\text{CH}_2\text{CH}_3$), 44.60 (1C, $-\text{CHC}(\text{O})\text{OH}$), 64.58 (1C, $-\text{C}(\text{O})\text{OCH}_2-$), 176.29 (1C, $-\text{C}(\text{O})\text{OH}$), 177.16 (1C, $-\text{C}(\text{O})\text{O}(\text{CH}_2)_3\text{CH}_3$)

HB P(AA-*b*-LMA): ^1H NMR (1:1 CDCl_3 : $\text{DMSO-}d^6$, 400 MHz) δ /ppm: 0.91 (br, 3H, $-\text{CH}_3$), 1.00 (br, 3H, $-(\text{CH}_2)_{11}\text{CH}_3$), 1.42 (br, 18H, $-(\text{CH}_2)_9\text{CH}_3$), 1.62 (br, 2H, $-(\text{CH}_2(\text{CH}_2)_9\text{CH}_3)$), 1.92 (br, 2H, $-\text{CH}_2\text{C}(\text{CH}_3)(\text{C}=\text{O})\text{O}(\text{CH}_2)_{11}\text{CH}_3$ and $-\text{CH}_2\text{CHCOOH}$), 3.94 (br, 2H, $\text{C}(\text{=O})\text{OCH}_2-$), 4.59 (br, 2H, $-\text{CH}_2\text{Ar}-$), 6.34 (br, 2H, Ar), 7.30-7.45 (br, 4H, Ar), 7.67 (br, 2H, Ar), 11.94 (s, 1H, $-\text{COOH}$)

^{13}C NMR (1:1 CDCl_3 : $\text{DMSO-}d^6$, 100 MHz) δ /ppm: 14.18 (1C, $-(\text{CH}_2)_{11}\text{CH}_3$), 22.62 (1C, $-(\text{CH}_2)_{10}\text{CH}_2\text{CH}_3$), 29.29 (3C, $-(\text{CH}_2)_6(\text{CH}_2)_3(\text{CH}_2)_2\text{CH}_3$), 29.61 (5C, $-\text{CH}_2(\text{CH}_2)_5(\text{CH}_2)_5\text{CH}_3$), 31.87 (1C, $-\text{CH}_2\text{CH}_2\text{CH}_3$), 64.69 (1C, $-\text{C}(\text{=O})\text{OCH}_2-$), 176.28 (1C, $-\text{C}(\text{=O})\text{OH}$), 177.41 (1C, $-\text{C}(\text{=O})\text{O}(\text{CH}_2)_{11}\text{CH}_3$)

10.18 RAFT Polymerisation of Alkyl Methacrylates and Acrylic acid using 4-Vinylbenzyl-1-pyrrolicarbodithioate to form HB Random Copolymer P(*n*MA-*co*-AA)



Each alkyl methacrylate monomer (methyl, butyl or lauryl), acrylic acid, 4-vinylbenzyl-1-pyrrole carbodithioate, ACVA and dioxane were mixed together in the desired ratio until the solid initiator had dissolved. The resulting solution was freeze-pump-thawed on a vacuum line (10^{-3} mbar, three cycles) then flame-sealed and heated in a thermostated water bath at $60\text{ }^\circ\text{C}$ for up to 24 h to undergo polymerisation. The products were then precipitated into rapidly stirring ice-cold petroleum ether. The non-solvent was removed by decanting and the polymer was dried in vacuo at room temperature for 24 h, giving polymer products as yellow amorphous solids.

HB P(MMA-*co*-AA): ^1H NMR (1:1 CDCl_3 : $\text{DMSO-}d^6$, 400 MHz) δ /ppm: 0.94-0.66 (br, 3H, $-\text{CH}_3$), 1.32-0.95 (br, 2H, $-\text{CH}_2\text{C}(\text{CH}_3)(\text{C}=\text{O})\text{OCH}_3$), 1.86 (br, 2H, $-\text{CH}_2\text{CHCOOH}$), 3.94 (br, 2H, $\text{C}(\text{=O})\text{OCH}_2-$), 4.59 (br, 2H, $-\text{CH}_2\text{Ar}-$), 6.34 (br, 2H, Ar), 7.30-7.45 (br, 4H, Ar), 7.67 (br, 2H, Ar), 11.94 (s, 1H, $-\text{COOH}$)

CH_2CHCOOH), 3.52 (br, 2H, C(=O)OCH_3), 4.57 (br, 2H, $-\text{CH}_2\text{Ar}-$), 6.34 (br, 2H, Ar), 7.30-7.45 (br, 4H, Ar), 7.67 (br, 2H, Ar), 11.87 (s, 1H, $-\text{COOH}$)

^{13}C NMR (1:1 CDCl_3 : $\text{DMSO}-d^6$, 100 MHz) δ /ppm: 22.77 (1C, $-\text{CH}_3$), 44.36 (1C, $-\text{CHC(=O)OH}$), 51.75 (1C, $-\text{C(=O)OCH}_3$), 176.88 (1C, $-\text{C(=O)OH}$), 177.26 (1C, $-\text{C(=O)OCH}_3$)

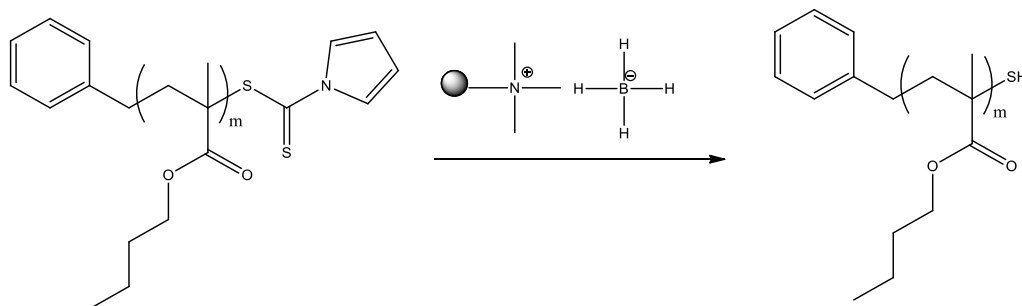
HB P(BMA-co-AA): ^1H NMR (1:1 CDCl_3 : $\text{DMSO}-d^6$, 400 MHz) δ /ppm: 0.89 (s, 3H, $-\text{CH}_3$), 1.00 (br, 3H, $-(\text{CH}_2)_3\text{CH}_3$), 1.42 (br, 2H, $-(\text{CH}_2)\text{CH}_3$), 1.62 (br, 2H, $-(\text{CH}_2\text{CH}_2\text{CH}_3)$), 1.92 (br, 4H, $-\text{CH}_2\text{C}(\text{CH}_3)(\text{C(=O)O}(\text{CH}_2)_3\text{CH}_3-$ and $-\text{CH}_2\text{CHCOOH}$), 3.96 (br, 2H, C(=O)OCH_2-), 4.57 (br, 2H, $-\text{CH}_2\text{Ar}-$), 6.34 (br, 2H, Ar), 7.30-7.45 (br, 4H, Ar), 7.67 (br, 2H, Ar), 11.96 (s, 1H, $-\text{COOH}$)

^{13}C NMR (1:1 CDCl_3 : $\text{DMSO}-d^6$, 100 MHz) δ /ppm: 13.91 (1C, $-(\text{CH}_2)_3\text{CH}_3$), 19.24 (1C, $-(\text{CH}_2)_2\text{CH}_2\text{CH}_3$), 30.36 (1C, $-\text{CH}_2\text{CH}_2\text{CH}_2\text{CH}_3$), 44.66 (1C, $-\text{CHC(=O)OH}$), 64.34 (1C, $-\text{C(=O)OCH}_2-$), 176.17 (1C, $-\text{C(=O)OH}$), 177.41 (1C, $-\text{C(=O)O}(\text{CH}_2)_3\text{CH}_3$)

HB P(LMA-co-AA): ^1H NMR (1:1 CDCl_3 : $\text{DMSO}-d^6$, 400 MHz) δ /ppm: 0.91 (br, 3H, $-\text{CH}_3$), 1.00 (br, 3H, $-(\text{CH}_2)_{11}\text{CH}_3$), 1.42 (br, 18H, $-(\text{CH}_2)_9\text{CH}_3$), 1.62 (br, 2H, $-(\text{CH}_2(\text{CH}_2)_9\text{CH}_3)$), 1.92 (br, 2H, $-\text{CH}_2\text{C}(\text{CH}_3)(\text{C(=O)O}(\text{CH}_2)_{11}\text{CH}_3$ and $-\text{CH}_2\text{CHCOOH}$), 3.94 (br, 2H, C(=O)OCH_2-), 4.59 (br, 2H, $-\text{CH}_2\text{Ar}-$), 6.34 (br, 2H, Ar), 7.30-7.45 (br, 4H, Ar), 7.67 (br, 2H, Ar), 11.94 (s, 1H, $-\text{COOH}$)

^{13}C NMR (1:1 CDCl_3 : $\text{DMSO}-d^6$, 100 MHz) δ /ppm: 14.25 (1C, $-(\text{CH}_2)_{11}\text{CH}_3$), 22.58 (1C, $-(\text{CH}_2)_{10}\text{CH}_2\text{CH}_3$), 29.25 (3C, $-(\text{CH}_2)_6(\text{CH}_2)_3(\text{CH}_2)_2\text{CH}_3$), 29.56 (5C, $-\text{CH}_2(\text{CH}_2)_5(\text{CH}_2)_5\text{CH}_3$), 31.82 (1C, $-\text{CH}_2\text{CH}_2\text{CH}_3$), 64.69 (1C, $-\text{C(=O)OCH}_2-$), 176.19 (1C, $-\text{C(=O)OH}$), 177.18 (1C, $-\text{C(=O)O}(\text{CH}_2)_{11}\text{CH}_3$)

10.19 Removal of RAFT End Groups using Polymer-Supported Borohydride Reducing Agent



PBMA with RAFT end groups (0.05 mmol) was dissolved in chloroform (10ml) in a small sample tube. Polymer-supported borohydride (on Amberlyst A26 or Amberlyst IRA-400) (0.2 mmol) was added and the tube closed and placed on a laboratory shaker for 24 hours. The suspension was then filtered to remove the resin and then the solvent was reduced to a minimal amount. This was then precipitated into rapidly stirring methanol to yield the product as a white powder, which was collected by decanting.

PBMA: ^1H NMR (CDCl_3 , 400 MHz) δ /ppm: 0.89 (s, 3H, $-\text{CH}_3$), 1.00 (br, 3H, $-(\text{CH}_2)_3\text{CH}_3$), 1.42 (br, 2H, $-(\text{CH}_2)\text{CH}_3$), 1.62 (br, 2H, $-(\text{CH}_2\text{CH}_2\text{CH}_3)$), 1.92 (br, 2H, $-\text{CH}_2\text{C}(\text{CH}_3)(\text{C}=\text{O})\text{O}(\text{CH}_2)_3\text{CH}_3-$), 3.96 (br, 2H, $\text{C}(\text{O})\text{OCH}_2-$), 4.63 (br, 1H, CHAr), 7.30-7.45 (br, 4H, Ar)

10.20 Preparation of Copolymer Dispersions

Dispersions were prepared using the solvent switch method. Copolymer samples were dissolved in THF at a concentration of 0.5 % w/v. Equivalent volumes of deionised water were added dropwise to the stirring solutions using a Razel R-99 syringe pump set to a rate of 0.1 ml min^{-1} , unless otherwise stated. Solutions were left to stir uncovered for three hours for the THF to evaporate, leaving the copolymers dispersed in H_2O . Study by ^1H NMR demonstrated that residual THF was not observed. The same method was additionally used to prepare dispersions in other solvent systems.

10.20.1 Preparation of Copolymer Dispersions at a Range of pH

Buffer solutions at the required pH were prepared by adding measured volumes of 1 mol dm^{-3} HCl or 1 mol dm^{-3} NaOH to known volumes of deionised water until the desired pH was obtained, monitored by a pH probe. NaCl was added as required to maintain constant ionic strength across all buffer solutions. Dispersions were prepared as above using buffer solutions in place of deionised water.

10.21 Annealing of Copolymer Dispersions

Copolymer dispersions prepared as above were sealed in sample tubes to prevent evaporation and placed into an oil bath thermostated to $45 \text{ }^\circ\text{C}$ whilst stirring for 12 hours or as otherwise stated.

10.22 Encapsulation and Release of Rhodamine B

Copolymer dispersions were prepared as above but with a solution of Rhodamine B in deionised water at a concentration of 0.2 mg ml^{-1} added dropwise instead of deionised water to allow Rhodamine B encapsulation. Dispersions were injected into pre-hydrated

3500 MWCO dialysis cassettes and were dialysed against deionised water for approximately 36 hours with regular water changes until no Rhodamine B was observed in the UV-vis spectra. The cassette was then transferred into a fresh volume of deionised water thermostated to 40 °C and Rhodamine B release was monitored by UV-vis spectrometry.

10.23 Equipment and Instrumentation

10.23.1 Freeze-Pump-Thaw Polymerisation

Ampoules were degassed on a high vacuum line equipped with a Pirani gauge. The reaction mixture was pipetted into a glass ampoule and placed onto the high vacuum line with the tap closed so the ampoule was not exposed to vacuum. The solution was frozen using liquid nitrogen and then opened to the vacuum until the gauge dropped to a steady output. Exposure to vacuum was then ceased by closing the tap and the ampoule was left for its contents to thaw. Thawing was aided by immersion of the ampoule in tepid water. Once thawing was complete, the full process was repeated until a negligible rise in pressure was observed when the ampoule was exposed to vacuum. The end pressure in the ampoule was approximately 3×10^{-3} mBar.

10.23.2 ^1H and ^{13}C NMR

All NMR spectra were recorded at ambient temperature on Bruker AV-250, AV-400 or DRX-500 at 250, 400 or 500 MHz (64 scans averaged per spectrum). Samples of mass 20-40 mg were dissolved in deuterated chloroform (CDCl_3) or alternative solvent system, filtered and placed in 7 mm NMR tubes.

10.23.3 Elemental Analysis

Elemental Analysis was performed on a Perkin-Elmer 2400 CHNS/O Series 2 Elemental Analyser. 5-10 mg of sample was combusted in the presence of excess oxygen and combustion reagent to form CO_2 and water. Levels of each element were detected using a thermal conductivity detection system.

10.23.4 Mass Spectrometry

Electron Ionisation (EI) MS was carried out using a VG Autospec Mass Spectrometer.

10.23.5 Gel Permeation Chromatography

Average molecular weight and molecular weight distributions were measured relative to PMMA standards by GPC with PL gel mixed-B (10 μm particle size, 100- 10^6 Å pore size, effective MW range 10^3 - 10^6 , 3x 30 cm + guard columns) (Polymer Laboratories, UK) on a RI detector. The mobile phase was THF (GPC grade) set at a flow rate of 1ml

min⁻¹. Sample concentration used was 2 mg ml⁻¹, filtered before injection. Samples were injected using a Gilson 234 auto injector. GPC-Viscometry was carried out using an Agilent 1260 Infinity solvent pump (flow rate 1 ml min⁻¹) and a Rheodyne 7725i injector with 200 µl loop. Columns were PL gel mixed-A (20µm particle size, 50-10⁶ Å pore size, effective MW range 2x10³ - 40x10⁶, 3x 30 cm + guard columns) (Polymer Laboratories, UK) thermostated at 30 °C. Detectors were an Agilent 1260 Infinity viscometer and a HP 1047A RI detector. Data acquisition and analysis were performed using Varian Cirrus multidetector software. The eluent was THF (GPC grade) filtered to 0.02 µm. Polymer samples were accurately weighed and made up to a concentration of 1 mg ml⁻¹.

10.23.6 Particle Sizing Analysis

Particle size analysis was carried out on a Brookhaven Instruments Corporation ZetaPALS Zeta Potential Analyser with the 90Plus/BI-MAS Multi Angle Particle Sizing Option. Samples were prepared at 0.5 % w/v concentration (5 mg ml⁻¹) by either dissolving directly in the required solvent (for THF results) or by using the solvent switch method. (Polymer samples were dissolved in THF then ultrapure H₂O was added dropwise to the stirring solutions. Samples were left to stir for several hours for the THF to evaporate). 15 µl of sample was then added to 3 ml of 10 mmol KCl solution, sonicated for 20 seconds and filtered through a 1 µm filter. Measurements were made at 25 °C unless otherwise stated. 10 analysis runs were made in triplicate for each sample.

10.23.7 Zeta Potential Measurements

Zeta potentials were measured on a Brookhaven Instruments Corporation ZetaPALS Zeta Potential Analyser. Samples were prepared in ultrapure H₂O using the same method as for particle size analysis. 15 µl of sample was added to 1.5 ml of 1 mmol KCl solution. Measurements were made at 25 °C in triplicate for each sample in 5 cycles of 2 minute runs.

10.23.8 Transmission Electron Microscopy

TEM imaging was carried out using a Philips CM 100 instrument operating at 100 kV. Polymer samples dispersed in ultrapure H₂O as described above, or ethanol where stated, were prepared for TEM by adsorbing a 5 µl drop of sample onto a glow-discharged carbon-coated grid for 1 minute. The grid was blotted, washed in a drop of distilled water and blotted again. The grid was then washed in a drop of uranyl formate,

blotted and then negatively stained by holding the grid in a drop of uranyl formate for 20 seconds before blotting.

10.23.9 Scanning Electron Microscopy

SEM imaging was carried out using a Philips XL-20 SEM operating at 20 kV. A TEM grid with sample adsorbed as described above was applied to an aluminium stub of 0.5 inch diameter using a carbonised sticky tab as an adhesive. Stubs were sputter-coated with gold using an Edwards S150b coater.

10.23.10 Small Angle Neutron Scattering

SANS measurements presented in this work were performed at the Rutherford Appleton Laboratory (ISIS Spallation Neutron Source, Didcot, UK) using the fixed-geometry, time-of-flight LOQ spectrometer. The LOQ instrument uses incident neutron wavelengths from 2.2 to 10.0 Å, which covers a scattering wavevector, Q , range of 0.009 to 1.3 Å⁻¹ at a sample-detector distance of 4.1 m. Polymer samples were prepared as 0.5% w/v solutions, 5 mg of polymer in 1 ml of the appropriate solvent system: d-THF, 1:1 d-THF/D₂O mixture, D₂O, 1:1 d-THF/CDCl₃ mixture and d-EtOH. All samples were transferred to 2 mm path-length quartz Hellma cells. The temperature was controlled by using circulating fluid baths to maintain constant temperature at 25 °C. Scattering intensities were reduced and normalized using the standard procedures on MantidPlot software to obtain the differential scattering cross section, $d\Sigma/d\Omega$, in absolute units (cm⁻¹), which is referred to here as $I(Q)$.

10.23.11 UV-Vis Spectrometry

UV-vis measurements were performed using a Perkin Elmer Lambda 35 UV-vis spectrometer with a double beam set-up employing deuterium and tungsten-halogen lamps. Glass sample cells were used with a pathlength of 1 cm. Deionised water was used as the reference. Spectra were recorded over a wavelength range of 500-600 nm. A calibration curve was constructed using solutions of known concentration to determine the extinction coefficient.

10.23.12 Atomic Force Microscopy

Force measurements were conducted by using molecular force probe-1D (MFP-1D) (Asylum Research, Santa Barbara, CA), which is a pN-sensitive instrument, to produce curves of force, F , against tip-sample separation distance. The experiments were conducted in Milli-Q water (15 MΩ cm resistivity, Elga PURElab option water purifier) at room temperature with z -piezo velocity of 400 nm s⁻¹, a z -piezo range of 200 nm, and

data acquisition rate of 10 000 points s⁻¹. Silicon (100) wafers with the native oxide layer intact were cut into pieces of approximately 10 mm × 10 mm. The small pieces were washed in ethanol, rinsed with Milli-Q water, and dried under nitrogen. The cantilever spring constant was calibrated before each measurement.

Samples were prepared by dissolving 5 mg of polymer in 3 ml of THF; three drops of this resulting solution were placed onto a clean silicon substrate set on the spincoater. Each sample was spin coated at 2000 or 4000 rpm for 20 seconds to obtain a suitable sample for AFM.

10.23.13 Contact Angle Measurements

Static contact angle measurements were carried out by the sessile drop method using a KSV CAM200 optical tensiometer, with OneAttention software used to calculate contact angles and corresponding surface energies. Contact angles were determined once drops had reached equilibrium, and at least 5 measurements were taken with each probe on each substrate to increase reproducibility of results. Substrates were prepared by coating high quality PMMA or PP sheets with copolymer solutions using K bars (RK Printcoat Instruments) of the required wire diameter to perform draw-downs.

10.23.14 ATR-FTIR

Infra Red spectra were recorded on a ThermoScientific Nicolet Avatar 370 FTIR spectrophotometer with Diamond ATR accessory, and OMNIC software. Samples were dissolved in a volatile solvent, dropped onto the window and recorded as a thin film following solvent evaporation.

10.23.15 Density Measurements

Densities were measured on an Anton Paar DMA 38 density meter which uses the oscillating U-tube method. The tube was filled with approximately 2 ml of fluid sample ensuring no air bubbles were present and then left for the reading to stabilise. Measurements were taken at 25 °C.

10.23.16 Viscometry

Dynamic viscosities were measured on an Anton Paar AMVn rolling ball viscometer. A glass capillary with 1.6 mm diameter was used together with a 1.5 mm diameter stainless steel ball, and filled with a 400 µl sample volume. The instrument was calibrated before use with deionised water. Viscosities were measured at 25 °C.

10.23.17 Printing Studies

Printing studies were carried out on either:

- a) A Domino G Series commercial printer using one print head with two rows of 150 nozzles linearly spaced at 85 μm , with the second row offset from the first. Maximum print height was 50.8 mm with 60-600 dpi resolution. Print speed capability varied from 300 m min^{-1} at 60 dpi to 30 m min^{-1} at 600 dpi. HP 45A-type cartridges were used which were manually filled up to a maximum volume of 42 ml.
- b) A Fujifilm Dimatix DMP 2831 research printer with 16 nozzles linearly spaced at 254 μm and a typical drop size of 1-10 pl. Maximum print height was 25 mm and the maximum print area was 200 mm x 300 mm. Cartridges were filled manually with sample solutions and had a minimum capacity of 1.5 ml.
- c) An ImageXpert JetXpert drop-in-flight analysis system was used in conjunction with a Domino G Series Printer. The Jet Xpert system involved an LED strobe with a pulse width of 100 to 1000 ns in 10 ns and a 752x480 pixel camera positioned either side of the drop curtain. A second 'wetting' camera was positioned in view of the nozzle plate. A built-in analysis system provided drop volume and velocity data.

References

1. T. K. Goh, S. Yamashita, K. Satoh, A. Blencowe, M. Kamigaito and G. G. Qiao, *Macromolecular Rapid Communications*, 2011, **32**, 456-461.
2. A. W. Bosman, H. M. Janssen and E. W. Meijer, *Chemical Reviews*, 1999, **99**, 1665-1688.
3. R. Yoshida, K. Uchida, Y. Kaneko, K. Sakai, A. Kikuchi, Y. Sakurai and T. Okano, *Nature*, 1995, **374**, 240-242.
4. D. M. Knauss and T. Z. Huang, *Macromolecules*, 2002, **35**, 2055-2062.
5. R. M. England and S. Rimmer, *Polymer Chemistry*, 2010, **1**, 1533-1544.
6. E. R. Gillies and J. M. J. Fréchet, *Drug Discovery Today*, 2005, **10**, 35-43.
7. R. van Heerbeek, P. C. J. Kamer, P. W. N. M. van Leeuwen and J. N. H. Reek, *Chemical Reviews*, 2002, **102**, 3717-3756.
8. S. Hopkins, S. R. Carter, J. W. Haycock, N. J. Fullwood, S. MacNeil and S. Rimmer, *Soft Matter*, 2009, **5**, 4928-4937.
9. S. Unal, I. Yilgor, E. Yilgor, J. P. Sheth, G. L. Wilkes and T. E. Long, *Macromolecules*, 2004, **37**, 7081-7084.
10. W. Ring, I. Mita, A. D. Jenkins and N. M. Bikales, *Pure and Applied Chemistry*, 1985, **57**, 1427-1440.
11. C. Feng, Y. J. Li, D. Yang, J. H. Hu, X. H. Zhang and X. Y. Huang, *Chemical Society Reviews*, 2011, **40**, 1282-1295.
12. M. F. Zhang and A. H. E. Muller, *Journal of Polymer Science Part A: Polymer Chemistry*, 2005, **43**, 3461-3481.
13. M. G. McKee, S. Unal, G. L. Wilkes and T. E. Long, *Progress in Polymer Science*, 2005, **30**, 507-539.
14. S. S. Sheiko, B. S. Sumerlin and K. Matyjaszewski, *Progress in Polymer Science*, 2008, **33**, 759-785.
15. H.-i. Lee, J. Pietrasik, S. S. Sheiko and K. Matyjaszewski, *Progress in Polymer Science*, 2010, **35**, 24-44.
16. S. S. Sheiko, F. C. Sun, A. Randall, D. Shirvanyants, M. Rubinstein, H. Lee and K. Matyjaszewski, *Nature*, 2006, **440**, 191-194.
17. I. Park, S. S. Sheiko, A. Nese and K. Matyjaszewski, *Macromolecules*, 2009, **42**, 1805-1807.
18. R. Barbey, L. Lavanant, D. Paripovic, N. Schuwer, C. Sugnaux, S. Tugulu and H. A. Klok, *Chemical Reviews*, 2009, **109**, 5437-5527.
19. K. Huang and J. Rzyayev, *Journal of the American Chemical Society*, 2009, **131**, 6880-6885.
20. J. Y. Yuan, Y. Y. Xu, A. Walther, S. Bolisetty, M. Schumacher, H. Schmalz, M. Ballauff and A. H. E. Muller, *Nature Materials*, 2008, **7**, 718-722.
21. L. Niimi, K. I. Serita, S. Hiraoka and T. Yokozawa, *Journal of Polymer Science Part A: Polymer Chemistry*, 2002, **40**, 1236-1242.
22. N. Hadjichristidis, M. Xenidou, H. Iatrou, M. Pitsikalis, Y. Poulos, A. Avgeropoulos, S. Sioula, S. Paraskeva, G. Velis, D. J. Lohse, D. N. Schulz, L. J. Fetters, P. J. Wright, R. A. Mendelson, C. A. Garcia-Franco, T. Sun and C. J. Ruff, *Macromolecules*, 2000, **33**, 2424-2436.
23. F. J. Hua, B. Liu, C. P. Hu and Y. L. Yang, *Journal of Polymer Science Part A: Polymer Chemistry*, 2002, **40**, 1876-1884.
24. J. M. G. Cowie and V. Arrighi, *Polymers: Chemistry and Physics of Modern Materials*, CRC Press, Boca Raton, 3rd edn., 2008.
25. D. C. Pepper, *Quarterly Reviews*, 1954, **8**, 88-121.
26. C. J. Hawker, A. W. Bosman and E. Harth, *Chemical Reviews*, 2001, **101**, 3661-3688.
27. D. H. Solomon, E. Rizzardo and P. Cacioli, *Chem. Abstr.*, 1985, **102**, 221335q.

28. K. Bian and M. F. Cunningham, *Journal of Polymer Science Part A: Polymer Chemistry*, 2006, **44**, 414-426.
29. Y. Guillaneuf, D. Gigmes, S. R. A. Marque, P. Astolfi, L. Greci, P. Tordo and D. Bertin, *Macromolecules*, 2007, **40**, 3108-3114.
30. T. Nakamura and M. Okubo, *Macromolecules*, 2007, **40**, 8663-8672.
31. E. Yoshida, *Colloid and Polymer Science*, 2010, **288**, 73-78.
32. D. Benoit, S. Grimaldi, S. Robin, J. P. Finet, P. Tordo and Y. Gnanou, *Journal of the American Chemical Society*, 2000, **122**, 5929-5939.
33. D. Benoit, V. Chaplinski, R. Braslau and C. J. Hawker, *Journal of the American Chemical Society*, 1999, **121**, 3904-3920.
34. D. Benoit, E. Harth, P. Fox, R. M. Waymouth and C. J. Hawker, *Macromolecules*, 2000, **33**, 363-370.
35. M. Kato, M. Kamigaito, M. Sawamoto and T. Higashimura, *Macromolecules*, 1995, **28**, 1721-1723.
36. J. S. Wang and K. Matyjaszewski, *Macromolecules*, 1995, **28**, 7572-7573.
37. Y. T. Li and S. P. Armes, *Macromolecules*, 2005, **38**, 8155-8162.
38. T. E. Patten, J. H. Xia, T. Abernathy and K. Matyjaszewski, *Science*, 1996, **272**, 866-868.
39. I. Y. Ma, E. J. Lobb, N. C. Billingham, S. P. Armes, A. L. Lewis, A. W. Lloyd and J. Salvage, *Macromolecules*, 2002, **35**, 9306-9314.
40. M. Save, J. V. M. Weaver, S. P. Armes and P. McKenna, *Macromolecules*, 2002, **35**, 1152-1159.
41. G. Odian, *Principles of Polymerisation*, Wiley & Sons, Hoboken N.J., 4th edn., 2004.
42. J. Chiefari, Y. K. Chong, F. Ercole, J. Krstina, J. Jeffery, T. P. T. Le, R. T. A. Mayadunne, G. F. Meijs, C. L. Moad, G. Moad, E. Rizzardo and S. H. Thang, *Macromolecules*, 1998, **31**, 5559-5562.
43. G. Moad, E. Rizzardo and S. H. Thang, *Accounts of Chemical Research*, 2008, **41**, 1133-1142.
44. G. Moad, F. Ercole, C. H. Johnson, J. Krstina, C. L. Moad, E. Rizzardo, T. H. Spurling, S. H. Thang and A. G. Anderson, *ACS Symposium Series*, 1998, **685**, 332-360.
45. R. T. Mayadunne, E. Rizzardo, J. Chiefari, J. Krstina, G. Moad, A. Postma and S. H. Thang, *Macromolecules*, 2000, **33**, 243-245.
46. J. F. Quinn, E. Rizzardo and T. P. Davis, *Chemical Communications*, 2001, 1044-1045.
47. D. Charmot, P. Corpart, H. Adam, S. Z. Zard, T. Biadatti and G. Bouhadir, *Macromolecular Symposia*, 2000, **150**, 23-32.
48. M. H. Stenzel, L. Cummins, G. E. Roberts, T. P. Davis, P. Vana and C. Barner-Kowollik, *Macromolecular Chemistry and Physics*, 2003, **204**, 1160-1168.
49. S. Perrier and P. Takolpuckdee, *Journal of Polymer Science Part A: Polymer Chemistry*, 2005, **43**, 5347-5393.
50. S. Kanagasabapathy, A. Sudalai and B. C. Benicewicz, *Macromolecular Rapid Communications*, 2001, **22**, 1076-1080.
51. A. B. Lowe and C. L. McCormick, *Progress in Polymer Science*, 2007, **32**, 283-351.
52. J. D. Biasutti, T. P. Davis, F. P. Lucien and J. P. A. Heuts, *Journal of Polymer Science Part A: Polymer Chemistry*, 2005, **43**, 2001-2012.
53. P. J. Flory, *Journal of the American Chemical Society*, 1952, **74**, 2718-2723.
54. Y. Kim, *Polymer Preprints (American Chemical Society, Division of Polymer Chemistry)*, 1988, **29**, 310-311.
55. Y. Ishida, A. C. F. Sun, M. Jikei and M.-A. Kakimoto, *Macromolecules*, 2000, **33**, 2832-2838.
56. W. Sinananwanich and M. Ueda, *Journal of Polymer Science Part A: Polymer Chemistry*, 2008, **46**, 2689-2700.

57. N. Liu, J. Vignolle, J.-M. Vincent, F. Robert, Y. Landais, H. Cramail and D. Taton, *Macromolecules*, 2014, **47**, 1532-1542.
58. J. M. J. Fréchet, M. Henmi, I. Gitsov, S. Aoshima, M. R. Leduc and R. B. Grubbs, *Science*, 1995, **269**, 1080-1083.
59. P. F. W. Simon, W. Radke and A. H. E. Müller, *Macromolecular Rapid Communications*, 1997, **18**, 865-873.
60. C. J. Hawker, J. M. J. Fréchet, R. B. Grubbs and J. Dao, *Journal of the American Chemical Society*, 1995, **117**, 10763-10764.
61. K. Matyjaszewski, S. G. Gaynor, A. Kulfan and M. Podwika, *Macromolecules*, 1997, **30**, 5192-5194.
62. Z. Wang, J. He, Y. Tao, L. Yang, H. Jiang and Y. Yang, *Macromolecules*, 2003, **36**, 7446-7452.
63. S. Carter, B. Hunt and S. Rimmer, *Macromolecules*, 2005, **38**, 4595-4603.
64. S. Carter, S. Rimmer, A. Sturdy and M. Webb, *Macromolecular Bioscience*, 2005, **5**, 373-378.
65. S. Perrier, P. Takolpuckdee and C. A. Mars, *Macromolecules*, 2005, **38**, 2033-2036.
66. A. Kumar, I. Y. Galaev and B. Mattiasson, *Biotechnology and Bioengineering*, 1998, **59**, 695-704.
67. J. K. Vasir, K. Tambwekar and S. Garg, *International Journal of Pharmaceutics*, 2003, **255**, 13-32.
68. J. E. Moses and A. D. Moorhouse, *Chemical Society Reviews*, 2007, **36**, 1249-1262.
69. H. Gao and K. Matyjaszewski, *Journal of the American Chemical Society*, 2007, **129**, 6633-6639.
70. C. Weber, C. R. Becer, R. Hoogenboom and U. S. Schubert, *Macromolecules*, 2009, **42**, 2965-2971.
71. V. Heroguez, Y. Gnanou and M. Fontanille, *Macromolecules*, 1997, **30**, 4791-4798.
72. L. Gu, Z. Shen, S. Zhang, G. Lu, X. Zhang and X. Huang, *Macromolecules*, 2007, **40**, 4486-4493.
73. S. Christodoulou, H. Iatrou, D. J. Lohse and N. Hadjichristidis, *Journal of Polymer Science Part A: Polymer Chemistry*, 2005, **43**, 4030-4039.
74. K. L. Beers, S. G. Gaynor, K. Matyjaszewski, S. S. Sheiko and M. Möller, *Macromolecules*, 1998, **31**, 9413-9415.
75. R. B. Grubbs, C. J. Hawker, J. Dao and J. M. J. Fréchet, *Angewandte Chemie International Edition in English*, 1997, **36**, 270-272.
76. Y. Zhang, Z. Shen, D. Yang, C. Feng, J. Hu, G. Lu and X. Huang, *Macromolecules*, 2009, **43**, 117-125.
77. H. Kipphan, *Handbook of Print Media: Technologies and Production Methods*, Springer, Berlin, 2001.
78. F. Savart, *Ann. Chim. Phys*, 1833, **53**, 337.
79. E. F. Goedde and M. C. Yuen, *Journal of Fluid Mechanics*, 1970, **40**, 495-511.
80. J. R. Castrejon-Pita, W. R. S. Baxter, J. Morgan, S. Temple, G. D. Martin and I. M. Hutchings, *Atomization and Sprays*, 2013, **23**, 541-565.
81. H. P. Le, *Journal of Imaging Science and Technology*, 1998, **42**, 49-62.
82. O. A. Basaran, H. J. Gao and P. P. Bhat, *Nonstandard Inkjets*, Annual Reviews, Palo Alto, 1st edn., 2013.
83. R. G. Sweet, *Review of Scientific Instruments*, 1965, **36**, 131-136.
84. <http://www.dp3project.org/technologies/digital-printing/inkjet>, (accessed 3rd September, 2014).
85. J. Brünahl and A. M. Grishin, *Sensors and Actuators A: Physical*, 2002, **101**, 371-382.
86. *GB Pat.*, GB2007162, 1979.

87. S. Magdassi, in *The Chemistry of Inkjet Inks*, World Scientific, Singapore, 2010, pp. 19-41.
88. J. G. Korvink, P. J. Smith, D. Y. Shin, O. Brand, G. K. Fedder, C. Hierold and O. Tabata, *Inkjet-based Micromanufacturing*, Wiley, Hoboken, 2012.
89. B. Derby and N. Reis, *MRS Bulletin*, 2003, **28**, 815-818.
90. M. Goldin, J. Yerushalmi, R. Pfeffer and R. Shinnar, *Journal of Fluid Mechanics*, 1969, **38**, 689-711.
91. R. P. Mun, J. A. Byars and D. V. Boger, *Journal of Non-Newtonian Fluid Mechanics*, 1998, **74**, 285-297.
92. D. C. Vadillo, S. D. Hoath, W.-K. Hsiao and M. R. Mackley, *NIP & Digital Fabrication Conference*, 2011, **2011**, 568-572.
93. C. Clasen, J. P. Plog, W.-M. Kulicke, M. Owens, C. Macosko, L. E. Scriven, M. Verani and G. H. McKinley, *Journal of Rheology (1978-present)*, 2006, **50**, 849-881.
94. S. D. Hoath, O. G. Harlen and I. M. Hutchings, *Journal of Rheology (1978-present)*, 2012, **56**, 1109-1127.
95. M. Cima, E. Sachs, L. Cima, J. Yoo, S. Khanuja, S. Borland, B. Wu and R. Giordano, Solid Freeform Fabrication Symposium Proceedings, Austin, Texas, 1994.
96. B. Utela, D. Storti, R. Anderson and M. Ganter, *Journal of Manufacturing Processes*, 2008, **10**, 96-104.
97. J. Bharathan and Y. Yang, *Applied Physics Letters*, 1998, **72**, 2660-2662.
98. J. F. Dijkman, P. C. Duineveld, M. J. J. Hack, A. Pierik, J. Rensen, J. E. Rubingh, I. Schram and M. M. Vernhout, *Journal of Materials Chemistry*, 2007, **17**, 511-522.
99. H. Sirringhaus, T. Kawase, R. H. Friend, T. Shimoda, M. Inbasekaran, W. Wu and E. P. Woo, *Science*, 2000, **290**, 2123-2126.
100. R. Parashkov, E. Becker, T. Riedl, H. Johannes and W. Kowalsky, *Proceedings of the IEEE*, 2005, **93**, 1321-1329.
101. T. F. Marinis, *Strain*, 2009, **45**, 208-220.
102. H. A. Stone, A. D. Stroock and A. Ajdari, *Annual Review of Fluid Mechanics*, 2004, **36**, 381-411.
103. R. M. Verkouteren, G. Gillen and D. W. Taylor, *Review of Scientific Instruments*, 2006, **77**, 085104.
104. E. Sachs, M. Cima, P. Williams, D. Brancazio and J. Cornie, *Journal of Manufacturing Science and Engineering*, 1992, **114**, 481-488.
105. K. A. M. Seerden, N. Reis, J. R. G. Evans, P. S. Grant, J. W. Halloran and B. Derby, *Journal of the American Ceramic Society*, 2001, **84**, 2514-2520.
106. B. V. Antohe and D. B. Wallace, ASME 2008 International Manufacturing Science and Engineering Conference collocated with the 3rd JSME/ASME International Conference on Materials and Processing, 2008.
107. B. Derby, *Science*, 2012, **338**, 921-926.
108. V. Mironov, T. Boland, T. Trusk, G. Forgacs and R. R. Markwald, *Trends in Biotechnology*, 2003, **21**, 157-161.
109. M. Nakamura, A. Kobayashi, F. Takagi, A. Watanabe, Y. Hiruma, K. Ohuchi, Y. Iwasaki, M. Horie, I. Morita and S. Takatani, *Tissue Engineering*, 2005, **11**, 1658-1666.
110. J. Sumerel, J. Lewis, A. Doraiswamy, L. F. Deravi, S. L. Sewell, A. E. Gerdon, D. W. Wright and R. J. Narayan, *Biotechnology Journal*, 2006, **1**, 976-987.
111. L. Setti, A. Fraleoni-Morgera, B. Ballarin, A. Filippini, D. Frascaro and C. Piana, *Biosensors and Bioelectronics*, 2005, **20**, 2019-2026.
112. M. Mutoh, *Physics of Fluids (1994-present)*, 2002, **14**, 1380-1388.
113. G. D. Martin, S. D. Hoath and I. M. Hutchings, *Journal of Physics: Conference Series*, 2008, **105**, 012001.

114. H. Dong, W. W. Carr and J. F. Morris, *Review of Scientific Instruments*, 2006, **77**, 085101.
115. K.-S. Kwon, *Journal of Micromechanics and Microengineering*, 2010, **20**, 115005.
116. M. C. Withiam, International Conference on Digital Printing Technologies, 1996.
117. H. K. Lee, M. K. Joyce, P. D. Fleming and J. Cameron, Proceedings of the TAPPI Coating Conference, 2002.
118. <http://www.pcimag.com/articles/dynamic-surface-tension-and-surface-energy-in-ink-formulations-and-substrates>, (accessed 4th September, 2014).
119. C. Poisson, V. Hervais, M. F. Lacrampe and P. Krawczak, *Journal of Applied Polymer Science*, 2006, **101**, 118-127.
120. F. Awaja, M. Gilbert, G. Kelly, B. Fox and P. J. Pigram, *Progress in Polymer Science*, 2009, **34**, 948-968.
121. A. Kinloch, *Journal of Material Science*, 1980, **15**, 2141-2166.
122. V. E. Basin, *Progress in Organic Coatings*, 1984, **12**, 213-250.
123. R.-Y. Qin and H. P. Schreiber, *Colloids and Surfaces A: Physicochemical and Engineering Aspects*, 1999, **156**, 85-93.
124. D. Schaubroeck, J. De Baets, T. Desmet, S. Van Vlierberghe, E. Schacht and A. Van Calster, *Applied Surface Science*, 2009, **255**, 8780-8787.
125. J.-H. Chen and E. Ruckenstein, *Journal of Colloid and Interface Science*, 1990, **135**, 496-507.
126. M. J. John and R. D. Anandjiwala, *Composites Part A: Applied Science and Manufacturing*, 2009, **40**, 442-448.
127. J. Lai, B. Sunderland, J. Xue, S. Yan, W. Zhao, M. Folkard, B. D. Michael and Y. Wang, *Applied Surface Science*, 2006, **252**, 3375-3379.
128. Q. F. Wei, *Materials Characterization*, 2004, **52**, 231-235.
129. B. Boschmans, M. Vanneste, L. Ruys, E. Temmerman, C. Leys and L. Van Vaeck, *Applied Surface Science*, 2006, **252**, 6660-6663.
130. N. Dilsiz, N. K. Erinc, E. Bayramli and G. Akovali, *Carbon*, 1995, **33**, 853-858.
131. V. Fombuena, D. Garcia-Sanoguera, L. Sanchez-Nacher, R. Balart and T. Boronat, *Journal of Adhesion Science and Technology*, 2014, **28**, 97-113.
132. H. N. A. M. Steenbakkers-Menting, P. E. L. Voets and P. J. Lemstra, *Journal of Adhesion Science and Technology*, 1995, **9**, 889-897.
133. M. Abdullin, A. Glazyrin, R. Asfandiyarov and R. Muslukhov, *Polymer Science Series B*, 2009, **51**, 303-308.
134. C. L. Aronson, L. G. Beholz, D. Beloskur, B. Burland and J. Perez, *Polymer Bulletin*, 2005, **53**, 401-412.
135. A. P. Kharitonov and L. N. Kharitonova, *Pure and Applied Chemistry*, 2009, **81**, 451-471.
136. A. Falsafi, F. S. Bates and M. Tirrell, *Macromolecules*, 2001, **34**, 1323-1327.
137. A. C. Balazs, M. Gempe and C. W. Lantman, *Macromolecules*, 1991, **24**, 168-176.
138. A. Baron, J. Rodriguez-Hernandez, E. Ibarboure, C. Derail and E. Papon, *International Journal of Adhesion and Adhesives*, 2009, **29**, 1-8.
139. C.-J. Hung, H.-Y. Chuang and F.-C. Chang, *Journal of Applied Polymer Science*, 2008, **107**, 831-839.
140. J. B. Zhang, P. J. Cole, U. Nagpal, C. W. Macosko and T. P. Lodge, *Journal of Adhesion*, 2006, **82**, 887-902.
141. C. Boyer, B. Boutevin and J. J. Robin, *Polymer Degradation and Stability*, 2005, **90**, 326-339.
142. K. Cho, S. Kyung Hoon, A. Tae Oan, K. Jungahn and K. Kwang Ung, *Polymer*, 1997, **38**, 4825-4830.
143. M. Y. Ju and F. C. Chang, *Polymer*, 2000, **41**, 1719-1730.
144. G. Jiang, H. Wu and S. Guo, *Polymer Engineering & Science*, 2010, **50**, 2273-2286.

145. B. Gupta, C. Plummer, I. Bisson, P. Frey and J. Hilborn, *Biomaterials*, 2002, **23**, 863-871.
146. C.-L. Li, C.-Y. Tu, J.-S. Huang, Y.-L. Liu, K.-R. Lee and J.-Y. Lai, *Surface and Coatings Technology*, 2006, **201**, 63-72.
147. H. Y. Kim, W. Joo and J. K. Kim, *Macromolecular Chemistry and Physics*, 2008, **209**, 746-753.
148. Z. S. Fu, M. Liu, J. T. Xu, Q. Wang and Z. Q. Fan, *Journal of Applied Polymer Science*, 2011, **119**, 1111-1121.
149. H. Shi, D. Shi, Z. Yao, S. Luan, J. Jin, J. Zhao, H. Yang, P. Stagnaro and J. Yin, *Polymer Chemistry*, 2011, **2**, 679-684.
150. G. Yilmaz, H. Toiserkani, D. O. Demirkol, S. Sakarya, S. Timur, Y. Yagci and L. Torun, *Journal of Polymer Science Part A: Polymer Chemistry*, 2011, **49**, 110-117.
151. S. R. Carter, R. M. England, B. J. Hunt and S. Rimmer, *Macromolecular Bioscience*, 2007, **7**, 975-986.
152. Y. K. Chong, T. P. T. Le, G. Moad, E. Rizzardo and S. H. Thang, *Macromolecules*, 1999, **32**, 2071-2074.
153. R. T. A. Mayadunne, J. Jeffery, G. Moad and E. Rizzardo, *Macromolecules*, 2003, **36**, 1505-1513.
154. G. Moad, R. T. A. Mayadunne, E. Rizzardo, M. Skidmore and S. H. Thang, *Macromolecular Symposia*, 2003, **192**, 1-12.
155. S. Carter, S. Rimmer, R. Rutkaite, L. Swanson, J. P. A. Fairclough, A. Sturdy and M. Webb, *Biomacromolecules*, 2006, **7**, 1124-1130.
156. Z. Muchtar, M. Schappacher and A. Deffieux, *Macromolecules*, 2001, **34**, 7595-7600.
157. T. Higashihara, M. Nagura, K. Inoue, N. Haraguchi and A. Hirao, *Macromolecules*, 2005, **38**, 4577-4587.
158. A. Hirao, A. Matsuo and T. Watanabe, *Macromolecules*, 2005, **38**, 8701-8711.
159. M. Babazadeh, *Journal of Applied Polymer Science*, 2006, **102**, 633-639.
160. J. F. Quinn, R. P. Chaplin and T. P. Davis, *Journal of Polymer Science Part A: Polymer Chemistry*, 2002, **40**, 2956-2966.
161. M. Stenzel-Rosenbaum, T. P. Davis, V. Chen and A. G. Fane, *Journal of Polymer Science Part A: Polymer Chemistry*, 2001, **39**, 2777-2783.
162. J. J. Vosloo, M. P. Tonge, C. M. Fellows, F. D'Agosto, R. D. Sanderson and R. G. Gilbert, *Macromolecules*, 2004, **37**, 2371-2382.
163. H. Mori and A. H. E. Müller, *Progress in Polymer Science*, 2003, **28**, 1403-1439.
164. E. Rizzardo, J. Chiefari, B. Y. K. Chong, F. Ercole, J. Krstina, J. Jeffery, T. P. T. Le, R. T. A. Mayadunne, G. F. Meijs, C. L. Moad, G. Moad and S. H. Thang, *Macromolecular Symposia*, 1999, **143**, 291-307.
165. D. E. Poree, M. D. Giles, L. B. Lawson, J. He and S. M. Grayson, *Biomacromolecules*, 2011, **12**, 898-906.
166. T. Krivorotova, R. Grigelis, J. Jonikaite and R. Makuska, *Chemija*, 2011, **22**, 248-254.
167. E. V. Dehmlow, *Angewandte Chemie International Edition in English*, 1974, **13**, 170-179.
168. C. M. Starks, C. L. Liotta and M. E. Halpern, *Phase-Transfer Catalysis*, Chapman & Hall, New York, 1994.
169. T. Ooi and K. Maruoka, *Angewandte Chemie International Edition*, 2007, **46**, 4222-4266.
170. J. K. Rasmussen and H. K. Smith, *Journal of the American Chemical Society*, 1981, **103**, 730-731.
171. T. Balakrishnan and S. Damodarkumar, *Journal of Applied Polymer Science*, 2000, **76**, 1564-1571.
172. T. D. N'Guyen, A. Deffieux and S. Boileau, *Polymer*, 1978, **19**, 423-426.

173. J. M. J. Fréchet, M. D. De Smet and M. J. Farrall, *The Journal of Organic Chemistry*, 1979, **44**, 1774-1779.
174. Y. Luo, J. Guo, Y. Liu, Q. Shao, C. Wang and D. Chu, *Journal of Membrane Science*, 2012, **423-424**, 209-214.
175. L. Couvreur, C. Lefay, J. Bellenev, B. Charleux, O. Guerret and S. Magnet, *Macromolecules*, 2003, **36**, 8260-8267.
176. H. Magnusson, E. Malmstrom, A. Hult and M. Johansson, *Polymer*, 2002, **43**, 301-306.
177. X. Y. Zhu, Y. F. Zhou and D. Y. Yan, *Journal of Polymer Science Part B-Polymer Physics*, 2011, **49**, 1277-1286.
178. S. Rimmer, S. Carter, R. Rutkaite, J. W. Haycock and L. Swanson, *Soft Matter*, 2007, **3**, 971-973.
179. J. Liu, Y. Wang, Q. Fu, X. Zhu and W. Shi, *Journal of Polymer Science Part A: Polymer Chemistry*, 2008, **46**, 1449-1459.
180. B. Yamada, O. Konosu, K. Tanaka and F. Oku, *Polymer*, 2000, **41**, 5625-5631.
181. S. Peleshanko, R. Gunawidjaja, S. Petrash and V. V. Tsukruk, *Macromolecules*, 2006, **39**, 4756-4766.
182. J. Chiefari, R. T. A. Mayadunne, C. L. Moad, G. Moad, E. Rizzardo, A. Postma, M. A. Skidmore and S. H. Thang, *Macromolecules*, 2003, **36**, 2273-2283.
183. F. A. Bovey, *Accounts of Chemical Research*, 1968, **1**, 175-185.
184. F. P. Price, *The Journal of Chemical Physics*, 1962, **36**, 209-218.
185. L. Merle and Y. Merle, *Macromolecules*, 1982, **15**, 360-366.
186. J. C. Randall, *Polymer Sequence Determination*, Academic Press, New York, 1st edn., 1977.
187. J. Schaefer and D. F. S. Natusch, *Macromolecules*, 1972, **5**, 416-427.
188. J. S. Román and M. Valero, *Polymer*, 1990, **31**, 1216-1221.
189. F. A. Bovey, *High Resolution NMR of Macromolecules*, Academic Press, New York, 1st edn., 1972.
190. M. Gaborieau, R. G. Gilbert, A. Gray-Weale, J. M. Hernandez and P. Castignolles, *Macromolecular Theory and Simulations*, 2007, **16**, 13-28.
191. L. Garamszegi, T. Q. Nguyen, C. J. G. Plummer and J. A. E. Månson, *Journal of Liquid Chromatography & Related Technologies*, 2003, **26**, 207-230.
192. A. Choucair and A. Eisenberg, *European Physical Journal E*, 2003, **10**, 37-44.
193. J.-F. Lutz, *Polymer International*, 2006, **55**, 979-993.
194. Y. Geng, F. Ahmed, N. Bhasin and D. E. Discher, *The Journal of Physical Chemistry B*, 2005, **109**, 3772-3779.
195. D. E. Discher and A. Eisenberg, *Science*, 2002, **297**, 967-973.
196. L. Zhang and A. Eisenberg, *Journal of the American Chemical Society*, 1996, **118**, 3168-3181.
197. A. Blanz, S. P. Armes and A. J. Ryan, *Macromolecular Rapid Communications*, 2009, **30**, 267-277.
198. M. Pitsikalis, J. Woodward, J. W. Mays and N. Hadjichristidis, *Macromolecules*, 1997, **30**, 5384-5389.
199. H. Hong, Y. Mai, Y. Zhou, D. Yan and J. Cui, *Macromolecular Rapid Communications*, 2007, **28**, 591-596.
200. K. Khanna, S. Varshney and A. Kakkar, *Polymer Chemistry*, 2010, **1**, 1171-1185.
201. Y. Zhou and D. Yan, *Chemical Communications*, 2009, 1172-1188.
202. Y. Zhou, W. Huang, J. Liu, X. Zhu and D. Yan, *Advanced Materials*, 2010, **22**, 4567-4590.
203. O. Glatter and O. Kratky, *Small Angle X-ray Scattering*, Academic Press, London, 1982.
204. J. S. Higgins and H. C. Benoit, *Polymers and Neutron Scattering*, Clarendon Press, Oxford, 1994.
205. J. Teixeira, *Journal of Applied Crystallography*, 1988, **21**, 781-785.

206. D. Stauffer, *Journal of the Chemical Society, Faraday Transactions 2: Molecular and Chemical Physics*, 1976, **72**, 1354-1364.
207. P.-G. De Gennes, *Scaling Concepts in Polymer Physics*, Cornell University Press, Ithaca, 1979.
208. http://www.ncnr.nist.gov/staff/hammouda/distance_learning/chapter_33.pdf, (accessed 10th March, 2015).
209. G. Guinier and A. Fournet, *Small Angle Scattering by X-Rays*, Wiley, New York, 1955.
210. M. Bergström, J. S. Pedersen, P. Schurtenberger and S. U. Egelhaaf, *The Journal of Physical Chemistry B*, 1999, **103**, 9888-9897.
211. S. Jain and F. S. Bates, *Science*, 2003, **300**, 460-464.
212. B. M. Discher, Y.-Y. Won, D. S. Ege, J. C.-M. Lee, F. S. Bates, D. E. Discher and D. A. Hammer, *Science*, 1999, **284**, 1143-1146.
213. L. Zhang and A. Eisenberg, *Science*, 1995, **268**, 1728-1731.
214. Y. Zhou and D. Yan, *Angewandte Chemie International Edition*, 2004, **43**, 4896-4899.
215. J. N. Israelachvili, D. J. Mitchell and B. W. Ninham, *Journal of the Chemical Society, Faraday Transactions 2: Molecular and Chemical Physics*, 1976, **72**, 1525-1568.
216. M. Antonietti and S. Förster, *Advanced Materials*, 2003, **15**, 1323-1333.
217. N. J. Warren and S. P. Armes, *Journal of the American Chemical Society*, 2014, **136**, 10174-10185.
218. O. Terreau, C. Bartels and A. Eisenberg, *Langmuir*, 2003, **20**, 637-645.
219. K. Yu and A. Eisenberg, *Macromolecules*, 1996, **29**, 6359-6361.
220. L. Li, K. Matsunaga, J. Zhu, T. Higuchi, H. Yabu, M. Shimomura, H. Jinnai, R. C. Hayward and T. P. Russell, *Macromolecules*, 2010, **43**, 7807-7812.
221. H. Yabu, T. Higuchi, K. Ijiro and M. Shimomura, *Chaos: An Interdisciplinary Journal of Nonlinear Science*, 2005, **15**, 047505.
222. S. Jain and F. S. Bates, *Macromolecules*, 2004, **37**, 1511-1523.
223. P. L. Ritger and N. A. Peppas, *Journal of Controlled Release*, 1987, **5**, 23-36.
224. J. Lukáš, R. N. S. Sodhi and M. V. Sefton, *Journal of Colloid and Interface Science*, 1995, **174**, 421-427.
225. I. Luzinov, S. Minko and V. V. Tsukruk, *Progress in Polymer Science*, 2004, **29**, 635-698.
226. D. Y. Kwok and A. W. Neumann, *Colloids and Surfaces A: Physicochemical and Engineering Aspects*, 2000, **161**, 31-48.
227. R. J. Good and C. J. van Oss, *The Modern Theory of Contact Angles and the Hydrogen Bond Components of Surface Energies*, Springer, New York, 1st edn., 1992.
228. F. M. Fowkes, *The Journal of Physical Chemistry*, 1962, **66**, 382-382.
229. D. K. Owens and R. C. Wendt, *Journal of Applied Polymer Science*, 1969, **13**, 1741-1747.
230. J. Kloubek, *The Journal of Adhesion*, 1974, **6**, 293-301.
231. S. Wu, *The Journal of Adhesion*, 1973, **5**, 39-55.
232. D. Li and A. W. Neumann, *Journal of Colloid and Interface Science*, 1992, **148**, 190-200.
233. J. Schultz, K. Tsutsumi and J.-B. Donnet, *Journal of Colloid and Interface Science*, 1977, **59**, 272-276.
234. T. Hugel and M. Seitz, *Macromolecular Rapid Communications*, 2001, **22**, 989-1016.
235. A. Noy, D. V. Vezenov and C. M. Lieber, *Annual Review of Materials Science*, 1997, **27**, 381-421.
236. M. Ludwig, W. Dettmann and H. E. Gaub, *Biophysical Journal*, 1997, **72**, 445-448.
237. M. Radmacher, R. W. Tillmann and H. E. Gaub, *Biophysical Journal*, 1993, **64**, 735-742.
238. H.-J. Butt, *Biophysical Journal*, 1992, **63**, 578-582.
239. W. F. Heinz and J. H. Hoh, *Biophysical Journal*, 1999, **76**, 528-538.
240. H.-J. Butt, B. Cappella and M. Kappl, *Surface Science Reports*, 2005, **59**, 1-152.
241. Z. Zhang, M. R. Tomlinson, R. Golestanian and M. Geoghegan, *Nanotechnology*, 2008, **19**, 035505.

242. C. Ortiz and G. Hadziioannou, *Macromolecules*, 1999, **32**, 780-787.
243. F. Andrea Alessandrini and Paolo, *Measurement Science and Technology*, 2005, **16**, R65.
244. H. Li, B. Liu, X. Zhang, C. Gao, J. Shen and G. Zou, *Langmuir*, 1999, **15**, 2120-2124.
245. S. Yamamoto, Y. Tsujii and T. Fukuda, *Macromolecules*, 2000, **33**, 5995-5998.
246. C. Liu, S. Cui, Z. Wang and X. Zhang, *The Journal of Physical Chemistry B*, 2005, **109**, 14807-14812.
247. Q. Xu, W. Zhang and X. Zhang, *Macromolecules*, 2001, **35**, 871-876.
248. S. Cui, C. Liu, W. Zhang, X. Zhang and C. Wu, *Macromolecules*, 2003, **36**, 3779-3782.
249. J. P. Aime, Z. Elkaakour, C. Odin, T. Bouhacina, D. Michel, J. Curely and A. Dautant, *Journal of Applied Physics*, 1994, **76**, 754-762.
250. H. A. Mizes, K. G. Loh, R. J. D. Miller, S. K. Ahuja and E. F. Grabowski, *Applied Physics Letters*, 1991, **59**, 2901-2903.
251. T. Han, J. M. Williams and T. P. Beebe Jr, *Analytica Chimica Acta*, 1995, **307**, 365-376.
252. C. Boyer, J. Q. Liu, V. Bulmus and T. P. Davis, *Australian Journal of Chemistry*, 2009, **62**, 830-847.
253. J. Xu, J. He, D. Fan, X. Wang and Y. Yang, *Macromolecules*, 2006, **39**, 8616-8624.
254. L. Barner and S. Perrier, in *Handbook of RAFT Polymerization*, ed. C. Barner-Kowollik, Wiley-VCH, Weinheim, 1st edn., 2008, pp. 455-482.
255. J. Brandrup, E. H. Immergut and E. A. Grulke, *Polymer Handbook*, Wiley, New York, 4th edn., 2003.
256. J. Eggers, *Reviews of Modern Physics*, 1997, **69**, 865-930.
257. www.kruss.de/services/education-theory/substance-data/solids, (accessed 7th January, 2015).

Appendix 1: Analysis of Variance (ANOVA)

One-Way ANOVA

The one-way ANOVA is used to determine whether there is a significant difference between three or more independent groups, based on the assumption that the populations are Gaussian.

The test determines whether there is any difference between related means. The null hypothesis states that the means are equal:

$$H_0: \mu_1 = \mu_2 = \mu_3 = \dots = \mu_k \quad \text{Equation A1.1}$$

where μ is the population mean and k is the number of related groups.

If the one-way ANOVA returns a significant result then the alternative hypothesis, H_A , is accepted. The alternative hypothesis states that the related means are not equal, and at least one mean is different to another mean. The test involves the fitting of a regression model.

In the ANOVA test, the total variability of the means is partitioned into variability within groups (due to the treatment) and variability between groups (residual variation). A mean sum of squares is determined both between groups (sum of squares of differences between group means and overall mean of all values in all groups, known as treatment sum of squares) and within groups (sum of squares of differences between each value and the group mean, known as residual sum of squares). Each sum of squares is associated with a certain number of degrees of freedom (DF) which is calculated from the number of subjects and the number of groups. The mean square (MS) is calculated by dividing the sum of squares by the appropriate number of degrees of freedom. This represents the variance.

The F -statistic is calculated as the ratio of the two mean square values. This is compared to a critical value, F_{crit} , obtained from statistical tables for the required DF. and significance level or α value. The α value used is often 0.05, which corresponds to a 95% confidence level. The null hypothesis is accepted when F is less than F_{crit} . P reports the significance level of the result. An R^2 value can be calculated to assess the model fit by calculating the ratio of the variation between groups to the variation within groups. R^2 is the fraction of the overall variance of all data which is attributable to differences

among the group means. A large R^2 value means that a large fraction of the variation is due to the treatment that defines the groups. It is a descriptive statistic that quantifies the strength of the relationship between group membership and the measured variable.

If the null hypothesis is true, F would be expected to have a value close to 1.0 most of the time. A large F ratio means that the variation among group means is greater than would be expected by chance. A large F ratio is seen both when the null hypothesis is wrong (the data are not sampled from populations with the same mean) and when large values in some groups and small values in others occurred due to random sampling. **Table A1.1** shows the results of a one-way ANOVA analysis on a sample dataset.

Table A1.1. Table showing results of one-way ANOVA analysis on sample data

Source of variation	Sum of squares	DF	MS	F	F_{crit}	P	R^2
Between groups	10600	6	1770	264	2.18	<0.0001	0.658
Within groups	5510	825	6.68				
Total	16100	831					

Two-Way ANOVA

The two-way ANOVA is an extension of the ANOVA method which is used to analyse variance in data sets where there are two independent variables. In this test, the variability among values is divided into four components: row factor, column factor, interaction between column and row factor (differences between rows that aren't the same at each column and differences between columns that aren't the same at each row), and the variation among replicates not due to systematic differences between rows and columns (residual variation). As in the one-way ANOVA, the sum-of-squares, degrees of freedom, mean square, and the F ratio are calculated for each component.

The two-way ANOVA tests three null hypotheses. The null hypothesis for the interaction term between column and row factor is that there is no interaction between

columns, representing data sets, and rows, in other words any systematic differences between columns are the same for each row and vice versa. The null hypothesis for the column factor is that the mean of each column is the same in the overall population and all differences are due to chance; with the equivalent null hypothesis for the row factor.

Table A1.2 shows the results of a one-way ANOVA analysis on a sample dataset.

Table A1.2. Table showing results of two-way ANOVA analysis on sample data

Source of variation	Sum of squares	DF	Variance	<i>F</i>	<i>F</i> _{crit}	P
Interaction	0.000327	18	1.82 x10 ⁻⁵	1.11	1.66	0.3511
Column factor	0.00121	3	4.04 x10 ⁻⁴	3.27	3.24	0.0488
Row factor	0.425	6	7.08 x10 ⁻²	4340	2.18	< 0.0001
Subjects (matching)	0.00198	16	1.24 x10 ⁻⁴	7.58	1.75	< 0.0001
Residual	0.00157	96	1.63 x10 ⁻⁵			

Tukey Post-Hoc Test

When a significant result is obtained from the ANOVA (i.e. the null hypothesis is rejected), the Tukey post-hoc test is used to determine which means are significantly different from each other. This applies the formula:

$$HSD = q\sqrt{\frac{MS_{within}}{n}} \quad \text{Equation A1.2}$$

where *HSD* is the honest significant difference, *MS_{within}* is obtained from the ANOVA results table, *n* is the number of values in each group and *q* is the studentised range statistic, obtained from statistical tables.

Once P values are obtained from the Tukey post-hoc test for each set of means, the results are displayed graphically using asterisks to display the significance level.

Appendix 2: Parameters obtained from Model Fitting to SANS Data

Results of Model Fitting to SANS Data of P(nMA-AA) Copolymers in d-THF

Table A2.1 Gaussian model

sample	M_w/M_n	$R_g / \text{\AA}$	dispersity in R_g	χ^2
HBR1	5.00	87.4	0.215	0.817
HBR2	4.10	74.2	0.004	0.768
HBR3	4.96	50.5	0.004	0.947
LR1	5.00	90.4	0.114	0.769
LR2	5.00	64.5	0.106	0.717
LR3	2.75	57.8	0.001	0.900
G1	1.04	98.7	0.072	0.799
G2	1.70	148.0	0.051	0.869
G3	1.86	68.7	0.332	1.430
HBM1	3.11	145.0	0.141	0.983
HBM2	3.43	90.5	0.094	0.800
HBM3	3.00	106.1	0.023	1.336

Results of Model Fitting to SANS Data of P(nMA-AA) Copolymers in 1:1 d-THF:D₂O Mixture

Table A2.2. Absolute Power Law

sample	m	χ^2
HBR1	3.22	2.497
HBR2	3.75	0.799
HBR3	0.87	1.057
LR1	1.24	1.712
LR2	1.09	0.888
LR3	4.01	3.795
G1	3.88	47.168
G2	3.66	245.150
G3	4.09	4.254
HBM1	3.99	0.732
HBM2	3.63	2.202
HBM3	3.68	255.740

Table A2.3 Gaussian model

sample	M_w/M_n	$R_g / \text{\AA}$	dispersity in R_g	χ^2
HBR1	1.00	572.8	0.018	2.889
HBR2	1.59	419.5	0.000	4.499
HBR3	5.00	65.2	0.034	1.057
LR1	2.95	69.1	0.000	0.776
LR2	1.00	559.7	0.000	46.191
LR3	5.99	424.6	0.000	110.950
G1	1.60	272.4	0.018	464.050
G2	2.69	251.4	0.000	1007.600
G3	1.35	318.3	0.016	368.480
HBM1	1.66	721.1	0.000	22.899
HBM2	1.31	491.7	0.011	12.252
HBM3	1.36	171.6	0.093	3408.000

Table A2.4. Fractal Model

sample	correlation length, $\xi / \text{\AA}$	fractal dimension	radius / \AA	SLD block / \AA^{-2}	dispersity in radius	χ^2
HBR1	1310.6	3.00	20.1	2.23×10^{-6}	0.300	0.864
HBR2	1711.7	3.01	20.9	2.29×10^{-6}	0.083	0.890
HBR3	110.2	1.09	3.6	1.33×10^{-6}	0.007	0.955
LR1	38.9	1.94	3.2	2.02×10^{-6}	0.005	0.767
LR2	1026.4	3.01	14.6	1.58×10^{-6}	0.001	0.982
LR3	1292.4	3.00	11.4	1.41×10^{-6}	0.079	1.217
G1	197.6	3.07	13.6	1.97×10^{-6}	0.127	3.740
G2	225.5	3.00	6.3	2.00×10^{-6}	0.009	43.478
G3	1383.5	3.00	6.9	1.40×10^{-6}	0.003	1.450
HBM1	1593.7	3.00	11.0	2.09×10^{-6}	0.173	0.968
HBM2	347.2	3.05	17.7	2.00×10^{-6}	0.617	0.976
HBM3	162.6	3.06	6.6	1.48×10^{-6}	0.349	5.954

TableA2.5. Sphere Model

sample	radius /Å	SLD sphere /Å ⁻²	dispersity in radius	χ^2
HBR1	1242.4	4.34 x10 ⁻⁶	0.075	2.419
HBR2	1324.6	4.51 x10 ⁻⁶	0.162	2.544
HBR3	1267.1	5.38 x10 ⁻⁶	0.033	4.726
LR1	1248.1	5.59 x10 ⁻⁶	0.036	16.85
LR2	1322.2	3.08 x10 ⁻⁶	0.095	1.555
LR3	712.2	3.17 x10 ⁻⁶	0.330	2.071
G1	437.4	3.54 x10 ⁻⁶	0.238	1.823
G2	443.0	2.33 x10 ⁻⁶	0.171	21.355
G3	898.0	1.58 x10 ⁻⁶	0.095	2.206
HBM1	1274.0	4.06 x10 ⁻⁶	0.140	1.087
HBM2	2125.7	2.08 x10 ⁻⁶	0.226	2.904
HBM3	1236.9	1.67 x10 ⁻⁶	0.063	19.561

Results of Model Fitting to SANS Data of P(nMA-AA) Copolymers in D₂O**Table A2.6. Absolute Power Law**

sample	range	<i>m</i>	χ^2	range	<i>m</i>	χ^2
HBR1	Q < 0.03	3.92	1.153	Q > 0.03	0.18	0.789
HBR2	Q < 0.03	4.20	0.591	Q > 0.03	0.36	0.789
HBR3	Q < 0.03	2.99	1.720	Q > 0.03	1.49 x10 ⁻⁴	0.735
LR1	Q < 0.03	4.13	0.962	Q > 0.03	0.63	0.865
LR2	Q < 0.03	3.81	1.937	Q > 0.03	1.00	0.811
LR3	Q < 0.03	3.42	3.199	Q > 0.03	1.367	0.742
G1	Q < 0.06	3.93	129.030	Q > 0.06	1.43	0.751
G2	Q < 0.06	4.21	226.230	Q > 0.06	1.33	0.756
G3	Q < 0.05	4.16	2.867	Q > 0.05	0.83	0.913
HBM1	Q < 0.03	3.83	0.622	Q > 0.03	0.74	0.874
HBM2	Q < 0.03	3.32	2.623	Q > 0.03	1.13	0.817
HBM3	Q < 0.09	2.93	589.910	Q > 0.09	0.93	0.686

Table A2.7. Gaussian model

sample	M_w/M_n	$R_g/\text{\AA}$	dispersity in R_g	χ^2
HBR1	1.000	133.5	0.0670	1.437
HBR2	1.000	136.9	0.0952	1.201
HBR3	2.292	99.9	0.100	0.832
LR1	0.998	73.6	0.000	15.073
LR2	1.000	200.0	0.000	15.326
LR3	1.000	208.4	0.000	6.301
G1	1.000	174.1	0.000	447.980
G2	1.487	209.9	0.000	940.240
G3	1.946	180.0	2.070×10^{-5}	174.420
HBM1	0.999	133.1	0.000	1.500
HBM2	1.432	299.6	0.029	21.204
HBM3	1.687	390.6	0.000	544.550

Table A2.8. Fractal Model

sample	correlation length, ξ / \AA	fractal dimension	radius / \AA	SLD block / \AA^{-2}	dispersity in radius	χ^2
HBR1	1614.0	3.02	13.6	4.59×10^{-6}	0.0490	0.800
HBR2	1012.8	3.02	14.9	3.90×10^{-6}	0.0878	0.778
HBR3	2799.5	3.01	9.7	4.18×10^{-6}	0.0592	0.792
LR1	943.1	3.02	3.8	4.16×10^{-6}	0.700	0.939
LR2	3425.6	3.00	4.0	2.04×10^{-6}	0.593	0.793
LR3	902.0	2.95	15.5	4.07×10^{-6}	0.410	0.832
G1	890.8	2.99	2.0	1.50×10^{-6}	0.800	24.772
G2	529.0	3.03	2.2	1.54×10^{-6}	8.674×10^{-19}	51.221
G3	1870.0	3.01	6.3	1.49×10^{-6}	0.000	1.195
HBM1	700.5	3.06	21.6	5.24×10^{-6}	0.175	0.804
HBM2	822.9	3.12	34.1	2.93×10^{-6}	8.565×10^{-19}	8.421
HBM3	1810.5	2.92	3.6	1.45×10^{-6}	0.0868	191.960

Table A2.9. Sphere Model

sample	radius /Å	SLD sphere /Å ⁻²	dispersity in radius	χ^2
HBR1	1383.2	4.42 x10 ⁻⁶	0.0483	0.803
HBR2	1386.9	4.00 x10 ⁻⁶	0.0456	0.777
HBR3	1776.0	5.83 x10 ⁻⁶	0.0340	0.767
LR1	1432.4	3.61 x10 ⁻⁶	0.0564	0.852
LR2	1255.2	4.16 x10 ⁻⁶	0.107	0.834
LR3	906.9	4.76 x10 ⁻⁶	0.106	2.531
G1	572.4	2.25 x10 ⁻⁶	0.163	22.368
G2	546.6	1.48 x10 ⁻⁶	0.163	83.214
G3	582.1	2.35 x10 ⁻⁶	0.169	1.156
HBM1	683.9	2.95 x10 ⁻⁶	0.256	0.938
HBM2	1261.3	3.36 x 10 ⁻⁶	0.059	32.424
HBM3	353.7	1.38 x10 ⁻⁶	0.265	423.31

Table A2.10. Lamellar ParaCrystal Model

sample	no. of layers	dispersity of spacing	SLD layer /Å ⁻²	spacing /Å	thickness /Å	dispersity of thickness	χ^2
LR3	2.10	0.241	3.77 x10 ⁻⁶	653.1	259.9	0.810	2.000
G1	2.00	0.316	1.40 x10 ⁻⁶	169.6	171.6	0.210	1.727
G2	1.61	0.047	1.81 x10 ⁻⁶	167.6	167.6	0.126	6.732
HBM1	2.44	0.250	3.71 x10 ⁻⁶	179.7	188.6	0.000	0.910
HBM2	10.37	0.221	2.07 x10 ⁻⁶	114.6	42.3	0.000	1.398
HBM3	2.60	0.235	2.29 x10 ⁻⁶	166.6	138.9	0.255	5.442

Results of Model Fitting to SANS Data of P(nMA-AA) Copolymers in 1:1 d-THF:CDCl₃ Mixture

Table A2.11. Absolute Power Law

sample	m	χ^2
HBR1	1.18	0.997
HBR2	1.25	0.870
HBR3	0.80	0.871
LR1	1.28	0.624
LR2	1.17	1.048
LR3	1.17	1.050
G1	2.34	1.708
G2	2.00	1.887
G3	1.60	2.132
HBM1	1.45	0.858
HBM2	2.18	1.136
HBM3	3.10	5.284

Table A2.12. Gaussian model

sample	M_w/M_n	$R_g/\text{\AA}$	dispersity in R_g	χ^2
HBR1	4.96	116.2	0.104	1.055
HBR2	4.84	85.3	0.025	0.795
HBR3	1.03	100.9	0.167	0.942
LR1	1.56	101.2	0.237	0.674
LR2	2.98	85.3	0.040	1.012
LR3	2.00	56.7	0.124	0.754
G1	1.00	144.8	0.153	3.177
G2	1.81	145.3	0.100	4.793
G3	2.48	116.8	0.206	1.190
HBM1	1.67	86.5	0.001	0.828
HBM2	1.00	186.7	0.008	1.428
HBM3	1.00	154.9	0.001	28.390

Table A2.13. Fractal Model

sample	correlation length, ξ / \AA	fractal dimension	radius / \AA	SLD block / \AA^{-2}	dispersity in radius	χ^2
HBR1	101.5	1.47	11.5	1.89×10^{-6}	0.099	0.974
HBR2	47.4	2.05	13.6	1.40×10^{-6}	0.001	0.778
HBR3	39.5	2.20	17.8	2.50×10^{-6}	0.000	0.948
LR1	262.2	1.38	4.6	1.40×10^{-6}	0.009	0.624
LR2	64.7	1.56	5.4	1.39×10^{-6}	0.039	0.939
LR3	47.5	1.68	6.3	1.40×10^{-6}	0.009	0.762
G1	328.1	2.36	4.9	3.19×10^{-6}	0.000	1.393
G2	499.7	2.03	4.0	1.54×10^{-6}	0.003	1.861
G3	81.0	1.99	10.0	1.48×10^{-6}	0.082	1.278
HBM1	578.1	1.51	4.7	3.19×10^{-6}	0.158	1.157
HBM2	364.7	2.10	5.0	4.34×10^{-6}	0.091	1.424
HBM3	102.7	3.01	3.8	2.31×10^{-6}	0.014	2.860

Table A2.14. Sphere Model

sample	radius /Å	SLD sphere	dispersity in radius	χ^2
HBR1	12461.0	1.93×10^{-6}	0.277	2.950
HBR2	2184.2	2.99×10^{-6}	0.354	5.740
HBR3	2793.1	3.98×10^{-6}	0.236	1.141
LR1	40006.0	1.41×10^{-6}	0.370	2.624
LR2	34011.0	1.51×10^{-6}	0.341	4.662
LR3	44675.0	1.40×10^{-6}	0.544	9.587
G1	1869.6	1.56×10^{-6}	0.028	2.982
G2	2211.6	1.43×10^{-6}	0.027	11.667
G3	4058.6	1.43×10^{-6}	0.014	68.502
HBM1	1310.0	3.40×10^{-6}	0.174	4.690
HBM2	1282.7	2.41×10^{-6}	0.182	9.425
HBM3	439.0	2.60×10^{-6}	0.144	9.150

Results of Model Fitting to SANS Data of P(nMA-AA) Copolymers in d-EtOH**Table A2.15. Absolute Power Law**

sample	m	χ^2
HBR2	1.13	1.498
LR2	1.03	1.226
G2	1.42	0.720
HBM2	1.70	0.927
HBA2	1.46	0.981
LB2	1.55	1.035

Table A2.16. Gaussian model

sample	M_w/M_n	$R_g/\text{Å}$	dispersity in R_g	χ^2
HBR2	2.38	56.0	0.118	0.918
LR2	3.99	48.5	0.026	0.851
G2	2.12	148.3	0.214	0.970
HBM2	1.05	163.4	0.005	1.432
HBA2	5.00	119.1	0.205	0.995
LB2	1.88	113.7	0.017	0.751

Table A2.17. Fractal Model

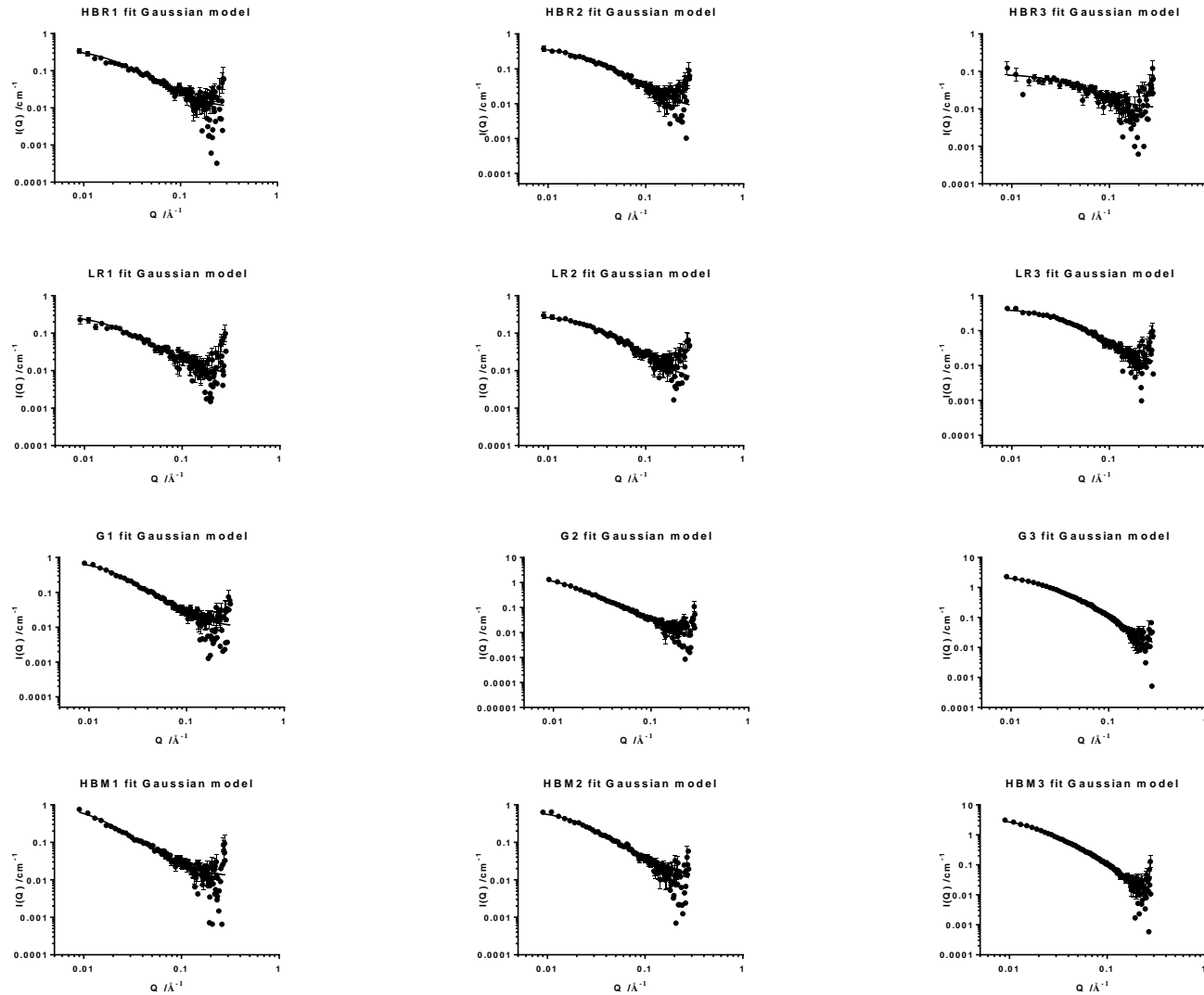
sample	correlation length, ξ /Å	fractal dimension	radius /Å	SLD block /Å ⁻²	dispersity in radius	χ^2
HBR2	540.2	1.13	6.7	1.40 x10 ⁻⁶	0.061	1.720
LR2	348.1	1.08	7.4	1.40 x10 ⁻⁶	0.000	1.259
G2	499.9	1.49	6.0	1.40 x10 ⁻⁶	0.000	0.753
HBM2	599.2	1.72	4.2	1.60 x10 ⁻⁶	0.005	0.957
HBA2	499.9	1.48	5.7	1.47 x10 ⁻⁶	0.000	1.189
LB2	166.1	1.57	5.3	1.40 x10 ⁻⁶	0.006	1.331

Table A2.18. Sphere Model

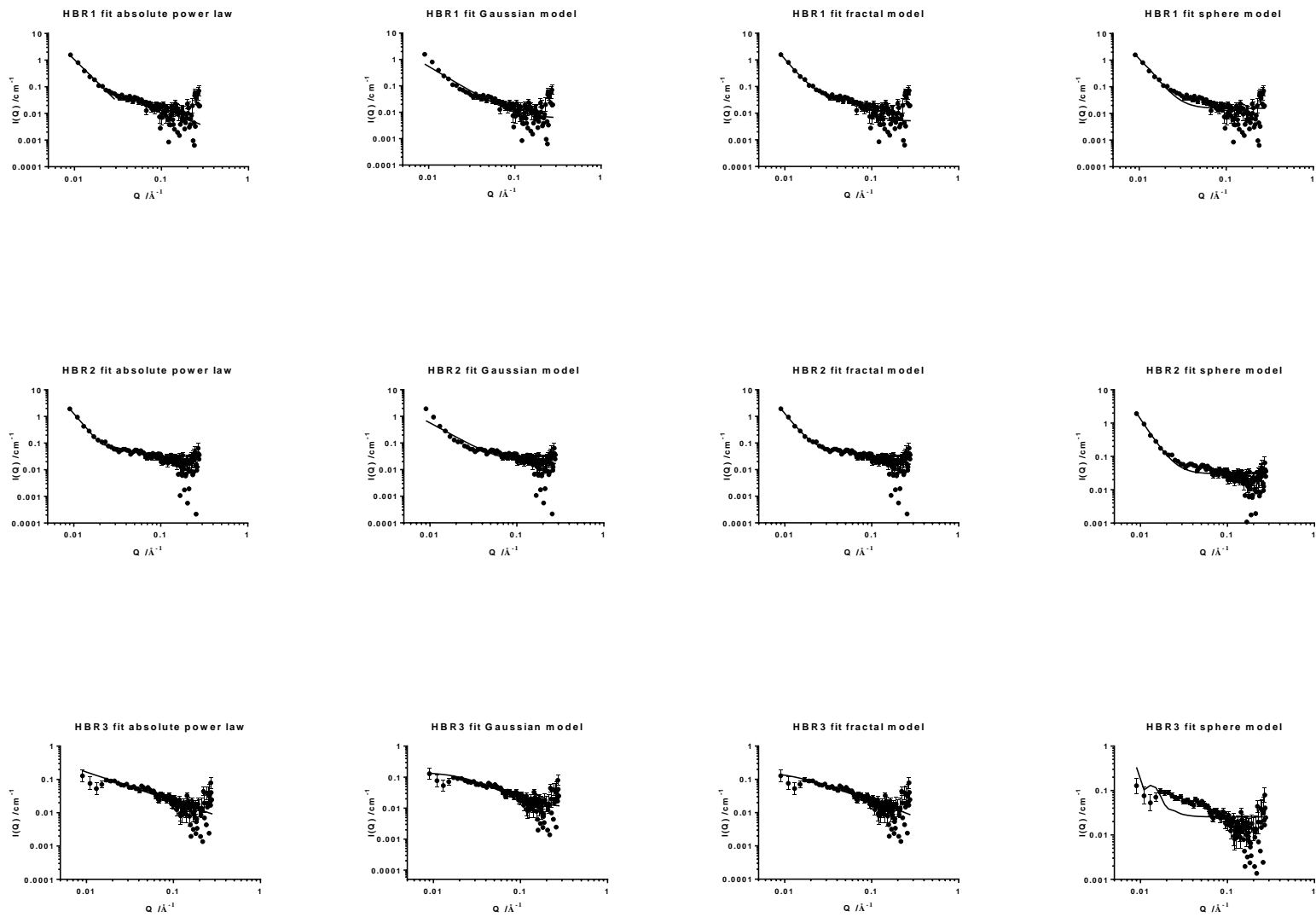
sample	radius /Å	SLD sphere /Å ⁻²	dispersity in radius	χ^2
HBR2	36.4	3.20 x10 ⁻⁶	0.236	1.279
LR2	29.0	1.40 x10 ⁻⁶	0.274	0.982
G2	42.1	1.46 x10 ⁻⁶	0.239	3.503
HBM2	38.2	3.63 x10 ⁻⁶	0.399	2.505
HBA2	42.7	4.16 x10 ⁻⁶	0.290	4.564
LB2	44.7	4.82 x10 ⁻⁶	0.280	5.891

Appendix 3: Model Fitting to SANS Data

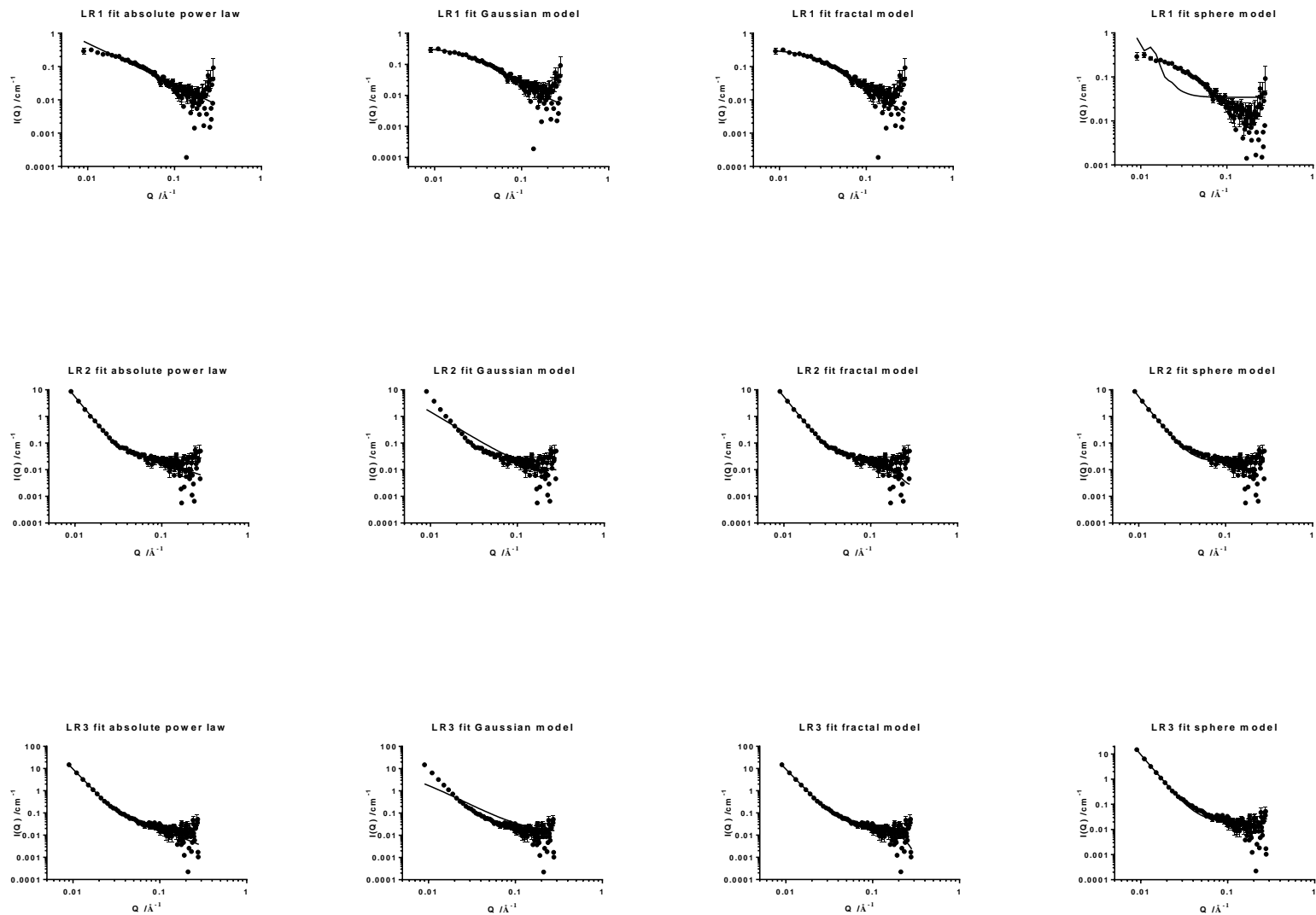
Results of Model Fitting to SANS Data from P(nMA-AA) Copolymers in d-THF



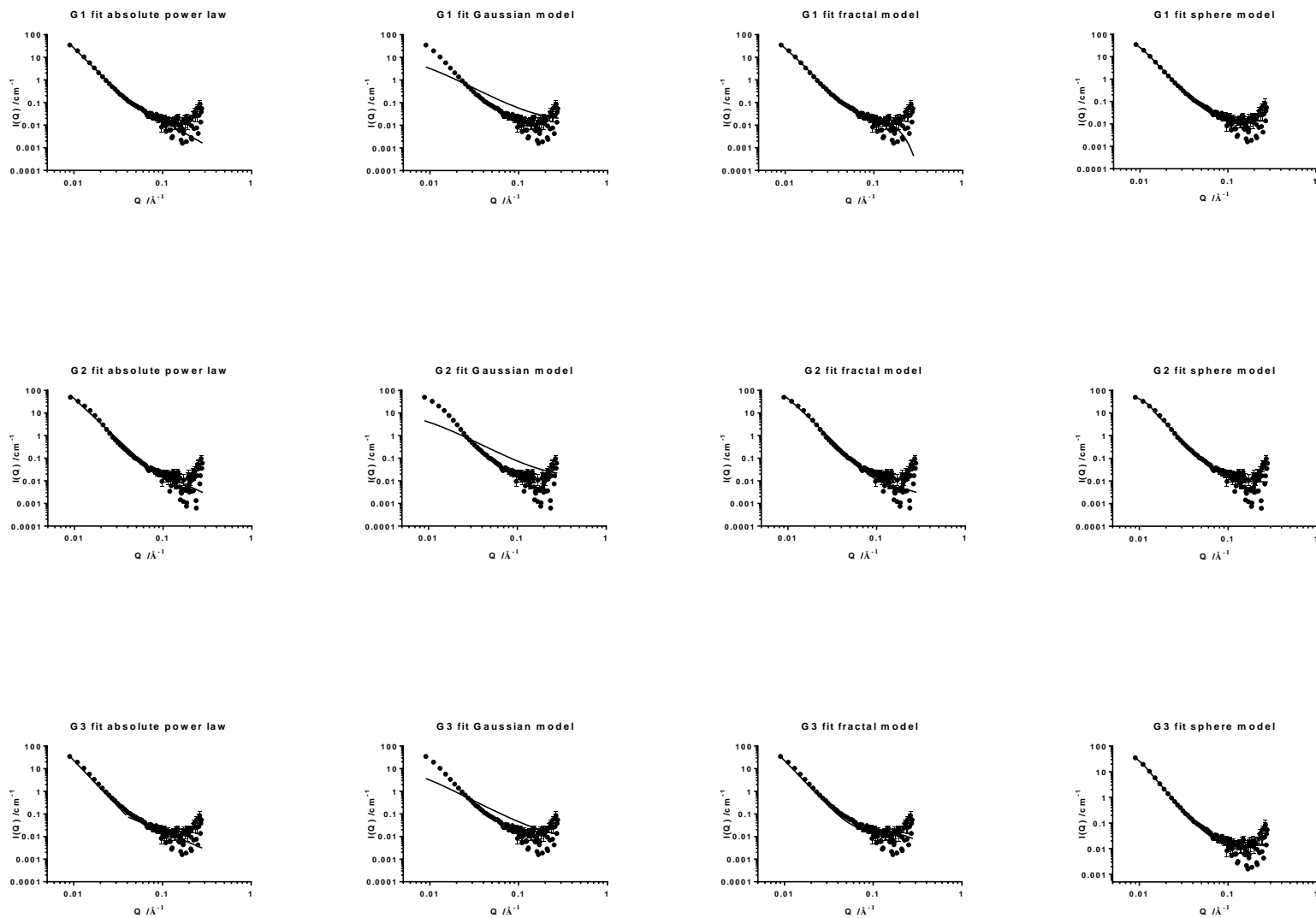
Results of Model Fitting to SANS Data from HB P(nMA-co-AA) Copolymers in d-THF:D₂O Mixture



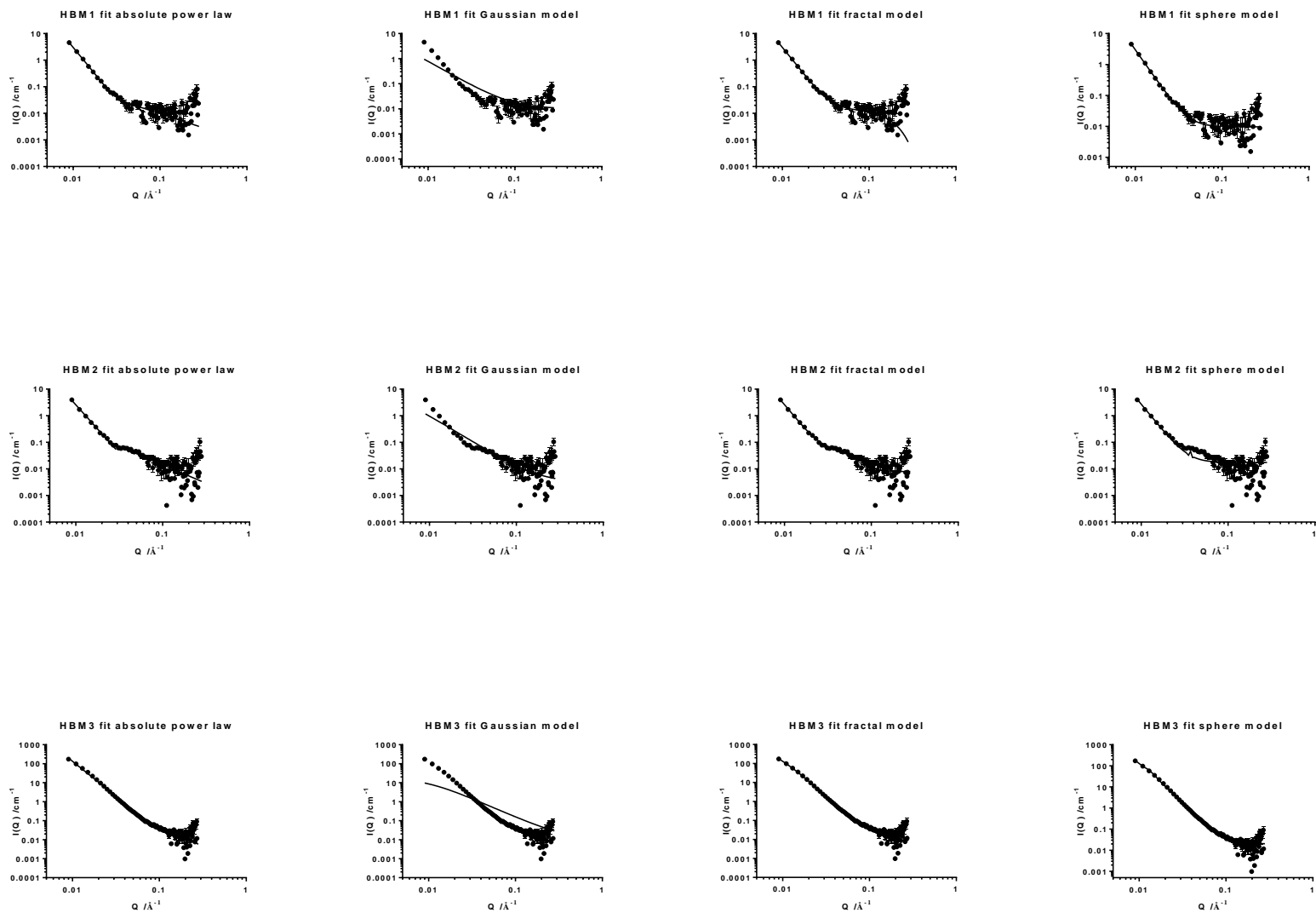
Results of Model Fitting to SANS Data from Linear P(nMA-co-AA) Copolymers in d-THF:D₂O Mixture



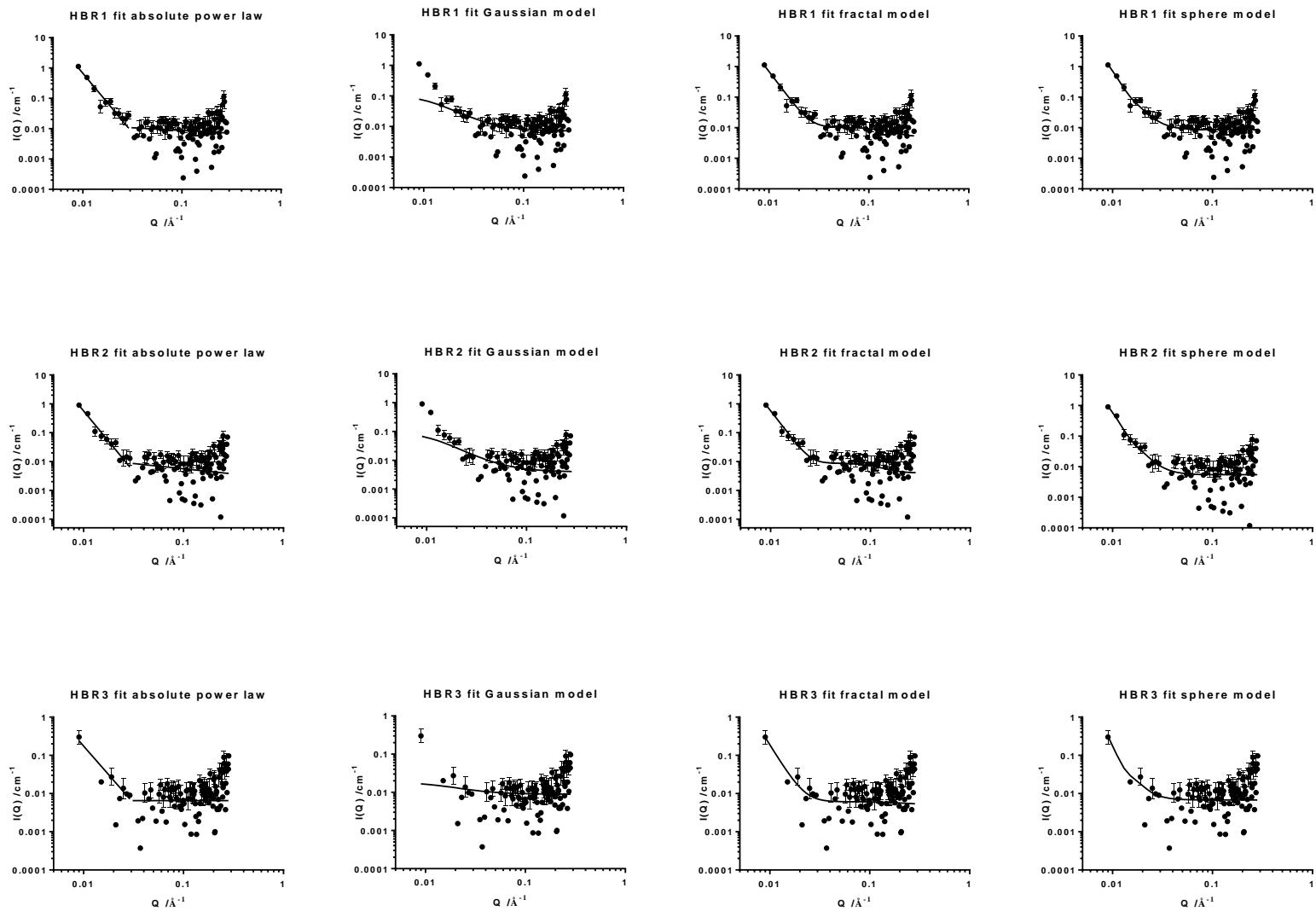
Results of Model Fitting to SANS Data from P(nMA-co-VBC-g-AA) Copolymers in d-THF:D₂O Mixture



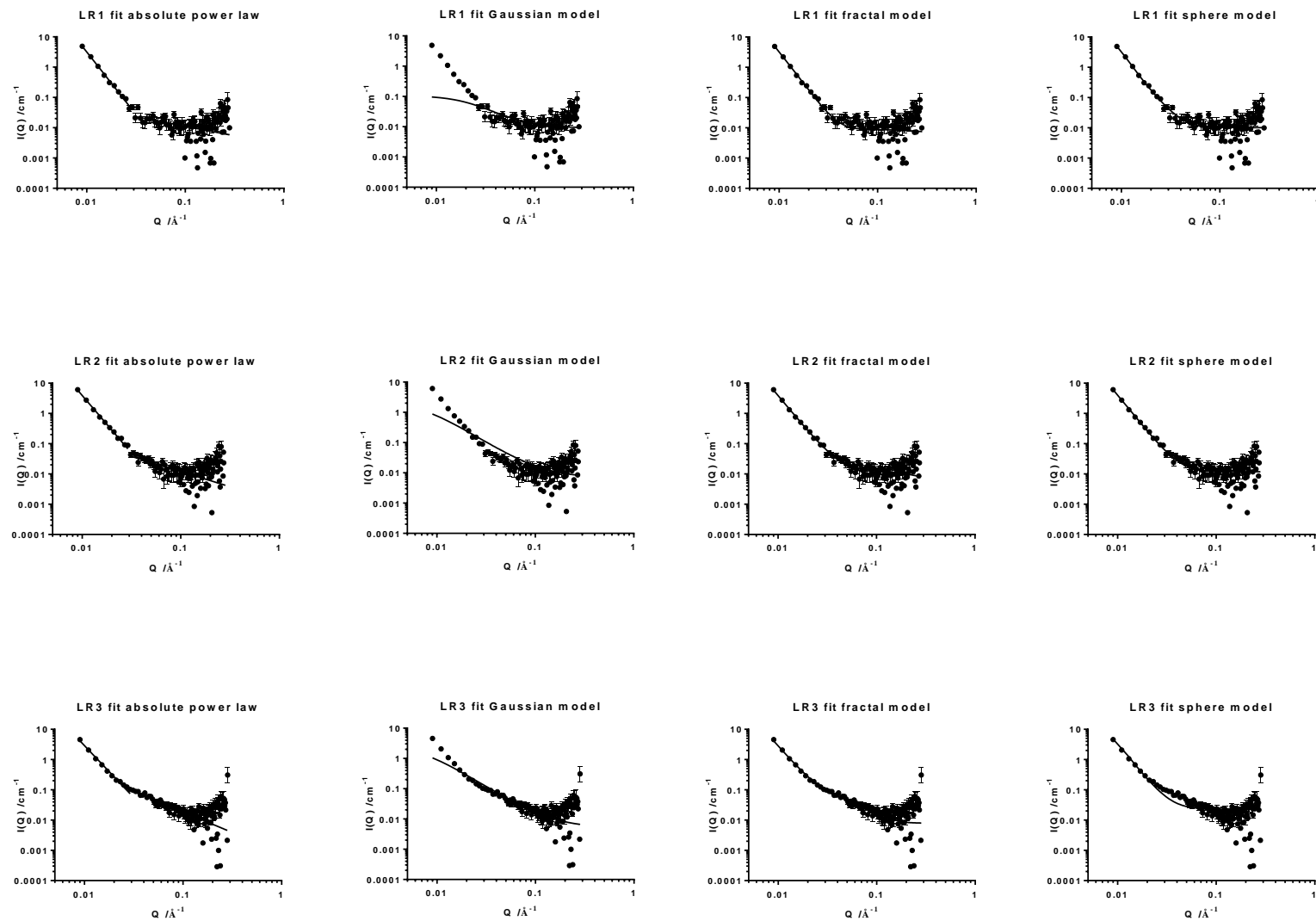
Results of Model Fitting to SANS Data from HB P(nMA-*b*-AA) Copolymers in d-THF:D₂O Mixture



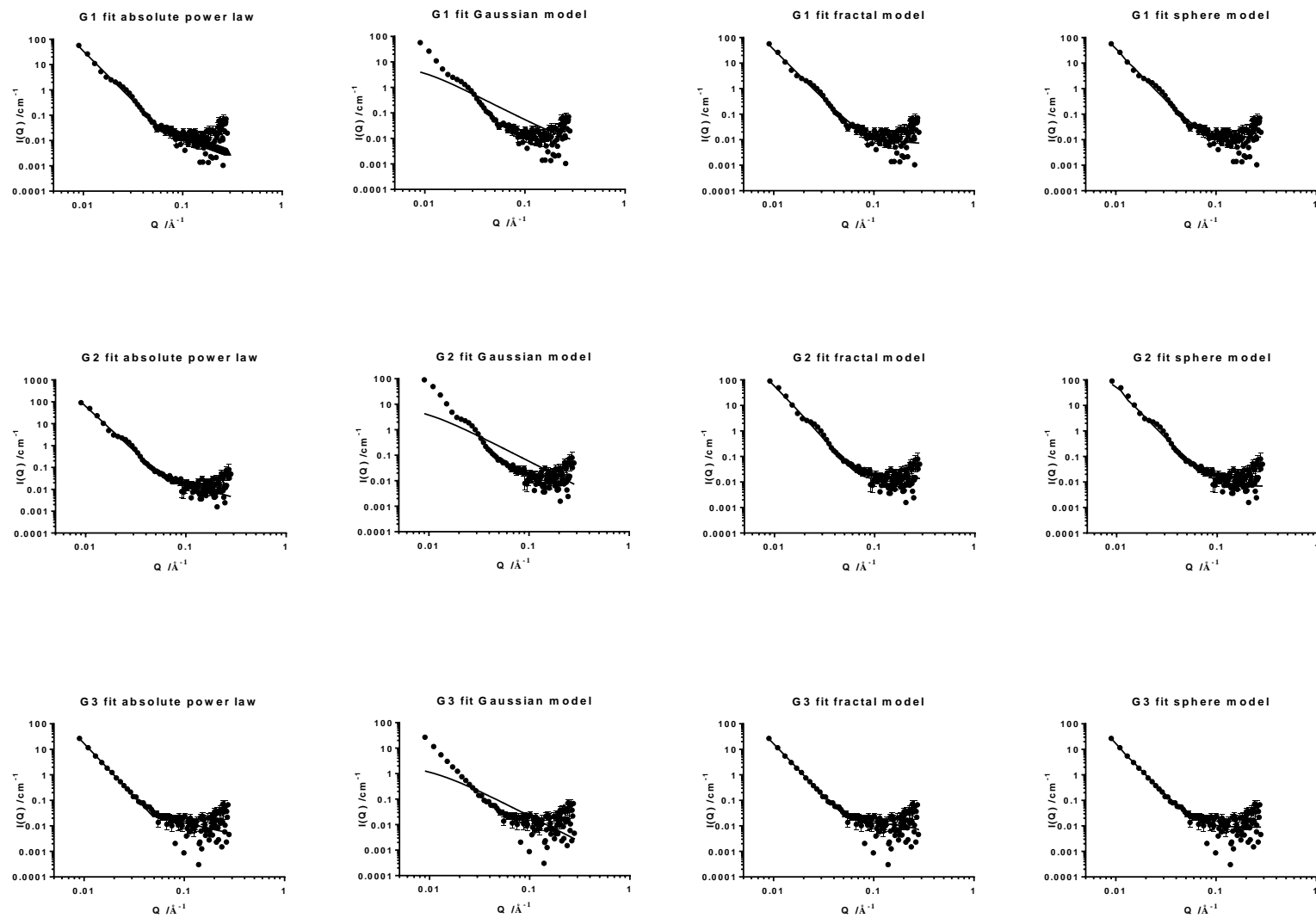
Results of Model Fitting to SANS Data from HB P(nMA-co-AA) Copolymers in D₂O



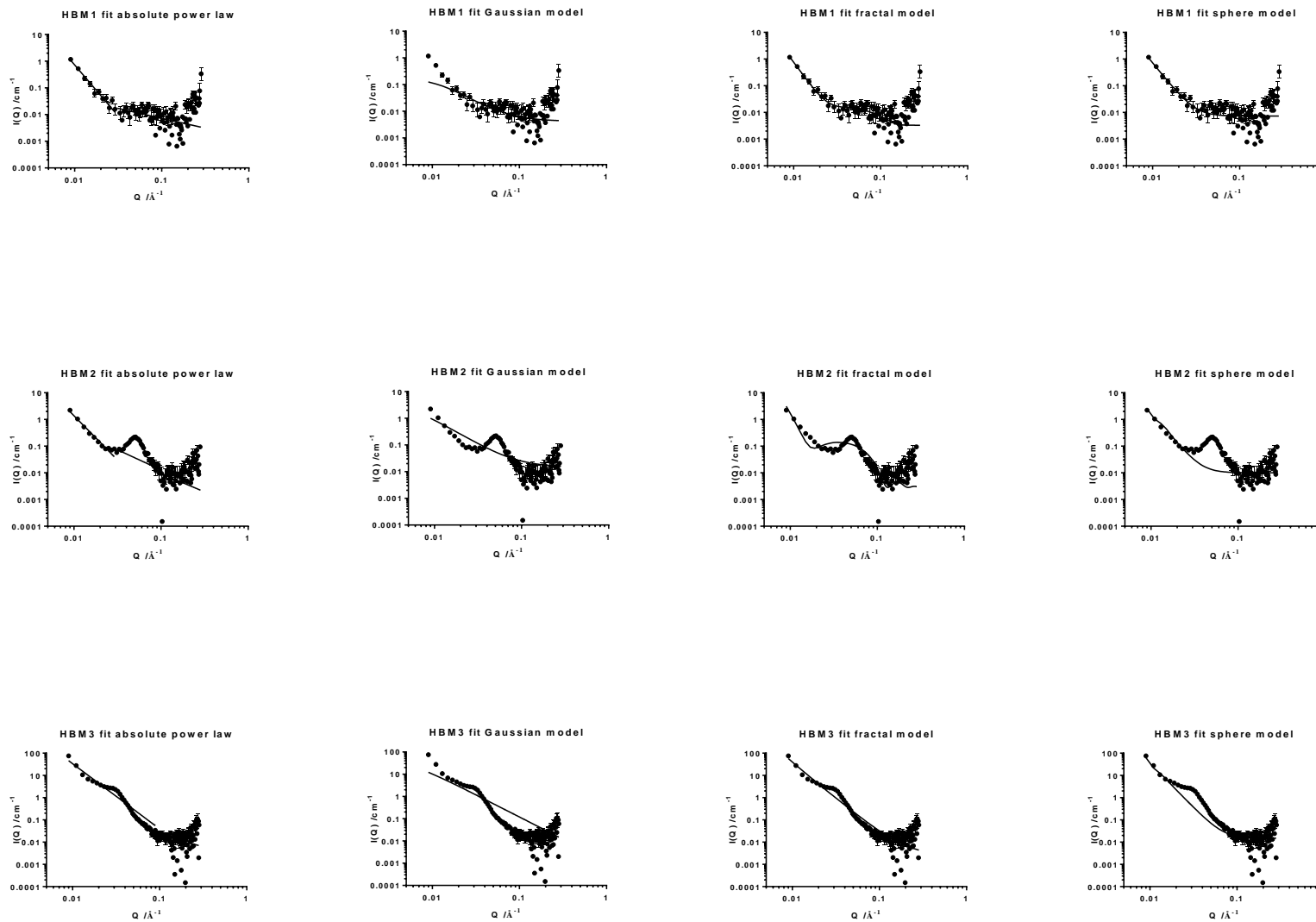
Results of Model Fitting to SANS Data from HB P(nMA-co-AA) Copolymers in D₂O



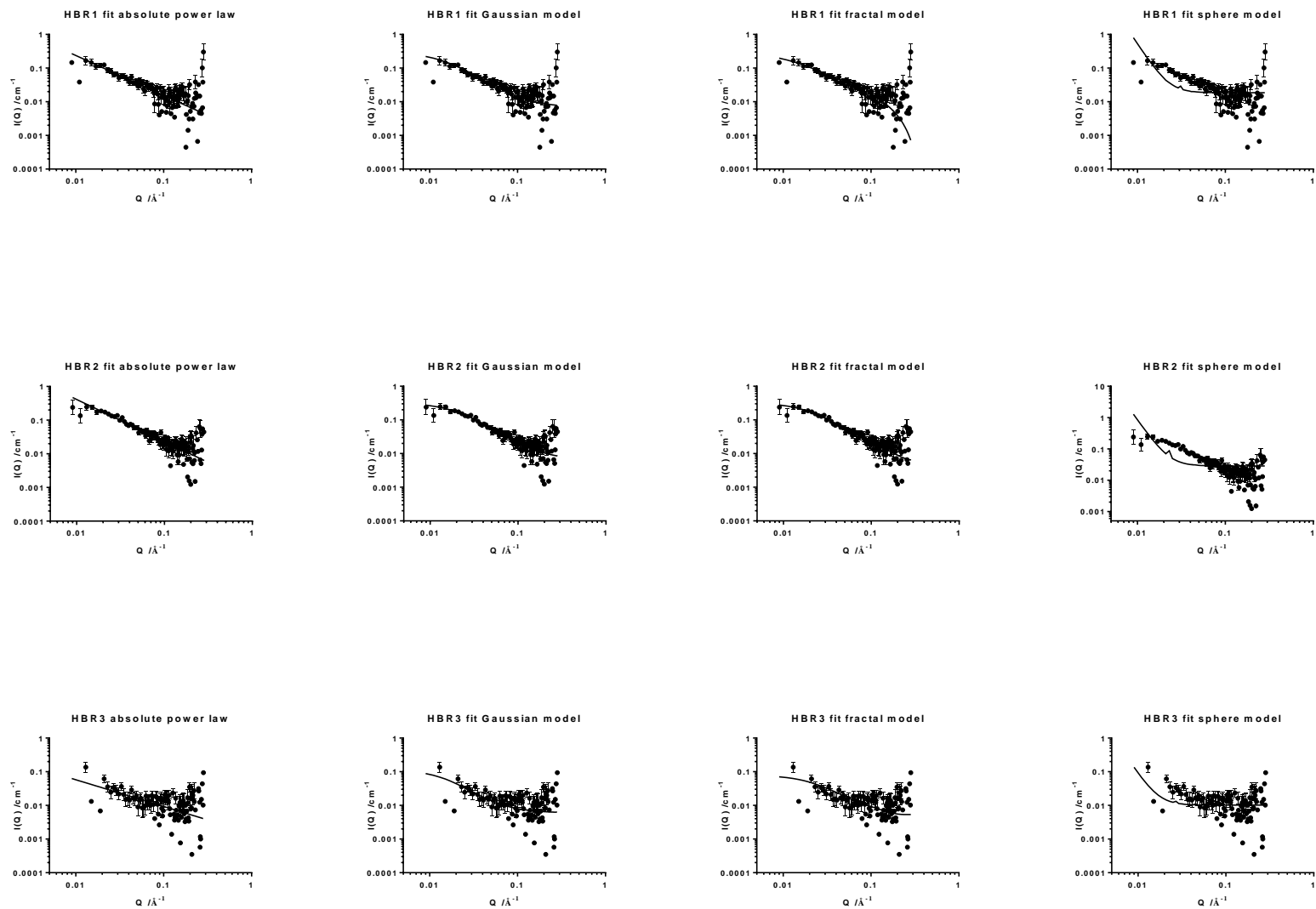
Results of Model Fitting to SANS Data from P(nMA-co-VBC-g-AA) Copolymers in D₂O



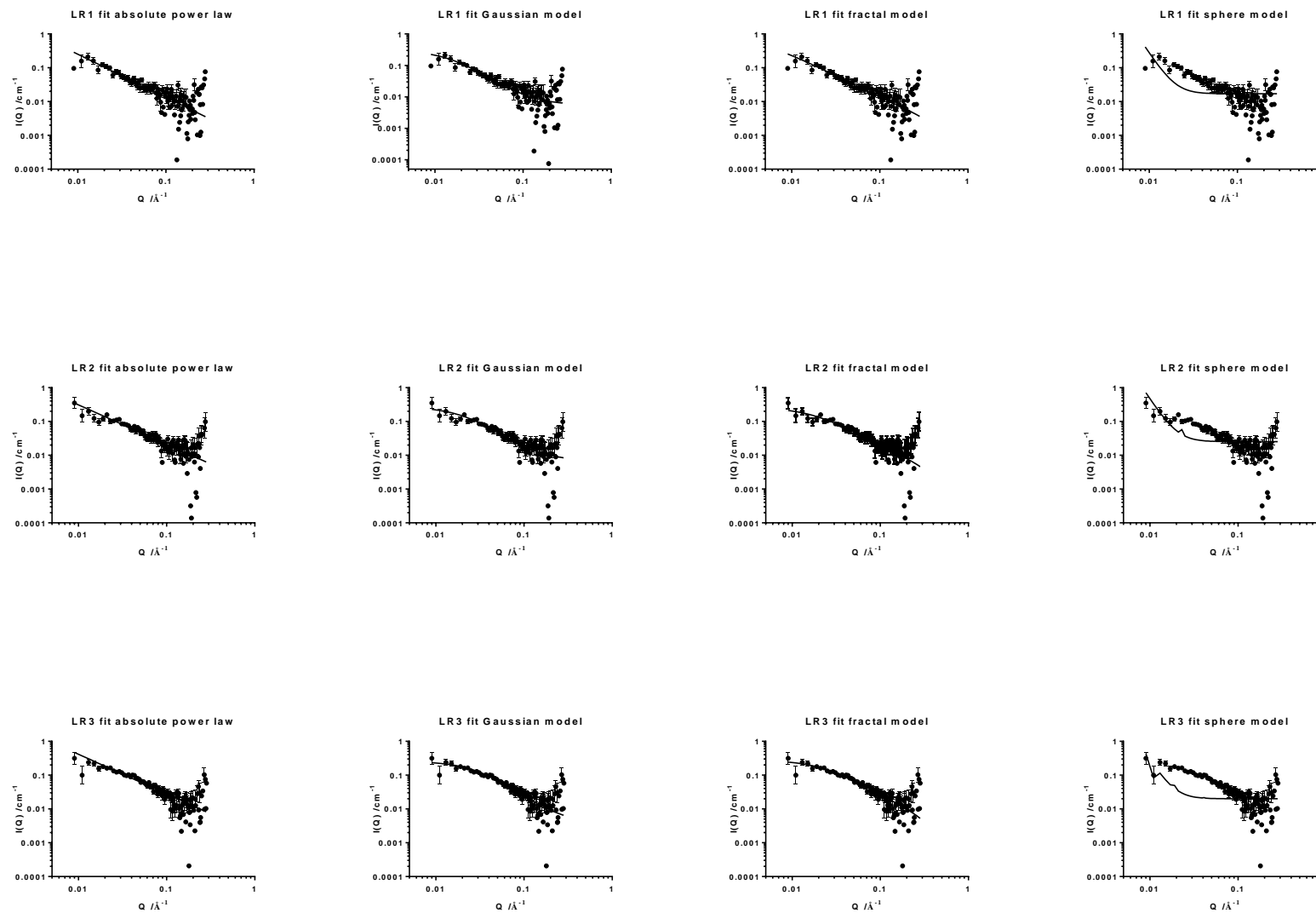
Results of Model Fitting to SANS Data from HB P(nMA-*b*-AA) Copolymers in D₂O

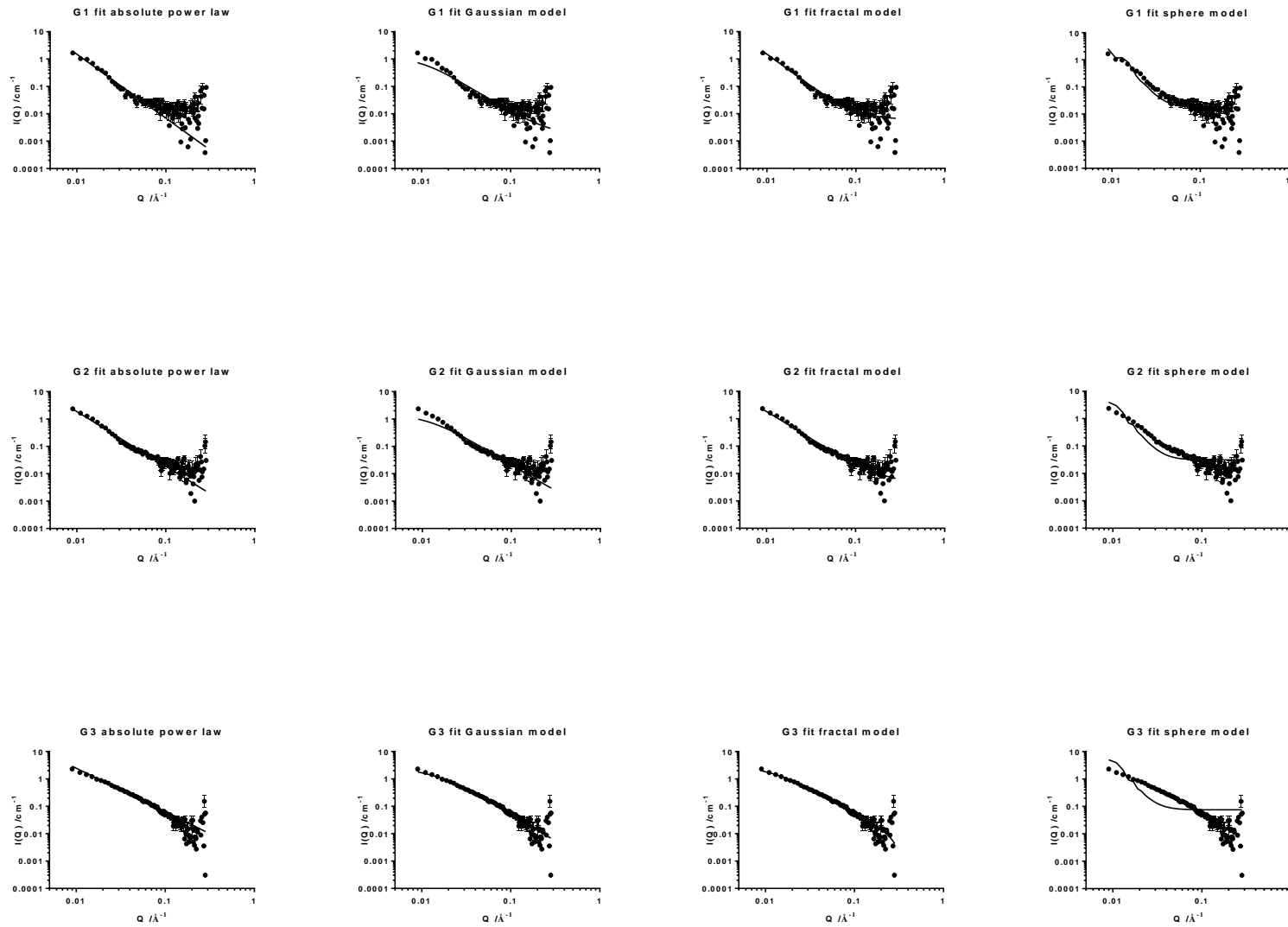


Results of Model Fitting to SANS Data from HB P(nMA-co-AA) Copolymers in d-THF:CDCl₃ Mixture

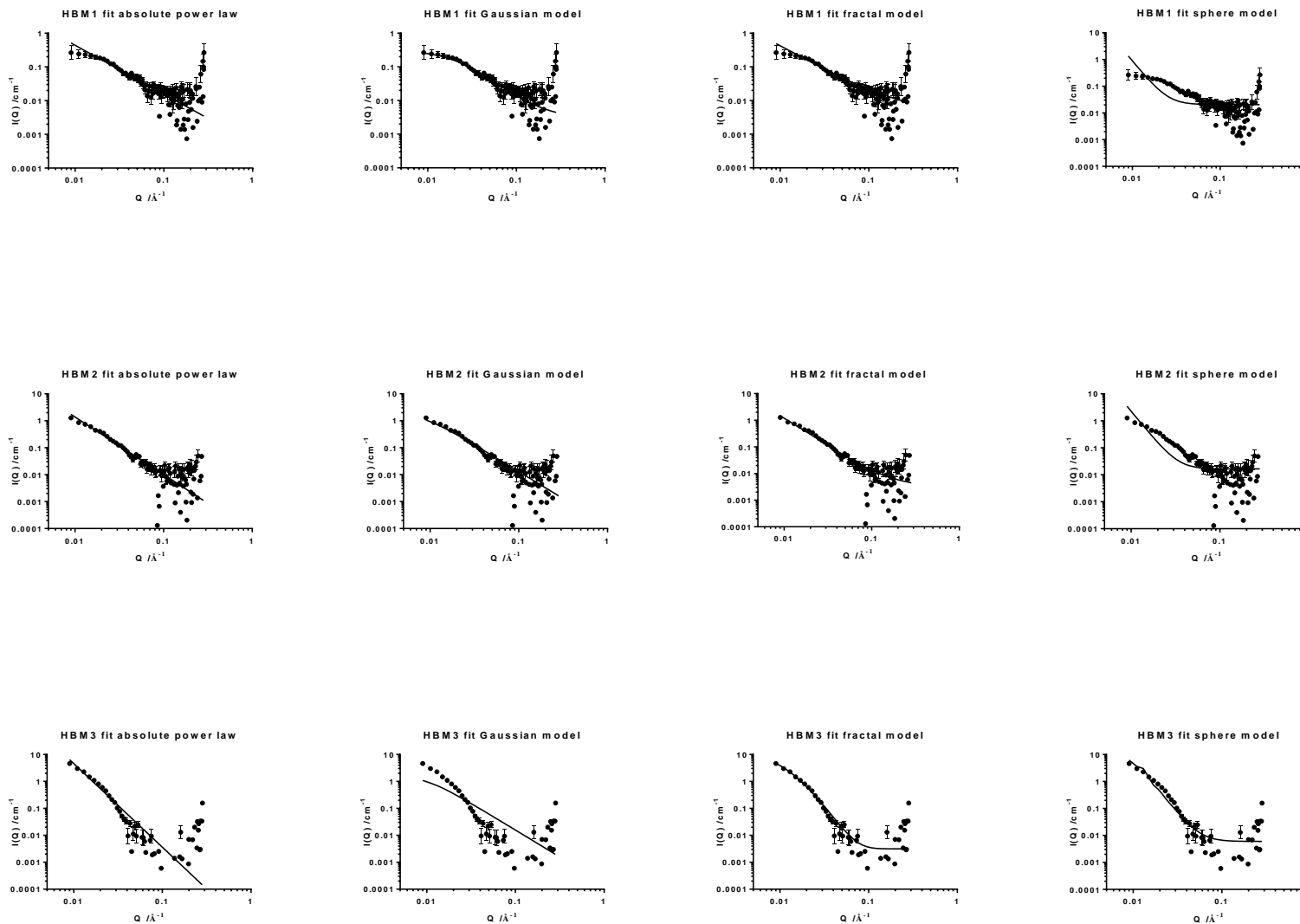


Results of Model Fitting to SANS Data from Linear P(nMA-co-AA) Copolymers in d-THF:CDCl₃ Mixture

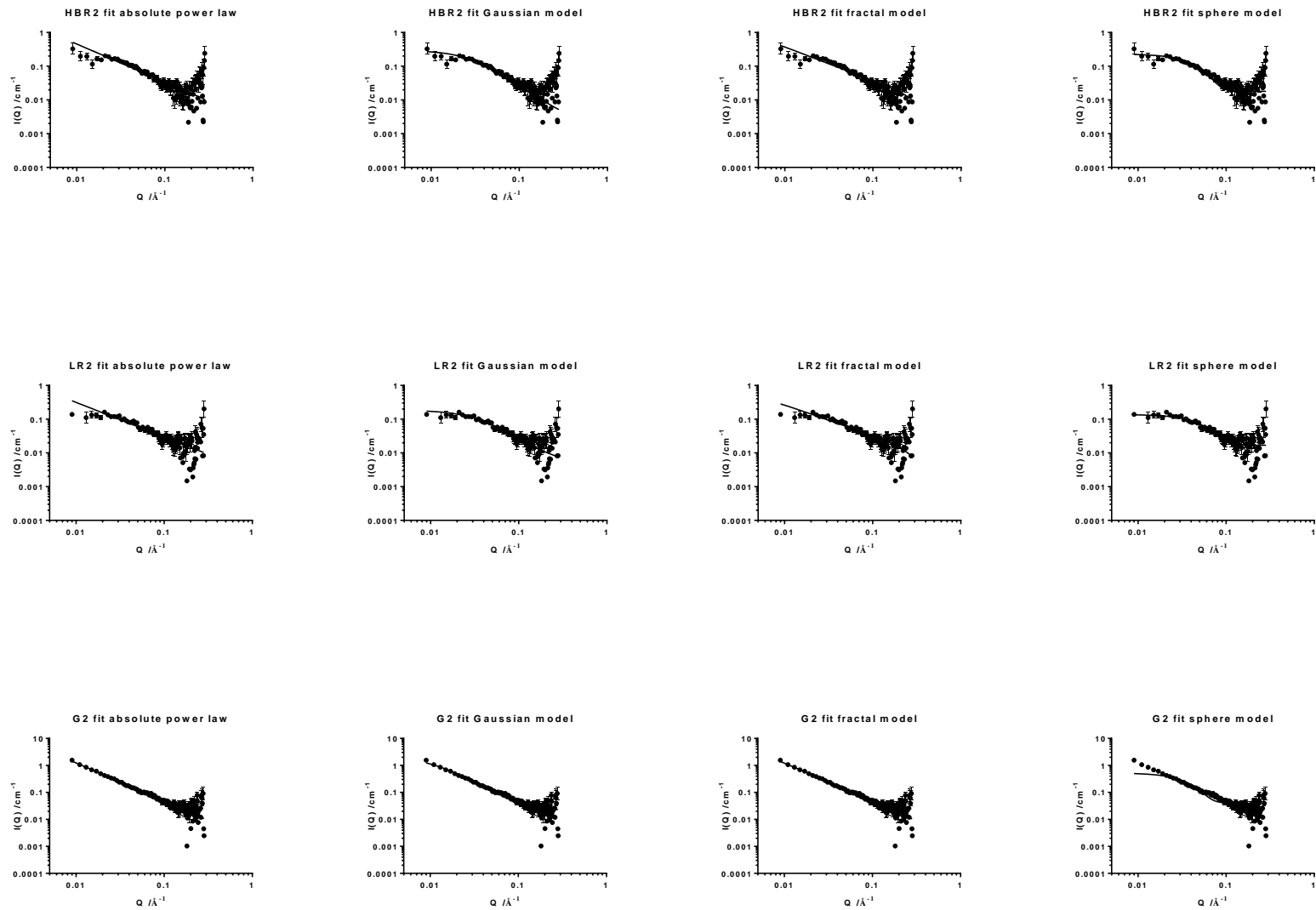


Results of Model Fitting to SANS Data from P(nMA-co-VBC-g-AA) Copolymers in d-THF:CDCl₃ Mixture

Results of Model Fitting to SANS Data from HB P(nMA-*b*-AA) Copolymers in d-THF:CDCl₃ Mixture



Results of Model Fitting to SANS Data from HB P(nMA-AA) Copolymers in d-EtOH



Results of Model Fitting to SANS Data from HB P(nMA-AA) Copolymers in d-EtOH

